Higher-Degree Immersed Finite Elements for Second-Order Elliptic Interface Problems

Mohamed Ben Romdhane

Dissertation submitted to the Faculty of the
Virginia Polytechnic Institute and State University
in partial fulfillment of the requirements for the degree of

Doctor of Philosophy
in
Mathematics

Slimane Adjerid, Chair
Tao Lin, Co-chair
George A. Hagedorn
Yuriko Renardy

August 1, 2011
Blacksburg, Virginia

Keywords: Interface Problems, Immersed Finite Elements,
Galerkin Method, Interior Penalty Method

Higher-Degree Immersed Finite Elements for Second-Order Elliptic Interface Problems

Mohamed Ben Romdhane

ABSTRACT

A wide range of applications involve interface problems. In most of the cases, mathematical modeling of these interface problems leads to partial differential equations with non-smooth or discontinuous inputs and solutions, especially across material interfaces. Different numerical methods have been developed to solve these kinds of problems and handle the non-smooth behavior of the input data and/or the solution across the interface. The main focus of our work is the immersed finite element method to obtain optimal numerical solutions for interface problems.

In this thesis, we present piecewise quadratic immersed finite element (IFE) spaces that are used with an immersed finite element (IFE) method with interior penalty (IP) for solving two-dimensional second-order elliptic interface problems without requiring the mesh to be aligned with the material interfaces. An analysis of the constructed IFE spaces and their dimensions is presented. Shape functions of Lagrange and hierarchical types are constructed for these spaces, and a proof for the existence is established. The interpolation errors in the proposed piecewise quadratic spaces yield optimal $\mathcal{O}(h^3)$ and $\mathcal{O}(h^2)$ convergence rates, respectively, in the L^2 and broken H^1 norms under mesh refinement. Furthermore, numerical results are presented to validate our theory and show the optimality of our quadratic IFE method.

Our approach in this thesis is, first, to establish a theory for the simplified case of a linear interface. After that, we extend the framework to quadratic interfaces. We, then, describe a general procedure for handling arbitrary interfaces occurring in real physical practical applications and present computational examples showing the optimality of the proposed method. Furthermore, we investigate a general procedure for extending our quadratic IFE spaces to p-th degree and construct hierarchical shape functions for $p = 3$.

In the name of Allah, the most gracious, the most merciful.

Acknowledgments

First of all, all praise and thanks are due to Allah for granting me the chance and the ability to successfully complete this work. Without his guidance and mercy, I would not be able to achieve this level of education.

I wish to express my sincere gratitude to my advisor, Professor Slimane Adjerid, for all his help, guidance, patience, and continuous encouragement to achieve this work. I have learned from his wide knowledge in numerical analysis and scientific computing, I have learned from his experience in research, and I have also learned so much from his personality. His invaluable guidance was critical for me in completing this work.

I would also like to thank my co-advisor and the co-chair of my committee, Professor Tao Lin, for all his help and guidance throughout this work. I appreciate his advice and continuous availability to help me complete this work. It is an honor to have worked with him and learned from him.

I would also like to thank Professor George Hagedorn and Professor Yuriko Renardy for agreeing to serve on my thesis committee and for their efforts in reviewing my work. I want also to thank all the professors of our department for teaching me and advising me throughout the years, as well as all the department staff.

Most importantly, I would like to thank my family. I believe that without their support and patience I would have never reached this point. Special thanks to my mother, the most important person in my life. After my father passed away, she strived to support me and made sacrifices to help me succeed in my life. I fail to find appropriate words to thank her; may Allah grant her the best reward. Special thanks to my wife as well, for her patience and support during our stay in Blacksburg. She was always close to me, ready to give me her support and encouragement, and was a continuous source of motivation and strength to achieve success in my work. I would like also to thank my son Hamza for waking me up during several nights and making me stay up during several whole nights, which helped me do more work.

Finally, I would like to thank all my friends in Blacksburg for the good time that we shared together in the past four years. Special thanks to my dear friend and colleague Idir Mechai for all his help, cooperation, and support. Special thanks also to Helmi Temimi and Mahboub Baccouch for their help and advice, especially during my first year in the United States. I also address my sincere acknowledgements and gratitude to Virginia Tech, as well as to the US National Science Foundation (NSF) for supporting this work by grants DMS-0713763 and DMS-1016313.

Contents

List of Tables

List of Figures

Chapter 1

Introduction

Mathematical modeling of a physical phenomenon in a domain consisting of multiple materials often leads to interface problems. Many important applications such as charging in space [25], projection methods for Navier-Stokes equation [19, 20], and shape and topology optimization [26] consist of solving interface problems. In this chapter, we first present the model second-order elliptic interface problem considered in this work. Next, we survey, from the literature, several existing methods that are used to solve interface problems and we briefly present the immersed finite element method. We conclude this chapter with an overview and the organization of this thesis.

1.1 The Model Interface Problem

We consider the following model interface problem

$$\begin{cases} -\nabla(\beta\nabla u) = f, & \text{on } \Omega, \\ u_{|\partial\Omega} = g. \end{cases} \tag{1.1.1a}$$

Without loss of generality, we assume that $\Omega \subset \mathbb{R}^2$ is a rectangular domain consisting of two sub-domains Ω^+ and Ω^- separated by an interface Γ as illustrated in Figure 1.1. The coefficient β is given by

$$\beta(x,y) = \begin{cases} \beta^+, & \text{on } \Omega^+, \\ \beta^-, & \text{on } \Omega^-, \end{cases} \tag{1.1.1b}$$

where β^+ and β^- are two positive constants. The true solution u and its flux are continuous across the interface Γ as

$$[u]_\Gamma = 0, \tag{1.1.2a}$$

and

$$[\beta\frac{\partial u}{\partial \boldsymbol{n}}]_\Gamma = 0, \tag{1.1.2b}$$

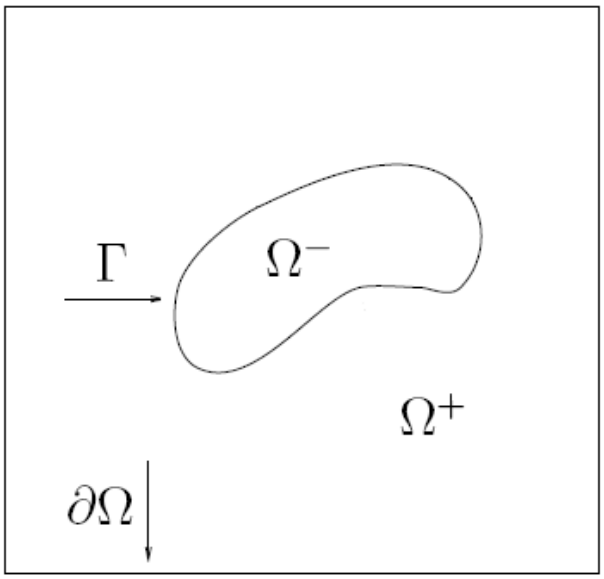

Figure 1.1: A two-material domain Ω.

where $[u]_\Gamma = u^+|_\Gamma - u^-|_\Gamma$ denotes the jump of u across the interface Γ. Here $u^\pm = u|_{\Omega^\pm}$ and $\frac{\partial u}{\partial \boldsymbol{n}} = \boldsymbol{n} \cdot \nabla u$ denotes the normal derivative of u on the interface Γ with $\boldsymbol{n}$ being a unit normal vector to Γ.

1.2 Applications of the Model Interface Problem

Interface problems with discontinuous coefficients across the interface are encountered in many fields such as: electromagnetics, materials science, and fluid dynamics. Thus, many applications involve our model interface problem. We will briefly mention two applications: electrostatic leviation of lunar dust and topology optimization.

1.2.1 Electrostatic Levitation of Lunar Dust

Lunar dust has an electrostatic charge that highly increases its ability to cling to everything, which may cause serious problems for spacecraft and astronauts such as: vision obscuration, false instrument readings, thermal control problems, and breathing problems for astronauts [25, 29]. To understand the interaction between the different space objects and its effect to the electric field, a simulation of the solar winds and the movement of the lunar dust is required. One efficient method to perform the simulation is called Particle-In-Cell (PIC) method [62], which involves solving an interface problem, similar to our model interface

problem, consisting of the equation

$$-\nabla(\beta\nabla\phi) = \rho, \tag{1.2.1}$$

where ϕ is the electric potential, ρ is the charge density, and β is the dielectric parameter which is piecewise constant.

1.2.2 Topology Optimization

Topology optimization constitutes an important step in designing continuous structures and mainly consists of finding the optimal material layout minimizing an objective functional under some constraints. In many practical applications, the constraint is a given partial differential equation similar to our model interface problem. For instance, for the heat conduction optimization problem treated in [26], if the domain Ω is a multi-material domain, a discontinuous optimal conductivity distribution $k(x)$ needs to be determined [29] so that the heat is minimized over the domain Ω, under the constraints

$$\nabla(k\nabla T) + f = 0, \quad \text{in } \Omega, \tag{1.2.2}$$

$$T = 0, \quad \text{on } \Gamma_D, \quad \textit{and} \quad (k\nabla T)\cdot \boldsymbol{n} = 0, \quad \text{on } \Gamma_N,$$

where T is the temperature, f is the heat source, Γ_D is the Dirichlet boundary, and Γ_N is the Neumann boundary with unit normal vector $\boldsymbol{n}$. The constraint (1.2.2) is the same as our model interface problem.

1.3 Methods to Solve the Model Interface Problem

First, let us note that solving the model problem (1.1.1a) with discontinuous coefficients and/or singular source terms using standard numerical methods does not usually lead to optimal accuracy of the solution across the interface, although these methods are efficient for smooth solutions. Hence, solving interface problems efficiently and accurately remains a challenge because of the non-smoothness or the discontinuity of the input data and/or the solutions, as well as the non-smoothness of the interface geometry in some applications. For instance, although in many applications the restriction of the solution to every sub-domain may be H^2 (as it is the case for our model second-order elliptic problem), the global solution is not H^2 on the whole domain, which causes many standard methods to fail to solve these problems efficiently.

Many numerical methods have been developed to solve the model interface problem (1.1.1a). We present a brief review of standard and recent methods for solving interface problems, related to this thesis.

1.3.1 The Standard Finite Element Methods

The standard finite element methods may be used to solve interface problems. The main feature of the standard finite elements is that the basis functions are developed independently from the problem, however, the mesh is formed according to the problem in order to ensure convergence and optimal convergence rates [9, 13, 18]. As a result, all conventional FE methods do not allow any interface to cut through the elements, and a body-fitted mesh has to be created according to the material interfaces. Hence, Galerkin finite element methods with body-fitted meshes and standard linear basis functions produce second-order accurate approximations to the solution of an interface problem [5, 13, 18, 28, 64]. However, the restriction of body-fitted meshes leads to many drawbacks, such as the need for multiple remeshing in applications with moving interfaces and the difficulty or impossibility of the use of uniform meshes. In fact, multiple body-fitted meshes generations is very difficult and time consuming for applications involving an interface or a domain with complicated geometry. This restriction becomes more severe with moving interfaces since a new mesh has to be generated at each time step. Another main restriction for solving interface problems using the standard finite elements theory is the need of higher-order approximation for the actual interface to obtain optimal convergence rates. In fact, it was shown by J. Li *et al.* [40] that when the FE method uses polynomials of degree p, the order of approximation of the interface has to be equal to $2p$, to guarantee optimal convergence rates in both L^2 and H^1 norms.

1.3.2 The Immersed Boundary Methods

The immersed boundary (IB) method was introduced in 1972 by Peskin [50, 51, 52] to study flow patterns around heart valves and study blood flow in the heart. Later, it has been applied to many other problems involving fluid dynamics in general, and in biophysics particularly. Different variants of the IB approach currently exist, due to several modifications and refinements of the method in many works during the 1980s and 1990s (for instance, Clarke *et al.* 1986, Zeeuw & Powell 1991, Berger & Aftosmis 1998) [47].

The immersed boundary method can be considered as a mathematical formulation based on a mixture of Eulerian and Lagrangian variables, as well as a numerical scheme. Eulerian variables and Lagrangian variables are related by interaction equations based on a Dirac delta function; and are defined, respectively, on a fixed Cartesian mesh and on a curvilinear mesh having the freedom to move through the fixed Cartesian mesh. The numerical scheme involves a smoothed approximation to the Dirac delta function based on the interaction equations. For instance, in the IB method applied to fluid dynamics, finite difference methods with periodic boundary conditions may be used in solving the interface problem by representing the entire fluid domain by a uniform background grid [46]. The main advantage of the IB method is that it overcomes the problem of computation cost in mesh update algorithms since the interface is automatically tracked. However, this method still has a major

disadvantage consisting of the assumption of a fiber-like one-dimensional immersed structure which limits accurate representation of immersed flexible solids occupying finite volumes, in addition to the limitations of this method in resolving fluid domains with complex shapes and boundary conditions.

Following the ideas and work on the IB method, the immersed interface methods (IIM) were developed as an alternative approach to treat interface problems.

1.3.3 The Immersed Interface Methods

The immersed interface methods (IIM) were first introduced by LeVeque and Li [38, 39] to solve elliptic problems with discontinuous coefficients using finite difference methods. The basic idea of the IIM is to discretize the equations on a uniform Cartesian grid and to explicitly incorporate the jumps into the finite difference equations. One main advantage of the IIM is its ability to efficiently produce solutions on uniform meshes using fast solvers, as well as to handle complex interface geometries.

1.4 Review of Immersed Finite Elements

1.4.1 Motivation of the Immersed Finite Element Methods

Immersed finite element (IFE) methods are very useful in solving many engineering and scientific problems, such as problems in material sciences, electromagnetism, fluid dynamics, and biological processes [27]. As mentioned in the previous section, the standard finite element method with body-fitted meshes can be used to solve interface problems with standard problem-independent finite element basis functions, but, in order to guarantee optimal convergence of standard finite element solutions, elements which are cut by the interface are not allowed [9, 13, 18]. This restriction leads to several drawbacks, for instance, *(i)* the need for large number of remeshing steps when solving problems with moving interfaces, *(ii)* excessive mesh refinement to resolve small structures such as thin layers in the domain, *(iii)* prohibition of the use of uniform meshes when solving general interface problems. In order to circumvent the limitations of the standard finite element method, optimal first-order IFE methods allowing elements to be cut by the interface were proposed [2, 3, 17, 27, 30, 31, 33, 34, 37, 41, 42, 43, 44]. IFE methods use meshes that are not necessarily body-fitted on which piecewise polynomial finite element spaces are constructed according to interface jump conditions. Elements that are cut by the interface are referred to as interface elements; otherwise, they are called non-interface elements. Similarly, the proposed meshes contain interface and non-interface edges.

1.4.2 Review of the IFE Methods

In the 1970s and 1980s, Babuska *et al.* [7, 8] proposed the generalized finite element method, based on the idea of locally solving the interface problem on an element and constructing the shape functions in that element. They developed local basis functions which may be non-polynomials and are capable of capturing many important features of the exact solution. As an extension of the framework developed by Babuska and Osborn [7, 8], the recently developed IFE methods [2, 3, 17, 27, 29, 30, 31, 33, 37, 41, 43, 44] are based on a similar idea and use the jump conditions to construct the reference shape functions with polynomials. The basic idea of IFE is to adapt the finite element method to handle interface problems by employing piecewise polynomial shape functions that satisfy the interface jump conditions. This idea is similar to Hsieh-Clough-Tocher macro elements [21] in which piecewise cubic polynomials on three sub-triangles are used to satisfy the required continuity. Optimal immersed finite element methods were first developed for piecewise linear and bilinear polynomial approximations [37, 41, 43, 44]. Adjerid and Lin [2, 3] developed optimal high-order IFE spaces and used them with local discontinuous Galerkin method in one-dimension. Numerical results were presented and optimal convergence rates has been achieved under both h and p refinements. Later, He, Lin and Lin [29, 32] investigated IFE discontinuous Galerkin formulations for two-dimensional problems. A bilinear IFE space was constructed in [30, 45] and used with a symmetric [22] and non-symmetric [49] DG method.

1.4.3 Description of the IFE Methods

The IFE method was developed to get rid of the limitation of the conventional finite element method in solving interface problems with discontinuous coefficients. It can also be considered as an alternative approach to the immersed boundary method, that is able to exhibit second-order convergence rates. The IFE method combines ideas from the finite element method and the immersed interface method. It incorporates the discretization from the finite element method into the framework of an immersed interface method leading Y. Gong, B. Li, and Z. Li [27] to call it "immersed-interface finite-element method". IFE method represents a fast and accurate solver of elliptic interface problems. For instance, in a long-time simulation of interface dynamics, IFE method may be able to solve such problems with no remeshing steps.

The IFE method allows using finite elements that are cut by the interface which eliminates the need for using body-fitted meshes and uses interface-independent meshes to solve interface problems. The main feature of the immersed finite elements is that the basis functions are constructed and developed according to the interface problem, while the mesh can be independent of the problem. As a result, meshes used by IFE methods consist of the following two types of elements:

1. **non-interface elements** which do not intersect the interface, and are equipped with

standard local FE basis functions;

2. **interface elements** which are cut by the interface, and are equipped with IFE basis functions satisfying interface jump conditions.

In general, the number of interface elements is much smaller than the number of non-interface elements, making the computational costs for the IFE method and the standard method comparable.

First, let us recall from [41] a description of the one-dimensional linear IFE spaces and shape functions developed in 2001 by Zhilin Li, who considered the model problem

$$\begin{aligned} &-(\beta(x)u'(x))' + q(x)u(x) = f(x), \qquad 0 \le x \le 1 \\ &u(0) = 0, \quad u(1) = 0. \end{aligned}$$

with

$$\alpha \in (0,1), \qquad \beta(x) = \begin{cases} \beta^-, & \text{for } x \in [0,\alpha), \\ \beta^+, & \text{for } x \in (\alpha,1]. \end{cases} \tag{1.4.1}$$

$$[u]_\alpha = [\beta u_x]_\alpha = 0. \tag{1.4.2}$$

In a uniform partition $0 = x_0 < x_1 < \cdots < x_n = 1$ of $[0,1]$ with step size h, assume that the interface point is inside the element $[x_j, x_{j+1}]$. Then, two piecewise linear basis functions at x_j and x_{j+1} were constructed as follows. The basis function ϕ_j can be written as

$$\phi_j(x) = \begin{cases} a_1\, x + b_1\ , & \text{for } \ x_{j-1} \le x < x_j \\ a_2\, x + b_2\ , & \text{for } \ x_j \le x < \alpha \\ a_3\, x + b_3\ , & \text{for } \ \alpha \le x < x_{j+1} \\ 0\ , & \textit{otherwise} \end{cases} \tag{1.4.3}$$

Enforcing the continuity at x_j, the two jump conditions (1.4.2) at α, and the three Lagrange nodal value conditions $\phi_j(x_j) = 1,\ \phi_j(x_{j-1}) = \phi_j(x_{j+1}) = 0$, the following expression for ϕ_j was obtained [41]:

$$\phi_j(x) = \begin{cases} \frac{x - x_{j-1}}{h}, & x_{j-1} \le x < x_j \\ \frac{x_j - x}{D} + 1, & x_j \le x < \alpha \\ \frac{(x_{j+1} - x)}{rD}, & \alpha \le x < x_{j+1} \\ 0, & \textit{otherwise}, \end{cases} \tag{1.4.4}$$

where $r = \frac{\beta^+}{\beta^-}$, and $D = h - \frac{\beta^+ - \beta^-}{\beta^+}\ (x_{j+1} - \alpha)$.

Similarly, the following ϕ_{j+1} was obtained [41]:

$$\phi_{j+1}(x) = \begin{cases} \frac{x - x_j}{D}, & x_j \leq x < \alpha \\ \frac{(x - x_{j+1})}{rD} + 1, & \alpha \leq x < x_{j+1} \\ \frac{x_{j+2} - x}{h}, & x_{j-1} \leq x_{j+1} < x_{j+2} \\ 0, & otherwise. \end{cases} \tag{1.4.5}$$

In this thesis, we extend IFE ideas to develop quadratic IFE spaces and methods that can be used to solve elliptic interface problems on either uniform or unstructured meshes. We recall the main features of these IFE methods:

i)- The interface is allowed to cut through edges of the mesh allowing the use of a static mesh, even for problems with moving interfaces. Furthermore, the IFE method may be used with any mesh, including a Cartesian mesh which may be highly desirable in many applications.

ii)- Physical jump conditions as well as eventual artificial jump conditions are enforced on the interface, and are extended locally to homogeneous jump conditions on every element in the mesh.

iii)- New finite element basis functions, satisfying the homogeneous jump conditions, are constructed on interface elements. These basis functions depend on the interface location and the enforced jump conditions [18, 35].

iv)- Optimal $\mathcal{O}(h^{p+1})$ convergence rates similar to those of the finite element method with a body-fitted mesh [13, 18, 27, 37, 41, 43, 44].

v)- Can be more efficient than conventional finite element method for some applications [24, 29].

1.5 Research Objectives

In our current research work, we propose quadratic IFE spaces combined with a penalized finite element formulation for solving two-dimensional interface problems. We present a general procedure for constructing optimal piecewise quadratic IFE spaces on triangular meshes and linear interfaces. Standard finite element shape functions are used on non-interface elements. On interface elements we construct piecewise quadratic shape functions

that satisfy the same interface jump conditions as the true solution, which have been used to construct linear and bilinear IFE shape functions [30, 43]. As observed in [17], extra constraints need to be carefully introduced in order to uniquely determine the higher-order IFE functions with optimal performance. Following the idea proposed in [2, 3], we require that each quadratic immersed shape function satisfies the continuity of a second-order elliptic operator. The proposed quadratic IFE spaces combined with a penalized finite element formulation are able to optimally represent the non-smooth behavior of the solution across the interface without requiring the mesh to be aligned with the material discontinuity.

1.6 Organization of the Thesis

This thesis is organized as follows. In Chapter 1, we introduce existing methods to solve interface problems and present a review of the IFE method to solve elliptic interface problems. In Chapter 2, we discuss the extended jump constraints and use them to construct quadratic IFE spaces, assuming a linear interface. In Chapter 3 we further show that such IFE spaces exist and determine their dimensions. In Chapter 4, we present numerical results to demonstrate the approximation capability of the proposed quadratic IFE spaces. In Chapter 5 we introduce an IFE method with interior penalty using the proposed quadratic IFE spaces and present numerical results showing the optimal convergence of the method. In Chapter 6, we discuss the extension of the quadratic IFE spaces to higher degree and present a general procedure for the construction of higher order IFE shape functions. In Chapter 7, we discuss the extension of our work to quadratic interfaces. Two approaches are proposed (isoparametric approach and an affine approach), then, numerical results are presented. Moreover, a procedure of handling general interfaces with quadratic IFE spaces is presented together with numerical results showing the optimality of the method. Finally, we conclude with a few remarks and discuss possible future work in Chapter 8.

Chapter 2

Quadratic Immersed Finite Element Spaces for Linear Interfaces

2.1 Introduction

In this chapter, we consider quadratic immersed finite elements for the model interface problem (1.1.1a) with a linear interface Γ defined by the equation

$$y = Ax + B. \tag{2.1.1}$$

We first discuss the jump conditions for constructing quadratic immersed finite element spaces that will be used later to solve the model interface problem. Next, we investigate the dimensions of these spaces and some of their properties.

2.2 Quadratic IFE Spaces

Let $\mathcal{P}_k$ denote the two-dimensional polynomial space in $\mathbb{R}^2$

$$\mathcal{P}_k = \{p, \mid p = \sum_{l=0}^{k} \sum_{i=0}^{l} c_i^l \xi^i \eta^{l-i}\}, \tag{2.2.1}$$

and let $\mathscr{T}_h$ be a regular triangular mesh of size h formed for the domain Ω, where h is the maximum diameter in the mesh, *i.e.*, $h = \max_{T \in \mathscr{T}_h} diam(T)$. The set of interface elements is denoted by $\mathscr{T}_h^i$. Similarly, edges that are cut by the interface are called interface edges; otherwise, they are referred to as non-interface edges. As illustrated in Figure 2.1, every interface element $T = \triangle V_1 V_2 V_3$ can be split as

$$T = T^+ \cup T^-, \text{ where } T^{\pm} = T \cap \Omega^{\pm}. \tag{2.2.2}$$

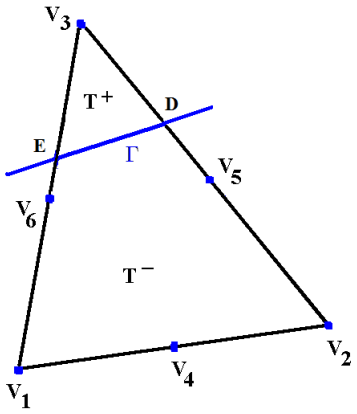

Figure 2.1: A physical interface element.

In the discussion from now on, we will use V_4, V_5 and V_6 to denote the midpoints of the edges of a triangular element $T = \triangle V_1V_2V_3$ such that

$$V_4 = \frac{1}{2}(V_1 + V_2),\ V_5 = \frac{1}{2}(V_2 + V_3),\ V_6 = \frac{1}{2}(V_3 + V_1).$$

We will also use D and E to denote the two intersection points of the interface Γ with the edges of the triangle T, as illustrated in Figure 2.1.

First, we introduce the following quadratic IFE spaces locally on an arbitrary interface element T

$$\mathcal{R}_1(T) = \{U,\ |\,U|_{T^\pm} \in \mathcal{P}_2,\ [U]_{T\cap\Gamma} = [\beta\frac{\partial U}{\partial \boldsymbol{n}}]_{T\cap\Gamma} = [\beta\Delta U]_{T\cap\Gamma} = 0\}, \tag{2.2.3a}$$

$$\mathcal{R}_2(T) = \{U,\ |\,U|_{T^\pm} \in \mathcal{P}_2,\ [U]_{T\cap\Gamma} = [\beta\frac{\partial U}{\partial \boldsymbol{n}}]_{T\cap\Gamma} = [\beta\frac{\partial^2 U}{\partial \boldsymbol{n}^2}]_{T\cap\Gamma} = 0\}. \tag{2.2.3b}$$

On an interface triangle T, let $\varphi(x, y)$ be a piecewise quadratic function written as

$$\varphi(x,y) = \begin{cases} \varphi^+(x,y)\ , & \text{on } T^+ \\ \varphi^-(x,y)\ , & \text{on } T^-, \end{cases} \tag{2.2.4}$$

where $\varphi^\pm(x, y) \in \mathcal{P}_2$. Thus, φ is determined by 12 independent parameters. A piecewise quadratic function $\varphi \in \mathcal{R}_1(T)$ satisfies

$$[\varphi]_\Gamma = 0, \tag{2.2.5a}$$

$$[\beta\ \boldsymbol{n}\cdot\nabla\varphi]_\Gamma = 0, \tag{2.2.5b}$$

$$[\beta\Delta\varphi]_\Gamma = 0. \tag{2.2.5c}$$

The two conditions (2.2.5a) and (2.2.5b) follow from the physical jump conditions (1.1.2a) and (1.1.2b), however the jump equation (2.2.5c) is suggested by the continuity of the right-hand side in (1.1.1a).

Guided by the work of the one-dimensional IFE methods in [2, 17] we can also construct piecewise quadratic functions that satisfy, instead of (2.2.5c), the following alternative condition for the second normal derivative

$$[\beta \frac{\partial^2 \varphi}{\partial \boldsymbol{n}^2}]_\Gamma = 0, \tag{2.2.6}$$

which leads to the piecewise quadratic polynomial space $\mathcal{R}_2(T)$.

Since interface jump conditions (2.2.5c) and (2.2.6) are not in the original interface problem, we call them the extended interface jump conditions. These extended jump conditions are needed to uniquely determine the quadratic IFE functions in $\mathcal{R}_i(T),\ i = 1, 2$, on each interface element $T \in \mathscr{T}_h$ and to guarantee the desired optimal approximation capability.

As it is often the case for finite element, the discussion is performed on a reference element, then every element of the mesh is mapped to the reference element. Hence, following this reasoning, we now describe how to use the reference triangle $\hat{T} = \triangle \hat{V}_1 \hat{V}_2 \hat{V}_3$ to define the functions in $\mathcal{R}_i(T),\ i = 1, 2$, where $\hat{V}_1 = (0, 0)^t$, $\hat{V}_2 = (1, 0)^t$ and $\hat{V}_3 = (0, 1)^t$. Without loss of generality, we assume that the vertices of each interface element $T = \triangle V_1 V_2 V_3 \in \mathscr{T}_h$ are arranged such that the vertex shared by its two interface edges is V_3. As usual, each element $T = \triangle V_1 V_2 V_3 \in \mathscr{T}_h$ with $V_i = (x_i, y_i)^t$ can be considered as the image of $\hat{T}$ through the affine mapping $F^{-1} : \hat{T} \to T$ defined by

$$F^{-1}(\hat{x}, \hat{y}) = V_1 + (V_2 - V_1)\hat{x} + (V_3 - V_1)\hat{y} = \begin{pmatrix} x \\ y \end{pmatrix}. \tag{2.2.7a}$$

Thus, the related mapping $F : T \to \hat{T}$ can be written as

$$F(x, y) = \mathbf{J} \begin{pmatrix} x \\ y \end{pmatrix} - \mathbf{J}\ V_1 = \begin{pmatrix} \hat{x} \\ \hat{y} \end{pmatrix}, \qquad \mathbf{J} = \begin{pmatrix} x_2 - x_1 & x_3 - x_1 \\ y_2 - y_1 & y_3 - y_1 \end{pmatrix}^{-1}. \tag{2.2.7b}$$

In order to construct the function φ on T, we construct a piecewise quadratic function $\hat{\varphi}$ on the reference element $\hat{T}$, then we use the mapping F defined in (2.2.7b) to obtain:

$$\varphi(x, y) = \hat{\varphi}(\hat{x}, \hat{y}) = \hat{\varphi}(F(x, y)). \tag{2.2.7c}$$

Since the interface is linear, it intersects two edges of every interface triangle creating 12 possible cases as shown in Figure 2.2. Furthermore, interface elements can be grouped into three types. Elements of Type I are shown in the first column with one vertex on one side of the interface and the remaining five nodes on the other side; elements of Type II are shown in the second column where two nodes are on one side and the remaining four nodes are on the other side, and elements of Type III are in the third column where the six nodes are

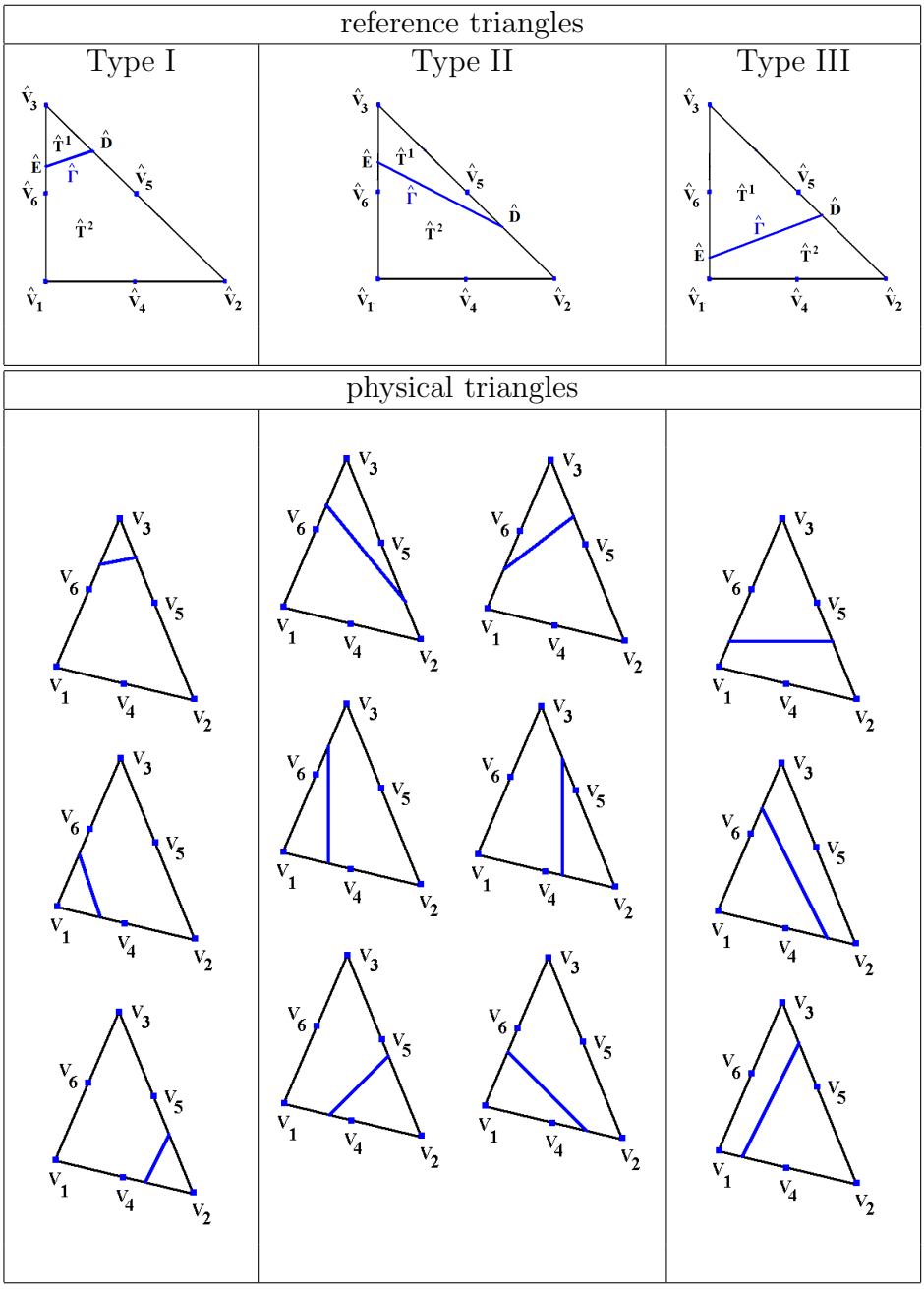

Figure 2.2: Interface elements of Type I and corresponding reference triangle (1^{st} column), elements of Type II and corresponding reference triangle (2^{nd} column), and elements of Type III and corresponding reference triangle (3^{rd} column).

equally distributed on both sides of the interface. All interface elements of a given type are mapped to the corresponding reference interface triangle shown in the first row of Figure 2.2.

For each type of reference triangles, we refer to the sub-domain of $\hat{T}$ containing vertex $\hat{V}_3$ as $\hat{T}^1$ and let $\hat{T}^2 = \hat{T} \setminus \hat{T}^1$.

The discontinuous material coefficient $\hat{\beta}$ on the reference interface triangle $\hat{T}$ is written as

$$\hat{\beta} = \begin{cases} \hat{\beta}^1, & \text{on } \hat{T}^1, \\ \hat{\beta}^2, & \text{on } \hat{T}^2, \end{cases} \tag{2.2.8}$$

where $\hat{\beta}^i = \beta^{\pm}$ if $\hat{T}^i = F(T^{\pm})$.

In order to construct piecewise quadratic functions on the reference triangles, we need to map the jump conditions to the reference triangles. First, we translate the interface jump conditions (1.1.2) to the piecewise quadratic function $\hat{\varphi}$ on $\hat{\Gamma} = F(\Gamma \cap T)$:

$$[\hat{\varphi}]_{\hat{\Gamma}} = 0, \tag{2.2.9a}$$

$$[\hat{\beta}\ \hat{\boldsymbol{n}} \cdot \hat{\nabla}\hat{\varphi}]_{\hat{\Gamma}} = 0, \tag{2.2.9b}$$

where $\hat{\boldsymbol{n}} = \mathbf{J}\boldsymbol{n}$ and $\hat{\nabla}\hat{\varphi} = (\partial_{\hat{x}}\hat{\varphi}, \partial_{\hat{y}}\hat{\varphi})^t$.

In fact, by chain rule, we have

$$\nabla\varphi(x, y) = \mathbf{J}^t \nabla\hat{\varphi}(\hat{x}, \hat{y}), \tag{2.2.10}$$

then

$$\boldsymbol{n} \cdot \nabla\varphi = \boldsymbol{n}^t \nabla\varphi = \boldsymbol{n}^t \mathbf{J}^t \nabla\hat{\varphi} = (\mathbf{J}\boldsymbol{n})^t \nabla\hat{\varphi}. \tag{2.2.11}$$

Hence

$$\boldsymbol{n} \cdot \nabla\varphi = \hat{\boldsymbol{n}} \cdot \hat{\nabla}\hat{\varphi}\ , \tag{2.2.12}$$

with

$$\hat{\boldsymbol{n}} = \mathbf{J}\boldsymbol{n}. \tag{2.2.13}$$

We notice that, in general, $\hat{\boldsymbol{n}}$ is not normal to $\hat{\Gamma} = F(\Gamma \cap T)$.

Next, we discuss how to translate the extended interface jump conditions (2.2.5c) and (2.2.6) to the reference element $\hat{T}$. Since $\nabla\varphi = \mathbf{J}^t\hat{\nabla}\hat{\varphi}$, we obtain

$$\Delta\varphi = \nabla \cdot \nabla\varphi = (\mathbf{J}^t\hat{\nabla}) \cdot (\mathbf{J}^t\hat{\nabla})\hat{\varphi}. \tag{2.2.14}$$

Then, on $\hat{T}$, the extended jump condition (2.2.5c) becomes

$$[\hat{\beta}(\mathbf{J}^t\hat{\nabla}) \cdot (\mathbf{J}^t\hat{\nabla})\hat{\varphi}]|_{\hat{\Gamma}} = 0. \tag{2.2.15}$$

We further note that the second normal derivative can be written as

$$\frac{\partial^2 \varphi}{\partial \boldsymbol{n}^2} = (\boldsymbol{n} \cdot \nabla)\,(\boldsymbol{n} \cdot \nabla)\,\varphi. \tag{2.2.16}$$

Thus, (2.2.6) leads to the following condition on $\hat{T}$:

$$[\hat{\beta}(\hat{\boldsymbol{n}} \cdot \hat{\nabla})(\hat{\boldsymbol{n}} \cdot \hat{\nabla})\hat{\varphi}]|_{\hat{\Gamma}} = [\hat{\beta}\frac{\partial^2 \hat{\varphi}}{\partial \hat{\boldsymbol{n}}^2}]_{\hat{\Gamma}} = 0. \tag{2.2.17}$$

Hence, on a reference element $\hat{T}$, we need to construct the following function space:

$$\hat{\mathcal{R}}_1(\hat{T}) = \{\hat{U} \in \hat{\mathcal{P}}_2(\hat{T}), |\ [\hat{U}]_{\hat{\Gamma}} = 0, [\hat{\beta}\frac{\partial \hat{U}}{\partial \hat{\boldsymbol{n}}}]_{\hat{\Gamma}} = 0, [\hat{\beta}(\mathbf{J}^t\nabla).(\mathbf{J}^t\nabla)\hat{U}]_{\hat{\Gamma}} = 0\}, \tag{2.2.18}$$

and

$$\hat{\mathcal{R}}_2(\hat{T}) = \{\hat{U} \in \hat{\mathcal{P}}_2(\hat{T}), |\ [\hat{U}]_{\hat{\Gamma}} = 0, [\hat{\beta}\frac{\partial \hat{U}}{\partial \hat{\boldsymbol{n}}}]_{\hat{\Gamma}} = 0, [\hat{\beta}\frac{\partial^2 \hat{U}}{\partial \hat{\boldsymbol{n}}^2}]_{\hat{\Gamma}} = 0\}, \tag{2.2.19}$$

where

$$\hat{\mathcal{P}}_2(\hat{T}) = \{\hat{p} \mid \hat{p}|_{\hat{T}^i} \in \mathcal{P}_2,\ i = 1, 2\}. \tag{2.2.20}$$

2.3 Properties of Quadratic IFE Spaces

We will now discuss the properties of the IFE spaces $\hat{\mathcal{R}}_k(\hat{T}),\ k = 1, 2$, determine their dimensions, and show how to construct their bases. In the discussion below, we note that any polynomial $\hat{\pi} \in \hat{\mathcal{P}}_2$ can be written as

$$\hat{\pi}(\hat{x}, \hat{y}) = \begin{cases} \sum_{i=1}^{6} c_i \hat{L}_i(\hat{x}, \hat{y}), & if\ (\hat{x}, \hat{y}) \in \hat{T}^1, \\ \sum_{i=1}^{6} c_{i+6} \hat{L}_i(\hat{x}, \hat{y}), & if\ (\hat{x}, \hat{y}) \in \hat{T}^2, \end{cases} \tag{2.3.1}$$

where $\hat{L}_j,\ j = 1, \ldots, 6$, are the standard Lagrange quadratic shape functions on $\hat{T}$ associated with nodes $\hat{V}_i, i = 1, 2, \cdots, 6$.

Let T be an arbitrary smooth interface triangle and let $\hat{T} = F(T)$ be the associated reference triangle cut by the interface $\hat{\Gamma} : \hat{y} = a\hat{x} + b$, as illustrated in Figure 2.2. We recall that F is the standard affine mapping given in (2.2.7) and that the unit normal vector $\boldsymbol{n}$ to the physical interface Γ is mapped to $\hat{\boldsymbol{n}} = \mathbf{J}\boldsymbol{n}$ which, in general, is not normal to $\hat{\Gamma}$.

In the next lemma we show that $\hat{\boldsymbol{n}} = (\hat{n}_x, \hat{n}_y)^t$ cannot be parallel to $\hat{\Gamma}$ when F is an invertible affine mapping.

Lemma 2.3.1. *Let T be an arbitrary interface element cut by a linear interface Γ. If F is the standard affine mapping from T to to the reference element $\hat{T}$, then*

$$a\hat{n}_x - \hat{n}_y \neq 0. \tag{2.3.2}$$

Proof. First, the unit normal vector to the interface $\hat{\Gamma}$ defined by the equation $\hat{y} = a\hat{x} + b$ can be written as

$$\hat{\mathbf{N}} = \frac{1}{\sqrt{1+a^2}}(a, -1)^t$$

with inner product

$$\hat{\boldsymbol{n}} \cdot \hat{\mathbf{N}} = \frac{a\hat{n}_x - \hat{n}_y}{\sqrt{1+a^2}}. \tag{2.3.3}$$

If $\hat{\boldsymbol{n}}$ is parallel to $\hat{\Gamma}$, then the inner product $\hat{\boldsymbol{n}} \cdot \hat{\mathbf{N}} = 0$. Hence the line containing Γ and all lines perpendicular to it are mapped onto the line containing $\hat{\Gamma}$. This means F maps $\mathbb{R}^2$ onto the line containing $\hat{\Gamma}$. This violates the one-to-one property of F and proves the lemma. □

2.3.1 Properties of $\hat{\mathcal{R}}_2(\hat{T})$

Here we prove that $\hat{\mathcal{R}}_2(\hat{T})$ is a non trivial linear space with dimension six.

Lemma 2.3.2. *Let $\hat{\pi} \in \hat{\mathcal{P}}_2(\hat{T})$ be defined by (2.3.1) with coefficients $\mathbf{c} = (c_1, c_2, \ldots, c_{12})^t \in \mathbb{R}^{12}$ and $P_1 = \hat{E}$, $P_2 = \hat{D}$ and $P_3 = (\hat{D} + \hat{E})/2$ as illustrated in Figure 2.2. Then*

$$\hat{\pi} \in \hat{\mathcal{R}}_2(\hat{T}) \quad \text{if and only if} \quad \mathbf{c} \in N(\mathbf{A}), \tag{2.3.4}$$

where $N(\mathbf{A})$ is the null space of the 6×12 rectangular matrix $\mathbf{A}$ defined by

$$\mathbf{A} = \begin{pmatrix} \mathbf{A}_0 & -\mathbf{A}_0 \\ \mathbf{A}_1 & -\hat{r}\mathbf{A}_1 \\ \mathbf{A}_2 & -\hat{r}\mathbf{A}_2 \end{pmatrix} \tag{2.3.5a}$$

with $\hat{r} = \frac{\hat{\beta}^2}{\hat{\beta}^1}$ and

$$\mathbf{A}_0 = \begin{pmatrix} \hat{L}_1(P_1) & \hat{L}_2(P_1) & \hat{L}_3(P_1) & \hat{L}_4(P_1) & \hat{L}_5(P_1) & \hat{L}_6(P_1) \\ \hat{L}_1(P_2) & \hat{L}_2(P_2) & \hat{L}_3(P_2) & \hat{L}_4(P_2) & \hat{L}_5(P_2) & \hat{L}_6(P_2) \\ \hat{L}_1(P_3) & \hat{L}_2(P_3) & \hat{L}_3(P_3) & \hat{L}_4(P_3) & \hat{L}_5(P_3) & \hat{L}_6(P_3) \end{pmatrix}, \tag{2.3.5b}$$

$$\mathbf{A}_1 = \begin{pmatrix} \frac{\partial \hat{L}_1}{\partial \hat{\boldsymbol{n}}}(P_1) & \frac{\partial \hat{L}_2}{\partial \hat{\boldsymbol{n}}}(P_1) & \frac{\partial \hat{L}_3}{\partial \hat{\boldsymbol{n}}}(P_1) & \frac{\partial \hat{L}_4}{\partial \hat{\boldsymbol{n}}}(P_1) & \frac{\partial \hat{L}_5}{\partial \hat{\boldsymbol{n}}}(P_1) & \frac{\partial \hat{L}_6}{\partial \hat{\boldsymbol{n}}}(P_1) \\ \\ \frac{\partial \hat{L}_1}{\partial \hat{\boldsymbol{n}}}(P_2) & \frac{\partial \hat{L}_2}{\partial \hat{\boldsymbol{n}}}(P_2) & \frac{\partial \hat{L}_3}{\partial \hat{\boldsymbol{n}}}(P_2) & \frac{\partial \hat{L}_4}{\partial \hat{\boldsymbol{n}}}(P_2) & \frac{\partial \hat{L}_5}{\partial \hat{\boldsymbol{n}}}(P_2) & \frac{\partial \hat{L}_6}{\partial \hat{\boldsymbol{n}}}(P_2) \end{pmatrix}, \tag{2.3.5c}$$

$$\mathbf{A}_2 = \begin{pmatrix} \frac{\partial^2 \hat{L}_1}{\partial \hat{\boldsymbol{n}}^2}(P_1) & \frac{\partial^2 \hat{L}_2}{\partial \hat{\boldsymbol{n}}^2}(P_1) & \frac{\partial^2 \hat{L}_3}{\partial \hat{\boldsymbol{n}}^2}(P_1) & \frac{\partial^2 \hat{L}_4}{\partial \hat{\boldsymbol{n}}^2}(P_1) & \frac{\partial^2 \hat{L}_5}{\partial \hat{\boldsymbol{n}}^2}(P_1) & \frac{\partial^2 \hat{L}_6}{\partial \hat{\boldsymbol{n}}^2}(P_1) \end{pmatrix}. \tag{2.3.5d}$$

Proof. We first show that the condition is necessary. Assume that $\hat{\pi} \in \hat{\mathcal{R}}_2(\hat{T})$, then

$$[\hat{p}]_{\hat{\Gamma}} = 0, \tag{2.3.6a}$$

$$[\hat{\beta}\frac{\partial \hat{p}}{\partial \hat{\boldsymbol{n}}}]_{\hat{\Gamma}} = 0, \tag{2.3.6b}$$

$$[\hat{\beta}\frac{\partial^2 \hat{p}}{\partial \hat{\boldsymbol{n}}^2}]_{\hat{\Gamma}} = 0. \tag{2.3.6c}$$

The jump condition (2.3.6a) is satisfied by enforcing $[\hat{\pi}](P_i) = 0,\ i = 1, 2, 3$, which can be written as

$$\sum_{j=1}^{6} c_j \hat{L}_j(P_i) - \sum_{j=1}^{6} c_{j+6} \hat{L}_j(P_i) = 0,\ i = 1, \ldots, 3,$$

or

$$\left(\mathbf{A}_0, -\mathbf{A}_0\right) \mathbf{c} = 0. \tag{2.3.7}$$

Similarly, the jump condition (2.3.6b) is satisfied by enforcing $[\hat{\beta}\frac{\partial \hat{\pi}}{\partial \hat{\boldsymbol{n}}}](P_i) = 0,\ i = 1, 2$, which can be written as

$$\sum_{j=1}^{6} c_j \frac{\partial \hat{L}_j}{\partial \hat{\boldsymbol{n}}}(P_i) - \hat{r} \sum_{j=1}^{6} c_{j+6} \frac{\partial \hat{L}_j}{\partial \hat{\boldsymbol{n}}}(P_i) = 0,\ i = 1, 2,$$

or

$$\left(\mathbf{A}_1, -\hat{r}\mathbf{A}_1\right) \mathbf{c} = 0. \tag{2.3.8}$$

The third condition (2.3.6c) is satisfied by enforcing $[\hat{\beta}\frac{\partial^2 \hat{\pi}}{\partial \hat{\boldsymbol{n}}^2}](P_1) = 0$, which can be written as

$$\sum_{j=1}^{6} c_j \frac{\partial^2 \hat{L}_j}{\partial \hat{\boldsymbol{n}}^2}(P_1) - \hat{r} \sum_{j=1}^{6} c_{j+6} \frac{\partial^2 \hat{L}_j}{\partial \hat{\boldsymbol{n}}^2}(P_1) = 0.$$

This is equivalent

$$\left(\mathbf{A}_2, -\hat{r}\mathbf{A}_2\right) \mathbf{c} = 0. \tag{2.3.9}$$

Combining (2.3.7), (2.3.8) and (2.3.9) yields $\mathbf{A}\mathbf{c} = 0$.

Reversing the arguments above can show that the condition is also sufficient. □

In the next lemma we show that the nullity of $\mathbf{A}$ defined in (2.3.5a) is equal to 6.

Lemma 2.3.3. *Under the assumptions of Lemma 2.3.2, the nullity of the matrix* $\mathbf{A}$ *defined in (2.3.5a) is equal to 6.*

Proof. Let us consider the 6×6 submatrix of $\mathbf{A}$

$$\mathbf{A}_c = \begin{pmatrix} \mathbf{A}_0 \\ \mathbf{A}_1 \\ \mathbf{A}_2 \end{pmatrix}. \tag{2.3.10}$$

A direct calculation gives its determinant as follows:

$$det(\mathbf{A}_c) = \frac{32}{(1+a)^4}(1-b)^4(a\hat{n}_x - \hat{n}_y)^4. \tag{2.3.11}$$

By the fact $b \neq 1$ and Lemma 2.3.1 we can show that $\mathbf{A}_c$ is invertible, hence, the rank of $\mathbf{A}$ is equal to 6. Then, we finish the proof by applying the the rank-nullity theorem:

$$rank(\mathbf{A}) + nullity(\mathbf{A}) = 12. \tag{2.3.12}$$

□

In the next lemma we establish the existence of an isomorphism between $\hat{\mathcal{R}}_2(\hat{T})$ and $N(\mathbf{A})$.

Theorem 2.3.1. *If* $\mathbf{A}$ *is the matrix defined by (2.3.5a), then the following statements hold*

1. *There exist an isomorphism* Ψ *from the quadratic IFE space* $\hat{\mathcal{R}}_2(\hat{T})$ *to the null space* $N(\mathbf{A})$.
2. *The dimension of* $\hat{\mathcal{R}}_2(\hat{T})$ *is equal to 6.*
3. *A set of vectors* $\{\mathbf{b}_i,\ i = 1, \ldots, 6\} \subset \mathbb{R}^{12}$ *form a basis of* $N(\mathbf{A})$ *if and only if* $\{\Psi^{-1}(\mathbf{b}_i),\ i = 1, \ldots, 6\}$ *form a basis of* $\hat{\mathcal{R}}_2(\hat{T})$.

Proof. For each $\hat{\pi} \in \hat{\mathcal{R}}_2(\hat{T})$ we can represent it in the form given in (2.3.1) and define the mapping $\Psi : \hat{\mathcal{R}}_2(\hat{T}) \to N(\mathbf{A})$ by

$$\Psi(\hat{\pi}) = (c_1, c_2, \ldots, c_{12})^t. \tag{2.3.13}$$

From the definition of Ψ, one can easily show that Ψ is linear, *i.e.*,

$$\Psi(\lambda \boldsymbol{a} + \mu \mathbf{b}) = \lambda \Psi(\boldsymbol{a}) + \mu \Psi(\mathbf{b}),\ \forall\ \boldsymbol{a}, \mathbf{b} \in \mathbb{R}^{12} \text{ and } \lambda, \mu \in \mathbb{R}. \tag{2.3.14}$$

Establishing that Ψ is injective is straight froward by setting $\Psi(\hat{\pi}) = \Psi(\hat{\zeta})$ we show that $\hat{\pi} = \hat{\zeta}$.

Next, we show that Ψ is surjective. In fact, for any $\mathbf{c} = (c_1, \ldots, c_{12})^t \in N(\mathbf{A})$, we can use Lemma 2.3.2 to form a piecewise quadratic polynomial $\hat{\pi} \in \hat{\mathcal{R}}_2(\hat{T})$ of the form (2.3.1). Thus, for all $\mathbf{c} \in N(\mathbf{A})$ there exists $\hat{\pi} \in \hat{\mathcal{R}}_2(\hat{T})$ such that $\Psi(\hat{\pi}) = \mathbf{b}$.

Hence, the mapping Ψ is an isomorphism between $\hat{\mathcal{R}}_2(\hat{T})$ and $N(\mathbf{A})$. Using Lemma 2.3.3 yields $dim(\hat{\mathcal{R}}_2(\hat{T})) = dim(N(\mathbf{A})) = 6$.

Since Ψ is an isomorphism, each basis of $N(\mathbf{A})$ is mapped into a basis of $\hat{\mathcal{R}}_2(\hat{T})$ which completes the proof. □

2.3.2 Properties of $\hat{\mathcal{R}}_1(\hat{T})$

In this section we will show that $\hat{\mathcal{R}}_1(\hat{T})$ has properties similar to those for $\hat{\mathcal{R}}_2(\hat{T})$.

Lemma 2.3.4. *Let $\hat{\pi} \in \hat{\mathcal{P}}_2(\hat{T})$ be defined by (2.3.1) with coefficients $\mathbf{c} = (c_1, c_2, \ldots, c_{12})^t \in \mathbb{R}^{12}$ and $P_1 = \hat{E}$, $P_2 = \hat{D}$ and $P_3 = (\hat{D} + \hat{E})/2$ as illustrated in Figure 2.2. Then*

$$\hat{\pi} \in \hat{\mathcal{R}}_1(\hat{T}) \quad \text{if and only if} \quad \mathbf{c} \in N(\mathbf{A}). \tag{2.3.15}$$

where the matrix $\mathbf{A}$ is defined by

$$\mathbf{A} = \begin{pmatrix} \mathbf{A}_0 & -\mathbf{A}_0 \\ \mathbf{A}_1 & -\hat{r}\mathbf{A}_1 \\ \mathbf{A}_2 & -\hat{r}\mathbf{A}_2 \end{pmatrix} \tag{2.3.16a}$$

with $\hat{r} = \frac{\hat{\beta}^2}{\hat{\beta}^1}$ and matrices $\mathbf{A}_0$ and $\mathbf{A}_1$, respectively, given by (2.3.5b) and (2.3.5c), and the matrix $\mathbf{A}_2$ is

$$\mathbf{A}_2 = \begin{pmatrix} a_1 & a_2 & \ldots & a_6 \end{pmatrix}, \quad a_j = (\mathbf{J}^t\nabla).(\mathbf{J}^t\nabla)\hat{L}_j(P_1),\ 1 \le j \le 6. \tag{2.3.16b}$$

Proof. The proof follows from the same arguments as those for Lemma 2.3.2:

If $\hat{\pi} \in \hat{\mathcal{R}}_1(\hat{T})$, then (2.3.6a), (2.3.6b) hold together with

$$[\hat{\beta}(\mathbf{J}^t\nabla).(\mathbf{J}^t\nabla)\hat{\pi}]_{\hat{\Gamma}} = 0. \tag{2.3.17}$$

Enforcing (2.3.6a) at $P_i,\ i = 1, 2, 3$, yields

$$\begin{pmatrix} \mathbf{A}_1 & -\mathbf{A}_1 \end{pmatrix} \mathbf{c} = 0, \tag{2.3.18}$$

while enforcing (2.3.6b) at P_1 and P_2 yields

$$\begin{pmatrix} \mathbf{A}_2 & -\hat{r}\mathbf{A}_2 \end{pmatrix} \mathbf{c} = 0. \tag{2.3.19}$$

Enforcing (2.3.17) at P_1 yields

$$\sum_{j=1}^{6} c_j(\mathbf{J}^t\nabla).(\mathbf{J}^t\nabla)\hat{L}_j(P_1) - \hat{r}\sum_{j=1}^{6} c_{j+6}(\mathbf{J}^t\nabla).(\mathbf{J}^t\nabla)\hat{L}_j(P_1) = 0, \tag{2.3.20}$$

which leads to

$$\begin{pmatrix} \mathbf{A}_3 & -\hat{r}\mathbf{A}_3 \end{pmatrix} \mathbf{c} = 0. \tag{2.3.21}$$

Combining (2.3.18), (2.3.19) and (2.3.21) we obtain $\mathbf{A}\mathbf{c} = 0$, which yields $\mathbf{c} \in N(\mathbf{A})$.

Reversing the arguments above can show that the condition is also sufficient. □

Lemma 2.3.5. *Under the assumptions of Lemma 2.3.4 the nullity of the matrix* $\mathbf{A}$ *defined by (2.3.16a) is equal to 6.*

Proof. Let the Jacobian of the affine mapping F be

$$\mathbf{J} = \begin{pmatrix} j_{11} & j_{12} \\ j_{21} & j_{22} \end{pmatrix}, \tag{2.3.22}$$

and, as before, we use the first six columns of $\mathbf{A}$ to define the 6×6 matrix $\mathbf{A}_c$. A direct computation leads to

$$\begin{aligned} det(\mathbf{A}_c) &= 16(1+a)(1-b)^4(a\hat{n}_x - \hat{n}_y)^2 \left((aj_{11} - j_{21})^2 + (aj_{12} - j_{22})^2\right) \\ &= 16(1+a)(1-b)^4(1+a^2)^2(\hat{\boldsymbol{n}} \cdot \hat{\mathbf{N}})^2 \, ||\mathbf{J}^t \hat{\mathbf{N}}||^2, \end{aligned} \tag{2.3.23}$$

where $||\cdot||$ denotes the Euclidian norm.

On all reference interface triangles $b \neq 1$ and $a > -1$. From Lemma 2.3.1 $\hat{\boldsymbol{n}} \cdot \hat{\mathbf{N}} \neq 0$ and since $\mathbf{J}$ is invertible $\mathbf{J}^t \hat{\mathbf{N}} \neq 0$. Thus, $det(\mathbf{A}_c) \neq 0$ and the rank of $\mathbf{A}$ is equal to 6. Finally, the result of this lemma follows from rank-nullity theorem. □

Theorem 2.3.2. *If the matrix* $\mathbf{A}$ *is defined by (2.3.16a), then the following statement hold*

1. *There exists an isomorphism* Ψ *from the piecewise quadratic space* $\hat{\mathcal{R}}_1(\hat{T})$ *to the null space* $N(\mathbf{A})$.
2. *The dimension of* $\hat{\mathcal{R}}_1(\hat{T})$ *is equal to 6.*
3. *The set of vectors* $\{\mathbf{b}_1, \ldots, \mathbf{b}_6\} \subset \mathbb{R}^{12}$ *form a basis of* $N(\mathbf{A})$ *if and only if* $\{\Psi^{-1}(\mathbf{b}_i),\ i = 1, \ldots, 6\}$ *form a basis of* $\hat{\mathcal{R}}_1(\hat{T})$.

Proof. The proof is the same as for Theorem 2.3.1 and is omitted. □

In conclusion, both quadratic IFE spaces $\hat{\mathcal{R}}_k(\hat{T})$, $k = 1, 2$, have dimension 6 and their elements can be represented as linear combinations of the piecewise quadratic shape functions obtained from a basis of the corresponding null space $N(\mathbf{A})$.

More conventional shape functions such as Lagrange and hierarchical shape functions may be constructed for these interface spaces. More details such as their existence and related algorithms for constructing them will be discussed in the forthcoming Chapters, where different bases for these spaces are developed and used with an interior penalty finite element method to solve elliptic interface problems.

2.4 The Global IFE Spaces

Let us first define the following IFE spaces over the whole domain:

$$\mathcal{W}_h^k = \{U \mid \ U|_T \in \mathcal{P}_2, \ for\ T \in \mathscr{T}_h \setminus \mathscr{T}_h^i \ \text{ and } \ U|_T \in \mathcal{R}_k(T), \ for\ T \in \mathscr{T}_h^i\}, \ k = 1, 2. \tag{2.4.1}$$

Then, to define the global quadratic IFE spaces over the whole simulation domain Ω, we let $\mathcal{N}_h$ be the set of nodes for the usual Lagrange quadratic finite element space defined on the mesh $\mathscr{T}_h$. As usual, for each node $\mathbf{v}_i \in \mathcal{N}_h$, we define a piecewise quadratic IFE basis function ψ_i^k over Ω as follows

$$\psi_i^k|_T \in \begin{cases} \mathcal{R}_k(T) \ \forall \ T \in \mathscr{T}_h^i \\ \\ \mathcal{P}_2 \ \forall \ T \in \mathscr{T}_h \setminus \mathscr{T}_h^i \end{cases}, \qquad \psi_i^k(\mathbf{v}_j) = \delta_{ij} \ \forall \ \mathbf{v}_j \in \mathcal{N}_h.$$

We note that the global quadratic IFE basis functions may be discontinuous across interface edges as discussed in Chapter 3. More precisely, the global IFE basis functions are continuous across non-interface edges while, in general, on interface edges they are continuous only at the two edge vertices and midpoint.

Without loss of generality, we assume that $\mathcal{N}_h$ contains N nodes among which the first N_I nodes are inside Ω while the rest of them are on the boundary of Ω. Finally, we define the global quadratic IFE spaces over the domain Ω as

$$\mathcal{S}_h^k = span\{\psi_j^k, \ j = 1, \ldots, N\}, \ k = 1, 2, \tag{2.4.2}$$

and define the space $\mathcal{S}_{h,0}^k$ as the span of all global quadratic IFE basis functions associated with interior nodes:

$$\mathcal{S}_{h,0}^k = span\{\psi_j^k, \ j = 1, \ldots, N_I\}, \ k = 1, 2. \tag{2.4.3}$$

Finally, we define the subsets of the spaces $\mathcal{S}_h^k, \ k = 1, 2$, consisting of functions interpolating the essential boundary condition g

$$\mathcal{S}_{h,E}^k = \left\{ U \in \mathcal{S}_h^k \,|\, U = \sum_{i=1}^{N_I} c_i \psi_i^k + \sum_{i=N_I+1}^{N} g(\mathbf{v}_i)\psi_i^k \right\}. \tag{2.4.4}$$

2.5 Conclusions

In this Chapter, we presented two IFE spaces $\mathcal{S}_h^k, \ k = 1, 2$, that can be used with a penalized finite element formulation or a with a discontinuous finite element formulation to solve interface problems. Assuming the interface is a straight line, we justified the use of the two sets of jump conditions to form IFE spaces locally on each interface element. We also investigated the dimensions of these IFE spaces and proved that the dimension of each space

is equal to 6. In Chapter 4, we will discuss the approximation capabilities of the two IFE spaces $\mathcal{S}_h^k,\ k = 1, 2$, and in Chapter 5, we will compute immersed finite element solutions of the problem (1.1.1a) using these spaces.

Chapter 3

Quadratic Immersed Finite Element Shape Functions

3.1 Introduction

In this chapter, we discuss quadratic immersed finite elements shape functions. We construct two basis for each of the two quadratic IFE spaces defined in Chapter 2, a basis of Lagrange type and a hierarchical basis. We establish a proof of the existence for Lagrange quadratic IFE shape functions on the space $\mathcal{S}_h^2$. Inspired by hierarchical standard finite element shape functions [61], we construct hierarchical IFE shape functions with a correction term to enforce the interface jump conditions. Then, we prove the linear independence of these hierarchical IFE shape functions.

3.2 Lagrange Quadratic IFE Shape Functions

3.2.1 Formulations of Lagrange IFE Shape Functions

Let $\hat{T}$ be a reference interface element of any of the three types described in Figure 2.2. In this section, we consider a basis for $\hat{\mathcal{R}}_k(\hat{T}),\ k = 1, 2$, consisting of the IFE shape functions of Lagrange type $\hat{\varphi}_i \in \hat{\mathcal{R}}_k(\hat{T}),\ i = 1, \ldots, 6,\ k = 1, 2$, satisfying the nodal constraints

$$\hat{\varphi}_i(\hat{V}_j) = \delta_{ij},\ j = 1, \ldots, 6, \tag{3.2.1}$$

On the reference element $\hat{T}$, each shape function can be written in a way such that it satisfies the corresponding jump constrains. We consider the change of coordinate from (x, y) to interface coordinate (ξ, η), where ξ is the coordinate in the the direction of the interface Γ, and η is the coordinate in the normal direction to $\Gamma : y = Ax + B$. Hence, (ξ, η) can be

defined as

$$\begin{cases} \xi = & x + Ay + C, \\ \eta = & \frac{1}{\sqrt{1+A^2}}\,(y - Ax - B), \end{cases} \tag{3.2.2}$$

where C is an arbitrary constant which represents the ξ coordinate of the Cartesian origin $(0, 0)$. In our work we have chosen $C = -AB$ in order to make the interface reference origin be the point with Cartesian coordinates $(0, B)$.

The coordinates (ξ, η) are mapped to $\hat{T}$ as $(\hat{\xi}, \hat{\eta})$, illustrated in Figure 3.1, and defined by

$$\begin{cases} \hat{\xi} = & \hat{n}_{\hat{x}}\hat{y} - \hat{n}_{\hat{y}}\hat{x} + c, \\ \hat{\eta} = & \frac{1}{\sqrt{1+a^2}}\,(\hat{y} - a\hat{x} - b), \end{cases} \tag{3.2.3}$$

where $\hat{n}_{\hat{x}}$ and $\hat{n}_{\hat{y}}$ are respectively the $\hat{x}$ and $\hat{y}$ coordinates of the vector $\hat{\boldsymbol{n}} = \mathbf{J}\boldsymbol{n}$, which is the mapping of the normal $\boldsymbol{n}$ to Γ, and where c is an arbitrary constant. In our work, we have chosen $c = -\hat{nxb}$ to get reference illustrated in the Figure 3.1. As previously mentioned, $\hat{\boldsymbol{n}} = \mathbf{J}\boldsymbol{n}$ is not orthogonal to $\hat{\Gamma}$ in general.

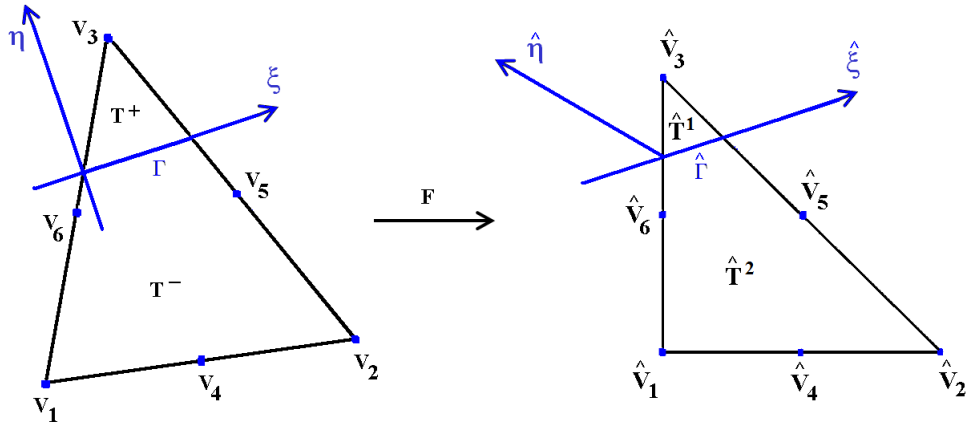

Figure 3.1: The interface coordinates systems (ξ, η) on T and $(\hat{\xi}, \hat{\eta})$ on $\hat{T} = F(T)$.

The coordinates $(\hat{\xi}, \hat{\eta})$ defined in (3.2.3) are well defined, as discussed in the Lemma 2.3.1. We note also that according to the definition in (3.2.3) of $\hat{\eta}$, we have

$$\frac{\partial}{\partial \hat{\boldsymbol{n}}} = \frac{\partial}{\partial \hat{\eta}}.$$

To construct a function $\varphi \in \hat{\mathcal{R}}_2(\hat{T})$, we use the interface coordinates on the reference element $(\hat{\xi}, \hat{\eta})$ defined above. Following the idea proposed by Adjerid and Lin [3] to write one-dimensional lagrange IFE shape functions, given the expression of $\hat{\varphi}$ on one side of $\hat{T}$, we write the expression on the other side of $\hat{T}$, such that $\hat{\varphi}$ satisfies the interface jump conditions

stated in (2.2.9).
For instance, given the expression $\hat{\varphi}^1(\hat{\xi},\hat{\eta})$ of $\hat{\varphi}$ on $\hat{T}^1$, we write $\hat{\varphi}$ on $\hat{T}^2$ as

$$\hat{\varphi}^2(\hat{\xi},\hat{\eta}) = \hat{\varphi}^1(\xi,0) + \frac{\hat{\beta}^1}{\hat{\beta}^2}\left(\hat{\varphi}^1(\hat{\xi},\hat{\eta}) - \hat{\varphi}^1(\hat{\xi},0)\right). \tag{3.2.4}$$

If we denote by $\hat{p}(\hat{x},\hat{y})$ the oblique projection on $\hat{\Gamma}$ in $\hat{\eta}$ direction of the point $(\hat{x},\hat{y})$ (i.e. $\hat{p}(\hat{x},\hat{y})$ is the mapping of the point $(\hat{\xi},0)$ to the Cartesian reference), then expression (3.2.4) becomes

$$\hat{\varphi}^2(\hat{x},\hat{y}) = \frac{\hat{\beta}^1}{\hat{\beta}^2}\hat{\varphi}^1(\hat{x},\hat{y}) + \left(1 - \frac{\hat{\beta}^1}{\hat{\beta}^2}\right)\tilde{\varphi}_i^1(\hat{x},\hat{y}), \tag{3.2.5}$$

with $\tilde{\varphi}_i^1(\hat{x},\hat{y}) = \hat{\varphi}_i^1(\hat{p}(\hat{x},\hat{y}))$.

Now, we define the following sets of indices: $\mathscr{I}_1$ the set of the indices of all the vertices of $\hat{T}$ that are on $\hat{T}^1$; and $\mathscr{I}_2$ the set of the indices of all the vertices of $\hat{T}$ that are on $\hat{T}^2$. Hence, considering the 3 types of reference elements shown in the first row of Figure 2.2, if $\hat{T}$ is of type I then $\mathscr{I}_1 = \{3\}$ and $\mathscr{I}_2 = \{1,2,4,5,6\}$; if $\hat{T}$ is of type II then $\mathscr{I}_1 = \{3,5\}$ and $\mathscr{I}_2 = \{1,2,4,6\}$; and if $\hat{T}$ is of type III then $\mathscr{I}_1 = \{3,5,6\}$ and $\mathscr{I}_2 = \{1,2,4\}$.

Now, we write the shape functions $\hat{\varphi}_i,\ i = 1,\ldots,6$, in terms of the standard quadratic shape functions of Lagrange type $\hat{L}_j(\hat{x},\hat{y}),\ j = 1,\ldots,6$, on the reference element, and such that each function $\hat{\varphi}_i$ satisfies the Lagrange nodal value conditions (3.2.1) on one side of $\hat{T}$, then we construct the expression of $\hat{\varphi}_i$ on the other side using equation (3.2.5).

Let us first define $\hat{r} = \frac{\hat{\beta}^1}{\hat{\beta}^2}$, then we write $\hat{\varphi}_i \in \hat{\mathcal{R}}_2(\hat{T}),\ i = 1,\ldots,6$, as follows.

For $i \in \mathscr{I}_1$, we write the shape function $\hat{\varphi}_i$ as

$$\hat{\varphi}_i(\hat{x},\hat{y}) = \begin{cases} \hat{\varphi}_i^2(\hat{x},\hat{y}) = \displaystyle\sum_{j\in\mathscr{I}_1} c_j\hat{L}_j(\hat{x},\hat{y})\ , & (\hat{x},\hat{y}) \in \hat{T}^2, \\ \hat{\varphi}_i^1(\hat{x},\hat{y}) = \frac{1}{\hat{r}}\ \hat{\varphi}_i^2(\hat{x},\hat{y}) + (1-\frac{1}{\hat{r}})\ \hat{\varphi}_i^2(\hat{p}(\hat{x},\hat{y}))\ , & (\hat{x},\hat{y}) \in \hat{T}^1. \end{cases} \tag{3.2.6}$$

For $i \in \mathscr{I}_2$, we write the shape function $\hat{\varphi}_i$ as

$$\hat{\varphi}_i(\hat{x},\hat{y}) = \begin{cases} \hat{\varphi}_i^1(\hat{x},\hat{y}) = \displaystyle\sum_{j\in\mathscr{I}_2} c_j\hat{L}_j(\hat{x},\hat{y})\ , & (\hat{x},\hat{y}) \in \hat{T}^1, \\ \\ \hat{\varphi}_i^2(\hat{x},\hat{y}) = \hat{r}\ \hat{\varphi}_i^1(\hat{x},\hat{y}) + (1-\hat{r})\ \hat{\varphi}_i^1(\hat{p}(\hat{x},\hat{y}))\ , & (\hat{x},\hat{y}) \in \hat{T}^2. \end{cases} \tag{3.2.7}$$

The remaining unknowns are determined by imposing the Lagrange nodal value conditions (3.2.1). Later in this section, we will discuss the existence and uniqueness of $\hat{\varphi}_i,\ i = 1,\ldots,6$.

Similarly for the quadratic IFE space $\hat{\mathcal{R}}_1(\hat{T})$, given the expression of a function $\hat{\varphi}$ on one side of $\hat{T}$, we can write the expression of $\hat{\varphi}$ on the other side of $\hat{T}$, such that it satisfies the interface jump conditions stated in (2.2.18). Then, given the expression $\hat{\varphi}^1(\hat{\xi},\hat{\eta})$ of $\hat{\varphi}$ on $\hat{T}^1$, we write $\hat{\varphi}$ on $\hat{T}^2$ as

$$\hat{\varphi}^2(\hat{x},\hat{y}) = \hat{r}\hat{\varphi}^1(\hat{x},\hat{y}) + (1-\hat{r})\tilde{\varphi}^1(\hat{x},\hat{y}) - \frac{(\hat{y}-a\hat{x}-b)^2}{2(1+a^2)}\,(1-\hat{r})(\mathbf{J}^t\hat{\nabla})\cdot(\mathbf{J}^t\hat{\nabla})\tilde{\varphi}^1(\hat{x},\hat{y})\ . \tag{3.2.8}$$

with $\tilde{\varphi}_i^1(\hat{x},\hat{y}) = \hat{\varphi}_i^1(\hat{p}(\hat{x},\hat{y}))$, and $\hat{p}(\hat{x},\hat{y})$ being the oblique projection on $\hat{\Gamma}$ in $\hat{\eta}$ direction.

Hence, the shape functions $\hat{\varphi}_i,\ i=1,\dots,6$, in $\hat{\mathcal{R}}_1(\hat{T})$ will be written as follows.

For $i \in \mathscr{I}_1$, we write the shape function $\hat{\varphi}_i$ as

$$\hat{\varphi}_i(\hat{x},\hat{y}) = \begin{cases} \hat{\varphi}_i^2(\hat{x},\hat{y}) = \sum\limits_{j\in\mathscr{I}_1} c_j\hat{L}_j(\hat{x},\hat{y}), & (\hat{x},\hat{y})\in\hat{T}^2, \\ \hat{\varphi}_i^1(\hat{x},\hat{y}) = \hat{r}\ \hat{\varphi}_i^2(\hat{x},\hat{y}) + (1-\hat{r})\tilde{\varphi}_i^2(\hat{x},\hat{y}) \\ \qquad\qquad - \ (1-\hat{r})\ \frac{(\hat{y}-a\hat{x}-b)^2}{2(1+a^2)}\hat{\Delta}\tilde{\varphi}_i^2(\hat{x},\hat{y}), & (\hat{x},\hat{y})\in\hat{T}^1, \end{cases}$$

and for $i \in \mathscr{I}_2$, we write the shape function $\hat{\varphi}_i$ as

$$\hat{\varphi}_i(\hat{x},\hat{y}) = \begin{cases} \hat{\varphi}_i^1(\hat{x},\hat{y}) = \sum\limits_{j\in\mathscr{I}_2} c_j\hat{L}_j(\hat{x},\hat{y}), & (\hat{x},\hat{y})\in\hat{T}^1, \\ \hat{\varphi}_i^2(\hat{x},\hat{y}) = \frac{1}{\hat{r}}\ \hat{\varphi}_i^1(\hat{x},\hat{y}) + (1-\frac{1}{\hat{r}})\tilde{\varphi}_i^1(\hat{x},\hat{y}) \\ \qquad\qquad - \ (1-\frac{1}{\hat{r}})\ \frac{(\hat{y}-a\hat{x}-b)^2}{2(1+a^2)}\hat{\Delta}\tilde{\varphi}_i^1(\hat{x},\hat{y}), & (\hat{x},\hat{y})\in\hat{T}^2, \end{cases}$$

with $\hat{r} = \frac{\hat{\beta}^1}{\hat{\beta}^2}$ and $\hat{\Delta} = (\mathbf{J}^t\hat{\nabla})\cdot(\mathbf{J}^t\hat{\nabla})$; and we recall that $\tilde{\varphi}_i^j = \varphi_i^j \circ \hat{p},\ j=1,2$.

In this dissertation, we establish the existence and uniqueness of the IFE shape functions on meshes consisting of right angle triangles where every interface triangle can be mapped to one of seven reference elements shown in Figure 3.2 such that $\hat{\boldsymbol{n}}$ is normal to $\hat{\Gamma}$. The interface Γ defined by $y = Ax + B$ is mapped to $\hat{\Gamma}$ defined by $\hat{y} = a\hat{x} + b$. The proof is presented only for the space $\mathcal{R}_2(T)$. The existence of Lagrange IFE shape functions for the space $\mathcal{R}_1(T)$ is the subject of future work, and should follow the same ideas as of the proof for the existence of Lagrange IFE shape functions for the space $\mathcal{R}_2(T)$, however it will include more computation and will be the subject of future investigation.

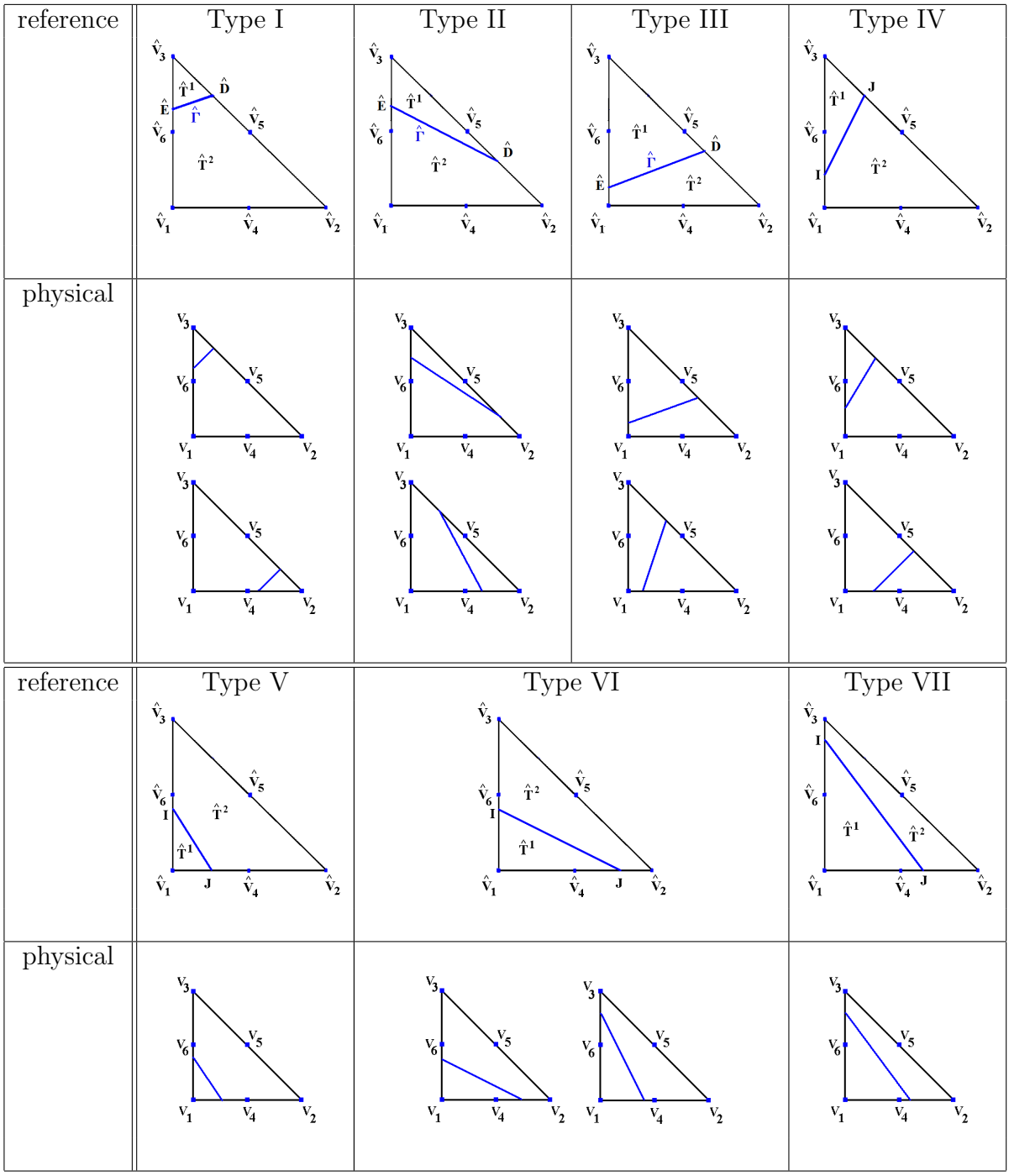

Figure 3.2: Reference triangles and associated right angle physical triangles.

3.2.2 Existence of Lagrange Basis for $\mathcal{R}_2(T)$

Before stating and proving the existence and uniqueness of our quadratic IFE shape functions we start by establishing several preliminary lemmas for each of the seven types shown in Figure 3.2. First, let us consider the projection $\hat{p}: \mathbb{R}^2 \to \hat{\Gamma}$ defined by

$$\hat{p}(\hat{x},\hat{y}) = \begin{pmatrix} 1 & a \\ -a & 1 \end{pmatrix}^{-1} \begin{pmatrix} 1 & a \\ 0 & 0 \end{pmatrix} \begin{pmatrix} \hat{x} \\ \hat{y} \end{pmatrix} + \begin{pmatrix} 1 & a \\ -a & 1 \end{pmatrix}^{-1} \begin{pmatrix} 0 \\ b \end{pmatrix}. \tag{3.2.9}$$

We can easily verify that $\hat{p}$ is an orthogonal projection from the plane $\mathbb{R}^2$ onto the line $\hat{\Gamma}$.

Lemma 3.2.1. *Let $\hat{L}_i$ be the standard Lagrange quadratic shape functions on the reference triangle of type I shown in Figure 3.2 and $\hat{p}$ denote the orthogonal projection defined by (3.2.9). Then, the eigenvalues of the matrix*

$$\mathbf{M}_2 = \begin{pmatrix} \hat{L}_1(\hat{p}(\hat{V}_1)) & \hat{L}_2(\hat{p}(\hat{V}_1)) & \hat{L}_4(\hat{p}(\hat{V}_1)) & \hat{L}_5(\hat{p}(\hat{V}_1)) & \hat{L}_6(\hat{p}(\hat{V}_1)) \\ \hat{L}_1(\hat{p}(\hat{V}_2)) & \hat{L}_2(\hat{p}(\hat{V}_2)) & \hat{L}_4(\hat{p}(\hat{V}_2)) & \hat{L}_5(\hat{p}(\hat{V}_2)) & \hat{L}_6(\hat{p}(\hat{V}_2)) \\ \hat{L}_1(\hat{p}(\hat{V}_4)) & \hat{L}_2(\hat{p}(\hat{V}_4)) & \hat{L}_4(\hat{p}(\hat{V}_4)) & \hat{L}_5(\hat{p}(\hat{V}_4)) & \hat{L}_6(\hat{p}(\hat{V}_4)) \\ \hat{L}_1(\hat{p}(\hat{V}_5)) & \hat{L}_2(\hat{p}(\hat{V}_5)) & \hat{L}_4(\hat{p}(\hat{V}_5)) & \hat{L}_5(\hat{p}(\hat{V}_5)) & \hat{L}_6(\hat{p}(\hat{V}_5)) \\ \hat{L}_1(\hat{p}(\hat{V}_6)) & \hat{L}_2(\hat{p}(\hat{V}_6)) & \hat{L}_4(\hat{p}(\hat{V}_6)) & \hat{L}_5(\hat{p}(\hat{V}_6)) & \hat{L}_6(\hat{p}(\hat{V}_6)) \end{pmatrix} \tag{3.2.10}$$

are in $[0,1]$, and $M_1 = \hat{L}_3(\hat{p}(\hat{V}_3))$ is in $[0,1]$, as well.

Proof. First we observe that for elements of Type I, cut by the interface $\hat{\Gamma}: \hat{y} = a\hat{x} + b$, a and b are in the domain

$$D = \{(a,b) \mid \frac{1}{2} \le b < 1, \quad 1 - 2b \le a \}, \tag{3.2.11}$$

as illustrated in Figure 3.3.

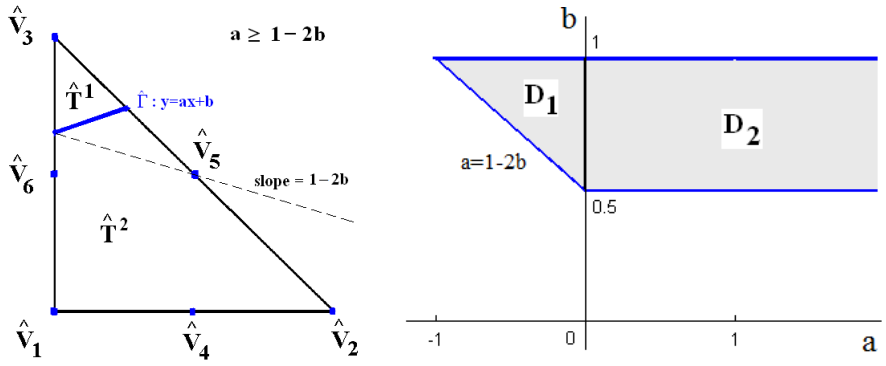

Figure 3.3: Interface elements of Type I (left) and associated domain for a and b (right).

A direct computation reveals that the five eigenvalues of $\mathbf{M}_2$ are $\{1, 1, 0, 0, \lambda\}$, with

$$\lambda = (1-b)\frac{(1+3a^2+2b)}{(1+a^2)^2}. \tag{3.2.12}$$

Next, we show that $\lambda \in [0, 1]$.

First, since $(1-b) > 0$, it is clear that $\lambda > 0$.

Now, to show that $\lambda \leq 1$, we define the function

$$v(a,b) = \lambda = (1-b)\frac{(1+3a^2+2b)}{(1+a^2)^2} \quad > \ 0\ , \qquad (a,b) \in D. \tag{3.2.13}$$

Note that $D = D_1 \cup D_2$, where

$$D_1 = \{(a,b) \mid \frac{1}{2} \leq b < 1,\ 1-2b < a \leq 0\}, \quad \text{and} \quad D_2 = \{(a,b) \mid \frac{1}{2} \leq b < 1,\ 0 < a\},$$

as illustrated in Figure 3.3.

A direct computation of the partial derivatives of v gives

$$\frac{\partial v}{\partial a}(a,b) = 2a(1-b)\frac{(1-4b-3a^2)}{(a^2+1)^3}, \tag{3.2.14}$$

and

$$\frac{\partial v}{\partial b}(a,b) = \frac{(1-4b-3a^2)}{(a^2+1)^2}. \tag{3.2.15}$$

Since $\frac{1}{2} \leq b < 1$, then $1-4b < 0$ which implies $(1-4b-3a^2) < 0$.

Thus $\frac{\partial v}{\partial b}(a,b)$ does not change sign, which implies that v has no critical point in $D_1 \cup D_2$.

Now, we will show that v does not exceed 1 over D_1, as well as over D_2.

The maximum of $v(a,b)$ over D_1 is reached on the boundary. A computation of the values of $v(a,b)$ on the boundary of D_1 gives

$$\begin{aligned}
v(a,1) &= 0, && (with \quad -1 \leq a \leq 0)\\
v(0,b) &= (1-b)(1+2b) = 1+b-2b^2, && (with \quad \frac{1}{2} \leq b < 1)\\
v(1-2b,b) &= (1-b)\frac{(6b^2-5b+2)}{2(2b^2-2b+1)^2} = w(b). && (with \quad \frac{1}{2} \leq b < 1)
\end{aligned}$$

Since $\frac{1}{2} \leq b$ (*i.e.* $1-2b < 0$), we have

$$v(0,b) = 1+b-2b^2 = 1+b(1-2b) \leq 1. \tag{3.2.16}$$

In order to prove that $w(b) \leq 1$, we compute

$$w'(b) = \frac{(2b^2 - 4b + 1)\,(6b^2 - 4b + 1)}{2\,(2b^2 - 2b + 1)^3}, \tag{3.2.17}$$

and note that for $\frac{1}{2} \leq b < 1$

$$6b^2 - 4b + 1 > 0\ , \quad 2b^2 - 2b + 1 > 0 \ \text{ and } \ 2b^2 - 4b + 1 < 0.$$

Thus $w'(b) < 0$, and $w(b)$ is decreasing over $[\frac{1}{2}, 1]$, which leads to $v(a, b) \leq 1$, on ∂D_1. Hence

$$w(b) \leq w(\frac{1}{2}) = 1.$$

i.e.

$$v(a, b) \leq 1, \quad \forall (a, b) \in D_1.$$

Over D_2, we can observe that $\frac{\partial v}{\partial a}(a, b) < 0$, which means that $v(a, b)$ is decreasing with respect to a. Then the maximum of $v(a, b)$ over D_2 is achieved on the boundary $a = 0$. Since we have already shown that $v(0, b) \leq 1$, then we conclude that

$$v(a, b) \leq 1, \quad \forall (a, b) \in D_1 \cup D_2.$$

Hence,

$$\lambda \in [0, 1] \quad \text{and} \quad \sigma(\mathbf{M}_2) \subset [0, 1].$$

A direct computation reveals that

$$\hat{L}_3(\hat{p}(\hat{V}_3)) = \frac{(a^2 + b)(a^2 - 1 + 2b)}{(1 + a^2)^2}. \tag{3.2.18}$$

We remark that $\hat{L}_3(\hat{p}(\hat{V}_3)) = 1 - \lambda$, where λ is the eigenvalue of $\mathbf{M}_2$ defined by (3.2.12).

Since $\lambda \in [0, 1]$, then $M_1 = \hat{L}_3(\hat{p}(\hat{V}_3)) \ \in [0, 1]$. □

Next, we will state and prove a result for interface elements of Type II.

Lemma 3.2.2. *Let $\hat{L}_i$ be the standard Lagrange quadratic shape functions on the reference element of type II shown in Figure 3.2, and $\hat{p}$ be the orthogonal projection on $\hat{\Gamma}$. Then the eigenvalues of the matrices*

$$\mathbf{M}_2 = \begin{pmatrix} \hat{L}_1(\hat{p}(\hat{V}_1)) & \hat{L}_2(\hat{p}(\hat{V}_1)) & \hat{L}_4(\hat{p}(\hat{V}_1)) & \hat{L}_6(\hat{p}(\hat{V}_1)) \\ \hat{L}_1(\hat{p}(\hat{V}_2)) & \hat{L}_2(\hat{p}(\hat{V}_2)) & \hat{L}_4(\hat{p}(\hat{V}_2)) & \hat{L}_6(\hat{p}(\hat{V}_2)) \\ \hat{L}_1(\hat{p}(\hat{V}_4)) & \hat{L}_2(\hat{p}(\hat{V}_4)) & \hat{L}_4(\hat{p}(\hat{V}_4)) & \hat{L}_6(\hat{p}(\hat{V}_4)) \\ \hat{L}_1(\hat{p}(\hat{V}_6)) & \hat{L}_2(\hat{p}(\hat{V}_6)) & \hat{L}_4(\hat{p}(\hat{V}_6)) & \hat{L}_6(\hat{p}(\hat{V}_6)) \end{pmatrix} \tag{3.2.19}$$

and

$$\mathbf{M}_1 = \begin{pmatrix} \hat{L}_3(\hat{p}(\hat{V}_3)) & \hat{L}_5(\hat{p}(\hat{V}_3)) \\ \hat{L}_3(\hat{p}(\hat{V}_5)) & \hat{L}_5(\hat{p}(\hat{V}_5)) \end{pmatrix} \tag{3.2.20}$$

are in $[0,1]$.

Proof. First we observe that for elements of Type II, cut by the interface $\hat{\Gamma} : \hat{y} = a\hat{x} + b$, a and b are in the domain

$$D = \{\ (a,b)\ |\ \frac{1}{2} \le b < 1\ ,\quad -b \le a \le 1-2b\ \}, \tag{3.2.21}$$

as illustrated in Figure 3.4. Thus, for $(a,b) \in D$, we have the inequalities

$$(1-b) > 0\ ,\quad (1-2b-a) \ge 0\ ,\quad a < 0\ ,\quad (2b-1) \ge 0\ ,\quad (a+b) \ge 0\ . \tag{3.2.22}$$

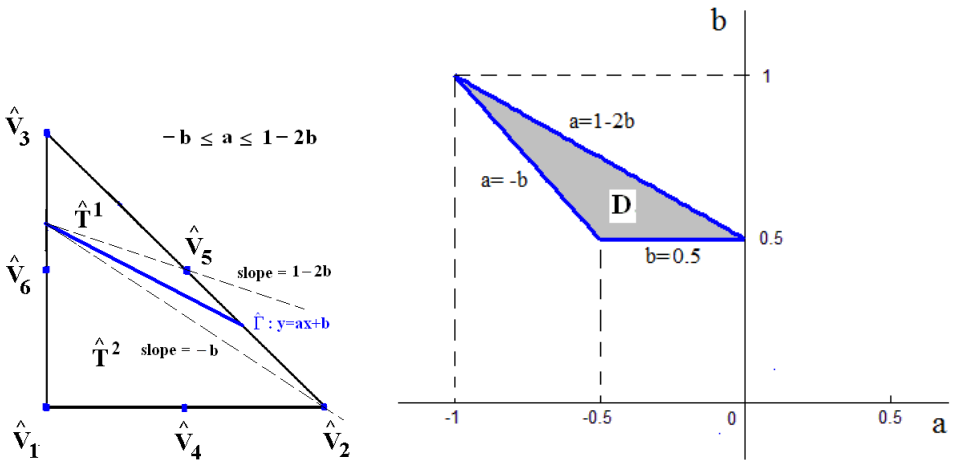

Figure 3.4: Interface elements of Type II (left) and associated domain for a and b (right).

A direct computation shows that the four eigenvalues of $\mathbf{M}_2$ are $\{\lambda_1, \lambda_2, 1, 0\}$, where λ_1 and λ_2 are roots of the quadratic equation

$$\begin{aligned} f(\lambda) \;&=\; \lambda^2 - \frac{2 + a^4 + a^3(2b-1) + a^2(3-b) - a(1+2b-4b^2) - b - 2b^2}{(1+a^2)^2}\,\lambda \\ &+\; \frac{(1-b)(1-2b-a)(1+a^2(2-a)+2b(1-a))}{(1+a^2)^3} = 0. \end{aligned} \tag{3.2.23}$$

Next, we will show that $f(0) \ge 0$, $f(b) < 0$ and $f(1) \ge 0$. In this case, since f is a continuous function, the quadratic equation $f(\lambda) = 0$ has a root in the interval $[0, b)$; and another root in the interval $(b, 1]$, which implies that both roots λ_1 and λ_2 are in the interval $[0, 1]$.

First, we observe that

$$f(0) = \frac{(1-b)(1-2b-a)(1+a^2(2-a)+2b(1-a))}{(1+a^2)^3}$$

From inequalities (3.2.22), we obtain

$$(1+a^2(2-a)+2b(1-a)) > 0,$$

and conclude that $f(0) \geq 0$.

Also, we observe that

$$f(1) = \frac{(a^2+b)(1-a)(2b-1)(a+2b+a^2)}{(1+a^2)^3}$$

From inequalities (3.2.22), we obtain

$$(a+2b+a^2) = (a+b)+b+a^2 > 0,$$

and conclude that $f(1) \geq 0$.

Moreover, we observe that we can write

$$\begin{aligned} f(b) = -\frac{(1-b)}{(1+a^2)^3} \qquad & (a^4b(1+a)^2 - 2a^3b(1-a-2b) \\ & +2a^2b(1-b) + (a+b)(a^2+2b-a^4)). \end{aligned}$$

From (3.2.21) and (3.2.22), we have $-1 < a \leq 0$, which implies $a^4 < 1$, combined with $2b \geq 1$ yields $(2b-a^4) \geq 0$, which, with the inequalities (3.2.22), imply $f(b) < 0$.

Hence, we conclude that $\sigma(\mathbf{M}_2) \subset [0,1]$.

A direct computation shows that the two eigenvalues of $\mathbf{M}_1$ are roots of the quadratic equation

$$\begin{aligned} g(\lambda) &= \lambda^2 - \frac{a^4+a^3+a^2+a+b+2ab+a^2b-2a^3b+2b^2-4ab^2}{(1+a^2)^2}\,\lambda \\ &+ \frac{(1-a)(a^2+b)(2b-1)(a+a^2+2b)}{(1+a^2)^3} = 0, \end{aligned}$$

where we note that for all λ, $g(\lambda) = f(1-\lambda)$, with f given in (3.2.23).

Thus, the roots of the equation $g(\lambda) = 0$ are equal to $1-\lambda_1$ and $1-\lambda_2$.

i.e. $\sigma(\mathbf{M}_1) \subset [0,1]$.

□

Lemma 3.2.3. *Let $\hat{L}_i$ be the standard Lagrange quadratic shape functions on the reference element of type III shown in Figure 3.2 and $\hat{p}$ be the orthogonal projection on $\hat{\Gamma}$. Then the eigenvalues of the matrices*

$$\mathbf{M}_2 = \begin{pmatrix} \hat{L}_1(\hat{p}(\hat{V}_1)) & \hat{L}_2(\hat{p}(\hat{V}_1)) & \hat{L}_4(\hat{p}(\hat{V}_1)) \\ \hat{L}_1(\hat{p}(\hat{V}_2)) & \hat{L}_2(\hat{p}(\hat{V}_2)) & \hat{L}_4(\hat{p}(\hat{V}_2)) \\ \hat{L}_1(\hat{p}(\hat{V}_4)) & \hat{L}_2(\hat{p}(\hat{V}_4)) & \hat{L}_4(\hat{p}(\hat{V}_4)) \end{pmatrix} \tag{3.2.24}$$

$$\mathbf{M}_1 = \begin{pmatrix} \hat{L}_3(\hat{p}(\hat{V}_3)) & \hat{L}_5(\hat{p}(\hat{V}_3)) & \hat{L}_6(\hat{p}(\hat{V}_3)) \\ \hat{L}_3(\hat{p}(\hat{V}_5)) & \hat{L}_5(\hat{p}(\hat{V}_5)) & \hat{L}_6(\hat{p}(\hat{V}_6)) \\ \hat{L}_3(\hat{p}(\hat{V}_6)) & \hat{L}_5(\hat{p}(\hat{V}_6)) & \hat{L}_6(\hat{p}(\hat{V}_6)) \end{pmatrix} \tag{3.2.25}$$

are in $[0,1]$.

Proof. First we observe that for elements of Type III, cut by the interface $\hat{\Gamma} : \hat{y} = a\hat{x} + b$, a and b are in the domain

$$D = \{\ (a,b)\ |\ \ 0 \le b < \frac{1}{2}\ ,\quad -b \le a \le 1-2b\ \}, \tag{3.2.26}$$

as illustrated in Figure 3.5. Thus, for $(a,b) \in D$, we have the inequalities

$$(1-b) > 0\ ,\quad (1-2b-a) \ge 0\ ,\quad (1-2b) > 0\ ,\quad (a+b) \ge 0\ ,\quad -\frac{1}{2} \le a \le 1\ . \tag{3.2.27}$$

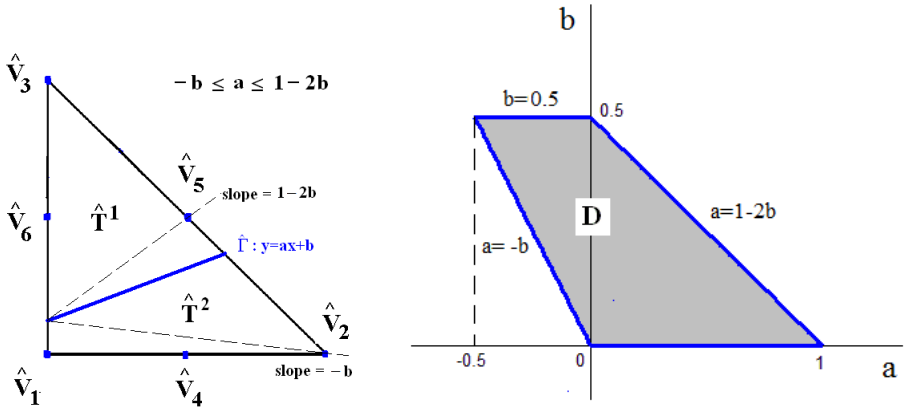

Figure 3.5: Interface elements of Type III (left) and associated domain for a and b (right).

A direct computation reveals that the three eigenvalues of $\mathbf{M}_2$ are $\{\lambda_1, \lambda_2, 1\}$, where λ_1 and λ_2 are roots of the quadratic equation

$$\begin{aligned} f(\lambda) &= \lambda^2 - \frac{(2 - a + a^2(1-b) - 5b + 2b^2)}{(1+a^2)^2}\,\lambda \\ &+ \frac{(1-b)(1-2b)(1-a-2b)}{(1+a^2)^3} = 0. \end{aligned} \tag{3.2.28}$$

Next, we will show that $f(0) \geq 0$ and $f(1) \geq 0$, and that for some $\alpha \in (0,1)$, we have $f(\alpha) < 0$. In this case, since f is continuous, we conclude that the quadratic equation $f(\lambda) = 0$ has one root in the interval $[0, \alpha)$; and another root in the interval $(\alpha, 1]$, which implies that both roots λ_1 and λ_2 are in the interval $[0, 1]$.

First, we observe that

$$f(0) = \frac{(1-b)(1-2b)(1-a-2b)}{(1+a^2)^3},$$

and

$$f(1) = \frac{2(1-2b-a)b^2 + (a+b)(a^2+3b) + b^2(1-b^2) + (a^2-b^2)^2 + a^6 + a^4 + a^4b + 5a^2b}{(1+a^2)^3},$$

From (3.2.26) and inequalities (3.2.27), we conclude that $f(0) \geq 0$, $f(1) \geq 0$.

Now, let us consider

$$\alpha = \frac{(1-a-2b) + (1-2b)(1-b)}{2(1+a^2)^2} \; > \; 0, \tag{3.2.29}$$

where we used (3.2.27).

Moreover, since $(a+b) \geq 0$, we can write

$$(1-2b-a) = (1-b) - (a+b) \; \leq \; (1-b),$$

which leads to

$$(1-a-2b) + (1-2b)(1-b) \; \leq \; (1-b) + (1-2b)(1-b) = 2(1-b)^2.$$

Hence,

$$\alpha = \frac{(1-a-2b) + (1-2b)(1-b)}{2(1+a^2)^2} \leq \frac{2(1-b)^2}{2(1+a^2)^2} = \left(\frac{1-b}{1+a^2}\right)^2 \; \leq \; 1. \tag{3.2.30}$$

We used the fact $\quad 0 < (1-b) \leq (1+a^2), \quad (\;\; (1-b) \leq 1 \;\; \text{and} \;\; 1 \leq (1+a^2) \;\;).$

We further note that the only case where $\alpha = 1$ is when $a = b = 0$, which corresponds to a non-interface element.

Hence, we proved that $\alpha \in (0,1)$.

We have

$$f(\alpha) = -\frac{4a^2b(1-a-2b)(1-b) + 2a^2(1-2b)(1-b)(a+b) + (a-b+2b^2)^2}{4(1+a^2)^4}.$$

From (3.2.26) and inequalities (3.2.27), we conclude that $f(0) > 0$, $f(1) > 0$ and $f(\alpha) < 0$, which yields $\sigma(\mathbf{M}_2) \subset [0,1]$.

A direct computation reveals that the three eigenvalues of $\mathbf{M}_1$ are 0 and the two roots of the quadratic equation

$$\begin{aligned} g(\lambda) &= \lambda^2 - \frac{a + 2a^4 + (5-2b)b + a^2(3+b)}{(1+a^2)^2}\,\lambda \\ &+ \frac{a^6 + 2a^4 + a^3 + 3ab + 6a^2b + a^4b + 6b^2 - 2ab^2 - 2a^2b^2 - 4b^3}{(1+a^2)^3} = 0. \end{aligned}$$

We note that for all $\lambda \in [0,1]$, $g(\lambda) = f(1-\lambda)$, where f is given in (3.2.28).

Since the roots of $f(\lambda) = 0$ are in $[0,1]$, Then $1-\lambda_1$ and $1-\lambda_2$ are the roots of the equation $g(\lambda) = 0$.

i.e. $\sigma(\mathbf{M}_1) \subset [0,1]$.

□

Lemma 3.2.4. *Let $\hat{L}_i$ be the standard Lagrange quadratic shape functions on the reference element of type IV shown in Figure 3.2 and $\hat{p}$ be the orthogonal projection on $\hat{\Gamma}$. Then the eigenvalues of the matrices*

$$\mathbf{M}_2 = \begin{pmatrix} \hat{L}_1(\hat{p}(\hat{V}_1)) & \hat{L}_2(\hat{p}(\hat{V}_1)) & \hat{L}_4(\hat{p}(\hat{V}_1)) & \hat{L}_5(\hat{p}(\hat{V}_1)) \\ \hat{L}_1(\hat{p}(\hat{V}_2)) & \hat{L}_2(\hat{p}(\hat{V}_2)) & \hat{L}_4(\hat{p}(\hat{V}_2)) & \hat{L}_5(\hat{p}(\hat{V}_2)) \\ \hat{L}_1(\hat{p}(\hat{V}_4)) & \hat{L}_2(\hat{p}(\hat{V}_4)) & \hat{L}_4(\hat{p}(\hat{V}_4)) & \hat{L}_5(\hat{p}(\hat{V}_4)) \\ \hat{L}_1(\hat{p}(\hat{V}_5)) & \hat{L}_2(\hat{p}(\hat{V}_5)) & \hat{L}_4(\hat{p}(\hat{V}_5)) & \hat{L}_5(\hat{p}(\hat{V}_5)) \end{pmatrix} \tag{3.2.31}$$

$$\mathbf{M}_1 = \begin{pmatrix} \hat{L}_3(\hat{p}(\hat{V}_3)) & \hat{L}_6(\hat{p}(\hat{V}_3)) \\ \hat{L}_3(\hat{p}(\hat{V}_6)) & \hat{L}_6(\hat{p}(\hat{V}_6)) \end{pmatrix} \tag{3.2.32}$$

are in $[0,1]$.

Proof. First we observe that for elements of Type IV, cut by the interface $\hat{\Gamma} : \hat{y} = a\hat{x} + b$, a and b are in the domain

$$D = \{\ (a,b) \mid\ 0 \le b < \frac{1}{2}\ ,\quad a \ge 1 - 2b\ \}, \tag{3.2.33}$$

as illustrated in Figure 3.6. Thus, for $(a,b) \in D$, we have the inequalities

$$(1-b) > 0\ ,\quad (a - 1 + 2b) \ge 0\ ,\quad (1-2b) > 0 \quad \text{and} \quad a > 0. \tag{3.2.34}$$

A direct computation reveals that the four eigenvalues of $\mathbf{M}_2$ are $\{\lambda_1, \lambda_2, 1, 0\}$, where λ_1 and λ_2 are roots of the quadratic equation

$$\begin{aligned} f(\lambda) &= \lambda^2 - \frac{2 + a^3(1-2b) + 3a^2(1-b) - 3b + 2a(1-2b)b + 2b^2}{(1+a^2)^2}\,\lambda \\ &+ \frac{(1-b)(1-2b)(1 + 2a^2 + a^3 + 2ab)}{(1+a^2)^3} = 0. \end{aligned} \tag{3.2.35}$$

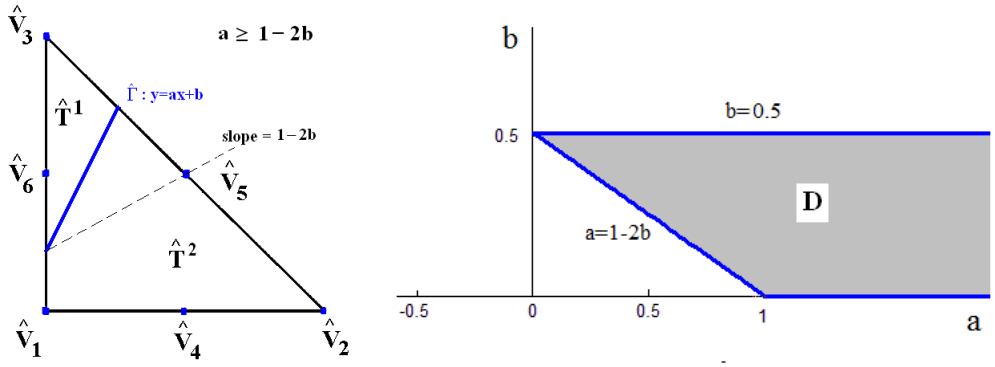

Figure 3.6: Interface elements of Type IV (left) and associated domain for a and b (right).

Next, we will show that $f(0) \geq 0$ and $f(1) \geq 0$, and that for some $\alpha \in (0,1)$, we have $f(\alpha) < 0$. In this case, since f is continuous, we conclude that the quadratic equation $f(\lambda) = 0$ has one root in the interval $[0, \alpha)$ and another root in the interval $(\alpha, 1]$, which implies that both roots λ_1 and λ_2 are in the interval $[0, 1]$.

First, we observe that

$$\begin{aligned} f(0) &= \frac{(1-b)(1-2b)(1+2a^2+a^3+2ab)}{(1+a^2)^3}, \\ f(1) &= \frac{a(a+2b-1)(a^2+b)(a^2+2b)}{(1+a^2)^3}. \end{aligned}$$

From inequalities (3.2.34), we conclude that $f(0) \geq 0$ and $f(1) \geq 0$.

Now, we define

$$\alpha = \frac{3a^2(1-b) + 2ab(1-2b) + 2}{2(1+a^2)^2} \ . \tag{3.2.36}$$

From inequalities (3.2.34), we observe that $\alpha > 0$.

Moreover, since $(1-b) < 1$, then

$$3a^2(1-b) < 3a^2. \tag{3.2.37}$$

We also have $(1-2b) \leq a$ and $a > 0$, which leads to

$$a(1-2b) \leq a^2 \ . \tag{3.2.38}$$

Since $2b < 1$, then $2ab(1-2b) \leq a(1-2b)$, which is combined with (3.2.38) to show

$$2ab(1-2b) \leq a^2. \tag{3.2.39}$$

Combining (3.2.37) and (3.2.39), we obtain $3(1-b)a^2 + 2ab(1-2b) \leq 3a^2 + a^2 = 4a^2$, then

$$\alpha = \frac{2 + 3(1-b)a^2 + 2ab(1-2b)}{2 + 4a^2 + 2a^4} \leq \frac{2 + 4a^2}{2 + 4a^2 + 2a^4} \; < \; 1.$$

We can write

$$f(\alpha) \;\; = \;\; -\frac{a}{4(1+a^2)^4} \; (\; Q(a,b) + R(a,b) \;),$$

where

$$\begin{aligned} Q(a,b) &= a^2(1-2b)\left(2a^2(1-b) + 4b(2-b) + a(1+12b)\right) + a^3b^2(1+16b), \\ R(a,b) &= 2b\left((1-2b)\left(4b^2 + 7ab + 2a\right) + 2b(a+2b-1) + 8ab^3 + a\right). \end{aligned}$$

From inequalities (3.2.34), $Q(a,b) > 0$ and $R(a,b) \geq 0$, which, in turn, imply $f(\alpha) < 0$. Hence, $\sigma(\mathbf{M}_2) \subset [0,1]$.

A direct computation reveals that the two eigenvalues of $\mathbf{M}_1$ are roots of the equation

$$\begin{aligned} g(\lambda) &= \lambda^2 - \frac{2a^4 + (3-2b)b + a^3(2b-1) + 2ab(2b-1) + a^2(1+3b)}{(1+a^2)^2} \; \lambda \\ &+ \frac{a(a^2+b)(a+2b-1)(a^2+2b)}{(1+a^2)^3} = 0, \end{aligned}$$

and note that $g(\lambda) = f(1-\lambda)$, where f is defined in (3.2.35).

Then, $1-\lambda_1$ and $1-\lambda_2$ are the roots of the equation $g(\lambda) = 0$.

i.e. $\sigma(\mathbf{M}_1) \subset [0,1]$.

□

Lemma 3.2.5. *Let $\hat{L}_i$ be the standard Lagrange quadratic shape functions on the reference element of type V shown in Figure 3.2 and $\hat{p}$ be the orthogonal projection on $\hat{\Gamma}$. Then the eigenvalues of the matrix*

$$\mathbf{M}_2 = \begin{pmatrix} \hat{L}_2(\hat{p}(\hat{V}_2)) & \hat{L}_3(\hat{p}(\hat{V}_2)) & \hat{L}_4(\hat{p}(\hat{V}_2)) & \hat{L}_5(\hat{p}(\hat{V}_2)) & \hat{L}_6(\hat{p}(\hat{V}_2)) \\ \hat{L}_2(\hat{p}(\hat{V}_3)) & \hat{L}_3(\hat{p}(\hat{V}_3)) & \hat{L}_4(\hat{p}(\hat{V}_3)) & \hat{L}_5(\hat{p}(\hat{V}_3)) & \hat{L}_6(\hat{p}(\hat{V}_3)) \\ \hat{L}_2(\hat{p}(\hat{V}_4)) & \hat{L}_3(\hat{p}(\hat{V}_4)) & \hat{L}_4(\hat{p}(\hat{V}_4)) & \hat{L}_5(\hat{p}(\hat{V}_4)) & \hat{L}_6(\hat{p}(\hat{V}_4)) \\ \hat{L}_2(\hat{p}(\hat{V}_5)) & \hat{L}_3(\hat{p}(\hat{V}_5)) & \hat{L}_4(\hat{p}(\hat{V}_5)) & \hat{L}_5(\hat{p}(\hat{V}_5)) & \hat{L}_6(\hat{p}(\hat{V}_5)) \\ \hat{L}_2(\hat{p}(\hat{V}_6)) & \hat{L}_3(\hat{p}(\hat{V}_6)) & \hat{L}_4(\hat{p}(\hat{V}_6)) & \hat{L}_5(\hat{p}(\hat{V}_6)) & \hat{L}_6(\hat{p}(\hat{V}_6)) \end{pmatrix} \tag{3.2.40}$$

are all in $[0,1]$, and $M_1 = \hat{L}_1(\hat{p}(\hat{V}_1))$ is in $[0,1]$, as well.

Proof. First, we observe that for element of type V, cut by the interface $\hat{\Gamma} : \hat{y} = a\hat{x} + b$, a and b are in the domain

$$D = \{\ (a,b)\ |\ \ 0 < b \leq \frac{1}{2}\ ,\quad a \leq -2b\ \}, \tag{3.2.41}$$

as illustrated in Figure 3.7.

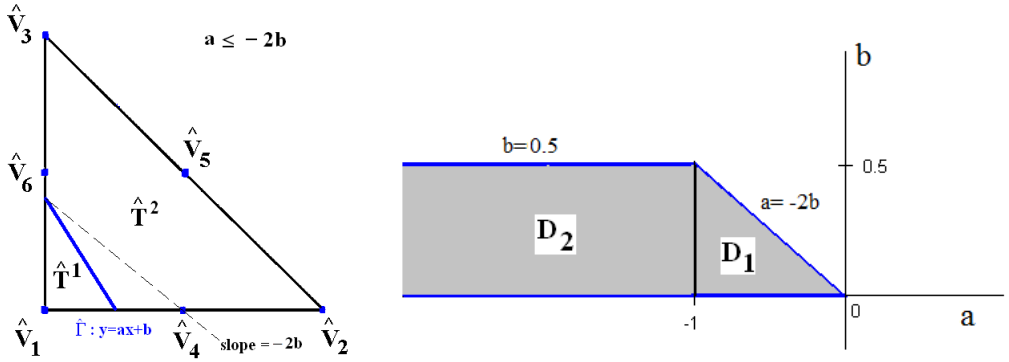

Figure 3.7: Interface elements of Type V (left) and associated domain for a and b (right).

A direct computation reveals that the five eigenvalues of $\mathbf{M}_2$ are $\{1, 1, 0, 0, \lambda\}$, with

$$\lambda = b(1-a)\frac{(3a^2 + 2ab - 2b + 3)}{(a^2+1)^2}. \tag{3.2.42}$$

Then, we write λ as

$$\begin{aligned} \lambda &= b(1-a)\frac{(2a^2 + a^2 + 2ab + b^2 - b^2 - 2b + 2 + 1)}{(a^2+1)^2} \\ &= b(1-a)\frac{(2a^2 + (a+b)^2 + (1-b^2) + 2(1-b))}{(a^2+1)^2} \ > \ 0. \end{aligned}$$

To show that $\lambda \leq 1$, we define the function

$$v(a,b) = \lambda = b(1-a)\frac{(3a^2 + 2ab - 2b + 3)}{(a^2+1)^2} \ > \ 0\ , \qquad \text{for } (a,b) \in D, \tag{3.2.43}$$

where $D = D_1 \cup D_2$, with

$$D_1 = \{(a,b) \mid 0 < b \leq \frac{1}{2},\ -1 \leq a \leq -2b\}, \quad \text{and} \quad D_2 = \{(a,b) \mid 0 < b \leq \frac{1}{2},\ a \leq -1\},$$

as illustrated in Figure 3.7.

A direct computation of the partial derivatives of v gives

$$\frac{\partial v}{\partial a}(a,b) = b\frac{(a^2-2a-1)\,(3a^2+4ab-4b+3)}{(a^2+1)^3}, \tag{3.2.44}$$

and

$$\frac{\partial v}{\partial b}(a,b) = (1-a)\frac{(3a^2+4ab-4b+3)}{(a^2+1)^2}. \tag{3.2.45}$$

We note that

$$3a^2+4ab-4b+3 = a^2+2(a+b)^2+1-2b^2+2(1-2b) \ > 0 \tag{3.2.46}$$

and since $(1-a) > 0$, then $\frac{\partial v}{\partial b}(a,b)$ does not change sign, which implies that v has no critical point in D.

Now, we will show that the $v(a,b)$ does not exceed 1 over D_1, as well as over D_2.

The maximum of $v(a,b)$ over D_1 is achieved on the boundary. A computation of the values of $v(a,b)$ on the boundary of D_1 gives

$$\begin{aligned}
v(a,0) &= 0 && (with \quad -1<a<0)\\
v(-1,b) &= -2b^2+3b = 1-(1-b)(1-2b) && (with \quad 0<b\leq\frac{1}{2})\\
v(-2b,b) &= b(2b+1)\frac{(8b^2-2b+3)}{(4b^2+1)^2} = w(b) && (with \quad 0<b\leq\frac{1}{2})
\end{aligned}$$

For $0<b\leq\frac{1}{2}$, we have $v(-1,b) = 1-(1-b)(1-2b) \leq 1$.

Furthermore, we have (for $0<b\leq\frac{1}{2}$)

$$w_1'(b) = -\frac{(4b^2-4b-1)\,(4b^2-4b+3)}{(4b^2+1)^3} = \frac{4-(2b-1)^4}{(4b^2+1)^3} \ > \ 0, \tag{3.2.47}$$

which implies that $w(b) \ \leq \ w(\frac{1}{2}) = 1$. Hence

$$0 \leq v(a,b) \leq 1, \quad \forall (a,b) \ \in D_1. \tag{3.2.48}$$

Now, for $v(a,b)$ over D_2, we notice that, since $a^2-2a-1>0$, for $a\leq -1$, and since we have, by (3.2.46), $(3a^2+4ab-4b+3)>0$, for $a\leq -1$, then $\frac{\partial v}{\partial a}(a,b)>0$, $\forall a\leq -1$.

Hence $v(a,b)$ is an increasing function for $a\in(-\infty,-1]$, its maximum is achieved on the line $a=-1$. Since we have already proved that $v(-1,b)\leq 1$, then we can conclude that the maximum of $v(a,b)$ over D_2 is less or equal to 1. Thus

$$0 \leq \lambda \leq 1, \quad \forall (a,b) \ \in D. \tag{3.2.49}$$

A direct computation of $\hat{L}_1(\hat{p}(\hat{V}_1))$ reveals that

$$\hat{L}_1(\hat{p}(\hat{V}_1)) = \frac{(a^2+2ab+1-2b)(a^2+ab+1-b)}{(a^2+1)^2}. \tag{3.2.50}$$

We note that $\hat{L}_1(\hat{p}(\hat{V}_1)) = 1-\lambda \in [0,1]$, where λ is the eigenvalue of $\mathbf{M}_2$ defined in (3.2.42). □

Lemma 3.2.6. *Let $\hat{L}_i$ be the standard Lagrange quadratic shape functions on the reference element of type VI shown in Figure 3.2 and $\hat{p}$ be the orthogonal projection on $\hat{\Gamma}$. Then the eigenvalues of the matrices*

$$\mathbf{M}_2 = \begin{pmatrix} \hat{L}_2(\hat{p}(\hat{V}_2)) & \hat{L}_3(\hat{p}(\hat{V}_2)) & \hat{L}_5(\hat{p}(\hat{V}_2)) & \hat{L}_6(\hat{p}(\hat{V}_2)) \\ \hat{L}_2(\hat{p}(\hat{V}_3)) & \hat{L}_3(\hat{p}(\hat{V}_3)) & \hat{L}_5(\hat{p}(\hat{V}_3)) & \hat{L}_6(\hat{p}(\hat{V}_3)) \\ \hat{L}_2(\hat{p}(\hat{V}_5)) & \hat{L}_3(\hat{p}(\hat{V}_5)) & \hat{L}_5(\hat{p}(\hat{V}_5)) & \hat{L}_6(\hat{p}(\hat{V}_5)) \\ \hat{L}_2(\hat{p}(\hat{V}_6)) & \hat{L}_3(\hat{p}(\hat{V}_6)) & \hat{L}_5(\hat{p}(\hat{V}_6)) & \hat{L}_6(\hat{p}(\hat{V}_6)) \end{pmatrix} \tag{3.2.51}$$

$$\mathbf{M}_1 = \begin{pmatrix} \hat{L}_1(\hat{p}(\hat{V}_1)) & \hat{L}_4(\hat{p}(\hat{V}_1)) \\ \hat{L}_1(\hat{p}(\hat{V}_4)) & \hat{L}_4(\hat{p}(\hat{V}_4)) \end{pmatrix} \tag{3.2.52}$$

are in $[0,1]$

Proof. First we observe that for elements of Type VI, cut by the interface $\hat{\Gamma} : \hat{y} = a\hat{x} + b$, a and b are in the domain

$$D = \{\ (a,b) \mid\ 0 < b \le \frac{1}{2}\ ,\quad -2b \le a \le -b\ \}, \tag{3.2.53}$$

as illustrated in Figure 3.8. Thus, for $(a,b) \in D$, we have the inequalities

$$(1-b) > 0\ ,\quad (1-2b) \ge 0\ ,\quad (a+2b) \ge 0\ ,\quad (a+b) \le 0\ , -1 \le a < 0\ . \tag{3.2.54}$$

A direct computation shows that the four eigenvalues of $\mathbf{M}_2$ are $\{\lambda_1, \lambda_2, 1, 0\}$, where λ_1 and λ_2 are roots of the quadratic equation

$$\begin{aligned} f(\lambda) &= \lambda^2 - \frac{a^4 + a^3b + a^2b(2b+1) - 3ab + a + b(5-2b)}{(a^2+1)^2}\lambda \\ &+ \frac{b(1-a)(a+2b)(a^2(2-a) - 2a(1-b) + (3-2b))}{(1+a^2)^3} = 0. \end{aligned} \tag{3.2.55}$$

Next, we will show the following. If $0 < b < \frac{1}{2}$, then $f(0) \ge 0$, $f(2b) < 0$ and $f(1) \ge 0$. In this case, since f is continuous, the quadratic equation $f(\lambda) = 0$ has one root in $[0, 2b)$, and

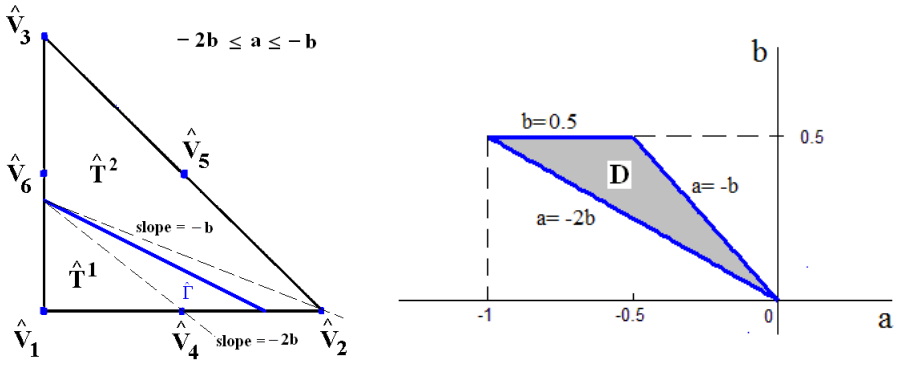

Figure 3.8: Interface elements of Type VI (left) and associated domain for a and b (right).

another root in $(2b, 1]$. However, if $b = \frac{1}{2}$, then $f(\lambda) = 0$ has one root equal to 1 and another root in $(0, 1)$.

Hence, oth λ_1 and λ_2 are in $[0, 1]$.

First, let us consider the case $0 < b < \frac{1}{2}$, where

$$f(0) = \frac{b(1-a)(a+2b)(a^2(2-a) - 2a(1-b) + (3-2b))}{(1+a^2)^3},$$

and

$$f(1) = \frac{(1-2b)\,(2a^2 + (1-a)(1-2b))\,(a(a+b) + 1 - b)}{(1+a^2)^3},$$

and

$$f(2b) = a\,\frac{b(1-2b)}{(1+a^2)^3}\,(a^4 - a^3(2a^2+5-2b) - 2(a+b)(2-a) - a + 1).$$

From inequalities (3.2.54), we conclude that $f(0) > 0$, $f(1) > 0$ and $f(2b) < 0$, which implies that λ_1 and λ_2 are in $[0, 1]$.

Now, let us consider the case $b = \frac{1}{2}$ (which implies that $-1 < a < -\frac{1}{2}$), where $f(\lambda) = 0$ becomes

$$\lambda^2 - \lambda\frac{(2a^4 + a^3 + 2a^2 - a + 4)}{2\,(a^2+1)^2} + \frac{(a-1)\,(a^2 - a - 2)}{2\,(a^2+1)^2} = 0 \qquad (3.2.56)$$

A direct computation of the solutions gives

$$\lambda_1 = 1 \qquad \textit{and} \qquad \lambda_2 = \frac{a^3 - 2a^2 - a + 2}{2\,(a^2+1)^2} = w(a). \qquad (3.2.57)$$

We just need to show that λ_2 is in $[0, 1]$.

Differentiate w to write

$$w'(a) = \frac{-a^4 + 4a^3 + 6a^2 - 12a - 1}{2\left(a^2+1\right)^3}. \tag{3.2.58}$$

For $-1 \leq a \leq -\frac{1}{2}$, we have

$$-a^4 + 4a^3 + 6a^2 - 12a - 1 = (1-a^2)(a^2-4a) - (2a+1) + 5a^2 - 6a \ > \ 0 \ , \tag{3.2.59}$$

Thus, $\quad w'(a) > 0$, leads to

$$w(-1) = 0 \ \leq \ w(a) = \lambda_2 \ \leq \ w(-\frac{1}{2}) = \frac{3}{5}.$$

Finally, we conclude that the eigenvalues of $\mathbf{M}_2$ are all in $[0,1]$.

A direct computation shows that the two eigenvalues of $\mathbf{M}_1$ are roots of the equation

$$\begin{aligned} g(\lambda) \ &= \ \lambda^2 - \frac{(a^4 - a^3b - a^2(2b^2+b-4) + a(3b-1) + 2b^2 - 5b + 2)}{(a^2+1)^2}\,\lambda \\ &+ \ \frac{(1-2b)(a^2+ab-b+1)\,(2a^2+(1-a)(1-2b))}{(a^2+1)^3} = 0. \end{aligned}$$

We note that for all λ, $g(\lambda) = f(1-\lambda)$, where f is defined in (3.2.55).

Since the roots of $f(\lambda) = 0$, λ_1 and λ_2, are in $[0,1]$, then the roots, $1-\lambda_1$ and $1-\lambda_2$, of the equation $g(\lambda) = 0$ are in $[0,1]$. This concludes the proof.

□

Lemma 3.2.7. *Let $\hat{L}_i$ be the standard Lagrange quadratic shape functions on the reference element of type VII shown in Figure 3.2 and $\hat{p}$ be the orthogonal projection on $\hat{\Gamma}$. Then the eigenvalues of the matrices*

$$\mathbf{M}_2 = \begin{pmatrix} \hat{L}_2(\hat{p}(\hat{V}_2)) & \hat{L}_3(\hat{p}(\hat{V}_2)) & \hat{L}_5(\hat{p}(\hat{V}_2)) \\ \hat{L}_2(\hat{p}(\hat{V}_3)) & \hat{L}_3(\hat{p}(\hat{V}_3)) & \hat{L}_5(\hat{p}(\hat{V}_3)) \\ \hat{L}_2(\hat{p}(\hat{V}_5)) & \hat{L}_3(\hat{p}(\hat{V}_5)) & \hat{L}_5(\hat{p}(\hat{V}_5)) \end{pmatrix} \tag{3.2.60}$$

and

$$\mathbf{M}_1 = \begin{pmatrix} \hat{L}_1(\hat{p}(\hat{V}_1)) & \hat{L}_4(\hat{p}(\hat{V}_1)) & \hat{L}_6(\hat{p}(\hat{V}_1)) \\ \hat{L}_1(\hat{p}(\hat{V}_4)) & \hat{L}_4(\hat{p}(\hat{V}_4)) & \hat{L}_6(\hat{p}(\hat{V}_4)) \\ \hat{L}_1(\hat{p}(\hat{V}_6)) & \hat{L}_4(\hat{p}(\hat{V}_6)) & \hat{L}_6(\hat{p}(\hat{V}_6)) \end{pmatrix} \tag{3.2.61}$$

are in $[0,1]$.

Proof. First we observe that for elements of Type VII, cut by the interface $\hat{\Gamma} : \hat{y} = a\hat{x} + b$, a and b are in the domain

$$D = \{ \ (a,b) \mid \ \frac{1}{2} < b < 1 \ , \quad -2b \leq a \leq -b \ \}, \tag{3.2.62}$$

as illustrated in Figure 3.9. Thus, for $(a,b) \in D$, we have the inequalities

$$(1-b) > 0 \ , \quad (1-2b) > 0 \ , \quad (a+2b) \geq 0 \ , \quad (a+b) \leq 0 \ , \quad -2 < a < -\frac{1}{2} \ . \tag{3.2.63}$$

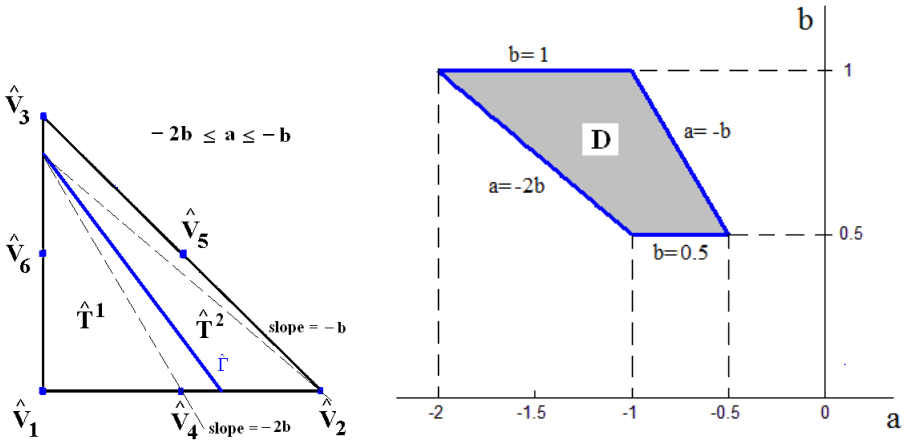

Figure 3.9: Interface elements of Type VII (left) and associated domain for a and b (right).

A direct computation reveals that the three eigenvalues of $\mathbf{M}_2$ are $\{\lambda_1, \lambda_2, 1\}$, where λ_1 and λ_2 are roots of the quadratic equation

$$\begin{aligned} f(\lambda) \ &= \ \lambda^2 - \frac{(1-a)\left(a^2(b-1) - 2ab^2 + a + b(2b+1)\right)}{\left(a^2+1\right)^2} \, \lambda \\ &+ \ \frac{b(2b-1)(a+2b)(1-a)^3}{\left(a^2+1\right)^3} = 0. \end{aligned} \tag{3.2.64}$$

Next, we will show that $f(0) \geq 0$ and $f(1) \geq 0$, and that for some $\alpha \in (0,1)$, we have $f(\alpha) < 0$. In this case, since f is continuous, we conclude that the quadratic equation $f(\lambda) = 0$ has one root in the interval $[0, \alpha)$ and another root in the interval $(\alpha, 1]$, which implies that both λ_1 and λ_2 are in $[0,1]$.

First, we observe that

$$f(0) = \frac{b(2b-1)(a+2b)(1-a)^3}{(1+a^2)^3}.$$

By the inequalities (3.2.63), we obtain that $f(0) \geq 0$.

Next, we define

$$\alpha = \frac{(1-a)(1+2b-a)(a+b-ab)}{2(1+a^2)^2}. \tag{3.2.65}$$

By the inequalities (3.2.63), we observe that

$$a+b-ab = \frac{1}{2}(2a+2b-2ab) = \frac{1}{2}(a+2b-a(2b-1)) > 0, \tag{3.2.66}$$

then $\alpha > 0$.

We further note that

$$1-\alpha = \frac{2(a+b^2)^2 + 2(a^4-b^4) + 2(1+a^2)(1-b^2) + (1-a)\left(a^2(1-b)-(a+b)\right)}{2(a^2+1)^2}.$$

By inequalities (3.2.63), we obtain that

$$a^4 - b^4 = (a-b)(a+b)(a^2+b^2) \ > \ 0\ . \tag{3.2.67}$$

Using (3.2.63) and (3.2.67), we conclude that $(1-\alpha) > 0$, i.e. $\alpha < 1$.

Hence $\alpha \in (0,1)$.

Next, we have

$$f(\alpha) = -\frac{(1-a)^2}{4(1+a^2)^4} \qquad ((a+b-ab)^2(1-a-2b)^2$$
$$+4b(1-a)(1+a)^2(a+2b-2b(a+b))) \ < \ 0,$$

where we used inequalities (3.2.63).

We also have

$$f(1) = \frac{(1+a^2)^3 + b(2b-1)(a+2b)(1-a)^3 - (1+a^2)(1-a)(1-a+2b)(a+b-ab)}{(1+a^2)^3}.$$

To show that $f(1) \geq 0$, let us consider the numerator

$$v(a,b) = (1+a^2)^3 + b(2b-1)(a+2b)(1-a)^3 - (1+a^2)(1-a)(1-a+2b)(a+b-ab) \tag{3.2.68}$$

The partial derivatives of $v(a,b)$ are

$$\frac{\partial v}{\partial a}(a,b) = 6a^5 - 5a^4(1-b) + 4a^3(5-4b^2) - 3a^2(4b^3-12b^2+b+2)$$
$$+2a(12b^3-16b^2+b+5) - 12b^3 + 12b^2 - 1,$$

$$\frac{\partial v}{\partial b}(a,b) = (a-1)\left(a^4 - a^3(8b-1) + 4a^2b(4-3b) + a(24b^2-16b+1) - 12b^2 + 8b + 1\right).$$

Now, we will show that $v(a,b)$ is decreasing with respect to b, *i.e.* $\frac{\partial v}{\partial b}(a,b) < 0$.

For $(a-1) < 0$, let us define

$$w(a,b) = \frac{v(a,b)}{(a-1)} = a^4 - a^3(8b-1) + 4a^2b(4-3b) + a(24b^2 - 16b + 1) - 12b^2 + 8b + 1.$$

A computation of the partial derivatives of $w(a,b)$ gives

$$\begin{aligned}
\frac{\partial w}{\partial a}(a,b) &= 4a^3 - (3a^2+1)(2b-1) + 2b(12a-7)(1-b) + 8b(a+b) - 2b(9a^2-b), \\
\frac{\partial w}{\partial b}(a,b) &= -8(1-a)\left(2b - 1 - a(a+2b) + a + b - ab\right).
\end{aligned}$$

Using (3.2.63) and (3.2.66), we see that $\frac{\partial w}{\partial b}(a,b) < 0$, which implies that w is decreasing with respect to b, for $b \in (\frac{1}{2}, 1)$.

Hence the minimum of $w(a,b)$ is achieved on the line $b = 1$ or on the line $a = -b$. A direct computation of $w(a,b)$ on these two boundaries gives

$$\begin{aligned}
w(a,1) &= a^4 - 7a^3 + 4a^2 + 9a - 3, \quad (-2 \le a < -1) \\
w(-b,b) &= -3b^4 - 9b^3 + 4b^2 + 7b + 1. \quad (\frac{1}{2} \le b < 1)
\end{aligned}$$

We can write

$$w(a,1) = 2(a+1)^2 + (a^2-1)(a^2+5) + a(a+1)(5-7a).$$

From inequalities (3.2.63), we have $a < -1$, then $w(a,1) > 0$.

We can also write

$$w(-b,b) = 1 - b^4 + b(1-b)(2b^2 + 11b + 7) \ > \ 0, \quad for \ \frac{1}{2} < b < 1.$$

Hence, we conclude that $w(a,b) > 0$, for $b \in (\frac{1}{2}, 1)$, which implies that

$$\frac{\partial v}{\partial b}(a,b) = (a-1)\ w(a,b) \ < 0.$$

Thus, v is decreasing with respect to b, for $b \in (\frac{1}{2}, 1)$. The minimum of $v(a,b)$ is achieved on the line $b = 1$ or on the line $a = -b$. A direct computation of $v(a,b)$ on these two boundaries gives

$$\begin{aligned}
v(a,1) &= a(a^5 + a^3 + 5a^2 + 2a - 1), \qquad (with \quad -2 \le a < -1) \\
v(-b,b) &= b^5 + 2b^4 - 5b^3 + b^2 + 1. \qquad (with \quad \frac{1}{2} < b < 1)
\end{aligned}$$

We can write

$$a^5 + a^3 + 5a^2 + 2a - 1 = (a+1)^2(a^3 - 2a^2 + 4a - 1) < 0,$$

and since $a < 0$, then it is clear that $v(a, 1) > 0$.

We can also write

$$b^5 + 2b^4 - 5b^3 + b^2 + 1 = (1-b)^2(b^3 + 4b^2 + 2b + 1) > 0,$$

and since $b > \frac{1}{2}$, then it is clear that $v(-b, b) > 0$, and we conclude that $v(a, b) > 0$, for $(a, b) \in D$.

Hence, we proved that $f(0) \geq 0$ and $f(1) \geq 0$, and for $0 < \alpha < 1$, $f(\alpha) < 0$, which yields

$$\sigma(\mathbf{M}_2) \subset [0, 1].$$

A direct computation reveals that the three eigenvalues of $\mathbf{M}_1$ are 0 and the two roots of the quadratic equation

$$g(\lambda) = \lambda^2 - \frac{2a^4 - a^3(1-b) - a^2(2b^2 + b - 6) + a(4b^2 + b - 1) - 2b^2 - b + 2}{(a^2+1)^2}\,\lambda$$
$$+ \frac{(1+a^2)^3 + b(2b-1)(a+2b)(1-a)^3 - (1+a^2)(1-a)(1-a+2b)(a+b-ab)}{(a^2+1)^3} = 0.$$

We note that for all $\lambda \in [0, 1]$

$$g(\lambda) = f(1 - \lambda)$$

where f is the function defined in (3.2.64).

Since the roots of $f(\lambda) = 0$ are in $[0, 1]$, Then $1 - \lambda_1$ and $1 - \lambda_2$ are the roots of the equation $g(\lambda) = 0$.

i.e. $\sigma(\mathbf{M}_1) \subset [0, 1]$. □

Now we are ready to prove the existence of the IFE shape functions on $\hat{\mathcal{R}}_2(\hat{T})$.

Theorem 3.2.1. *Let $\hat{T}$ be a reference interface element cut by the interface $\hat{\Gamma} : \hat{y} = a\hat{x} + b$, and let $\hat{\mathcal{R}}_2(\hat{T})$ be the quadratic polynomial space defined in (2.2.19), with $\hat{\boldsymbol{n}}$ orthogonal to $\hat{\Gamma}$. There exists six shape functions $\hat{\varphi}_i$, $i = 1, \ldots, 6$, in $\hat{\mathcal{R}}_2(\hat{T})$ satisfying the Lagrange nodal value conditions (3.2.1). The shape functions $\hat{\varphi}_i$, $i = 1, \ldots, 6$, are unique.*

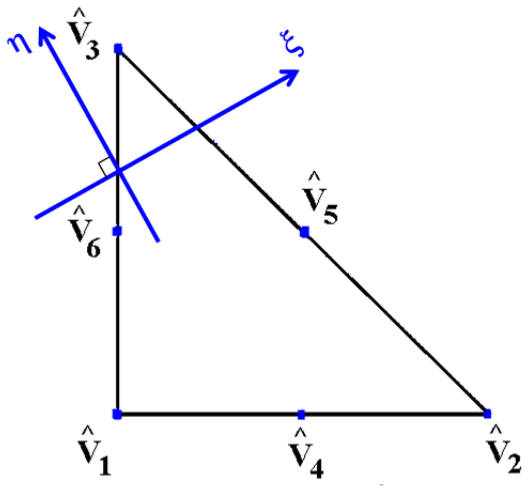

Figure 3.10: Interface coordinates system on the reference element of Type I with $\hat{\mathbf{n}}$ orthogonal to $\hat{\Gamma}$.

Proof. Let $\hat{T}$ be a reference interface element, with vertices $\hat{V}_i,\ i = 1, 2, 3$, and midpoints of the edges $\hat{V}_i,\ i = 4, 5, 6$, of one of the 7 types described in Table 3.2. Considering the interface coordinates (ξ, η) described in Figure 3.1 and their mapping $(\hat{\xi}, \hat{\eta})$ to $\hat{T}$ such that $\hat{\boldsymbol{n}} = \mathbf{J}\boldsymbol{n}$ is orthogonal to the $\hat{\xi}$ coordinate, as illustrated in Figure 3.10, for Type I.

First, for elements of Type I we write the expressions of $\hat{\varphi}_i,\ i = 1, \ldots, 6$, as in (3.2.6) and (3.2.7), with $\mathscr{I}_1 = \{3\}$ and $\mathscr{I}_2 = \{1, 2, 4, 5, 6\}$, respectively.

The shape function $\hat{\varphi}_3$ is given by

$$\hat{\varphi}_3(\hat{x}, \hat{y}) = \begin{cases} \hat{\varphi}_3^2(\hat{x}, \hat{y}) = c_3 \hat{L}_3(\hat{x}, \hat{y}) \ , & (\hat{x}, \hat{y}) \in \hat{T}^2. \\ \\ \hat{\varphi}_3^1(\hat{x}, \hat{y}) = \frac{1}{\hat{r}}\ \hat{\varphi}_3^2(\hat{x}, \hat{y}) + (1 - \frac{1}{\hat{r}})\ \hat{\varphi}_3^2(\hat{p}(\hat{x}, \hat{y})) \ , & (\hat{x}, \hat{y}) \in \hat{T}^1. \end{cases} \tag{3.2.69}$$

For $i \in \mathscr{I}_2$, we can write the shape function $\hat{\varphi}_i$ as

$$\hat{\varphi}_i(\hat{x}, \hat{y}) = \begin{cases} \hat{\varphi}_i^1(\hat{x}, \hat{y}) = \displaystyle\sum_{j \in \mathscr{I}_2} c_j \hat{L}_j(\hat{x}, \hat{y}) \ , & (\hat{x}, \hat{y}) \in \hat{T}^1, \\ \\ \hat{\varphi}_i^2(\hat{x}, \hat{y}) = \hat{r}\ \hat{\varphi}_i^1(\hat{x}, \hat{y}) + (1 - \hat{r})\ \hat{\varphi}_i^1(\hat{p}(\hat{x}, \hat{y})) \ , & (\hat{x}, \hat{y}) \in \hat{T}^2, \end{cases} \tag{3.2.70}$$

with $\hat{r} = \frac{\hat{\beta}^1}{\hat{\beta}^2}$.

Each shape function is in $\hat{\mathcal{R}}_2(\hat{T})$, and the constants c_j are determined by imposing the Lagrange nodal value conditions (3.2.1).

Hence, imposing (3.2.1) to $\hat{\varphi}_3$, at the node $\hat{V}_3$, leads to one equation for c_3

$$\left(\frac{1}{\hat{r}} + (1 - \frac{1}{\hat{r}})\lambda_6\right) c_3 = 1, \tag{3.2.71}$$

with $\lambda_6 = \hat{L}_3(\hat{p}(\hat{V}_3))$.

By Lemma 3.2.1, we have $\lambda_6 \in [0, 1]$, thus

$$\frac{1}{\hat{r}} + (1 - \frac{1}{\hat{r}})\lambda_6 \neq 0 \ ,$$

and we can solve for c_3,

$$c_3 = \frac{\hat{r}}{1 + (\hat{r} - 1)\lambda_6}.$$

For $i \in \mathscr{I}_2$, imposing the Lagrange nodal value conditions (3.2.1) at $\hat{V}_j, j = 1, 2, 4, 5, 6$, leads to the following linear system for $\mathbf{c} = (c_1, c_2, c_4, c_5, c_6)^t$

$$\mathbf{A}_2 \ \mathbf{c} \ = \ \mathbf{e}_{\delta(i)}, \qquad \text{with} \qquad \mathbf{A}_2 = \hat{r} \ \mathbf{I} + (1 - \hat{r}) \ \mathbf{M}_2, \tag{3.2.72}$$

where $\mathbf{e}_i$ is the canonical vector in $\mathbb{R}^5$, δ is the mapping defined by

$$\delta(1) = 1, \ \delta(2) = 2, \ \delta(4) = 3, \ \delta(5) = 4, \ \delta(6) = 5,$$

and $\mathbf{M}_2$ is the matrix defined in (3.2.10), with eigenvalue $\lambda_k \in [0, 1], \ k = 1, \ldots, 6$, as shown in Lemma 3.2.1.

The eigenvalues of the matrix $\mathbf{A}_2$

$$\mu_k = \hat{r} + (1 - \hat{r}) \ \lambda_k \ , \quad k = 1, \ldots, 5, \tag{3.2.73}$$

are bounded as

$$min(1, \hat{r}) \ \leq \ \mu_k \ \leq \ max(1, \hat{r}) \ , \qquad k = 1, \ldots, 5. \tag{3.2.74}$$

Thus, $\mu_k > 0 \ , \ k = 1, \ldots, 5$, and the system (3.2.72) has a unique solution.

For elements of Type II, we write the expressions of $\hat{\varphi}_i, \ i = 1, \ldots, 6$, as in (3.2.6) and (3.2.7), with $\mathscr{I}_1 = \{3, 5\}$ and $\mathscr{I}_2 = \{1, 2, 4, 6\}$, as illustrated in Figure 3.11. For $i \in \mathscr{I}_1$, the shape function $\hat{\varphi}_i$ is given by

$$\hat{\varphi}_i(\hat{x}, \hat{y}) = \begin{cases} \hat{\varphi}_i^2(\hat{x}, \hat{y}) = \displaystyle\sum_{j \in \mathscr{I}_1} c_j \hat{L}_j(\hat{x}, \hat{y}) \ , & (\hat{x}, \hat{y}) \in \hat{T}^2, \\ \\ \hat{\varphi}_i^1(\hat{x}, \hat{y}) = \frac{1}{\hat{r}} \ \hat{\varphi}_i^2(\hat{x}, \hat{y}) + (1 - \frac{1}{\hat{r}}) \ \hat{\varphi}_i^2(\hat{p}(\hat{x}, \hat{y})) \ , & (\hat{x}, \hat{y}) \in \hat{T}^1. \end{cases} \tag{3.2.75}$$

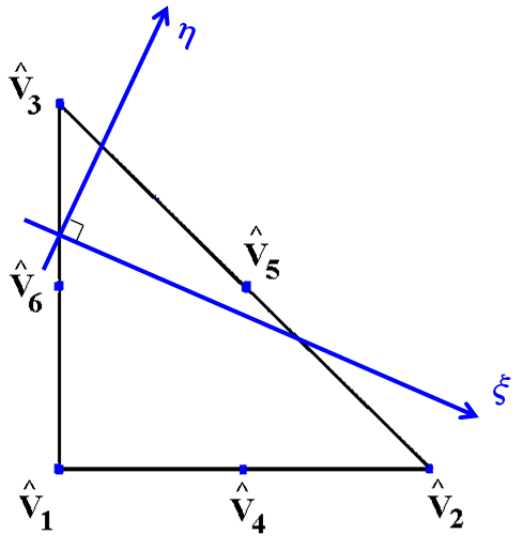

Figure 3.11: Interface coordinates system on the reference element of Type II with $\hat{\mathbf{n}}$ orthogonal to $\hat{\Gamma}$.

For $i \in \mathscr{I}_2$, the shape function $\hat{\varphi}_i$ is given by

$$\hat{\varphi}_i(\hat{x},\hat{y}) = \begin{cases} \hat{\varphi}_i^1(\hat{x},\hat{y}) = \displaystyle\sum_{j\in\mathscr{I}_2} c_j \hat{L}_j(\hat{x},\hat{y}) \ , & (\hat{x},\hat{y}) \in \hat{T}^1, \\ \\ \hat{\varphi}_i^2(\hat{x},\hat{y}) = \hat{r}\ \hat{\varphi}_i^1(\hat{x},\hat{y}) + (1-\hat{r})\ \hat{\varphi}_i^1(\hat{p}(\hat{x},\hat{y})) \ , & (\hat{x},\hat{y}) \in \hat{T}^2, \end{cases} \tag{3.2.76}$$

with $\hat{r} = \frac{\hat{\beta}^1}{\hat{\beta}^2}$.

Following the same reasoning as for Type I, the coefficients c_j are determined by imposing the Lagrange nodal value conditions (3.2.1).

For $i \in \mathscr{I}_1$, imposing the Lagrange nodal value conditions (3.2.1) at $\hat{V}_j, j = 3, 5$, leads to the following linear system for $\mathbf{c} = (c_3, c_5)^t$

$$\mathbf{A}_1\ \mathbf{c}\ =\ \mathbf{e}_{\delta(i)}, \qquad \text{with} \qquad \mathbf{A}_1 = \frac{1}{\hat{r}}\ \mathbf{I} + (1-\frac{1}{\hat{r}})\ \mathbf{M}_1, \tag{3.2.77}$$

where $\mathbf{e}_i$ is the canonical vector in $\mathbb{R}^2$, δ is the mapping defined by

$$\delta(3) = 1,\ \delta(5) = 2,$$

and $\mathbf{M}_1$ is the matrix defined in (3.2.20), with eigenvalues $\lambda_k \in [0,1],\ k = 1, 2$, as shown in Lemma 3.2.2.

The eigenvalues of $\mathbf{A}_1$

$$\mu_k = \frac{1}{\hat{r}} + (1-\frac{1}{\hat{r}})\ \lambda_k \ , \quad k = 1, 2, \tag{3.2.78}$$

are bounded as

$$min(1, \frac{1}{\hat{r}}) \ \leq \ \mu_k \ \leq \ max(1, \frac{1}{\hat{r}}) \ , \qquad k = 1, 2. \tag{3.2.79}$$

Thus, $\mu_k > 0$, $k = 1, 2$, and the system (3.2.77) has a unique solution.

For $i \in \mathscr{I}_2$, imposing the Lagrange nodal value conditions (3.2.1) at $\hat{V}_j, j = 1, 2, 4, 6$, leads to the following linear system for $\mathbf{c} = (c_1, c_2, c_4, c_6)^t$

$$\mathbf{A}_2 \ \mathbf{c} \ = \ \mathbf{e}_{\delta(i)}, \qquad \text{with} \qquad \mathbf{A}_2 = \hat{r} \ \mathbf{I} + (1 - \hat{r}) \ \mathbf{M}_2, \tag{3.2.80}$$

where $\mathbf{e}_i$ is the canonical vector in $\mathbb{R}^4$, δ is the mapping defined by

$$\delta(1) = 1, \ \delta(2) = 2, \ \delta(4) = 3, \ \delta(6) = 4,$$

and $\mathbf{M}_2$ is the matrix defined in (3.2.19), with eigenvalues $\lambda_k \in [0, 1], \ k = 1, \ldots, 4$, as shown in Lemma 3.2.2.

The eigenvalues of $\mathbf{A}_2$

$$\mu_k = \hat{r} + (1 - \hat{r}) \ \lambda_k \ , \quad k = 1, \ldots, 4, \tag{3.2.81}$$

are bounded as

$$min(1, \hat{r}) \ \leq \ \mu_k \ \leq \ max(1, \hat{r}) \ , \qquad k = 1, \ldots, 4. \tag{3.2.82}$$

Thus, $\mu_k > 0$, $k = 1, \ldots, 4$, and the system (3.2.80) has a unique solution.

For elements of Type III, we write the expressions of $\hat{\varphi}_i, \ i = 1, \ldots, 6$, as in (3.2.6) and (3.2.7), with $\mathscr{I}_1 = \{3, 4, 5\}$ and $\mathscr{I}_2 = \{1, 2, 4\}$, as illustrated in Figure 3.12. For $i \in \mathscr{I}_1$, the shape function $\hat{\varphi}_i$ is given by

$$\hat{\varphi}_i(\hat{x}, \hat{y}) = \begin{cases} \hat{\varphi}_i^2(\hat{x}, \hat{y}) = \displaystyle\sum_{j \in \mathscr{I}_1} c_j \hat{L}_j(\hat{x}, \hat{y}) \ , & (\hat{x}, \hat{y}) \in \hat{T}^2, \\ \\ \hat{\varphi}_i^1(\hat{x}, \hat{y}) = \frac{1}{\hat{r}} \ \hat{\varphi}_i^2(\hat{x}, \hat{y}) + (1 - \frac{1}{\hat{r}}) \ \hat{\varphi}_i^2(\hat{p}(\hat{x}, \hat{y})) \ , & (\hat{x}, \hat{y}) \in \hat{T}^1. \end{cases} \tag{3.2.83}$$

For $i \in \mathscr{I}_2$, the shape function $\hat{\varphi}_i$ is given by

$$\hat{\varphi}_i(\hat{x}, \hat{y}) = \begin{cases} \hat{\varphi}_i^1(\hat{x}, \hat{y}) = \displaystyle\sum_{j \in \mathscr{I}_2} c_j \hat{L}_j(\hat{x}, \hat{y}) \ , & (\hat{x}, \hat{y}) \in \hat{T}^1, \\ \\ \hat{\varphi}_i^2(\hat{x}, \hat{y}) = \hat{r} \ \hat{\varphi}_i^1(\hat{x}, \hat{y}) + (1 - \hat{r}) \ \hat{\varphi}_i^1(\hat{p}(\hat{x}, \hat{y})) \ , & (\hat{x}, \hat{y}) \in \hat{T}^2, \end{cases} \tag{3.2.84}$$

with $\hat{r} = \frac{\hat{\beta}^1}{\hat{\beta}^2}$.

The coefficients c_j are determined by imposing the Lagrange nodal value conditions (3.2.1).

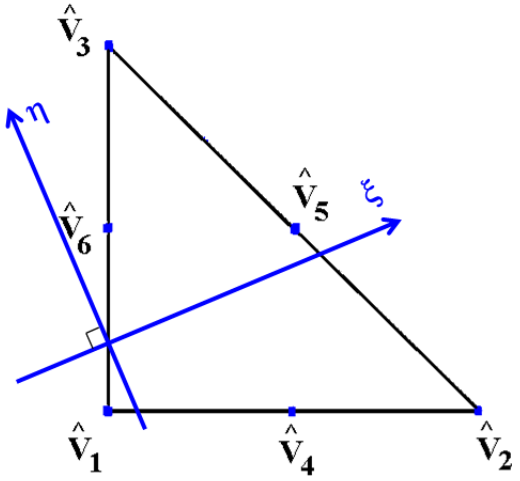

Figure 3.12: Interface coordinates system on the reference element of Type III with $\hat{\mathbf{n}}$ orthogonal to $\hat{\Gamma}$.

For $i \in \mathscr{I}_1$, imposing the Lagrange nodal value conditions (3.2.1) at $\hat{V}_j, j = 3, 5, 6$, leads to the following linear system for $\mathbf{c} = (c_3, c_5, c_6)^t$

$$\mathbf{A}_1 \ \mathbf{c} \ = \ \mathbf{e}_{\delta(i)}, \qquad \text{with} \qquad \mathbf{A}_1 = \frac{1}{\hat{r}} \ \mathbf{I} + (1 - \frac{1}{\hat{r}}) \ \mathbf{M}_1, \tag{3.2.85}$$

where $\mathbf{e}_i$ is the canonical vector in $\mathbb{R}^3$, δ is the mapping defined by

$$\delta(3) = 1, \ \delta(5) = 2, \ \delta(6) = 3,$$

and $\mathbf{M}_1$ is the matrix defined in (3.2.25), with eigenvalues $\lambda_k \in [0, 1], \ k = 1, \ldots, 3$, as shown in Lemma 3.2.3.

The eigenvalues of $\mathbf{A}_1$

$$\mu_k = \frac{1}{\hat{r}} + (1 - \frac{1}{\hat{r}}) \ \lambda_k \ , \quad k = 1, 2, 3, \tag{3.2.86}$$

are bounded as

$$min(1, \frac{1}{\hat{r}}) \ \leq \ \mu_k \ \leq \ max(1, \frac{1}{\hat{r}}) \ , \qquad k = 1, 2, 3. \tag{3.2.87}$$

Thus, $\mu_k > 0 \ , \ k = 1, 2$, and the system (3.2.85) has a unique solution.

For $i \in \mathscr{I}_2$, imposing the Lagrange nodal value conditions (3.2.1) at $\hat{V}_j, j = 1, 2, 4$ leads to the following linear system for $\mathbf{c} = (c_1, c_2, c_4)^t$

$$\mathbf{A}_2 \ \mathbf{c} \ = \ \mathbf{e}_{\delta(i)}, \qquad \text{with} \qquad \mathbf{A}_2 = \hat{r} \ \mathbf{I} + (1 - \hat{r}) \ \mathbf{M}_2, \tag{3.2.88}$$

where $\mathbf{e}_i$ is the canonical vector in $\mathbb{R}^3$, δ is the mapping defined by

$$\delta(1) = 1,\ \delta(2) = 2,\ \delta(4) = 3,$$

and $\mathbf{M}_2$ is the matrix defined in (3.2.24), with eigenvalues $\lambda_k \in [0,1],\ k = 1,\ldots,3$, as shown in Lemma 3.2.3.

The eigenvalues of $\mathbf{A}_2$

$$\mu_k = \hat{r} + (1-\hat{r})\ \lambda_k\ , \quad k = 1,2,3, \tag{3.2.89}$$

are bounded as

$$min(1,\hat{r})\ \leq\ \mu_k\ \leq\ max(1,\hat{r})\ , \qquad k = 1,\ldots,3. \tag{3.2.90}$$

Thus, $\mu_k > 0\ ,\ k = 1,\ldots,3$, and the system (3.2.80) has a unique solution.

For elements of Type IV, we write the expressions of $\hat{\varphi}_i,\ i = 1,\ldots,6$, as in (3.2.6) and (3.2.7), with $\mathscr{I}_1 = \{3,6\}$ and $\mathscr{I}_2 = \{1,2,4,5\}$, as illustrated in Figure 3.13. For $i \in \mathscr{I}_1$, the

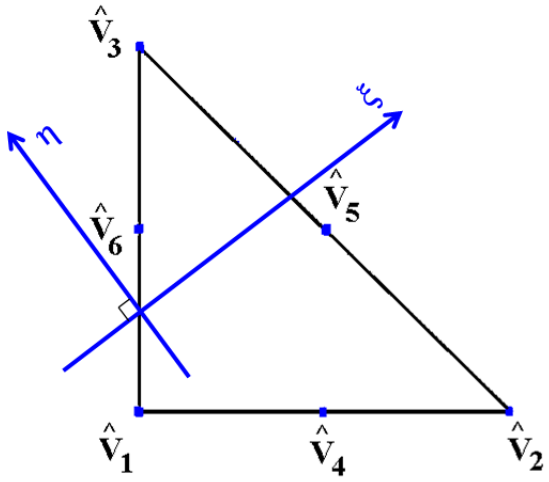

Figure 3.13: Interface coordinates system on the reference element of Type IV with $\hat{\mathbf{n}}$ orthogonal to $\hat{\Gamma}$.

shape function $\hat{\varphi}_i$ is given by

$$\hat{\varphi}_i(\hat{x},\hat{y}) = \begin{cases} \hat{\varphi}_i^2(\hat{x},\hat{y}) = \displaystyle\sum_{j\in\mathscr{I}_1} c_j \hat{L}_j(\hat{x},\hat{y})\ , & (\hat{x},\hat{y}) \in \hat{T}^2, \\ \\ \hat{\varphi}_i^1(\hat{x},\hat{y}) = \frac{1}{\hat{r}}\ \hat{\varphi}_i^2(\hat{x},\hat{y}) + (1-\frac{1}{\hat{r}})\ \hat{\varphi}_i^2(\hat{p}(\hat{x},\hat{y}))\ , & (\hat{x},\hat{y}) \in \hat{T}^1. \end{cases} \tag{3.2.91}$$

For $i \in \mathscr{I}_2$, the shape function $\hat{\varphi}_i$ is given by

$$\hat{\varphi}_i(\hat{x},\hat{y}) = \begin{cases} \hat{\varphi}_i^1(\hat{x},\hat{y}) = \displaystyle\sum_{j\in\mathscr{I}_2} c_j \hat{L}_j(\hat{x},\hat{y})\ , & (\hat{x},\hat{y}) \in \hat{T}^1, \\ \\ \hat{\varphi}_i^2(\hat{x},\hat{y}) = \hat{r}\ \hat{\varphi}_i^1(\hat{x},\hat{y}) + (1-\hat{r})\ \hat{\varphi}_i^1(\hat{p}(\hat{x},\hat{y}))\ , & (\hat{x},\hat{y}) \in \hat{T}^2, \end{cases} \tag{3.2.92}$$

with $\hat{r} = \frac{\hat{\beta}^1}{\hat{\beta}^2}$.

The coefficients c_j are determined by imposing the Lagrange nodal value conditions (3.2.1).

For $i \in \mathscr{I}_1$,imposing the Lagrange nodal value conditions (3.2.1) at $\hat{V}_j, j = 3, 6$, leads to the following linear system for $\mathbf{c} = (c_3, c_6)^t$

$$\mathbf{A}_1 \ \mathbf{c} \ = \ \mathbf{e}_{\delta(i)}, \qquad \text{with} \qquad \mathbf{A}_1 = \frac{1}{\hat{r}} \ \mathbf{I} + (1 - \frac{1}{\hat{r}}) \ \mathbf{M}_1, \tag{3.2.93}$$

where $\mathbf{e}_i$ is the canonical vector in $\mathbb{R}^2$, δ is the mapping defined by

$$\delta(3) = 1, \ \delta(6) = 2,$$

and $\mathbf{M}_1$ is the matrix defined in (3.2.20), with eigenvalues $\lambda_k \in [0, 1], \ k = 1, 2$, as shown in Lemma 3.2.4.

The eigenvalues of $\mathbf{A}_1$

$$\mu_k = \frac{1}{\hat{r}} + (1 - \frac{1}{\hat{r}}) \ \lambda_k \ , \quad k = 1, 2, \tag{3.2.94}$$

are bounded as

$$min(1, \frac{1}{\hat{r}}) \ \leq \ \mu_k \ \leq \ max(1, \frac{1}{\hat{r}}) \ , \qquad k = 1, 2. \tag{3.2.95}$$

Thus, $\mu_k > 0 \ , \ k = 1, 2$, and the system (3.2.93) has a unique solution.

For $i \in \mathscr{I}_2$, imposing the Lagrange nodal value conditions (3.2.1) at $\hat{V}_j, j = 1, 2, 4, 5$, leads to the following linear system for $\mathbf{c} = (c_1, c_2, c_4, c_5)^t$

$$\mathbf{A}_2 \ \mathbf{c} \ = \ \mathbf{e}_{\delta(i)}, \qquad \text{with} \qquad \mathbf{A}_2 = \hat{r} \ \mathbf{I} + (1 - \hat{r}) \ \mathbf{M}_2, \tag{3.2.96}$$

where $\mathbf{e}_i$ is the canonical vector in $\mathbb{R}^4$, δ is the mapping defined by

$$\delta(1) = 1, \ \delta(2) = 2, \ \delta(4) = 3, \ \delta(5) = 4,$$

and $\mathbf{M}_2$ is the matrix defined in (3.2.31), with eigenvalues $\lambda_k \in [0, 1], \ k = 1, \ldots, 4$, as shown in Lemma 3.2.4.

The eigenvalues of $\mathbf{A}_2$

$$\mu_k = \hat{r} + (1 - \hat{r}) \ \lambda_k \ , \quad k = 1, \ldots, 4, \tag{3.2.97}$$

are bounded as

$$min(1, \hat{r}) \ \leq \ \mu_k \ \leq \ max(1, \hat{r}) \ , \qquad k = 1, \ldots, 4. \tag{3.2.98}$$

Thus, $\mu_k > 0 \ , \ k = 1, \ldots, 4$, and the system (3.2.96) has a unique solution.

For elements of Type V we write the expressions of $\hat{\varphi}_i, \ i = 1, \ldots, 6$, as in (3.2.6) and (3.2.7), with $\mathscr{I}_1 = \{1\}$ and $\mathscr{I}_2 = \{2, 3, 4, 5, 6\}$, as illustrated in Figure 3.14. The shape function $\hat{\varphi}_1$

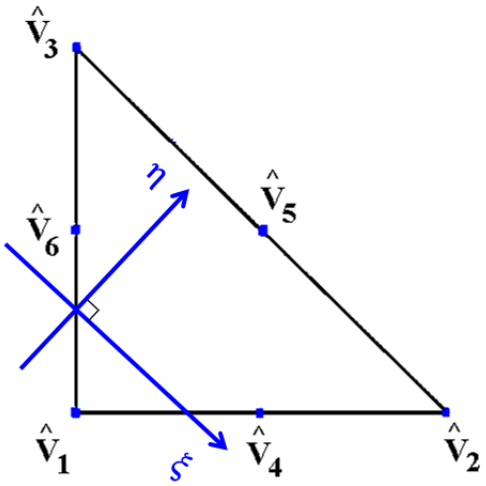

Figure 3.14: Interface coordinates system on the reference element of Type V with $\hat{\mathbf{n}}$ orthogonal to $\hat{\Gamma}$.

is given by

$$\hat{\varphi}_1(\hat{x},\hat{y}) = \begin{cases} \hat{\varphi}_1^2(\hat{x},\hat{y}) = c_1 \hat{L}_1(\hat{x},\hat{y}) \ , & (\hat{x},\hat{y}) \in \hat{T}^2, \\ \\ \hat{\varphi}_1^1(\hat{x},\hat{y}) = \frac{1}{\hat{r}}\ \hat{\varphi}_1^2(\hat{x},\hat{y}) + (1-\frac{1}{\hat{r}})\ \hat{\varphi}_1^2(\hat{p}(\hat{x},\hat{y})) \ , & (\hat{x},\hat{y}) \in \hat{T}^1. \end{cases} \tag{3.2.99}$$

For $i \in \mathscr{I}_2$, we can write the shape function $\hat{\varphi}_i$ as

$$\hat{\varphi}_i(\hat{x},\hat{y}) = \begin{cases} \hat{\varphi}_i^1(\hat{x},\hat{y}) = \displaystyle\sum_{j\in\mathscr{I}_2} c_j \hat{L}_j(\hat{x},\hat{y}) \ , & (\hat{x},\hat{y}) \in \hat{T}^1, \\ \\ \hat{\varphi}_i^2(\hat{x},\hat{y}) = \hat{r}\ \hat{\varphi}_i^1(\hat{x},\hat{y}) + (1-\hat{r})\ \hat{\varphi}_i^1(\hat{p}(\hat{x},\hat{y})) \ , & (\hat{x},\hat{y}) \in \hat{T}^2, \end{cases} \tag{3.2.100}$$

with $\hat{r} = \frac{\hat{\beta}^1}{\hat{\beta}^2}$.

Each shape function is in $\hat{\mathcal{R}}_2(\hat{T})$, and the constants c_j are determined by imposing the Lagrange nodal value conditions (3.2.1).

Hence, imposing the Lagrange nodal value conditions (3.2.1) to $\hat{\varphi}_1$ at $\hat{V}_1$, leads to one equation for c_1

$$\left(\frac{1}{\hat{r}} + (1-\frac{1}{\hat{r}})\lambda_6\right) c_1 = 1 \tag{3.2.101}$$

with $\lambda_6 = \hat{L}_1(\hat{p}(\hat{V}_1))$

By Lemma 3.2.5, we have $\lambda_6 \in [0,1]$, then

$$\frac{1}{\hat{r}} + (1-\frac{1}{\hat{r}})\lambda_6 \neq 0 \ ,$$

and we can solve for c_5,

$$c_5 = \frac{\hat{r}}{1 + (\hat{r} - 1)\lambda_6}.$$

For $i \in \mathscr{I}_2$, imposing the Lagrange nodal value conditions (3.2.1) at $\hat{V}_j, j = 2, 3, 4, 5, 6$, leads to the following linear system for $\mathbf{c} = (c_2, c_3, c_4, c_5, c_6)^t$

$$\mathbf{A}_2 \ \mathbf{c} \ = \ \mathbf{e}_{\delta(i)}, \qquad \text{with} \qquad \mathbf{A}_2 = \hat{r} \ \mathbf{I} + (1 - \hat{r}) \ \mathbf{M}_2, \tag{3.2.102}$$

where $\mathbf{e}_i$ is the canonical vector in $\mathbb{R}^5$, δ is the mapping defined by

$$\delta(2) = 1, \ \delta(3) = 2, \ \delta(4) = 3, \ \delta(5) = 4, \ \delta(6) = 5,$$

and $\mathbf{M}_2$ is the matrix defined in (3.2.40), with eigenvalue $\lambda_k \in [0, 1], \ k = 1, \ldots, 5$, as shown in Lemma 3.2.5.

The eigenvalues of the matrix $\mathbf{A}_2$

$$\mu_k = \hat{r} + (1 - \hat{r}) \ \lambda_k \ , \quad k = 1, \ldots, 5, \tag{3.2.103}$$

are bounded as

$$min(1, \hat{r}) \ \leq \ \mu_k \ \leq \ max(1, \hat{r}) \ , \qquad k = 1, \ldots, 5. \tag{3.2.104}$$

Thus, $\mu_k > 0 \ , \ k = 1, \ldots, 5$, and the system (3.2.102) has a unique solution.

For elements of Type VI, we write the expressions of $\hat{\varphi}_i, \ i = 1, \ldots, 6$, as in (3.2.6) and (3.2.7), with $\mathscr{I}_1 = \{1, 4\}$ and $\mathscr{I}_2 = \{2, 3, 5, 6\}$, as illustrated in Figure 3.15. For $i \in \mathscr{I}_1$, the shape function $\hat{\varphi}_i$ is given by

$$\hat{\varphi}_i(\hat{x}, \hat{y}) = \begin{cases} \hat{\varphi}_i^2(\hat{x}, \hat{y}) = \displaystyle\sum_{j \in \mathscr{I}_1} c_j \hat{L}_j(\hat{x}, \hat{y}) \ , & (\hat{x}, \hat{y}) \in \hat{T}^2, \\ \\ \hat{\varphi}_i^1(\hat{x}, \hat{y}) = \frac{1}{\hat{r}} \ \hat{\varphi}_i^2(\hat{x}, \hat{y}) + (1 - \frac{1}{\hat{r}}) \ \hat{\varphi}_i^2(\hat{p}(\hat{x}, \hat{y})) \ , & (\hat{x}, \hat{y}) \in \hat{T}^1. \end{cases} \tag{3.2.105}$$

For $i \in \mathscr{I}_2$, the shape function $\hat{\varphi}_i$ is given by

$$\hat{\varphi}_i(\hat{x}, \hat{y}) = \begin{cases} \hat{\varphi}_i^1(\hat{x}, \hat{y}) = \displaystyle\sum_{j \in \mathscr{I}_2} c_j \hat{L}_j(\hat{x}, \hat{y}) \ , & (\hat{x}, \hat{y}) \in \hat{T}^1, \\ \\ \hat{\varphi}_i^2(\hat{x}, \hat{y}) = \hat{r} \ \hat{\varphi}_i^1(\hat{x}, \hat{y}) + (1 - \hat{r}) \ \hat{\varphi}_i^1(\hat{p}(\hat{x}, \hat{y})) \ , & (\hat{x}, \hat{y}) \in \hat{T}^2, \end{cases} \tag{3.2.106}$$

with $\hat{r} = \frac{\hat{\beta}^1}{\hat{\beta}^2}$.

The coefficients c_j are determined by imposing the Lagrange nodal value conditions (3.2.1).

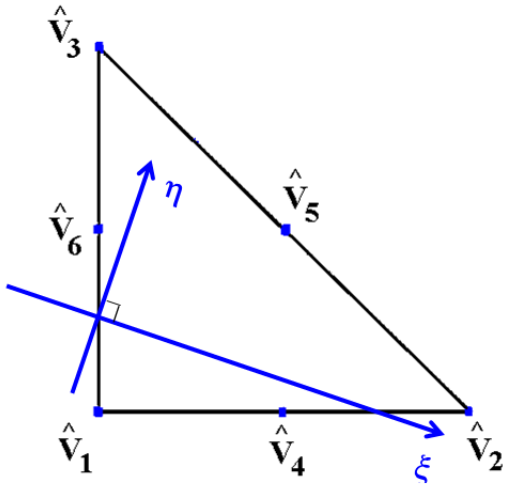

Figure 3.15: Interface coordinates system on the reference element of Type VI with $\hat{\mathbf{n}}$ orthogonal to $\hat{\Gamma}$.

For $i \in \mathscr{I}_1$, imposing the Lagrange nodal value conditions (3.2.1) at $\hat{V}_j, j = 1, 4$, leads to the following linear system for $\mathbf{c} = (c_1, c_4)^t$

$$\mathbf{A}_1 \ \mathbf{c} \ = \ \mathbf{e}_{\delta(i)}, \qquad \text{with} \qquad \mathbf{A}_1 = \frac{1}{\hat{r}} \ \mathbf{I} + (1 - \frac{1}{\hat{r}}) \ \mathbf{M}_1, \tag{3.2.107}$$

where $\mathbf{e}_i$ is the canonical vector in $\mathbb{R}^2$, δ is the mapping defined by

$$\delta(1) = 1, \ \delta(4) = 2,$$

and $\mathbf{M}_1$ is the matrix defined in (3.2.52), with eigenvalues $\lambda_k \in [0, 1], \ k = 1, 2$, as shown in Lemma 3.2.6.

The eigenvalues of $\mathbf{A}_1$

$$\mu_k = \frac{1}{\hat{r}} + (1 - \frac{1}{\hat{r}}) \ \lambda_k \ , \quad k = 1, 2, \tag{3.2.108}$$

are bounded as

$$min(1, \frac{1}{\hat{r}}) \ \leq \ \mu_k \ \leq \ max(1, \frac{1}{\hat{r}}) \ , \qquad k = 1, 2. \tag{3.2.109}$$

Thus, $\mu_k > 0 \ , \ k = 1, 2$, and the system (3.2.107) has a unique solution.

For $i \in \mathscr{I}_2$, imposing the Lagrange nodal value conditions (3.2.1) at $\hat{V}_j, j = 2, 3, 5, 6$, leads to the following linear system for $\mathbf{c} = (c_2, c_3, c_5, c_6)^t$

$$\mathbf{A}_2 \ \mathbf{c} \ = \ \mathbf{e}_{\delta(i)}, \qquad \text{with} \qquad \mathbf{A}_2 = \hat{r} \ \mathbf{I} + (1 - \hat{r}) \ \mathbf{M}_2, \tag{3.2.110}$$

where $\mathbf{e}_i$ is the canonical vector in $\mathbb{R}^4$, δ is the mapping defined by

$$\delta(2) = 1,\ \delta(3) = 2,\ \delta(5) = 3,\ \delta(6) = 4,$$

and $\mathbf{M}_2$ is the matrix defined in (3.2.51), with eigenvalues $\lambda_k \in [0,1],\ k = 1,\ldots,4$, as shown in Lemma 3.2.6.

The eigenvalues of $\mathbf{A}_2$

$$\mu_k = \hat{r} + (1-\hat{r})\ \lambda_k\ , \quad k = 1,\ldots,4, \tag{3.2.111}$$

are bounded as

$$min(1,\hat{r})\ \leq\ \mu_k\ \leq\ max(1,\hat{r})\ , \qquad k = 1,\ldots,4. \tag{3.2.112}$$

Thus, $\mu_k > 0\ ,\ k = 1,\ldots,4$, and the system (3.2.110) has a unique solution.

For elements of Type VII, we write the expressions of $\hat{\varphi}_i,\ i = 1,\ldots,6$, as in (3.2.6) and (3.2.7), with $\mathscr{I}_1 = \{1,4,6\}$ and $\mathscr{I}_2 = \{2,3,5\}$, as illustrated in Figure 3.16. For $i \in \mathscr{I}_1$, the

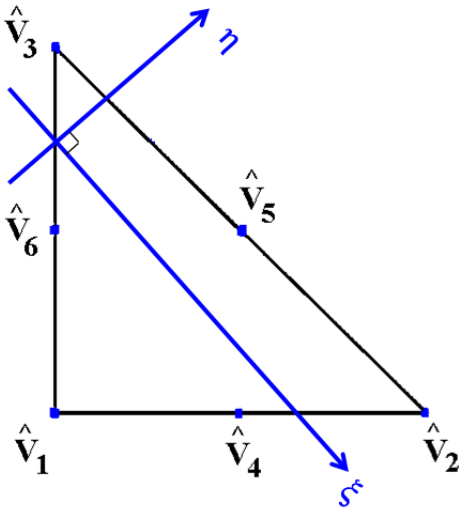

Figure 3.16: Interface coordinates system on the reference element of Type VII with $\hat{\mathbf{n}}$ orthogonal to $\hat{\Gamma}$.

shape function $\hat{\varphi}_i$ is given by

$$\hat{\varphi}_i(\hat{x},\hat{y}) = \begin{cases} \hat{\varphi}_i^2(\hat{x},\hat{y}) = \displaystyle\sum_{j\in\mathscr{I}_1} c_j \hat{L}_j(\hat{x},\hat{y})\ , & (\hat{x},\hat{y}) \in \hat{T}^2, \\ \\ \hat{\varphi}_i^1(\hat{x},\hat{y}) = \frac{1}{\hat{r}}\ \hat{\varphi}_i^2(\hat{x},\hat{y}) + (1-\frac{1}{\hat{r}})\ \hat{\varphi}_i^2(\hat{p}(\hat{x},\hat{y}))\ , & (\hat{x},\hat{y}) \in \hat{T}^1. \end{cases} \tag{3.2.113}$$

For $i \in \mathscr{I}_2$, the shape function $\hat{\varphi}_i$ is given by

$$\hat{\varphi}_i(\hat{x},\hat{y}) = \begin{cases} \hat{\varphi}_i^1(\hat{x},\hat{y}) = \sum_{j\in\mathscr{I}_2} c_j \hat{L}_j(\hat{x},\hat{y}) \ , & (\hat{x},\hat{y}) \in \hat{T}^1, \\ \\ \hat{\varphi}_i^2(\hat{x},\hat{y}) = \hat{r}\ \hat{\varphi}_i^1(\hat{x},\hat{y}) + (1-\hat{r})\ \hat{\varphi}_i^1(\hat{p}(\hat{x},\hat{y})) \ , & (\hat{x},\hat{y}) \in \hat{T}^2, \end{cases} \tag{3.2.114}$$

with $\hat{r} = \frac{\hat{\beta}^1}{\hat{\beta}^2}$.

The coefficients c_j are determined by imposing the Lagrange nodal value conditions (3.2.1).

For $i \in \mathscr{I}_1$, imposing the Lagrange nodal value conditions (3.2.1) at $\hat{V}_j, j = 1,4,6$, leads to the following linear system for $\mathbf{c} = (c_1, c_4, c_6)^t$

$$\mathbf{A}_1\ \mathbf{c}\ =\ \mathbf{e}_{\delta(i)}, \qquad \text{with} \qquad \mathbf{A}_1 = \frac{1}{\hat{r}}\ \mathbf{I} + (1-\frac{1}{\hat{r}})\ \mathbf{M}_1, \tag{3.2.115}$$

where $\mathbf{e}_i$ is the canonical vector in $\mathbb{R}^3$, δ is the mapping defined by

$$\delta(1) = 1,\ \delta(4) = 2,\ \delta(6) = 3,$$

and $\mathbf{M}_1$ is the matrix defined in (3.2.61), with eigenvalues $\lambda_k \in [0,1],\ k = 1,2$, as shown in Lemma 3.2.7.

The eigenvalues of $\mathbf{A}_1$

$$\mu_k = \frac{1}{\hat{r}} + (1-\frac{1}{\hat{r}})\ \lambda_k \ , \quad k = 1,2, \tag{3.2.116}$$

are bounded as

$$min(1,\frac{1}{\hat{r}})\ \leq\ \mu_k\ \leq\ max(1,\frac{1}{\hat{r}}) \ , \qquad k = 1,2. \tag{3.2.117}$$

Thus, $\mu_k > 0\ ,\ k = 1,2$, and the system (3.2.115) has a unique solution.

For $i \in \mathscr{I}_2$,imposing the Lagrange nodal value conditions (3.2.1) at $\hat{V}_j, j = 2,3,5$, leads to the following linear system for $\mathbf{c} = (c_2, c_3, c_5)^t$

$$\mathbf{A}_2\ \mathbf{c}\ =\ \mathbf{e}_{\delta(i)}, \qquad \text{with} \qquad \mathbf{A}_2 = \hat{r}\ \mathbf{I} + (1-\hat{r})\ \mathbf{M}_2, \tag{3.2.118}$$

where $\mathbf{e}_i$ is the canonical vector in $\mathbb{R}^3$, δ is the mapping defined by

$$\delta(2) = 1,\ \delta(3) = 2,\ \delta(5) = 3,$$

and $\mathbf{M}_2$ is the matrix defined in (3.2.60), with eigenvalues $\lambda_k \in [0,1],\ k = 1,\ldots,3$, as shown in Lemma 3.2.7.

The eigenvalues of $\mathbf{A}_2$

$$\mu_k = \hat{r} + (1-\hat{r})\ \lambda_k \ , \quad k = 1,2,3, \tag{3.2.119}$$

are bounded as

$$min(1, \hat{r}) \ \leq \ \mu_k \ \leq \ max(1, \hat{r}) \ , \qquad k = 1, \ldots, 3. \tag{3.2.120}$$

Thus, $\mu_k > 0 \ , \ k = 1, \ldots, 3$, and the system (3.2.118) has a unique solution.

□

Corollary 3.2.1. *Under the assumptions of Theorem 3.2.1, the shape functions $\hat{\varphi}_i \in \hat{\mathcal{R}}_2(\hat{T}),\ i = 1, \ldots, 6$, satisfying the Lagrange nodal value conditions $\hat{\varphi}_i(\hat{V}_j) = \delta_{ij},\ i, j = 1, \ldots, 6$, form a basis of $\hat{\mathcal{R}}_2(\hat{T})$.*

Proof. The conditions $\hat{\varphi}_i(\hat{V}_j) = \delta_{ij},\ i, j = 1, \ldots, 6$, trivially implies the independency of the shape functions $\hat{\varphi}_i,\ i = 1, \ldots, 6$. Since the dimension of $\hat{\mathcal{R}}_2(\hat{T})$ is equal to 6, then the result follows. □

Corollary 3.2.2. *Under the assumptions of Theorem 3.2.1, $\hat{\varphi}_i,\ i = 1, \ldots, 6$, form a partition of unity for the space $\hat{\mathcal{R}}_2(\hat{T})$, i.e.*

$$\sum_{i=1}^{6} \hat{\varphi}_i(\hat{x}, \hat{y}) = 1, \qquad \forall (\hat{x}, \hat{y}) \in \hat{T}. \tag{3.2.121}$$

Proof. Let $\hat{\varphi}_i,\ i = 1, \ldots, 6$, be the Lagrange basis of $\hat{\mathcal{R}}_2(\hat{T})$. Since the constant function $\hat{\varphi}_0(\hat{x}, \hat{y}) = 1$ is in $\hat{\mathcal{R}}_2(\hat{T})$, then, there exists $d_i,\ i = 1, \ldots, 6$, such that

$$1 = \sum_{i=1}^{6} d_i \hat{\varphi}_i(\hat{x}, \hat{y}). \tag{3.2.122}$$

Since $\hat{\varphi}_i(\hat{V}_j) = \delta_{ij},\ i, j = 1, \ldots, 6$, then evaluating equation (3.2.122) at $\hat{V}_j$ implies

$$1 = d_j, \qquad j = 1, \ldots, 6, \tag{3.2.123}$$

which completes the proof. □

Now, we will prove the existence of a basis $\hat{\varphi}_i,\ i = 1, \ldots, 6$, for $\mathcal{R}_2(T)$, on any isosceles right triangle interface element T.

Corollary 3.2.3. *Let T be an isosceles right triangular interface element with nodes $V_i,\ i = 1, \ldots, 6$. The Lagrange nodal value conditions $\varphi_i(V_j) = \delta_{ij},\ j = 1, \ldots, 6$, uniquely determine a basis $\varphi_i,\ i = 1, \ldots, 6$, of $\mathcal{R}_2(T)$.*

Proof. T can be mapped, using the mapping F defined in (2.2.7) to a reference interface element $\hat{T}$ which represents one of the 7 types described in Table 3.2, and such that the

mapping F is the composition of a translation t, a rotation r, a dilation d, and a reflection l. Hence, F can be written as

$$F = t \circ r \circ d \circ l \ .$$

Since the all transformations t, r, d, and l preserve the right angle, the mapped normal $\hat{\boldsymbol{n}}$ is orthogonal to the mapped interface $\hat{\Gamma}$.

From Theorem 3.2.1, we conclude the existence of six shape functions $\hat{\varphi}_i,\ i = 1, \ldots, 6$, in $\hat{\mathcal{R}}_2(\hat{T})$ that are uniquely determined by the Lagrange nodal value conditions. Since $dim(\mathcal{R}_2(T)) = 6$, and the shape functions

$$\varphi_i(x, y) = \hat{\varphi}_i(F(x, y)) \in \mathcal{R}_2(T), \quad i = 1, \ldots, 6,$$

are linearly independent, thus, they form a basis of $\mathcal{R}_2(T)$.

□

We note that the assumption of uniform meshes with isosceles right triangular elements is an acceptable assumption, since the IFE method is generally used (in practical applications) with Cartesian meshes. Thus, following the standard procedure for constructing global finite element basis functions, we apply Corollary 3.2.3 to show the existence of global IFE basis function for the space $\mathcal{S}_h^2$ on uniform meshes with isosceles right angle elements. In the next section we give few examples of such global IFE basis functions.

3.2.3 Examples of Lagrange IFE Basis Functions

We consider a mesh with two triangular elements over the domain $\Omega = (0, 1)^2$ cut by the linear interface $y = \frac{1}{2}x + \frac{1}{5}$ to two sub-domains $\Omega^+ = \{(x, y) \mid y > \frac{1}{2}x + \frac{1}{5}\}$ and $\Omega^- = \{(x, y) \mid y < \frac{1}{2}x + \frac{1}{5}\}$ as illustrated in Figure 3.17, with $r = \frac{\beta^+}{\beta^-} = 5$.

We present six Lagrange global immersed basis functions $\psi_i,\ i = 1, \ldots, 6$, defined on this mesh, in Figures 3.18 and 3.19. We see that the global IFE basis functions are continuous across non-interface edges while, in general, on interface edges they are continuous only at the two vertices of the edge and at its midpoint.

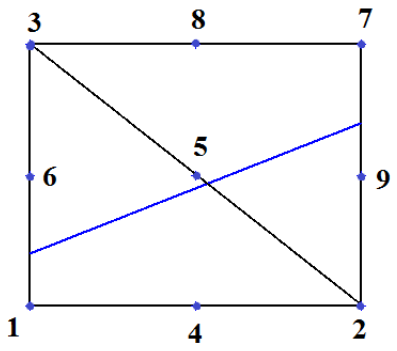

Figure 3.17: A mesh having two elements for $\Omega = (0,1)^2$ cut by the interface $y = \frac{x}{2} + \frac{1}{5}$ with $r = 5$.

3.3 Hierarchical Quadratic IFE Shape Functions

The idea and the construction of hierarchical shape functions was treated in the late 1970's by Piano, as a way for p-extensions [53, 54, 55], and by Szabo and Babuska [61]. Later, other published work treated new hierarchical finite element bases such as Shephard, Dey and Flaherty [59], and hierarchical finite elements bases on triangular elements such as Adjerid, Aiffa and Flaherty [1].

A hierarchical basis of degree $p+1$ is considered as a correction of the basis of degree p. Hence, the finite element space is enriched by adding new shape functions to the existing ones, without changing them nor the degrees of freedom, but just add new shape functions. Thus, when increasing the polynomial degree, the whole basis need not to be reconstructed. Only a set of functions of degree $p+1$ is added to the basis of degree p. This property is very desirable and essential, especially in the case of p refinement [1].

Hierarchical shape functions on triangular meshes are classified into three categories: nodal shape functions, side modes, and internal modes [61]. For standard finite elements of degree p, we have :

- Nodal shape functions : which are the same as the three linear shape functions of Lagrange type.
- Side modes : which are $3(p-1)$ functions. They are non zero on one edge of the triangle, and vanish on the other two edges.
- Internal modes : which are $\frac{(p-1)(p-2)}{2}$ functions. The first one, $N_1^{(0)}$ is the product of the three nodal shape functions, and the others are the products of $N_1^{(0)}$ by Legendre polynomials and products of Legendre polynomials.

For the immersed finite elements, the idea is the same and the number of nodal shape functions, side modes, and internal modes is the same, however the shape functions are

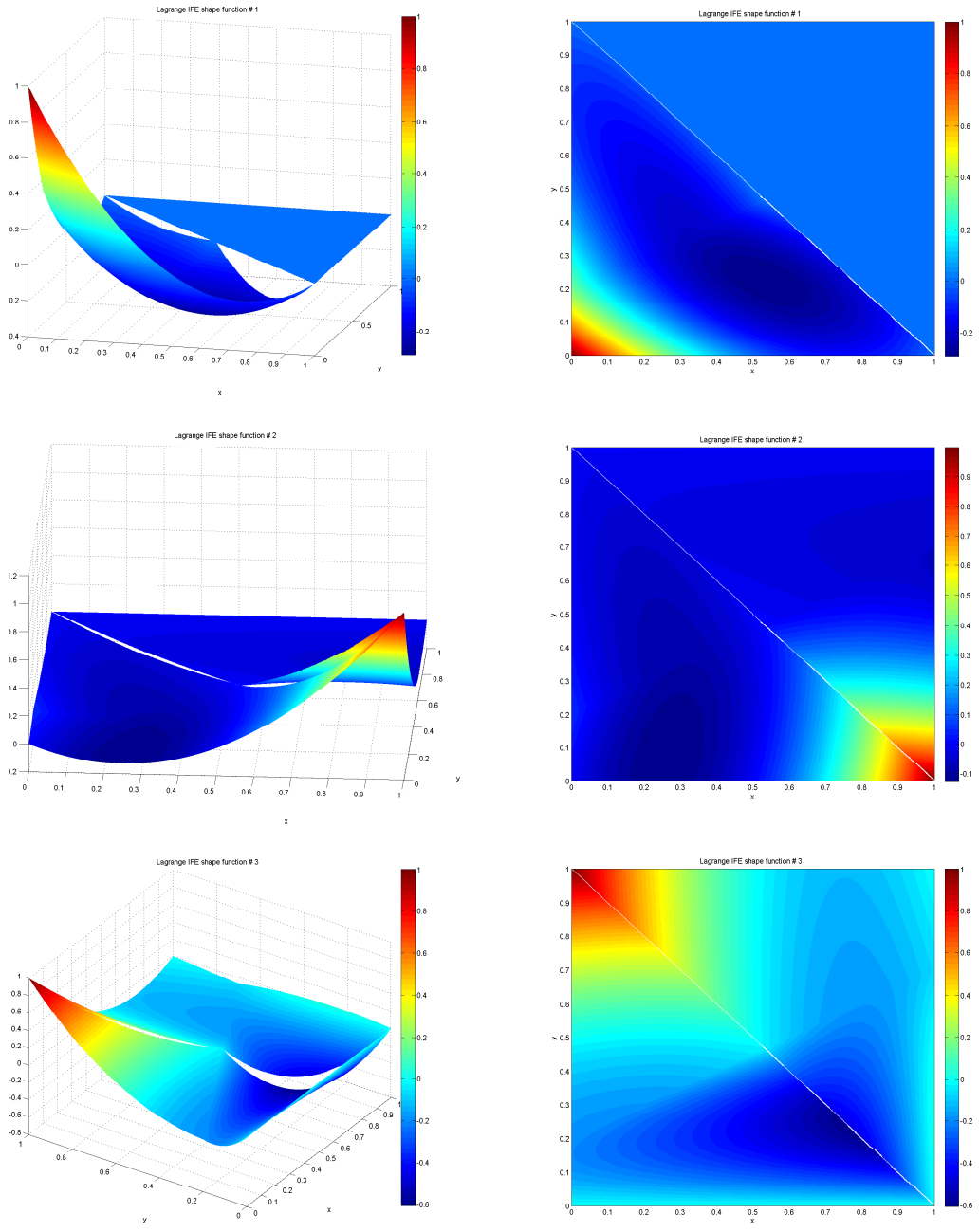

Figure 3.18: Lagrange immersed basis functions $\psi_i,\ i = 1, \ldots, 3$ (respectively from the top to the bottom) on the 2 elements mesh in Figure 3.17.

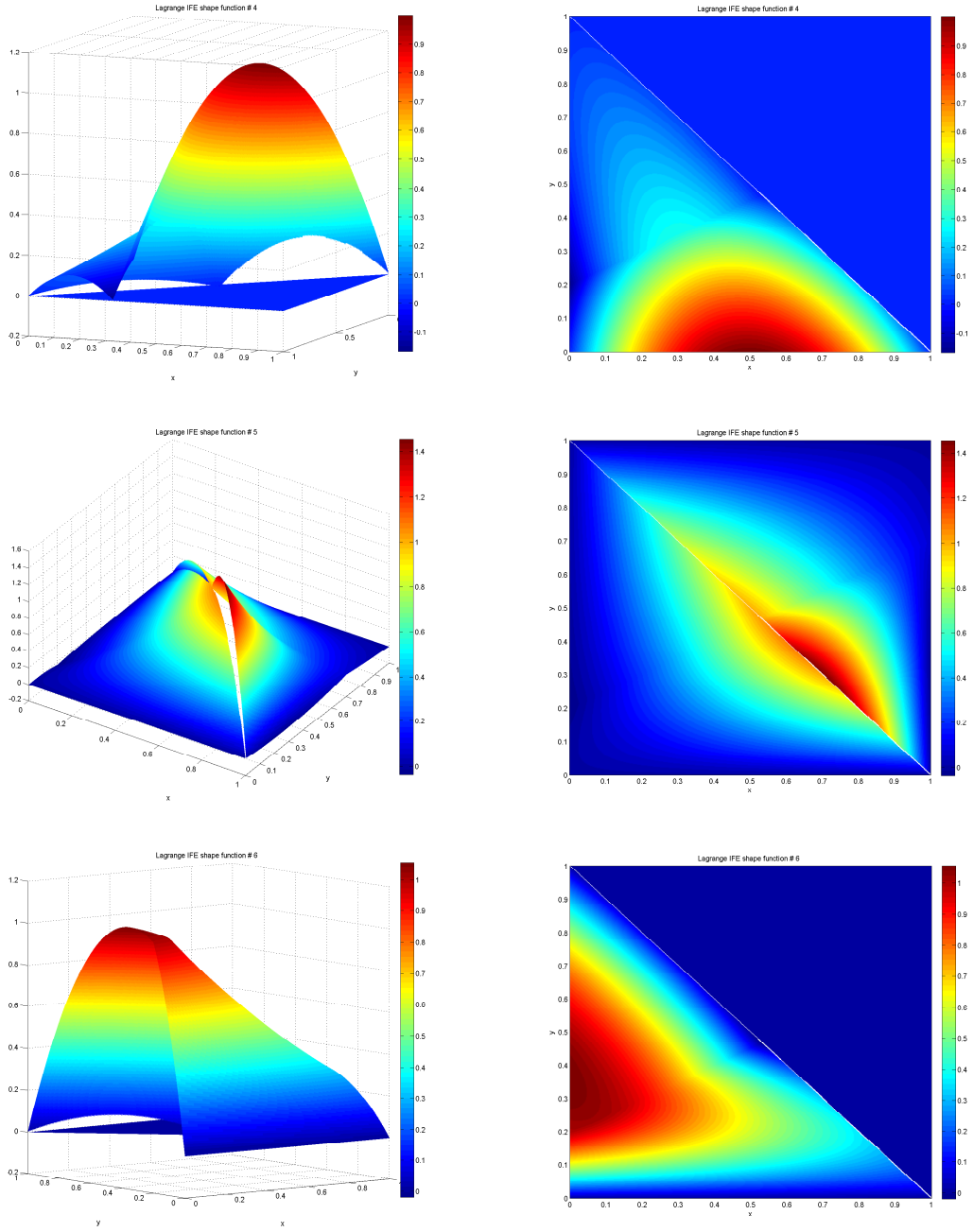

Figure 3.19: Lagrange immersed basis functions $\psi_i,\ i = 4, \ldots, 6$ (respectively from the top to the bottom) on the 2 elements mesh in Figure 3.17.

piecewise polynomials, taking into consideration the interface jump conditions. Hierarchical IFE shape functions in one-dimension have been developed by Adjerid and Lin [3].

As mentioned above, the main advantage of hierarchical shape functions is their efficiency in p refinement, since the whole basis need not to be reconstructed, when the degree of the finite element increases. Another advantage of hierarchical bases appears when solving the finite element problem. In fact, hierarchical bases lead to systems with stiffness matrices having a controllable condition number. This is due to the orthogonality properties of the hierarchical shape functions in one-dimension, and in two-dimensions with rectangular meshes. Although, hierarchical shape functions in two-dimensions with triangular meshes may lead to stiffness matrices with condition number that grows exponentially with p-refinement, Adjerid, Aiffa and Flaherty [1] showed that this problem can be overcame by reducing the coupling between the face and region shape functions through orthogonalization. Hence, stiffness matrices with condition numbers that have a quadratic growth with degree p, are obtained.

3.3.1 Linear IFE Shape Functions

We consider a reference interface element $\hat{T}$ with vertices $\hat{V}_1 = (0,0)^t,\ \hat{V}_2 = (1,0)^t,\ \hat{V}_3 = (0,1)^t$, cut by the interface $\hat{\Gamma}$. Li, Lin, Lin and Rogers [42] showed that there exist three piecewise linear IFE shape functions $\hat{\varphi}_i,\ i = 1,2,3$, which are uniquely determined by the Lagrange nodal value conditions (3.2.1):

$$\hat{\varphi}_i(\hat{V}_j) = \delta_{ij},\ j = 1,2,3,$$

and the physical jump conditions on the reference element (2.2.9):

$$[\hat{\varphi}_i]_{\hat{\Gamma}} = 0,$$

$$[\hat{\beta}\ \frac{\partial \hat{\varphi}_i}{\partial \hat{\boldsymbol{n}}}]_{\hat{\Gamma}} = 0.$$

We note that these linear IFE shape functions $\hat{\varphi}_i,\ i = 1,2,3$, belong to both quadratic IFE spaces $\hat{\mathcal{R}}_1(\hat{T})$ and $\hat{\mathcal{R}}_2(\hat{T})$. For completeness, we recall their expressions, according to Li, Lin, Lin and Rogers [42]. These shape functions are defined on any reference interface element of the three types illustrated in Figure 2.2. We let $\hat{D}$ and $\hat{E}$ the intersection points of the interface with the sides of the reference triangle, and we call $(0, \hat{y}_1)$ the coordinates of the point $\hat{E}$ and $(1-\hat{y}_2, \hat{y}_2)$ the coordinates of the point $\hat{D}$. We recall also that the physical normal is mapped to $\hat{\boldsymbol{n}} = \mathbf{J}\boldsymbol{n} = (\hat{n}_x, \hat{n}_y)^t$. Then, according to [42], $\hat{\varphi}_i,\ i = 1,2,3$, can be written as:

$$\hat{\varphi}_1(\hat{\xi},\hat{\eta}) = \begin{cases} \hat{a}_{11}\hat{x} + \hat{a}_{21}(\hat{y}-1) & ,\quad (\hat{x},\hat{y}) \in \hat{T}^1, \\ \\ 1 - \hat{x} + \hat{b}_{21}\hat{y} & ,\quad (\hat{x},\hat{y}) \in \hat{T}^2, \end{cases} \tag{3.3.1a}$$

$$\hat{\varphi}_2(\hat{\xi},\hat{\eta}) = \begin{cases} \hat{a}_{12}\hat{x} + \hat{a}_{22}(\hat{y}-1) & , \quad (\hat{x},\hat{y}) \in \hat{T}^1, \\ \hat{x} + \hat{b}_{22}\hat{y} & , \quad (\hat{x},\hat{y}) \in \hat{T}^2, \end{cases} \tag{3.3.1b}$$

$$\hat{\varphi}_3(\hat{\xi},\hat{\eta}) = \begin{cases} 1 + \hat{a}_{13}\hat{x} + \hat{a}_{23}(\hat{y}-1) & , \quad (\hat{x},\hat{y}) \in \hat{T}^1, \\ \hat{b}_{23}\hat{y} & , \quad (\hat{x},\hat{y}) \in \hat{T}^2, \end{cases} \tag{3.3.1c}$$

with

$$a_{1i} = \begin{cases} \frac{\alpha(1-\hat{r})}{\hat{y}_1+\hat{a}\alpha+\hat{r}(1-\hat{y}_1)}, & i=1, \\ \frac{-(1+\hat{a}\alpha)\hat{r}+(1+\alpha)(\hat{r}-1)\hat{y}_2}{\hat{y}_1+\hat{a}\alpha+\hat{r}(1-\hat{y}_1)}, & i=2, \\ \frac{\hat{r}+\alpha(-1+\hat{r}+\hat{a}\hat{r}-(1+\alpha)(\hat{r}-1)\hat{y}_2}{\hat{y}_1+\hat{a}\alpha+\hat{r}(1-\hat{y}_1)}, & i=3, \end{cases} \tag{3.3.2a}$$

$$a_{2i} = \begin{cases} \frac{\hat{a}\alpha+\hat{r}}{\hat{y}_1+\hat{a}\alpha+\hat{r}(1-\hat{y}_1)}, & i=1, \\ \frac{-(1+\hat{a}\alpha)\hat{r}+\hat{a}(1+\alpha)(\hat{r}-1)\hat{y}_2}{\hat{y}_1+\hat{a}\alpha+\hat{r}(1-\hat{y}_1)}, & i=2, \\ -\frac{\hat{a}(-1+\hat{r})+(-\alpha+(1+\alpha)\hat{y}_2}{\hat{y}_1+\hat{a}\alpha+\hat{r}(1-\hat{y}_1)}, & i=3, \end{cases} \tag{3.3.2b}$$

$$b_{2i} = \begin{cases} \frac{\hat{a}\alpha+1}{\hat{y}_1+\hat{a}\alpha+\hat{r}(1-\hat{y}_1)}, & i=1, \\ \frac{-1-\hat{a}(-1+\hat{r}+\alpha\hat{r})+\hat{a}(1+\alpha)(\hat{r}-1)\hat{y}_2}{\hat{y}_1+\hat{a}\alpha+\hat{r}(1-\hat{y}_1)}, & i=2, \\ -\frac{\hat{a}(1+\alpha)(-1+\hat{r})+(-1+\hat{y}_2}{\hat{y}_1+\hat{a}\alpha+\hat{r}(1-\hat{y}_1)}, & i=3, \end{cases} \tag{3.3.2c}$$

and

$$\alpha = \frac{\hat{y}_2 - \hat{y}_1}{1-\hat{y}_2}, \tag{3.3.2d}$$

$$\hat{a} = -\frac{\hat{n}_x}{\hat{n}_y}, \tag{3.3.2e}$$

$$\hat{r} = \frac{\hat{\beta}^2}{\hat{\beta}^1}. \tag{3.3.2f}$$

Next, we construct three quadratic IFE edge shape functions $\hat{\varphi}_4$, $\hat{\varphi}_5$, and $\hat{\varphi}_6$ on the reference interface element, for each of the spaces $\hat{\mathcal{R}}_1(\hat{T})$ and $\hat{\mathcal{R}}_2(\hat{T})$. To construct these three IFE edge shape functions, we use the coordinates $(\hat{\xi},\hat{\eta})$ defined in (3.2.3), as previously illustrated in Figure 3.1.

3.3.2 Hierarchical Shape Functions on $\hat{\mathcal{R}}_2(\hat{T})$

Guided by hierarchical quadratic shape functions for the standard finite elements [61], we write the IFE edge shape functions $\hat{\varphi}_4$, $\hat{\varphi}_5$, and $\hat{\varphi}_6$ as

$$\hat{\varphi}_4(\hat{\xi},\hat{\eta}) = \begin{cases} \hat{\varphi}_1^1(\hat{\xi},\hat{\eta})\hat{\varphi}_2^1(\hat{\xi},\hat{\eta}) + \hat{c}_4\hat{\eta}^2 \ , & (\hat{x},\hat{y}) \in \hat{T}^1, \\ \hat{\varphi}_1^2(\hat{\xi},\hat{\eta})\hat{\varphi}_2^2(\hat{\xi},\hat{\eta}) \ , & (\hat{x},\hat{y}) \in \hat{T}^2, \end{cases} \tag{3.3.3a}$$

$$\hat{\varphi}_5(\hat{\xi},\hat{\eta}) = \begin{cases} \hat{\varphi}_2^1(\hat{\xi},\hat{\eta})\hat{\varphi}_3^1(\hat{\xi},\hat{\eta}) + \hat{c}_5\hat{\eta}^2 \ , & (\hat{x},\hat{y}) \in \hat{T}^1, \\ \hat{\varphi}_2^2(\hat{\xi},\hat{\eta})\hat{\varphi}_3^2(\hat{\xi},\hat{\eta}) \ , & (\hat{x},\hat{y}) \in \hat{T}^2, \end{cases} \tag{3.3.3b}$$

$$\hat{\varphi}_6(\hat{\xi},\hat{\eta}) = \begin{cases} \hat{\varphi}_1^1(\hat{\xi},\hat{\eta})\hat{\varphi}_3^1(\hat{\xi},\hat{\eta}) + \hat{c}_6\hat{\eta}^2 \ , & (\hat{x},\hat{y}) \in \hat{T}^1, \\ \hat{\varphi}_1^2(\hat{\xi},\hat{\eta})\hat{\varphi}_3^2(\hat{\xi},\hat{\eta}) \ , & (\hat{x},\hat{y}) \in \hat{T}^2, \end{cases} \tag{3.3.3c}$$

where $\hat{c}_4,\ \hat{c}_5,$ and $\hat{c}_6$, are selected such that (2.2.17) is satisfied:

$$[\hat{\beta}\ \frac{\partial^2\hat{\varphi}_k}{\partial\hat{\boldsymbol{n}}^2}]_{\hat{\Gamma}} = 0, \qquad k = 4,5,6.$$

First, we recall that according to the definition of $\hat{\eta}$ in (3.2.3), we have

$$\frac{\partial}{\partial\hat{\eta}} = \frac{\partial}{\partial\hat{\boldsymbol{n}}}.$$

Hence, the derivative of $\hat{\varphi}_k,\ k = 4,5,6$, in the direction of $\hat{\boldsymbol{n}}$ can be written as

$$\frac{\partial\hat{\varphi}_k}{\partial\hat{\boldsymbol{n}}}(\hat{\xi},\hat{\eta}) = \begin{cases} \frac{\partial\hat{\varphi}_i^1}{\partial\hat{\boldsymbol{n}}}(\hat{\xi},\hat{\eta})\ \hat{\varphi}_j^1(\hat{\xi},\hat{\eta}) + \hat{\varphi}_i^1(\hat{\xi},\hat{\eta})\ \frac{\partial\hat{\varphi}_j^1}{\partial\hat{\boldsymbol{n}}}(\hat{\xi},\hat{\eta}) + 2\hat{c}_k\hat{\eta} \ , & (\hat{x},\hat{y}) \in \hat{T}^1, \\ \frac{\partial\hat{\varphi}_i^2}{\partial\hat{\boldsymbol{n}}}(\hat{\xi},\hat{\eta})\ \hat{\varphi}_j^2(\hat{\xi},\hat{\eta}) + \hat{\varphi}_i^2(\hat{\xi},\hat{\eta})\ \frac{\partial\hat{\varphi}_j^2}{\partial\hat{\boldsymbol{n}}}(\hat{\xi},\hat{\eta}) \ , & (\hat{x},\hat{y}) \in \hat{T}^2, \end{cases} \tag{3.3.4}$$

where i and j are such that $\hat{V}_k$ is the mid-point of the edge $\hat{V}_i\ \hat{V}_j$.

Since the second derivatives of $\hat{\varphi}_1$, $\hat{\varphi}_2$ and $\hat{\varphi}_3$ are equal to zero , then the second derivative of $\hat{\varphi}_k,\ k = 4,5,6$, in the direction of $\hat{\boldsymbol{n}}$ can be written as

$$\frac{\partial^2\hat{\varphi}_k}{\partial\hat{\boldsymbol{n}}^2}(\hat{\xi},\hat{\eta}) = \begin{cases} 2\ \frac{\partial\hat{\varphi}_i^1}{\partial\hat{\boldsymbol{n}}}(\hat{\xi},\hat{\eta})\frac{\partial\hat{\varphi}_j^1}{\partial\hat{\boldsymbol{n}}}(\hat{\xi},\hat{\eta}) + 2\ \hat{c}_k \ , & (\hat{x},\hat{y}) \in \hat{T}^1, \\ 2\ \frac{\partial\hat{\varphi}_i^2}{\partial\hat{\boldsymbol{n}}}(\hat{\xi},\hat{\eta})\frac{\partial\hat{\varphi}_j^2}{\partial\hat{\boldsymbol{n}}}(\hat{\xi},\hat{\eta}) \ , & (\hat{x},\hat{y}) \in \hat{T}^2, \end{cases} \tag{3.3.5}$$

Enforcing the jump condition (2.2.17) yields

$$\hat{\beta}^1 \frac{\partial \hat{\varphi}_i^1}{\partial \hat{\boldsymbol{n}}}(\hat{\xi}, 0^+) \frac{\partial \hat{\varphi}_j^1}{\partial \hat{\boldsymbol{n}}}(\hat{\xi}, 0^+) + \ \hat{\beta}^1 \ \hat{c}_k \ = \hat{\beta}^2 \frac{\partial \hat{\varphi}_i^2}{\partial \hat{\boldsymbol{n}}}(\hat{\xi}, 0^-) \frac{\partial \hat{\varphi}_j^2}{\partial \hat{\boldsymbol{n}}}(\hat{\xi}, 0^-),$$

which leads to

$$\hat{c}_k = -\frac{\hat{\beta}^1 \ \hat{\boldsymbol{n}} \cdot \hat{\varphi}_i^1(\hat{\xi}, 0^+) \ \ \hat{\boldsymbol{n}} \cdot \hat{\varphi}_j^1(\hat{\xi}, 0^+) - \hat{\beta}^2 \ \hat{\boldsymbol{n}} \cdot \hat{\varphi}_i^2(\hat{\xi}, 0^-) \ \ \hat{\boldsymbol{n}} \cdot \hat{\varphi}_j^2(\hat{\xi}, 0^-)}{\hat{\beta}^1} \ , \quad k = 4, 5, 6.$$

$\hat{c}_k$ can, alternatively, be written as

$$\hat{c}_k = -\frac{1}{\hat{\beta}^1} \left[\hat{\beta} \frac{\partial \hat{\varphi}_i}{\partial \hat{\boldsymbol{n}}} \frac{\partial \hat{\varphi}_j}{\partial \hat{\boldsymbol{n}}} \right]_{\hat{\Gamma}} \ , \qquad k = 4, 5, 6. \tag{3.3.6}$$

Now, we prove some properties of $\hat{\varphi}_k$, $k = 4, 5, 6$. First, we will prove in the next lemma that they satisfy the jump conditions (2.2.9).

Lemma 3.3.1. *The three IFE edge functions $\hat{\varphi}_k$, $k = 4, 5, 6$, defined in (3.3.3), satisfy the jump conditions (2.2.9) on the reference interface element.*
Thus, $\hat{\varphi}_k \in \hat{\mathcal{R}}_2(\hat{T})$, $k = 4, 5, 6$.

Proof. Since $\hat{\varphi}_1$, $\hat{\varphi}_2$ and $\hat{\varphi}_3$ are continuous at the interface $\hat{\Gamma} : \hat{\eta} = 0$, then $\hat{\varphi}_k$, $k = 4, 5, 6$, satisfy the jump condition (2.2.9a).

The derivative of $\hat{\varphi}_k$, in the direction of $\hat{\boldsymbol{n}}$, is (3.3.4), which implies that

$$\hat{\beta} \frac{\partial \hat{\varphi}_k}{\partial \hat{\boldsymbol{n}}}(\hat{\xi}, \hat{\eta}) = \begin{cases} \hat{\beta}^1 \ \frac{\partial \hat{\varphi}_i^1}{\partial \hat{\boldsymbol{n}}}(\hat{\xi}, \hat{\eta}) \ \hat{\varphi}_j^1(\hat{\xi}, \hat{\eta}) \ + \ \hat{\beta}^1 \ \frac{\partial \hat{\varphi}_j^1}{\partial \hat{\boldsymbol{n}}}(\hat{\xi}, \hat{\eta}) \ \hat{\varphi}_i^1(\hat{\xi}, \hat{\eta}) \ + \ 2 \ \hat{\beta}^1 \ \hat{c}_k \ \hat{\eta} \ , & \text{on } \hat{T}^1, \\ \hat{\beta}^2 \ \frac{\partial \hat{\varphi}_i^2}{\partial \hat{\boldsymbol{n}}}(\hat{\xi}, \hat{\eta}) \ \hat{\varphi}_j^2(\hat{\xi}, \hat{\eta}) \ + \ \hat{\beta}^2 \ \frac{\partial \hat{\varphi}_j^2}{\partial \hat{\boldsymbol{n}}}(\hat{\xi}, \hat{\eta}) \ \hat{\varphi}_i^2(\hat{\xi}, \hat{\eta}) & , \text{ on } \hat{T}^2. \end{cases}$$

Since, $\hat{\varphi}_i$ and $\hat{\varphi}_j$, $i, j = 1, 2, 3$, satisfy the jump conditions (2.2.9) at the interface $\hat{\Gamma} : \hat{\eta} = 0$, then $\hat{\varphi}_k$, $k = 4, 5, 6$, satisfy the jump condition (2.2.9b). □

Now, we prove the linear independence of the shape functions $\hat{\varphi}_k$, $k = 4, 5, 6$.

Lemma 3.3.2. *The functions $\hat{\varphi}_k$, $k = 4, 5, 6$, defined in (3.3.3), are linearly independent.*

Proof. Let γ_4, γ_5, γ_6 be constants such that

$$\gamma_4 \ \hat{\varphi}_4(\hat{x}, \hat{y}) \ + \ \gamma_5 \ \hat{\varphi}_5(\hat{x}, \hat{y}) \ + \ \gamma_6 \ \hat{\varphi}_6(\hat{x}, \hat{y}) = 0 \ , \qquad \forall (\hat{x}, \hat{y}) \in \hat{T}. \tag{3.3.7}$$

In particular, over $\hat{T}^2$, we have

$$\gamma_4 \ \hat{\varphi}_1^2(\hat{x}, \hat{y}) \ \hat{\varphi}_2^2(\hat{x}, \hat{y}) + \gamma_5 \ \hat{\varphi}_2^2(\hat{x}, \hat{y}) \ \hat{\varphi}_3^2(\hat{x}, \hat{y}) + \gamma_6 \ \hat{\varphi}_1^2(\hat{x}, \hat{y}) \ \hat{\varphi}_3^2(\hat{x}, \hat{y}) = 0 \ , \quad \forall (\hat{x}, \hat{y}) \in \hat{T}^2. \tag{3.3.8}$$

At $\hat{V}_4$, as $\hat{\varphi}_1(\hat{V}_4) = \hat{\varphi}_2(\hat{V}_4) = \frac{1}{2}$ and $\hat{\varphi}_3(\hat{V}_4) = 0$, (3.3.8) becomes

$$\frac{1}{4}\gamma_4 \ = 0 \ , \qquad i.e. \quad \gamma_4 \ = 0.$$

Then, the relation(3.3.8) becomes

$$\hat{\varphi}_3^2(\hat{x},\hat{y}) \left(\gamma_5 \ \hat{\varphi}_2^2(\hat{x},\hat{y}) \ + \ \gamma_6 \ \hat{\varphi}_1^2(\hat{x},\hat{y})\right) = 0 \ , \qquad \forall (\hat{x},\hat{y}) \in \hat{T}^2.$$

Since, on any subset of non-zero measure, $\hat{\varphi}_3$ is not identically zero, then

$$\gamma_5 \ \hat{\varphi}_2^2(\hat{x},\hat{y}) \ + \ \gamma_6 \ \hat{\varphi}_1^2(\hat{x},\hat{y}) = 0 \ , \qquad \text{almost everywhere in } \hat{T}^2. \tag{3.3.9}$$

The independence of $\hat{\varphi}_1(\hat{x},\hat{y})$ and $\hat{\varphi}_2(\hat{x},\hat{y})$ implies that $\gamma_5 = \gamma_6 = 0$, which concludes the proof.

□

Theorem 3.3.1. *Let $\hat{\varphi}_k, \ k = 1,2,3,$ be the three linear IFE shape functions on a reference interface element $\hat{T}$, and let $\hat{\varphi}_k, \ k = 4,5,6,$ be the quadratic IFE edge shape functions defined in (3.3.3). The six IFE shape functions $\hat{\varphi}_k, \ k = 1,\ldots,6,$ form a basis of $\hat{\mathcal{R}}_2(\hat{T})$.*

Proof. The piecewise linear IFE shape functions $\hat{\varphi}_k, \ k = 1,2,3,$ are linearly independent by construction ; and the piecewise quadratic IFE edge shape functions $\hat{\varphi}_k, \ k = 4,5,6,$ are linearly independent as well, by Lemma 3.3.2.

Let us denote

$$\begin{aligned} \mathcal{V}_1 &= span\{\hat{\varphi}_1, \hat{\varphi}_2, \hat{\varphi}_3\}, \\ \mathcal{V}_2 &= span\{\hat{\varphi}_4, \hat{\varphi}_5, \hat{\varphi}_6\}, \\ \mathcal{V} &= span\{\hat{\varphi}_1, \hat{\varphi}_2, \hat{\varphi}_3, \hat{\varphi}_4, \hat{\varphi}_5, \hat{\varphi}_6\} \subset \hat{\mathcal{R}}_2(\hat{T}). \end{aligned}$$

From basic linear algebra, we know that

$$\begin{aligned} dim(\mathcal{V}) &= dim(\mathcal{V}_1) + dim(\mathcal{V}_2) - dim(\mathcal{V}_1 \cap \mathcal{V}_2) \\ &= 6 - dim(\mathcal{V}_1 \cap \mathcal{V}_2) \end{aligned}$$

We want to prove that $dim(\mathcal{V}_1 \cap \mathcal{V}_2) = 0, \ \ i.e. \ \mathcal{V}_1 \cap \mathcal{V}_2 = \{0\}$.

Let $v \in \mathcal{V}_1 \cap \mathcal{V}_2$, then

$$v(\hat{x},\hat{y}) = \sum_{k=1}^{3} \gamma_k \hat{\varphi}_k(\hat{x},\hat{y}) = \sum_{k=4}^{6} \gamma_k \hat{\varphi}_k(\hat{x},\hat{y}), \qquad \forall (\hat{x},\hat{y}) \in \hat{T}, \tag{3.3.10}$$

which implies

$$\sum_{k=1}^{3} \gamma_k \hat{\varphi}_k(\hat{x},\hat{y}) - \sum_{k=4}^{6} \gamma_k \hat{\varphi}_k(\hat{x},\hat{y}) = 0, \qquad \forall (\hat{x},\hat{y}) \in \hat{T}. \tag{3.3.11}$$

We note that

$$\hat{\varphi}_i(\hat{V}_j) = \delta_{ij}, \quad i,j = 1,2,3,$$

$$\hat{\varphi}_1(\hat{V}_4) \neq 0,\ \hat{\varphi}_2(\hat{V}_4) \neq 0, \quad \hat{\varphi}_3(\hat{V}_4) = 0,$$

which yields

$$\hat{\varphi}_k(\hat{V}_1) = 0, \quad \hat{\varphi}_k(\hat{V}_2) = 0, \quad k = 4,5,6,$$

$$\hat{\varphi}_4(\hat{V}_4) \neq 0, \quad \hat{\varphi}_5(\hat{V}_4) = \hat{\varphi}_6(\hat{V}_4) = 0.$$

At $\hat{V}_1$, $\hat{V}_2$ and $\hat{V}_4$, respectively, equation (3.3.11) becomes

$$\gamma_1 = 0,$$

$$\gamma_2 = 0,$$

$$\gamma_1\hat{\varphi}_1(\hat{V}_4) + \gamma_2\hat{\varphi}_2(\hat{V}_4) - \gamma_4\hat{\varphi}_4(\hat{V}_4) = 0.$$

which yields

$$\gamma_1 = \gamma_2 = \gamma_4 = 0,$$

Thus, equation (3.3.11) becomes

$$\gamma_3\hat{\varphi}_3(\hat{x},\hat{y}) - \gamma_5\hat{\varphi}_5(\hat{x},\hat{y}) - \gamma_6\hat{\varphi}_6(\hat{x},\hat{y}) = 0\ , \qquad \forall(\hat{x},\hat{y}) \in \hat{T}.$$

Next, we show that $\gamma_3 = \gamma_5 = \gamma_6 = 0$, by using the previous equation on $\hat{T}^2$

$$\gamma_3\hat{\varphi}_3^2(\hat{x},\hat{y}) - \gamma_5\hat{\varphi}_2^2(\hat{x},\hat{y})\hat{\varphi}_3^2(\hat{x},\hat{y}) - \gamma_6\hat{\varphi}_1^2(\hat{x},\hat{y})\hat{\varphi}_3^2(\hat{x},\hat{y}) = 0, \qquad \forall(\hat{x},\hat{y}) \in \hat{T}^2.$$

Then

$$\hat{\varphi}_3(\hat{x},\hat{y})\left(\gamma_3 - \gamma_5\hat{\varphi}_2(\hat{x},\hat{y}) - \gamma_6\hat{\varphi}_1(\hat{x},\hat{y})\right) = 0, \qquad \forall(\hat{x},\hat{y}) \in \hat{T}^2.$$

Since $\hat{\varphi}_3(\hat{x},\hat{y})$, is non zero polynomial over $\hat{T}^2$

$$\gamma_3 - \gamma_5\hat{\varphi}_2(\hat{x},\hat{y}) - \gamma_6\hat{\varphi}_1(\hat{x},\hat{y}) = 0, \qquad \text{on } \hat{T}^2. \tag{3.3.12}$$

By the relation [42],

$$\hat{\varphi}_1(\hat{x},\hat{y}) + \hat{\varphi}_2(\hat{x},\hat{y}) + \hat{\varphi}_3(\hat{x},\hat{y}) = 1\ , \qquad \forall(\hat{x},\hat{y}) \in \hat{T}, \tag{3.3.13}$$

(3.3.12) becomes

$$\gamma_3(\hat{\varphi}_1^2(\hat{x},\hat{y}) + \hat{\varphi}_2^2(\hat{x},\hat{y}) + \hat{\varphi}_3^2(\hat{x},\hat{y})) + \gamma_5\hat{\varphi}_2^2(\hat{x},\hat{y}) + \gamma_6\hat{\varphi}_1^2(\hat{x},\hat{y}) = 0\ , \qquad \text{on } \hat{T}^2,$$

which can be written also as

$$\gamma_3\ \hat{\varphi}_3^2(\hat{x},\hat{y}) + (\gamma_3+\gamma_5)\ \hat{\varphi}_2^2(\hat{x},\hat{y}) + (\gamma_3+\gamma_6)\ \hat{\varphi}_1^2(\hat{x},\hat{y}) = 0\ , \qquad \text{on } \hat{T}^2.$$

The linear independence of $\hat{\varphi}_i,\ i=1,2,3$, implies that $\gamma_3=\gamma_5=\gamma_6=0$, which gives

$$v = 0 \qquad i.e. \qquad \mathcal{V}_1 \cap \mathcal{V}_2 = \{0\}, \tag{3.3.14}$$

which completes the proof, since $dim(\mathcal{V}) = dim(\hat{\mathcal{R}}_2(\hat{T})) = 6$.

□

3.3.3 Hierarchical Shape Functions on $\hat{\mathcal{R}}_1(\hat{T})$

To construct three quadratic IFE edge shape functions for the space $\hat{\mathcal{R}}_1(\hat{T})$, we construct $\hat{\varphi}_4$, $\hat{\varphi}_5$, and $\hat{\varphi}_6$, as in (3.3.3) and select $\hat{c}_4,\ \hat{c}_5,\ \hat{c}_6$ such that the shape functions $\hat{\varphi}_k,\ k=4,5,6$, satisfy the jump condition (2.2.15)

$$[\hat{\beta}\ (\mathbf{J}^t\hat{\nabla})\cdot(\mathbf{J}^t\hat{\nabla})\hat{\varphi}_k]_{\hat{\Gamma}} = 0.$$

First, we transform the expression (3.3.3) for $\hat{\varphi}_k,\ k=4,5,6$, from the reference $(\hat{\xi},\hat{\eta})$ defined in (3.2.3) to the Cartesian reference $(\hat{x},\hat{y})$, as

$$\hat{\varphi}_k(\hat{x},\hat{y}) = \begin{cases} \hat{\varphi}_i^1(\hat{x},\hat{y})\hat{\varphi}_j^1(\hat{x},\hat{y}) + \ \hat{c}_k\ \frac{(\hat{y}-a\hat{x}-b)^2}{(1+a^2)}\ , & (\hat{x},\hat{y}) \in \hat{T}^1, \\ \hat{\varphi}_i^2(\hat{x},\hat{y})\hat{\varphi}_j^2(\hat{x},\hat{y})\ , & (\hat{x},\hat{y}) \in \hat{T}^2. \end{cases} \tag{3.3.15}$$

Applying $(\mathbf{J}^t\hat{\nabla})$ leads to

$$(\mathbf{J}^t\hat{\nabla})\hat{\varphi}_k(\hat{x},\hat{y}) = \begin{cases} (\mathbf{J}^t\hat{\nabla})\hat{\varphi}_i^1\ \hat{\varphi}_j^1 + \hat{\varphi}_i^1\ (\mathbf{J}^t\hat{\nabla})\hat{\varphi}_j^1 + \frac{\hat{c}_k}{(1+a^2)}(\mathbf{J}^t\hat{\nabla})\left((\hat{y}-a\hat{x}-b)^2\right),\ (\hat{x},\hat{y}) \in \hat{T}^1, \\ (\mathbf{J}^t\hat{\nabla})\hat{\varphi}_i^2\ \hat{\varphi}_j^2 + \hat{\varphi}_i^2\ (\mathbf{J}^t\hat{\nabla})\hat{\varphi}_j^2\ , & (\hat{x},\hat{y}) \in \hat{T}^2, \end{cases}$$

which yields

$$(\mathbf{J}^t\hat{\nabla})\cdot(\mathbf{J}^t\hat{\nabla})\hat{\varphi}_k(\hat{x},\hat{y}) = \begin{cases} 2\ (\mathbf{J}^t\hat{\nabla})\hat{\varphi}_i^1\cdot(\mathbf{J}^t\hat{\nabla})\hat{\varphi}_j^1 \\ \qquad + \frac{\hat{c}_k}{(1+a^2)}\ (\mathbf{J}^t\hat{\nabla})\cdot(\mathbf{J}^t\hat{\nabla})\left((\hat{y}-a\hat{x}-b)^2\right)\ , & (\hat{x},\hat{y}) \in \hat{T}^1, \\ 2\ (\mathbf{J}^t\hat{\nabla})\hat{\varphi}_i^2\cdot(\mathbf{J}^t\hat{\nabla})\hat{\varphi}_j^2\ , & (\hat{x},\hat{y}) \in \hat{T}^2. \end{cases}$$

This can be written as

$$(\mathbf{J}^t\hat{\nabla})\cdot(\mathbf{J}^t\hat{\nabla})\hat{\varphi}_k(\hat{x},\hat{y}) = \begin{cases} 2\ (\mathbf{J}^t\hat{\nabla})\hat{\varphi}_i^1\cdot(\mathbf{J}^t\hat{\nabla})\hat{\varphi}_j^1 + \frac{2\ \hat{c}_k}{(1+a^2)}(\mathbf{v}\cdot\mathbf{v})\ , & (\hat{x},\hat{y}) \in \hat{T}^1, \\ 2\ (\mathbf{J}^t\hat{\nabla})\hat{\varphi}_i^2\cdot(\mathbf{J}^t\hat{\nabla})\hat{\varphi}_j^2\ , & (\hat{x},\hat{y}) \in \hat{T}^2, \end{cases}$$

where $\mathbf{v} = (\mathbf{J}^t\hat{\nabla})(\hat{y} - a\hat{x} - b)$. We note that $\mathbf{v}$ is constant vector.

This can be written as

$$(\mathbf{J}^t\hat{\nabla}) \cdot (\mathbf{J}^t\hat{\nabla})\hat{\varphi}_k(\hat{x},\hat{y}) = \begin{cases} 2\ (\mathbf{J}^t\hat{\nabla})\hat{\varphi}_i^1 \cdot (\mathbf{J}^t\hat{\nabla})\hat{\varphi}_j^1 + 2\ \frac{\hat{c}_k}{(1+a^2)}||\mathbf{v}||_2^2\ , & (\hat{x},\hat{y}) \in \hat{T}^1, \\ 2\ (\mathbf{J}^t\hat{\nabla})\hat{\varphi}_i^2 \cdot (\mathbf{J}^t\hat{\nabla})\hat{\varphi}_j^2 \quad , & (\hat{x},\hat{y}) \in \hat{T}^2, \end{cases}$$

combined with the jump condition (2.2.15) yields

$$\hat{\beta}^1(\mathbf{J}^t\hat{\nabla})\hat{\varphi}_i^1 \cdot (\mathbf{J}^t\hat{\nabla})\hat{\varphi}_j^1 + \hat{\beta}^1\ ||\mathbf{v}||_2^2\ \frac{\hat{c}_k}{(1+a^2)} = \hat{\beta}^2\ (\mathbf{J}^t\hat{\nabla})\hat{\varphi}_i^2 \cdot (\mathbf{J}^t\hat{\nabla})\hat{\varphi}_j^2,$$

which leads to

$$\hat{c}_k = -(1+a^2)\frac{\hat{\beta}^1\ (\mathbf{J}^t\hat{\nabla}\hat{\varphi}_i^1).(\mathbf{J}^t\hat{\nabla}\hat{\varphi}_j^1) - \hat{\beta}^2\ (\mathbf{J}^t\hat{\nabla}\varphi_i^2).(\mathbf{J}^t\hat{\nabla}\hat{\varphi}_j^2)}{\hat{\beta}^1\ ||\mathbf{v}||_2^2}\ , \qquad k = 4,5,6.$$

The coefficient $\hat{c}_k$ can, alternatively, be written as

$$\hat{c}_k = -(1+a^2)\frac{[\hat{\beta}\ (\mathbf{J}^t\hat{\nabla}\hat{\varphi}_i) \cdot (\mathbf{J}^t\hat{\nabla}\hat{\varphi}_j)]_{\hat{\Gamma}}}{\hat{\beta}^1\ ||\mathbf{v}||_2^2}\ , \qquad k = 4,5,6. \tag{3.3.16}$$

Now, we prove some properties of the functions $\hat{\varphi}_k$, $k = 4,5,6$. First, we will prove in the next lemma that they satisfy the jump conditions (2.2.9).

Lemma 3.3.3. *The three IFE edge functions $\hat{\varphi}_k$, $k = 4,5,6$, defined in (3.3.3), with $\hat{c}_k$, $k = 4,5,6$, given by (3.3.16), satisfy the jump conditions (2.2.9) on the reference interface element. Thus, $\hat{\varphi}_k \in \hat{\mathcal{R}}_1(\hat{T})$, $k = 4,5,6$.*

Proof. The proof is similar to the proof of Lemma 3.3.1. □

The shape functions $\hat{\varphi}_k$, $k = 1,\ldots,6$, form a basis of $\hat{\mathcal{R}}_1(\hat{T})$ as stated in the following theorem.

Theorem 3.3.2. *Let $\hat{\varphi}_k$, $k = 1,2,3$, be the three linear IFE shape functions on a reference interface element $\hat{T}$, and $\hat{\varphi}_k$, $k = 4,5,6$, be the quadratic IFE edge shape functions defined in (3.3.3), where the constants $\hat{c}_k$, $k = 4,5,6$, are given by (3.3.16). Then, the six IFE shape functions $\hat{\varphi}_k$, $k = 1,\ldots,6$, form a basis of $\hat{\mathcal{R}}_1(\hat{T})$.*

Proof. The proof is similar to the proof of Theorem 3.3.1. □

3.4 Conclusions

In this Chapter, we discussed the construction of Lagrange and hierarchical shape functions on interface elements. We presented general formulas to construct functions belonging to both spaces $\mathcal{R}_k(T),\ k = 1, 2$, for an arbitrary interface element T, proved the existence of six Lagrange shape functions on the interface element T, and formed a basis for the space $\mathcal{R}_2(T)$. The same idea can be also used to prove the existence of a Lagrange basis for the space $\mathcal{R}_1(T)$, however the proof will need more work. The main reason is that the construction of functions belonging to $\mathcal{R}_2(T)$ is much easier than the construction of functions belonging to the space $\mathcal{R}_1(T)$. Furthermore, we proved the existence of a hierarchical basis for each of the spaces $\mathcal{R}_k(T),\ k = 1, 2$, on an arbitrary interface element T. Although the Lagrange shape functions have the advantage of satisfying the nodal value conditions at all the mesh nodes, they do not have enough flexibility and efficiency to be easily extended to higher-degrees. Instead, hierarchical shape functions can easily be extended to obtain p-th degree shape functions and construct a basis for p-th degree IFE spaces. Such an idea is discussed in Chapter 6.

Chapter 4

Approximation Capability of Quadratic Immersed Finite Element Spaces

4.1 Introduction

In this chapter, we discuss the approximation capability of the proposed quadratic IFE spaces, and we present numerical results for several interface problems to demonstrate the optimal convergence of the quadratic IFE spaces. We expect to obtain the same optimal approximation capability as the standard finite elements spaces, *i.e.*, $p+1=3$ in the L^2 norm and $p=2$ in the broken H^1 norm.

We use the following norms to measure approximation errors:

$$||w||_0^2 = \int_\Omega w^2 \, dxdy, \tag{4.1.1a}$$

$$||w_t||_{0,h}^2 = \sum_{T\in\mathscr{T}_h} \int_T w_t^2 \, dxdy, \quad t = x, y. \tag{4.1.1b}$$

The norm (4.1.1a) is the standard L^2-norm, however the norm (4.1.1b) is a broken L^2-norm used to compute the errors in the derivatives w_t, $t = x, y$, of a function w, where $w_t \in L^2(T), \forall\, T \in \mathscr{T}_h$, but not in $L^2(\Omega)$.

We also recall the standard H^1-norm

$$||w||_1^2 = ||w||_0^2 + ||w_x||_0^2 + ||w_y||_0^2 = \int_\Omega (w^2 + w_x^2 + w_y^2) \, dxdy, \tag{4.1.2}$$

and the broken H^1-norm:

$$||w||_{1,h}^2 = ||w||_0^2 + ||w_x||_{0,h}^2 + ||w_y||_{0,h}^2 = \int_\Omega w^2 \, dxdy + \sum_{T\in\mathscr{T}_h} \int_T (w_x^2 + w_y^2) \, dxdy. \tag{4.1.3}$$

It is well known that when standard quadratic basis functions are used, with a body-fitted mesh, to interpolate a function $u \in H^3(\Omega^\pm)$ and solution of the interface problem (1.1.1a) with a linear interface, then the interpolation error satisfies the following inequalities [12, 14]:

$$||u - I_h u||_0 \ \leq \ Ch^3, \tag{4.1.4a}$$
$$||u - I_h u||_1 \ \leq \ Ch^2, \tag{4.1.4b}$$

where $I_h u$ is the interpolant of the function u in the finite element space with a mesh size h.

In this chapter, we conduct several numerical experiments to demonstrate the optimal approximation capabilities of our Lagrange quadratic IFE spaces $\mathcal{S}_h^1$ and $\mathcal{S}_h^2$ and hierarchical IFE spaces W_h^1 and W_h^2 constructed in Chapter 2. All of the numerical results demonstrate the optimal approximation capability for these IFE spaces, i.e., under h refinement, the following hold:

$$||u - I_h u||_0 \ \approx \ Ch^3, \tag{4.1.5a}$$
$$||u_x - (I_h u)_x||_{0,h} \ \approx \ Ch^2, \tag{4.1.5b}$$
$$||u_y - (I_h u)_y||_{0,h} \ \approx \ Ch^2. \tag{4.1.5c}$$

4.2 Approximation Capability using Lagrange IFE Shape Functions for the Spaces $\mathcal{S}_h^1$ and $\mathcal{S}_h^2$

We define a piecewise Lagrange type IFE interpolant $I_h u(x,y)$ of $u(x,y)$ such that $\forall\ T \in \mathscr{T}_h$

$$I_h u(x,y)|_T = \sum_{i=1}^{6} u(V_i)\phi_i(x,y), \tag{4.2.1}$$

where $V_i,\ i = 1,\ldots,6$, are the nodes on T and $\phi_i(x,y),\ i = 1,\ldots,6$ are the six Lagrange FE or IFE shape functions depending on whether T is a non-interface or an interface element.

Example 4.2.1.

In this example we assume that the domain $\Omega = [0,1]^2$ is cut by the interface $y = x + \frac{2}{3}$ such that $\Omega^+ = \{y > x + \frac{2}{3}\}$ and $\Omega^- = \{y < x + \frac{2}{3}\}$, and consider $u \in \mathcal{S}(\Omega)$ defined by

$$u(x,y) = \begin{cases} \frac{(6x^2+6xy-4x+3)\ \cos(y^2-x^2-\frac{4}{3}y+\frac{4}{9})+(2+3x-3y)\ \sin(\frac{2}{3}-x-y)}{3\beta^+}; & \text{on } \Omega^+, \\ \\ \frac{(\frac{\beta^-}{\beta^+}-1)(3-8x+12xy)+(6x^2+6xy-4x+3)\ \cos(y^2-x^2-\frac{4}{3}y+\frac{4}{9})+(2+3x-3y)\ \sin(\frac{2}{3}-x-y)}{3\beta^-}; & \text{on } \Omega^-, \end{cases} \tag{4.2.2}$$

with $r = \frac{\beta^+}{\beta^-} = 5$ and $r = \frac{\beta^+}{\beta^-} = 10^3$ representing a moderate and a large jump in the coefficient β.

The uniform triangular mesh $\mathscr{T}_h$ is formed by partitioning Ω into $(1/h)^2$ squares, $h = \frac{1}{2^m}$, $m = 2, 3, 4, 5, 6, 7$, then forming the triangular elements by joining the lower left and upper right vertices of the squares.

We present errors in $I_h u$ and their orders of convergence in Tables 4.1, 4.2, 4.3 and 4.4. We observe that, since functions in $\mathcal{S}_h^1$ satisfy the jump conditions of $\mathcal{S}(\Omega)$, the interpolant in $\mathcal{S}_h^1$ yields $\mathcal{O}(h^3)$ optimal convergence rates for u and $\mathcal{O}(h^2)$ for its derivatives. Interpolation in the non-consistent IFE space $\mathcal{S}_h^2$ shows near optimal convergence rates.

h	$\|\|u - I_h u\|\|_0$	order	$\|\|u_x - (I_h u)_x\|\|_{0,h}$	order	$\|\|u_y - (I_h u)_y\|\|_{0,h}$	order
$\frac{1}{4}$	1.824818e-03	N/A	5.509363e-02	N/A	3.422630e-02	N/A
$\frac{1}{8}$	2.286751e-04	2.9963	1.383511e-02	1.9935	8.736473e-03	1.9699
$\frac{1}{16}$	2.857819e-05	3.0003	3.454655e-03	2.0017	2.189569e-03	1.9964
$\frac{1}{32}$	3.573301e-06	2.9995	8.640540e-04	1.9993	5.482050e-04	1.9978
$\frac{1}{64}$	4.465973e-07	3.0002	2.159648e-04	2.0003	1.370356e-04	2.0001
$\frac{1}{128}$	5.582714e-08	2.9999	5.399578e-05	1.9999	3.426435e-05	1.9998

Table 4.1: L^2 interpolation errors and orders for u, u_x and u_y for the function (4.2.2) with $r = 5$ using the IFE space $\mathcal{S}_h^1$.

h	$\|\|u - I_h u\|\|_0$	order	$\|\|u_x - (I_h u)_x\|\|_{0,h}$	order	$\|\|u_y - (I_h u)_y)\|\|_{0,h}$	order
$\frac{1}{4}$	1.825604e-03	N/A	5.512166e-02	N/A	3.428669e-02	N/A
$\frac{1}{8}$	2.307696e-04	2.9838	1.395794e-02	1.9815	8.880656e-03	1.9489
$\frac{1}{16}$	2.857665e-05	3.0135	3.454740e-03	2.0144	2.189942e-03	2.0197
$\frac{1}{32}$	3.579449e-06	2.9970	8.654861e-04	1.9969	5.499555e-04	1.9935
$\frac{1}{64}$	4.465694e-07	3.0027	2.159599e-04	2.0027	1.370315e-04	2.0048
$\frac{1}{128}$	5.584678e-08	2.9993	5.401489e-05	1.9993	3.428750e-05	1.9987

Table 4.2: L^2 interpolation errors and orders for u, u_x and u_y for the function (4.2.2) with $r = 10^3$ using the IFE space $\mathcal{S}_h^1$.

h	$\|\|u - I_h u\|\|_0$	order	$\|\|u_x - (I_h u)_x\|\|_{0,h}$	order	$\|\|u_y - (I_h u)_y\|\|_{0,h}$	order
$\frac{1}{4}$	1.839495e-03	N/A	5.532437e-02	N/A	3.514150e-02	N/A
$\frac{1}{8}$	2.330852e-04	2.9803	1.396273e-02	1.9863	9.073591e-03	1.9534
$\frac{1}{16}$	2.990975e-05	2.9621	3.593021e-03	1.9583	2.430470e-03	1.9004
$\frac{1}{32}$	3.857176e-06	2.9549	9.083393e-04	1.9838	6.220373e-04	1.9661
$\frac{1}{64}$	5.284785e-07	2.8676	2.524459e-04	1.8472	1.908056e-04	1.7048
$\frac{1}{128}$	7.184269e-08	2.8789	6.471950e-05	1.9637	4.976721e-05	1.9388

Table 4.3: L^2 interpolation errors and orders for u, u_x and u_y for the function (4.2.2) with $r = 5$ using the IFE space $\mathcal{S}_h^2$.

h	$\|\|u - I_h u\|\|_0$	order	$\|\|u_x - (I_h u)_x\|\|_{0,h}$	order	$\|\|u_y - (I_h u)_y)\|\|_{0,h}$	order
$\frac{1}{4}$	1.835268e-03	N/A	5.552221e-02	N/A	3.513217e-02	N/A
$\frac{1}{8}$	2.283991e-04	3.0063	1.382844e-02	2.0054	8.749940e-03	2.0054
$\frac{1}{16}$	2.958586e-05	2.9485	3.628863e-03	1.9300	2.464341e-03	1.8280
$\frac{1}{32}$	3.586461e-06	3.0442	8.704789e-04	2.0596	5.587641e-04	2.1408
$\frac{1}{64}$	5.101100e-07	2.8136	2.597386e-04	1.7447	1.994275e-04	1.4863
$\frac{1}{128}$	5.677858e-08	3.1673	5.576483e-05	2.2196	3.700960e-05	2.4298

Table 4.4: L^2 interpolation errors and orders for u, u_x and u_y for the function (4.2.2) with $r = 10^3$ using the IFE space $\mathcal{S}_h^2$.

4.3 Approximation Capability using Hierarchical IFE Shape Functions for the Spaces $\mathcal{W}_h^1$ and $\mathcal{W}_h^2$

We define a piecewise quadratic IFE interpolant $I_h u(x,y)$ of $u(x,y)$ using hierarchical shape functions as

$$I_h u(x,y)|_T = \sum_{j=1}^{6} c_j \phi_j(x,y), \quad \forall\ T \in \mathscr{T}_h, \tag{4.3.1}$$

where $\phi_j(x,y),\ j=1,\ldots,6$, are the six quadratic FE or IFE shape functions depending on whether T is a non-interface or an interface element, and $c_j,\ j=1,\ldots,6$, are six constants such that $I_h u(V_i) = u(V_i),\ i=1,\ldots,6$, with $V_i,\ i=1,\ldots,6$, being the nodes on T.

To compute the interpolation errors, we use the L^2-norm defined in (4.1.1a), and the broken H^1 norm defined in (4.1.3).

Example 4.3.1.

We consider the function from Example 6.4.1, and use hierarchical IFE shape functions developed in Chapter 3 to test the approximation capability of the spaces $\mathcal{W}_h^k,\ k=1,2$. We obtain results presented in Tables 4.5 and 4.6 for hierarchical IFE shape functions in $\mathcal{W}_h^1$, and in Tables 4.7 and 4.8 for hierarchical IFE shape functions in $\mathcal{W}_h^2$. We obtain the same conclusions as for the spaces $\mathcal{S}_h^1$ and $\mathcal{S}_h^2$ in the previous section. In fact, we observe that the interpolant in $\mathcal{W}_h^1$ yields $\mathcal{O}(h^3)$ optimal convergence rates for u and $\mathcal{O}(h^2)$ for its derivatives, while, interpolation in the IFE space $\mathcal{W}_h^2$ shows near optimal convergence rates.

h	$\|\|u - I_h u\|\|_0$	order	$\|\|u_x - (I_h u)_x\|\|_{0,h}$	order	$\|\|u_y - (I_h u)_y\|\|_{0,h}$	order
$\frac{1}{4}$	1.824818e-03	N/A	5.509363e-02	N/A	3.422630e-02	N/A
$\frac{1}{8}$	2.286751e-04	2.9963	1.383511e-02	1.9935	8.736473e-03	1.9699
$\frac{1}{16}$	2.857819e-05	3.0003	3.454655e-03	2.0017	2.189569e-03	1.9964
$\frac{1}{32}$	3.573301e-06	2.9995	8.640540e-04	1.9993	5.482050e-04	1.9978
$\frac{1}{64}$	4.465973e-07	3.0002	2.159648e-04	2.0003	1.370356e-04	2.0001
$\frac{1}{128}$	5.582714e-08	2.9999	5.399578e-05	1.9998	3.426435e-05	1.9997

Table 4.5: Interpolation errors and orders for u, u_x and u_y for the function (4.2.2) with $r=5$, using hierarchical IFE shape functions in $\mathcal{W}_h^1$.

h	$\|\|u - I_h u\|\|_0$	order	$\|\|u_x - (I_h u)_x\|\|_{0,h}$	order	$\|\|u_y - (I_h u)_y\|\|_{0,h}$	order
$\frac{1}{4}$	1.825604e-03	N/A	5.512166e-02	N/A	3.428669e-02	N/A
$\frac{1}{8}$	2.307696e-04	2.9838	1.395794e-02	1.9815	8.880656e-03	1.9489
$\frac{1}{16}$	2.857665e-05	3.0135	3.454740e-03	2.0144	2.189942e-03	2.0197
$\frac{1}{32}$	3.579449e-06	2.9970	8.654861e-04	1.9969	5.499555e-04	1.9935
$\frac{1}{64}$	4.465694e-07	3.0027	2.159599e-04	2.0027	1.370315e-04	2.0048
$\frac{1}{128}$	5.584678e-08	2.9993	5.401489e-05	1.9993	3.428750e-05	1.9987

Table 4.6: Interpolation errors and orders for u, u_x and u_y for the function (4.2.2) with $r = 1000$, using hierarchical IFE shape functions in $\mathcal{W}_h^1$.

h	$\|\|u - I_h u\|\|_0$	order	$\|\|u_x - (I_h u)_x\|\|_{0,h}$	order	$\|\|u_y - (I_h u)_y\|\|_{0,h}$	order
$\frac{1}{4}$	1.839495e-03	N/A	5.532437e-02	N/A	3.514150e-02	N/A
$\frac{1}{8}$	2.330852e-04	2.9803	1.396273e-02	1.9863	9.073591e-03	1.9534
$\frac{1}{16}$	2.990975e-05	2.9621	3.593021e-03	1.9583	2.430470e-03	1.9004
$\frac{1}{32}$	3.857176e-06	2.9549	9.083393e-04	1.9838	6.220373e-04	1.9661
$\frac{1}{64}$	5.284785e-07	2.8676	2.524459e-04	1.8472	1.908056e-04	1.7048
$\frac{1}{128}$	7.184269e-08	2.8789	6.471950e-05	1.9637	4.976721e-05	1.9388

Table 4.7: Interpolation errors and orders for u, u_x and u_y for the function (4.2.2) with $r = 5$, using hierarchical IFE shape functions in $\mathcal{W}_h^2$.

h	$\|\|u - I_h u\|\|_0$	order	$\|\|u_x - (I_h u)_x\|\|_{0,h}$	order	$\|\|u_y - (I_h u)_y\|\|_{0,h}$	order
$\frac{1}{4}$	1.835268e-03	N/A	5.552221e-02	N/A	3.513217e-02	N/A
$\frac{1}{8}$	2.283991e-04	3.0063	1.382844e-02	2.0054	8.749940e-03	2.0054
$\frac{1}{16}$	2.958586e-05	2.9485	3.628863e-03	1.9300	2.464341e-03	1.8280
$\frac{1}{32}$	3.586461e-06	3.0442	8.704789e-04	2.0596	5.587641e-04	2.1408
$\frac{1}{64}$	5.101100e-07	2.8136	2.597386e-04	1.7447	1.994275e-04	1.4863
$\frac{1}{128}$	5.677858e-08	3.1673	5.576483e-05	2.2196	3.700960e-05	2.4298

Table 4.8: Interpolation errors and orders for u, u_x and u_y for the function (4.2.2) with $r = 1000$, using hierarchical IFE shape functions in $\mathcal{W}_h^2$.

4.4 Conclusions

In this chapter, we recalled and defined broken H^s, $s = 0, 1$, norms, and we used these norms to show the approximation capability of the IFE spaces $\mathcal{S}_h^k, k = 1, 2$, and $\mathcal{W}_h^k, k = 1, 2$, defined in Chapter 2. In all the examples we presented, using Lagrange shape functions for $\mathcal{S}_h^k, k = 1, 2$, and hierarchical shape functions for $\mathcal{W}_h^k, k = 1, 2$, the interpolation error is of order $\mathcal{O}(h^3)$ in L^2-norm and of order $\mathcal{O}(h^2)$ in broken H^1-norm. This behavior is similar to the behavior of standard finite elements where the interpolation error for the finite element spaces is proved to be of order $\mathcal{O}(h^{p+1})$ in L^2-norm and of order $\mathcal{O}(h^p)$ in H^1-norm, which is the same optimal approximation capability as the standard quadratic finite element spaces. Thus, the proposed IFE spaces $\mathcal{S}_h^k, k = 1, 2$, exhibit optimal approximation capability in both L^2 and broken H^1 norms. A future work would be to analytically investigate the approximation capability of theses spaces and prove the inequalities (4.1.5), which were investigated numerically in this chapter.

Chapter 5

Immersed Finite Element Methods

5.1 Introduction

In this chapter, we develop two finite element methods for solving the interface problem (1.1.1) with the quadratic IFE spaces $\mathcal{S}_h^1$ and $\mathcal{S}_h^2$, defined in (2.4.2). We assume that the true solution u belongs to the function space

$$\mathcal{S}(\Omega) = \{u,\ u|_{\Omega^\pm} \in H^3(\Omega^\pm),\ [u]_\Gamma = [\beta\ \boldsymbol{n} \cdot \nabla u]_\Gamma = 0\}. \tag{5.1.1}$$

The developed immersed finite element solutions, denoted as U^h, will belong to the function spaces $\mathcal{S}_{h,E}^k,\ k = 1, 2$, defined in (2.4.4).

It is well known [14, 61] that solutions obtained by the standard finite element method satisfy the following inequalities

$$||u - U^h||_r \ \leq\ C\ h^{3-r}, \quad r = 0, 1, \tag{5.1.2a}$$

and

$$||u_x - U_x^h||_0 \ \leq\ C\ h^2, \tag{5.1.2b}$$
$$||u_y - U_y^h||_0 \ \leq\ C\ h^2. \tag{5.1.2c}$$

In Chapter 4, we showed numerically that we have the optimal approximation capability of the IFE spaces S_h^1 and S_h^2, represented by the inequalities (4.1.5). In this chapter, numerical experiments will show that inequalities (5.1.2) hold for solutions obtained by immersed finite element methods. We first use a continuous Galerkin formulation, similar to the method used in [3, 30, 43]. While this method will not exhibit optimal convergence rates, its modification with an interior penalty method that penalizes the discontinuities of the shape functions across the non-interface edges yields optimal convergence rates. We will show numerically that solutions obtained by this interior penalty immersed finite element method exhibits an

optimal convergence rates S_h^1, and nearly optimal rate in S_h^2, *i.e.*, under h refinement the following estimates hold:

$$||u - U^h||_0 \approx C\ h^3, \tag{5.1.3}$$
$$||u_x - U_x^h||_{0,h} \approx C\ h^2, \tag{5.1.4}$$
$$||u_y - U_y^h||_{0,h} \approx C\ h^2. \tag{5.1.5}$$

5.2 Continuous Galerkin Finite Element formulation

Let us recall the non-penalized IFE method which exhibited optimal convergence rates for linear, bilinear, or one-dimensional higher degree IFE spaces [3, 30, 43]. The weak formulation used in this IFE method is obtained by multiplying the equation (1.1.1a) by a test function $v \in H_0^1(\Omega)$ and integrating over Ω through all elements of $\mathscr{T}_h$, as follows:

$$\int_\Omega -\nabla(\beta\nabla u)\ v\ dxdy = \int_\Omega f\ v\ dxdy,$$

which can be written also as

$$\int_{\Omega^+} -\nabla(\beta\nabla u)\ v\ dxdy + \int_{\Omega^-} -\nabla(\beta\nabla u)\ v\ dxdy = \int_\Omega f\ v\ dxdy.$$

Applying integration by parts on Ω^+ and Ω^- then combining the terms, we obtain

$$\int_\Omega \beta\nabla u \cdot \nabla v\ dxdy = \int_\Omega f\ v\ dxdy,$$

which leads to non-penalized IFE method as follows: determining $U^h \in \mathcal{S}_{h,E}^k,\ k = 1, 2$, such that

$$\sum_{T\in\mathscr{T}_h} \int_T \beta\nabla U^h\nabla \cdot V^h dxdy = \sum_{T\in\mathscr{T}_h} \int_T fV^h dxdy,\ \forall\ V^h \in \mathcal{S}_{h,0}^k. \tag{5.2.1}$$

However, our numerical results in Example 5.4.1 indicate that this non-penalized IFE formulation does not converge optimally from the point of view of quadratic polynomials used in $\mathcal{S}_{h,E}^k,\ k = 1, 2$. To overcome this defect, we propose to employ penalization and stabilization in the quadratic IFE method. This penalization idea is based on the Non Symmetric Interior Penalty (NIPG) method [15, 57], where we apply penalization on interface edges only and use discontinuous IFE spaces.

5.3 Non-symmetric Interior Penalty Galerkin (NIPG) Formulation

The IFE spaces proposed in this manuscript are not continuous across interface edges. Thus, in developing suitable finite element methods for solving interface problems with these IFE spaces, we borrow penalization techniques used in discontinuous finite element methods for solving second-order elliptic problems.

5.3.1 Review of Interior Penalty Methods

Interior penalty methods were proposed in many works in 1970s and was used as a new way of imposing Dirichlet boundary conditions in a weak form for elliptic problems. The first works were introduced independently by Nitsche [48] in 1971, by Babuska [6] in 1973, and by Douglas in 1976 [36]. In 1978, Wheeler [63] made a study of the consistency, symmetrization, and adding penalty terms on each edge to penalize the jump of the function across the edge. In the 1990, techniques of IP methods were applied to local discontinuous Galerkin methods. The interior penalty method was used to solve second-order elliptic problems [58, 11]. In this matter, the original method of Bassi and Rebay was studied by Brezzi *et al.* [16], the discontinuous Galerkin (DG) method of Baumann and Oden was studied by Oden, Babuska and Baumann in [49] and by Riviere and Wheeler in [57]. A synthesization of the elliptic, parabolic, and hyperbolic theory was done by Suli, Schwab, and Houston [60] who applied the analysis of DG methods to partial differential equations with non-negative characteristic form. Later on, Arnold, Brezzi, Cockburn and Marini made a recast of most of the previously developed methods for elliptic problems within a single framework in [4] and presented a unified analysis of the DG methods applied to elliptic problems [23]. In 2005, a stabilization of the IP methods and discontinuous Galerkin methods was proposed by Brezzi, Cockburn, Marini, and Suli [15].

5.3.2 The Interior Penalty IFE Method

We now introduce a few notations and conventions in order to describe the formulation with interior penalty terms. Let $\mathscr{E}_h$, $\mathscr{E}_h^0$, $\mathscr{E}_h^i$ and $\mathscr{E}_h^{0,i}$ be the set of all the edges, interior edges, interface edges and interior interface edges in a mesh $\mathscr{T}_h$, respectively.

For $e \in \mathscr{E}_h^0$ shared by the two elements T_1 and T_2, let the vectors $\boldsymbol{n}_1$ and $\boldsymbol{n}_2$, respectively, be the unit vectors normal to e, pointing towards the exterior of the elements T_1 and T_2. Following [23], for a scalar piecewise smooth function φ, we let $\varphi|_{T_i} = \varphi_i,\ i = 1, 2$, and we will use the average and jump of φ on an edge e defined by

$$\{\varphi\} = \frac{1}{2}(\varphi_1 + \varphi_2) \qquad \text{and} \qquad [\varphi] = \varphi_1 \mathbf{n_1} + \varphi_2 \mathbf{n_2}. \tag{5.3.1a}$$

Similarly for a vector-valued piecewise smooth function $\boldsymbol{\tau}$ such that $\boldsymbol{\tau}|_{T_i} = \boldsymbol{\tau}_i,\ i = 1, 2$ we define its average and jump by

$$\{\boldsymbol{\tau}\} = \frac{1}{2}(\boldsymbol{\tau}_1 + \boldsymbol{\tau}_2) \qquad \text{and} \qquad [\boldsymbol{\tau}] = \boldsymbol{\tau}_1 \cdot \mathbf{n_1} + \boldsymbol{\tau}_2 \cdot \mathbf{n_2}. \tag{5.3.1b}$$

We will also use the following notations

$$(u, v)_{\mathscr{T}_h} = \sum_{T \in \mathscr{T}_h} \int_T u\ v\ \ dxdy, \text{ and } < u, v >_{\mathscr{E}_h^t} = \sum_{e \in \mathscr{E}_h^t} \int_e u\ v\ \ ds, \tag{5.3.2}$$

where $t = 0, i$ or $(0, i)$.

Now, we recall the standard NIPG weak formulation on a mesh $\mathscr{T}_h$ of the model elliptic problem (1.1.1a) is [15, 56]:

$$(\beta\nabla u, \nabla v)_{\mathscr{T}_h} - \sum_{T \in \mathscr{T}_h} \int_{\partial T} \beta\ \frac{\partial u}{\partial \boldsymbol{n}}\ v\ ds + < [u]\,, \{\beta\nabla v\} >_{\mathscr{E}_h^0} + < [\beta\nabla u], \{v\} >_{\mathscr{E}_h^0}$$
$$+ s < [u]\,, [v] >_{\mathscr{E}_h^0} = (f,\ v)_{\mathscr{T}_h}, \tag{5.3.3}$$

where $s > 0$ is the penalty parameter. Following [23] and (5.3.1) we can write the integral

$$\sum_{T \in \mathscr{T}_h} \int_{\partial T} \beta\ \frac{\partial u}{\partial \boldsymbol{n}}\ v\ ds =$$

$$< \{\beta\nabla u\}, [v] >_{\mathscr{E}_h^0} + < [\beta\nabla u], \{v\} >_{\mathscr{E}_h^0} + \sum_{e \in \mathscr{E}_h \cap \partial\Omega} \int_e \beta\nabla u \cdot \boldsymbol{n}\ v\ ds. \tag{5.3.4}$$

Combining (5.3.3) and (5.3.4) leads to the following weak form:

$$(\beta\nabla u, \nabla v)_{\mathscr{T}_h} - < \{\beta\nabla u\}, [v] >_{\mathscr{E}_h^0} - \int_{\mathscr{E}_h \cap \partial\Omega} \beta\nabla u \cdot \boldsymbol{n}\ v\ ds + < [u], \{\beta\nabla v\} >_{\mathscr{E}_h^0}$$
$$+ s < [u], [v] >_{\mathscr{E}_h^0} = (f,\ v)_{\mathscr{T}_h}.$$

Note that, for all functions $V^h \in \mathcal{S}_h^k$, we have $[V^h]_e = 0$ if e is a non-interface edge, and if $V^h \in \mathcal{S}_{h,0}^k$ then $V^h|_e = 0$ on non-interface boundary edges while $V^h|_e \neq 0$ on boundary interface edges. Hence, applying the above weak form to $\mathcal{S}_{h,E}^k$ leads to the quadratic IFE method: find $U \in \mathcal{S}_{h,E}^k$ such that

$$(\beta\nabla U^h, \nabla V^h)_{\mathscr{T}_h} + < [U^h], \{\beta\nabla V^h\} >_{\mathscr{E}_h^{0,i}} - < \{\beta\nabla U^h\}, [V^h] >_{\mathscr{E}_h^{0,i}} +$$
$$s < [U^h], [V^h] >_{\mathscr{E}_h^{0,i}} - \int_{\mathscr{E}_h^i \cap \partial\Omega} \beta\nabla U^h \cdot \boldsymbol{n}\ V^h\ ds = (f,\ V^h)_{\mathscr{T}_h}, \qquad \forall\ V^h \in \mathcal{S}_{h,0}^k. \tag{5.3.5}$$

In the discussions below, we select $s = 1$ and refer to this method as the Interior Penalty IFE method.

5.4 Numerical Results

In this section we present numerical results for several interface problems to demonstrate the optimal convergence of the quadratic IFE spaces. We will use the norms (4.1.1a) and (4.1.1b) defined in Chapter 4 to measure errors in an approximation.

Example 5.4.1.

In this example, we will show that the original non-conforming Galerkin formulation does not converge when it is used with the quadratic IFE spaces even though this non-conforming Galerkin formulation works optimally with the linear, bilinear, and 1D higher degree IFE spaces. Then, we demonstrate that the interior penalty IFE methods can produce solutions to the interface problems with optimal convergence rates.

We consider the interface problem (1.1.1) with the same domain Ω and the same true solution , as in Example 6.4.1, where $\frac{\beta^+}{\beta^-} = 5$. We recall the true solution:

$$u(x,y) = \begin{cases} \frac{(6x^2+6xy-4x+3)\ \cos(y^2-x^2-\frac{4}{3}y+\frac{4}{9})+(2+3x-3y)\ \sin(\frac{2}{3}-x-y)}{3\beta^+}\ ; & \text{on } \Omega^+, \\ \frac{(\frac{\beta^-}{\beta^+}-1)(3-8x+12xy)+(6x^2+6xy-4x+3)\ \cos(y^2-x^2-\frac{4}{3}y+\frac{4}{9})+(2+3x-3y)\ \sin(\frac{2}{3}-x-y)}{3\beta^-}\ ; & \text{on } \Omega^-. \end{cases}$$

Numerical results in Table 5.1 clearly suggest that the quadratic IFE solutions produced by the original non-conforming Galerkin formulation do not converge to the true solution under mesh refinement.

h	$\|\|u-U^h\|\|_0$	order	$\|\|u_x-U^h_x\|\|_{0,h}$	order	$\|\|u_y-U^h_y\|\|_{0,h}$	order
$\frac{1}{4}$	1.895109e-03	N/A	5.541022e-02	N/A	3.524658e-02	N/A
$\frac{1}{8}$	4.842859e-04	1.9683	1.849617e-02	1.5829	1.451450e-02	1.2799
$\frac{1}{16}$	6.071277e-05	2.9957	4.626621e-03	1.9991	3.856017e-03	1.9123
$\frac{1}{32}$	5.041339e-05	0.2681	5.654537e-03	-0.2894	5.481738e-03	-0.5075
$\frac{1}{64}$	6.476201e-06	2.9605	1.545544e-03	1.8712	1.543935e-03	1.8280
$\frac{1}{128}$	6.674539e-06	-0.0435	2.706456e-03	-0.8082	2.683355e-03	-0.7974

Table 5.1: L^2 errors and orders for u and its derivatives for Example 5.4.1 with $r = 5$ using the method (5.2.1) with $\mathcal{S}_h^1$.

Example 5.4.2.

Next, we solve the same interface problem as in Example 5.4.1 for $\frac{\beta^+}{\beta^-} = 5$ and $\frac{\beta^+}{\beta^-} = 10^3$ on the same meshes by the interior penalty IFE method (5.3.5) using quadratic IFE spaces $\mathcal{S}_h^1$ and $\mathcal{S}_h^2$. The related datum are presented in Tables 5.2, 5.3, 5.4, and 5.5. From these datum, we can easily observe that the interior penalty IFE method with the IFE space $\mathcal{S}_h^1$ performs optimally, while it performs near optimally with the space $\mathcal{S}_h^2$.

h	$\|\|u - U^h\|\|_0$	order	$\|\|u_x - U_x^h\|\|_{0,h}$	order	$\|\|u_y - U_y^h\|\|_{0,h}$	order
$\frac{1}{4}$	2.185943e-03	N/A	1.862205e-02	N/A	2.458501e-02	N/A
$\frac{1}{8}$	2.746045e-04	2.9928	4.496799e-03	2.0500	6.257552e-03	1.9741
$\frac{1}{16}$	3.426104e-05	3.0027	1.105460e-03	2.0242	1.565315e-03	1.9991
$\frac{1}{32}$	4.284828e-06	2.9992	2.757968e-04	2.0029	3.916519e-04	1.9988
$\frac{1}{64}$	5.355157e-07	3.0002	6.883339e-05	2.0024	9.787855e-05	2.0005
$\frac{1}{128}$	5.582693e-08	3.0001	5.399404e-05	1.9999	3.426510e-05	1.9998

Table 5.2: L^2 errors and orders for u and its derivatives for Example 5.4.2 with $r = 5$ using the interior penalty IFE method with $\mathcal{S}_h^1$.

h	$\|\|u - U^h\|\|_0$	order	$\|\|u_x - U_x^h\|\|_{0,h}$	order	$\|\|u_y - U_y^h\|\|_{0,h}$	order
$\frac{1}{4}$	2.008170e-03	N/A	5.644459e-02	N/A	3.510983e-02	N/A
$\frac{1}{8}$	2.340102e-04	3.1012	1.383754e-02	2.0282	8.805326e-03	1.9954
$\frac{1}{16}$	2.891611e-05	3.0166	3.464429e-03	1.9978	2.199582e-03	2.0011
$\frac{1}{32}$	3.584640e-06	3.0119	8.641624e-04	2.0032	5.489480e-04	2.0024
$\frac{1}{64}$	4.473714e-07	3.0022	2.160397e-04	2.0000	1.371766e-04	2.0006
$\frac{1}{128}$	5.585713e-08	3.0017	5.399635e-05	2.0002	3.427253e-05	2.0010

Table 5.3: L^2 errors and orders for u and its derivatives for Example 5.4.2 with $r = 10^3$ using the interior penalty IFE method with $\mathcal{S}_h^1$.

h	$\|\|u - U^h\|\|_0$	order	$\|\|u_x - U_x^h\|\|_{0,h}$	order	$\|\|u_y - U_y^h\|\|_{0,h}$	order
$\frac{1}{4}$	1.850654e-03	N/A	5.517477e-02	N/A	3.508381e-02	N/A
$\frac{1}{8}$	2.355202e-04	2.9741	1.396110e-02	1.9826	9.091639e-03	1.9481
$\frac{1}{16}$	3.014075e-05	2.9660	3.561352e-03	1.9709	2.386854e-03	1.9294
$\frac{1}{32}$	3.899650e-06	2.9503	9.046449e-04	1.9770	6.167033e-04	1.9524
$\frac{1}{64}$	5.462242e-07	2.8357	2.449317e-04	1.8849	1.808684e-04	1.7696
$\frac{1}{128}$	7.834247e-08	2.8016	6.361485e-05	1.9449	4.831422e-05	1.9044

Table 5.4: L^2 errors and orders for u and its derivatives for Example 5.4.2 with $r = 5$ using the interior penalty IFE method with $\mathcal{S}_h^2$.

h	$\|\|u - U^h\|\|_0$	order	$\|\|u_x - U_x^h\|\|_{0,h}$	order	$\|\|u_y - U_y^h\|\|_{0,h}$	order
$\frac{1}{4}$	2.094214e-03	N/A	5.715809e-02	N/A	3.542342e-02	N/A
$\frac{1}{8}$	2.330975e-04	3.1674	1.384422e-02	2.0456	8.817699e-03	2.0062
$\frac{1}{16}$	2.906282e-05	3.0036	3.468043e-03	1.9970	2.203575e-03	2.0005
$\frac{1}{32}$	3.589693e-06	3.0172	8.680604e-04	1.9982	5.554346e-04	1.9881
$\frac{1}{64}$	4.480319e-07	3.0021	2.164614e-04	2.0036	1.379888e-04	2.0090
$\frac{1}{128}$	5.830773e-08	2.9418	5.502787e-05	1.9758	3.589954e-05	1.9425

Table 5.5: L^2 errors and orders for u and its derivatives for Example 5.4.2 with $r = 10^3$ using the interior penalty IFE method with $\mathcal{S}_h^2$.

Example 5.4.3.

There are many applications with great potentials to take advantages of the key feature of IFE methods: their meshes can be independent of the location of interfaces. We now use a thin layer interface problem to illustrate this.

We consider the interface problem (1.1.1) on $\Omega = (0,1)^2$ consisting of two materials, one of them forms a thin layer in the top part of the domain. More specifically, we assume that the interface is defined by

$$y = 1 - \epsilon,\ 0 < \epsilon < 1, \tag{5.4.1}$$

which separates Ω into Ω^+ defined by $y > 1-\epsilon$ and Ω^- defined by $y < 1-\epsilon$ as illustrated in Figure 5.1. The boundary conditions and the source term f are selected such that the true solution is

$$u(x,y) = \begin{cases} \frac{(1+x^3(y+e-1))\cos(x(y+e-1))+\sin(x(y+e-1))}{\beta^+}, & \text{on } \Omega^+, \\ \frac{(1+x^3(y+e-1))\cos(x(y+e-1))+\sin(x(y+e-1))-1}{\beta^-} + \frac{1}{\beta^+}, & \text{on } \Omega^-. \end{cases} \tag{5.4.2}$$

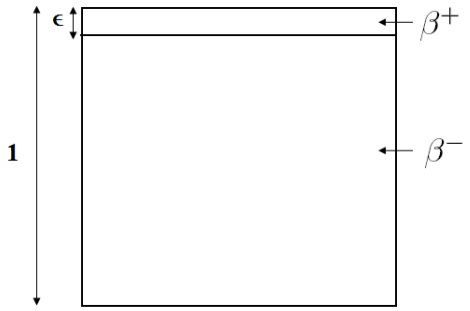

Figure 5.1: A two-material domain with a thin layer of width ϵ for Example 5.4.3.

We solve this problem for $\epsilon = 10^{-3}$ and $\frac{\beta^+}{\beta^-} = 5$ using the interior penalty IFE method (5.3.5) on uniform meshes with $2n^2$ right-angle triangles using the space $\mathcal{S}_h^1$. We present the L^2 errors for the quadratic IFE solutions to u and it derivatives in Table 5.6. As a comparison, we also solve this problem by the standard quadratic finite element method with body-fitted meshes. The related computations are carried out through the software *COMSOL* using its default parameters except for "max element size" $hmax = 1/8, 1/16, 1/32$ and $1/64$. A typical mesh used in COMSOL for $hmax = 1/16$ and $\epsilon = 10^{-3}$ is shown in Figure 5.2. We present the finite element errors in Table 5.7 and plot the L^2 errors versus the number of degrees of freedom for both methods in Figure 5.3. From these data, we observe that, to produce numerical solutions with comparable accuracies, the standard finite element method based on body-fitted meshes require much more global degree of freedoms than the interior penalty IFE method.

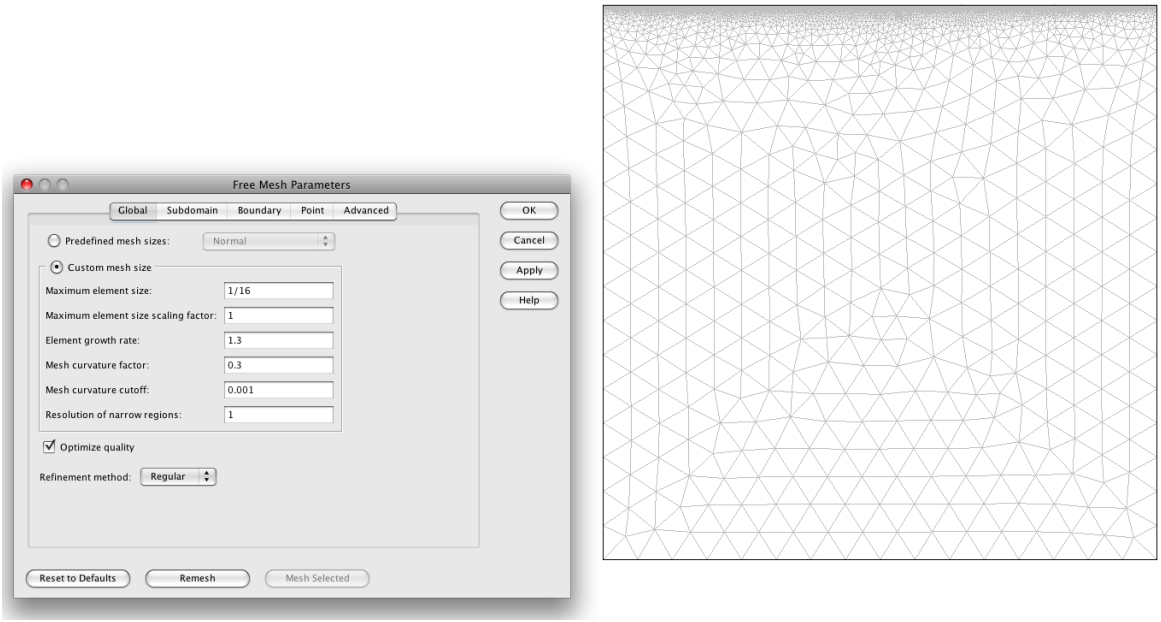

Figure 5.2: COMSOL interface with a mesh for the two-material domain of Figure 5.1 with $\epsilon = 10^{-3}$.

DOF	$\|\|u - U^h\|\|_0$	$\|\|u_x - U^h_x\|\|_{0,h}$	$\|\|u_y - U^h_y\|\|_{0,h}$
289	1.689638e-04	4.136825e-03	3.268165e-03
1089	2.137912e-05	1.041716e-03	8.173907e-04
4225	2.684222e-06	2.610211e-04	2.043138e-04
16641	3.362449e-07	6.529878e-05	5.107821e-05

Table 5.6: L^2 errors and orders for u and its derivatives for Example 5.4.3 with $\epsilon = 10^{-3}$ using the interior penalty IFE method (5.3.5) with $\mathcal{S}_h^1$.

DOF	$\|\|u - U^h\|\|_0$	$\|\|u_x - U^h_x\|\|_{0,h}$	$\|\|u_y - U^h_y\|\|_{0,h}$
25550	1.838226e-04	5.894349e-03	4.736762e-03
25706	2.488306e-05	1.633209e-03	1.391346e-03
27182	3.049056e-06	4.049628e-04	3.783127e-04
32890	3.796342e-07	1.038044e-04	9.289677e-05

Table 5.7: L^2 errors and orders for u and its derivatives for Example 5.4.3 with $\epsilon = 10^{-3}$ using the standard finite element method in COMSOL software on body-fitted meshes.

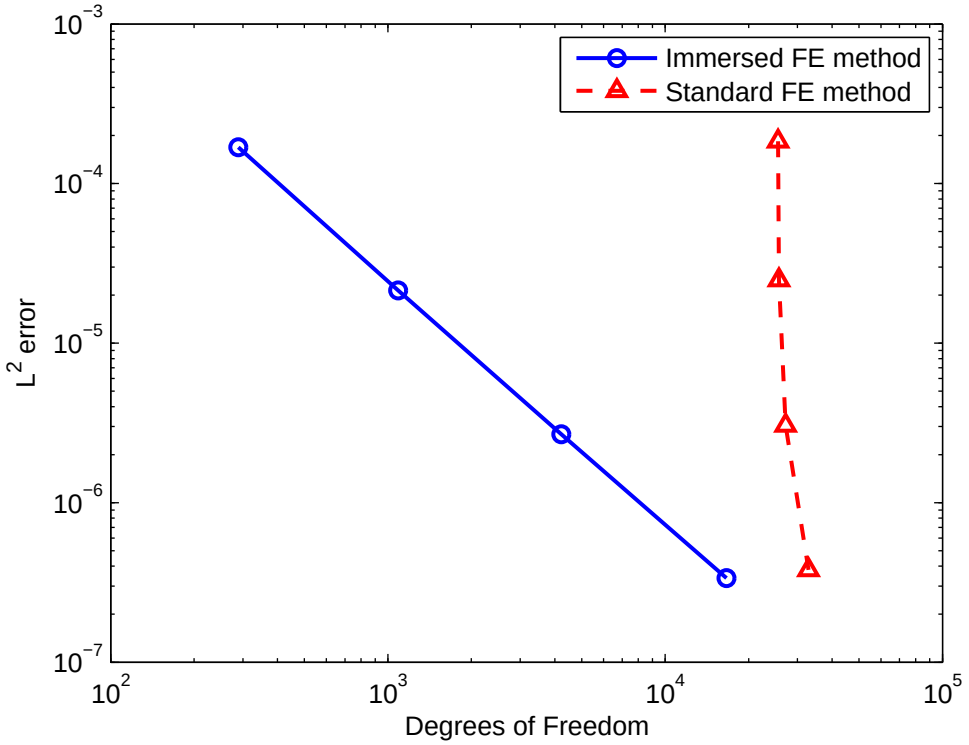

Figure 5.3: L^2 errors versus the number of degrees of freedom for immersed method on uniform meshes and for standard finite element method on body-fitted meshes using COMSOL for Example 5.4.3.

5.5 Conclusions

The interior penalty IFE methods presented in this chapter rely on the specially designed piecewise quadratic IFE spaces $\mathcal{S}_h^k,\ k = 1, 2$, presented in chapter 2, and lead to $\mathcal{O}(h^{3-s})$ optimal convergence rates in broken $H^s,\ s = 0, 1$, norms. In addition to the optimality of the method in finding numerical solutions to interface problems, our numerical results showed also that this method is more efficient than the standard finite element method for solving some particular interface problems such as problems involving thin layers. A future work will consist of testing a discontinuous Galerkin formulation and a selective discontinuous Galerkin formulation [29] with these quadratic IFE spaces $\mathcal{S}_h^k,\ k = 1, 2$.

Chapter 6

p-th Degree Immersed Finite Element Spaces for Linear Interface

6.1 Introduction

In this chapter, we discuss immersed finite element spaces of degree $p \geq 3$, which represent a generalization of the quadratic IFE spaces developed in Chapter 2, considering the same model problem and a linear interface $\Gamma : y = Ax + B$. First, we discuss the jump conditions on interface elements and present some properties of the p-th degree IFE spaces. Next, we discuss the construction of IFE shape functions for such spaces. A detailed construction of hierarchical cubic IFE shape functions is presented, and general procedure is given for the construction of hierarchical IFE shape functions of degree p.

6.2 p-the Degree IFE Spaces and Jump Conditions

We first define the p-th degree IFE spaces $\mathcal{R}_1^p(T)$ and $\mathcal{R}_2^p(T)$ locally on an arbitrary interface element T. $\mathcal{R}_1^p(T)$ and $\mathcal{R}_2^p(T)$ are the extensions of the quadratic IFE spaces $\mathcal{R}_1(T)$ and $\mathcal{R}_2(T)$ defined in (2.2.3a) and (2.2.3b).

$U \in \mathcal{R}_1^p(T)$, if and only if $U|_{T^\pm} \in \mathcal{P}_p$ and U satisfies the following conditions

$$[U]_{T\cap\Gamma} = 0 \tag{6.2.1a}$$

$$[\beta \frac{\partial U}{\partial \boldsymbol{n}}]_{T\cap\Gamma} = 0 \tag{6.2.1b}$$

$$[\beta \Delta U]_{T\cap\Gamma} = 0 \tag{6.2.1c}$$

$$[\ \frac{\partial^l}{\partial \boldsymbol{n}^l}(\beta \Delta U)\ ]_{T\cap\Gamma} = 0\ , \qquad l = 1, 2, \ldots, (p-2). \tag{6.2.1d}$$

$U \in \mathcal{R}_2^p(T)$, if and only if $U|_{T^\pm} \in \mathcal{P}_p$ and U satisfies the jump conditions (6.2.1a) and (6.2.1b) in addition to the conditions

$$[\ \beta \frac{\partial^2 U}{\partial \boldsymbol{n}^2}\ ]_{T\cap\Gamma} = 0\ , \tag{6.2.2a}$$

$$[\ \beta \frac{\partial^l U}{\partial \boldsymbol{n}^l}\ ]_{T\cap\Gamma} = 0\ , \qquad l = 3, 4, \ldots, p. \tag{6.2.2b}$$

We define the global IFE spaces over the whole solution domain Ω:

$$\mathcal{S}_h^{p,k} = \{U,\ |\ \ U|_T \in \mathcal{P}_p,\ for\ T \in \mathscr{T}_h \setminus \mathscr{T}_h^i\ \text{ and }\ U|_T \in \mathcal{R}_k^p(T),\ for\ T \in \mathscr{T}_h^i\},\ k = 1, 2. \tag{6.2.3}$$

In our computations, we will use the subspaces:

$$\mathcal{S}_{h,0}^{p,k} = \{U,\ |\ \ U \in \mathcal{S}_h^{p,k},\ and\ [U]_e = 0,\ for\ e \in \mathscr{E}_h \setminus \mathscr{E}_h^i\},\ k = 1, 2, \tag{6.2.4}$$

in solving the interface problem.

We note that equations (6.2.1a), (6.2.1b) and (6.2.1c) are the jump conditions used to define the quadratic IFE space $\mathcal{R}_1(T)$; and equations (6.2.1d) are an extension of the condition (6.2.1c).
Similarly, we note that equations (6.2.1a), (6.2.1b) and (6.2.2a) are the jump conditions used to define the quadratic IFE space $\mathcal{R}_2(T)$; and equations (6.2.2b) are an extension of the condition (6.2.2a).

Remark 6.2.1. *Using the notations introduced above, we can denote the quadratic IFE spaces $\mathcal{R}_1(T)$ and $\mathcal{R}_2(T)$ as $\mathcal{R}_1^2(T)$ and $\mathcal{R}_2^2(T)$, respectively.*
On any physical element T, we have:

$$\mathcal{R}_2^{p-1}(T) \subset \mathcal{R}_2^p(T), \quad for\ p \geq 3, \tag{6.2.5}$$

$$\mathcal{R}_1^{p-1}(T) \subset \mathcal{R}_1^p(T), \quad for\ p \geq 3. \tag{6.2.6}$$

As discussed previously, an interface finite element function is computed by mapping each interface element T in the mesh into a reference interface triangle $\hat{T}$, using the affine mapping F defined in (2.2.7). Thus, we develop reference IFE spaces $\hat{\mathcal{R}}_1^p(\hat{T})$ and $\hat{\mathcal{R}}_2^p(\hat{T})$ over $\hat{T}$, where $\hat{T} = F(T)$.

Hence, on a reference element $\hat{T}$, we construct the following IFE function spaces:

$$\hat{\mathcal{R}}_1^p(\hat{T}) = \{\hat{U} \in \hat{\mathcal{P}}_p(\hat{T}), |\ [\hat{U}]_{\hat{\Gamma}} = [\hat{\beta}\frac{\partial \hat{U}}{\partial \hat{\boldsymbol{n}}}]_{\hat{\Gamma}} = [\frac{\partial^l}{\partial \hat{\boldsymbol{n}}^l}(\hat{\beta}(\mathbf{J}^t\hat{\nabla}).(\mathbf{J}^t\hat{\nabla})\hat{U})]_{\hat{\Gamma}} = 0,\ l = 0, \ldots, p-2\}, \tag{6.2.7}$$

and

$$\hat{\mathcal{R}}_2^p(\hat{T}) = \{\hat{U} \in \hat{\mathcal{P}}_p(\hat{T}), |\ [\hat{U}]_{\hat{\Gamma}} = 0,\ [\hat{\beta}\frac{\partial^l \hat{U}}{\partial \hat{\boldsymbol{n}}^l}]_{\hat{\Gamma}} = 0,\ l = 1, \ldots, p\}, \tag{6.2.8}$$

where

$$\hat{\mathcal{P}}_p = \{\hat{p} \mid \hat{p}|_{\hat{T}^i} \in \mathcal{P}_p \ , \quad i = 1, 2 \ \}, \tag{6.2.9}$$

$$\hat{\Gamma} = F(\Gamma), \qquad \hat{\boldsymbol{n}} = J\boldsymbol{n}, \qquad \text{and} \qquad \hat{\nabla}\hat{U} = (\partial_{\hat{x}}\hat{U}, \partial_{\hat{y}}\hat{U})^t. \tag{6.2.10}$$

Now, we construct hierarchical IFE shape functions of degree $p = 3$, and we conclude a general procedure for constructing p-th degree hierarchical IFE shape functions.

6.3 Hierarchical p-th Degree IFE Shape Functions

Guided by the constructing procedure of hierarchical quadratic IFE shape functions in Chapter 3, we construct hierarchical higher-degree IFE shape functions. We consider the same reference interface element $\hat{T}$ with vertices $\hat{V}_1 = (0,0)^t$, $\hat{V}_2 = (1,0)^t$, $\hat{V}_3 = (0,1)^t$, cut by a linear interface $\hat{\Gamma} : \hat{y} = a\hat{x} + b$, as described in Figure 3.1.

Hierarchical Cubic IFE Shape Functions on $\hat{\mathcal{R}}_2^3(\hat{T})$

In Chapter 3, we constructed a basis of $\hat{\varphi}_i \in \hat{\mathcal{R}}_2(\hat{T})$ formed by three piecewise linear IFE shape functions developed by Li, Lin, Lin and Rogers [42], in addition to three piecewise quadratic IFE shape functions, as proved in Theorem 3.3.1.

We have $\hat{\varphi}_i \in \hat{\mathcal{R}}_2(\hat{T}) \subset \hat{\mathcal{R}}_2^3(\hat{T}),\ i = 1, \ldots, 6.$

Now, guided by our work for quadratic IFE spaces as well as the cubic standard finite element theory, we construct four cubic IFE shape functions $\hat{\varphi}_i,\ i = 7 \ldots 10$, which satisfy the physical jump conditions (2.2.9) and the extended jump conditions (6.2.2a), and (6.2.2b) with $l = 3$:

$$[\frac{\partial^3 \hat{U}}{\partial \hat{\boldsymbol{n}}^3}]_{\hat{\Gamma}} = 0. \tag{6.3.1}$$

Thus, $\hat{\varphi}_7$, $\hat{\varphi}_8$, $\hat{\varphi}_9$ and $\hat{\varphi}_{10}$ can be written as

$$\hat{\varphi}_7(\hat{\xi}, \hat{\eta}) = \begin{cases} \hat{\varphi}_1(\hat{\xi}, \hat{\eta})\hat{\varphi}_4(\hat{\xi}, \hat{\eta}) + \hat{c}_7\hat{\eta}^2 + \hat{d}_7\hat{\eta}^3 \ , & (\hat{x}, \hat{y}) \in \hat{T}^1 \\ \hat{\varphi}_1(\hat{\xi}, \hat{\eta})\hat{\varphi}_4(\hat{\xi}, \hat{\eta}), & (\hat{x}, \hat{y}) \in \hat{T}^2 \end{cases} \tag{6.3.2a}$$

$$\hat{\varphi}_8(\hat{\xi}, \hat{\eta}) = \begin{cases} \hat{\varphi}_2(\hat{\xi}, \hat{\eta})\hat{\varphi}_5(\hat{\xi}, \hat{\eta}) + \hat{c}_8\hat{\eta}^2 + \hat{d}_8\hat{\eta}^3 \ , & (\hat{x}, \hat{y}) \in \hat{T}^1 \\ \hat{\varphi}_2(\hat{\xi}, \hat{\eta})\hat{\varphi}_5(\hat{\xi}, \hat{\eta}), & (\hat{x}, \hat{y}) \in \hat{T}^2 \end{cases} \tag{6.3.2b}$$

$$\hat{\varphi}_9(\hat{\xi},\hat{\eta}) = \begin{cases} \hat{\varphi}_3(\hat{\xi},\hat{\eta})\hat{\varphi}_6(\hat{\xi},\hat{\eta}) + \hat{c}_9\hat{\eta}^2 + \hat{d}_9\hat{\eta}^3 \ , & (\hat{x},\hat{y}) \in \hat{T}^1 \\ \hat{\varphi}_3(\hat{\xi},\hat{\eta})\hat{\varphi}_6(\hat{\xi},\hat{\eta}), & (\hat{x},\hat{y}) \in \hat{T}^2. \end{cases} \tag{6.3.2c}$$

$$\hat{\varphi}_{10}(\hat{\xi},\hat{\eta}) = \begin{cases} \hat{\varphi}_1(\hat{\xi},\hat{\eta})\hat{\varphi}_5(\hat{\xi},\hat{\eta}) + \hat{c}_{10}\hat{\eta}^2 + \hat{d}_{10}\hat{\eta}^3 \ , & (\hat{x},\hat{y}) \in \hat{T}^1 \\ \hat{\varphi}_1(\hat{\xi},\hat{\eta})\hat{\varphi}_5(\hat{\xi},\hat{\eta}), & (\hat{x},\hat{y}) \in \hat{T}^2 \end{cases} \tag{6.3.2d}$$

First, we show in the following lemma that the shape function $\hat{\varphi}_k$, $k = 7, \ldots, 10$, satisfy the physical jump conditions on the reference element.

Lemma 6.3.1. *The four IFE shape functions $\hat{\varphi}_k$, $k = 7, \ldots, 10$, defined in (6.3.2), satisfy the jump conditions (2.2.9a) and (2.2.9b).*

Proof. Since $\hat{\varphi}_i$ and $\hat{\varphi}_j$ are continuous, and the interface $\hat{\Gamma}$ is $\hat{\eta} = 0$, then $[\hat{\varphi}_k]_{\hat{\Gamma}} = 0$.

The derivative of $\hat{\varphi}_k$ in the direction od $\hat{\boldsymbol{n}}$ is given by (6.3.3), then

$$\hat{\beta}\frac{\partial\hat{\varphi}_k}{\partial\hat{\boldsymbol{n}}}(\hat{\xi},\hat{\eta}) = \begin{cases} \hat{\beta}^1\frac{\partial\hat{\varphi}_i}{\partial\hat{\boldsymbol{n}}}(\hat{\xi},\hat{\eta})\hat{\varphi}_j(\hat{\xi},\hat{\eta}) + \hat{\beta}^1\hat{\varphi}_i(\hat{\xi},\hat{\eta})\frac{\partial\hat{\varphi}_j}{\partial\hat{\boldsymbol{n}}}(\hat{\xi},\hat{\eta}) + 2\hat{\beta}^1\hat{c}_k\hat{\eta} \ + 3\hat{\beta}^1\hat{d}_k\hat{\eta}^2 \ , & \text{on } \hat{T}^1 \\ \hat{\beta}^2\frac{\partial\hat{\varphi}_i}{\partial\hat{\boldsymbol{n}}}(\hat{\xi},\hat{\eta})\hat{\varphi}_j(\hat{\xi},\hat{\eta}) + \hat{\beta}^2\hat{\varphi}_i(\hat{\xi},\hat{\eta})\frac{\partial\hat{\varphi}_j}{\partial\hat{\boldsymbol{n}}}(\hat{\xi},\hat{\eta}) & , \text{ on } \hat{T}^2 \end{cases}$$

Since $\hat{\varphi}_i$, $\hat{\varphi}_j$, $\hat{\beta}\frac{\partial\hat{\varphi}_i}{\partial\hat{\boldsymbol{n}}}$ and $\hat{\beta}\frac{\partial\hat{\varphi}_j}{\partial\hat{\boldsymbol{n}}}$ are continuous over $\hat{\Gamma} : \hat{\eta} = 0$, then we obtain that $\hat{\beta}\frac{\partial\hat{\varphi}_k}{\partial\hat{\boldsymbol{n}}}$ is continuous, as well.

□

Next, to have $\varphi_k \in \hat{\mathcal{R}}_2^3(\hat{T})$ $k = 7, \ldots, 10$, we select the values of $\hat{c}_k$ and $\hat{d}_k$ such that the shape functions $\hat{\varphi}_k$, $k = 7, \ldots, 10$ satisfy the conditions (2.2.17) and (6.3.1).

We have, the derivative of $\hat{\varphi}_k$ in the direction od $\hat{\boldsymbol{n}}$ can be written as

$$\frac{\partial\hat{\varphi}_k}{\partial\hat{\boldsymbol{n}}}(\hat{\xi},\hat{\eta}) = \begin{cases} \frac{\partial\hat{\varphi}_i}{\partial\hat{\boldsymbol{n}}}(\hat{\xi},\hat{\eta})\hat{\varphi}_j(\hat{\xi},\hat{\eta}) + \hat{\varphi}_i(\hat{\xi},\hat{\eta})\frac{\partial\hat{\varphi}_j}{\partial\hat{\boldsymbol{n}}}(\hat{\xi},\hat{\eta}) + 2\hat{c}_k\hat{\eta} \ + 3\hat{d}_k\hat{\eta}^2 \ , & \text{on } \hat{T}^1 \\ \frac{\partial\hat{\varphi}_i}{\partial\hat{\boldsymbol{n}}}(\hat{\xi},\hat{\eta})\hat{\varphi}_j(\hat{\xi},\hat{\eta}) + \hat{\varphi}_i(\hat{\xi},\hat{\eta})\frac{\partial\hat{\varphi}_j}{\partial\hat{\boldsymbol{n}}}(\hat{\xi},\hat{\eta}) & , \text{ on } \hat{T}^2 \end{cases} \tag{6.3.3}$$

The second normal derivative of $\hat{\varphi}_k$, $k = 7, \ldots, 10$ is

$$\frac{\partial^2\hat{\varphi}_k}{\partial\hat{\boldsymbol{n}}^2}(\hat{\xi},\hat{\eta}) = \begin{cases} \hat{\varphi}_i^1(\hat{\xi},\hat{\eta})\frac{\partial^2\hat{\varphi}_j^1}{\partial\hat{\boldsymbol{n}}^2}(\hat{\xi},\hat{\eta}) + 2\ \frac{\partial\hat{\varphi}_i^1}{\partial\hat{\boldsymbol{n}}}(\hat{\xi},\hat{\eta})\frac{\partial\hat{\varphi}_j^1}{\partial\hat{\boldsymbol{n}}}(\hat{\xi},\hat{\eta}) + 2\ \hat{c}_k + 6\ \hat{d}_k\hat{\eta} \ , & \text{on } \hat{T}^1 \\ \hat{\varphi}_i^2(\hat{\xi},\hat{\eta})\frac{\partial^2\hat{\varphi}_j^2}{\partial\hat{\boldsymbol{n}}^2}(\hat{\xi},\hat{\eta}) + 2\ \frac{\partial\hat{\varphi}_i^2}{\partial\hat{\boldsymbol{n}}}(\hat{\xi},\hat{\eta})\frac{\partial\hat{\varphi}_j^2}{\partial\hat{\boldsymbol{n}}}(\hat{\xi},\hat{\eta}) & , \text{ on } \hat{T}^2 \end{cases} \tag{6.3.4}$$

Since $\hat{\beta}\hat{\varphi}_i\frac{\partial^2\hat{\varphi}_j}{\partial\hat{\boldsymbol{n}}^2}$ is continuous, enforcing the jump condition (2.2.17) yields

$$\hat{\beta}^1\frac{\partial\hat{\varphi}_i^1}{\partial\hat{\boldsymbol{n}}}(\hat{\xi},0^+)\frac{\partial\hat{\varphi}_j^1}{\partial\hat{\boldsymbol{n}}}(\hat{\xi},0^+)+\ \hat{\beta}^1\ \hat{c}_k\ =\hat{\beta}^2\frac{\partial\hat{\varphi}_i^2}{\partial\hat{\boldsymbol{n}}}(\hat{\xi},0^-)\frac{\partial\hat{\varphi}_j^2}{\partial\hat{\boldsymbol{n}}}(\hat{\xi},0^-). \tag{6.3.5}$$

Hence, we choose $\hat{c}_k$ as

$$\hat{c}_k=-\frac{\hat{\beta}^1\ \hat{\boldsymbol{n}}\cdot\hat{\varphi}_i^1(\hat{\xi},0^+)\ \ \hat{\boldsymbol{n}}\cdot\hat{\varphi}_j^1(\hat{\xi},0^+)-\hat{\beta}^2\ \hat{\boldsymbol{n}}\cdot\hat{\varphi}_i^2(\hat{\xi},0^-)\ \ \hat{\boldsymbol{n}}\cdot\hat{\varphi}_j^2(\hat{\xi},0^-)}{\hat{\beta}^1}, \tag{6.3.6}$$

which can, alternatively, be written as

$$\hat{c}_k=-\frac{1}{\hat{\beta}^1}\left[\hat{\beta}\frac{\partial\hat{\varphi}_i}{\partial\hat{\boldsymbol{n}}}\frac{\partial\hat{\varphi}_j}{\partial\hat{\boldsymbol{n}}}\right]_{\hat{\Gamma}}. \tag{6.3.7}$$

Notice that this expression is the same as (3.3.6) used for the quadratic IFE shape functions.

Now, consider the third normal derivative of $\varphi_k,\ k=7,\ldots,10$

$$\frac{\partial^3\hat{\varphi}_k}{\partial\hat{\boldsymbol{n}}^3}(\hat{\xi},\hat{\eta})=\begin{cases}3\ \frac{\partial\hat{\varphi}_i^1}{\partial\hat{\boldsymbol{n}}}(\hat{\xi},\hat{\eta})\frac{\partial^2\hat{\varphi}_j^1}{\partial\hat{\boldsymbol{n}}^2}(\hat{\xi},\hat{\eta})+6\ \hat{d}_k\ , & (\hat{x},\hat{y})\in\hat{T}^1\\ 3\ \frac{\partial\hat{\varphi}_i^2}{\partial\hat{\boldsymbol{n}}}(\hat{\xi},\hat{\eta})\frac{\partial^2\hat{\varphi}_j^2}{\partial\hat{\boldsymbol{n}}^2}(\hat{\xi},\hat{\eta}) & , \quad (\hat{x},\hat{y})\in\hat{T}^2\end{cases} \tag{6.3.8}$$

Enforcing the jump condition (6.3.1) yields

$$\hat{\beta}^1\frac{\partial\hat{\varphi}_i^1}{\partial\hat{\boldsymbol{n}}}(\hat{\xi},0^+)\frac{\partial^2\hat{\varphi}_j^1}{\partial\hat{\boldsymbol{n}}^2}(\hat{\xi},0^+)+\ 2\ \hat{\beta}^1\ \hat{c}_k\ =\hat{\beta}^2\frac{\partial\hat{\varphi}_i^2}{\partial\hat{\boldsymbol{n}}}(\hat{\xi},0^-)\frac{\partial^2\hat{\varphi}_j^2}{\partial\hat{\boldsymbol{n}}^2}(\hat{\xi},0^-). \tag{6.3.9}$$

Hence, we choose $\hat{d}_k$ as

$$\hat{d}_k=-\frac{1}{2\hat{\beta}^1}\left(\hat{\beta}^1\frac{\partial\hat{\varphi}_i^1}{\partial\hat{\boldsymbol{n}}}(\hat{\xi},0^+)\frac{\partial^2\hat{\varphi}_j^1}{\partial\hat{\boldsymbol{n}}^2}(\hat{\xi},0^+)-\hat{\beta}^2\frac{\partial\hat{\varphi}_i^2}{\partial\hat{\boldsymbol{n}}}(\hat{\xi},0^-)\frac{\partial^2\hat{\varphi}_j^2}{\partial\hat{\boldsymbol{n}}^2}(\hat{\xi},0^-)\right), \tag{6.3.10}$$

which can, alternatively, be written as

$$\hat{d}_k=-\frac{1}{2\ \hat{\beta}^1}\left[\hat{\beta}\frac{\partial\hat{\varphi}_i}{\partial\hat{\boldsymbol{n}}}\frac{\partial^2\hat{\varphi}_j}{\partial\hat{\boldsymbol{n}}^2}\right]_{\hat{\Gamma}}. \tag{6.3.11}$$

In a similar way, we can construct IFE shape functions for the space $\hat{\mathcal{R}}_1^3(\hat{T})$.

p-th degree IFE Shape Functions on $\hat{\mathcal{R}}_2^p(\hat{T})$

Guided by the standard finite elements theory, we expect that the dimension of the space $\hat{\mathcal{R}}_2^p(\hat{T})$ is $N_p=\frac{(p+1)(p+2)}{2}$. Following the same pattern of the quadratic and cubic IFE

shape functions, we construct hierarchical IFE shape functions for the p-th degree IFE space $\hat{\mathcal{R}}_2^p(\hat{T})$, assuming that we have $N_{p-1} = \frac{p(p+1)}{2}$ hierarchical IFE shape functions for the $(p-1)$-th order IFE space $\hat{\mathcal{R}}_2^{p-1}(\hat{T})$. Hence, we use the IFE shape functions of $\hat{\mathcal{R}}_2^{p-1}(\hat{T})$ and we construct $p+1$ IFE shape functions $\hat{\varphi}_k,\ k = N_{p-1}+1, N_{p-1}+2, \ldots, N_p$. In fact, recall that $\hat{\varphi}_i \in \hat{\mathcal{R}}_2^{p-1}(\hat{T}) \subset \hat{\mathcal{R}}_2^p(\hat{T}),\ i = 1, 2, \ldots, N_{p-1}$.

In the current section, we will proceed by induction. We assume that we have shape functions of the IFE space $\hat{\mathcal{R}}_2^{p-1}(\hat{T})$ and we will construct $p+1$ IFE shape functions $\hat{\varphi}_k,\ k = N_{p-1} + 1, N_{p-1}+2, \ldots, N_p$, which satisfy the physical jump conditions (2.2.9), the extended jump condition of second order (2.2.17) and the higher-order extended jump conditions (6.3.1) for $l = 3, 4, \ldots, p$.

Thus, $\hat{\varphi}_k,\ k = N_{p-1}+1, N_{p-1}+2, \ldots, N_p$ can be written as

$$\hat{\varphi}_k(\hat{\xi},\hat{\eta}) = \begin{cases} \hat{\varphi}_i^1(\hat{\xi},\hat{\eta})\hat{\varphi}_j^1(\hat{\xi},\hat{\eta}) + \sum_{s=2}^{p} \hat{c}_{k,s}\hat{\eta}^s\ , & (\hat{x},\hat{y}) \in \hat{T}^1, \\ \\ \hat{\varphi}_i^2(\hat{\xi},\hat{\eta})\hat{\varphi}_j^2(\hat{\xi},\hat{\eta}) & , \quad (\hat{x},\hat{y}) \in \hat{T}^2. \end{cases} \tag{6.3.12}$$

where $\hat{\varphi}_i$ and $\hat{\varphi}_j$ are, respectively, a linear and $(p-1)$-th degree IFE shape functions.

Lemma 6.3.2. *The $(p+1)$ IFE shape functions $\hat{\varphi}_k,\ k = N_{p-1}+1, N_{p-1}+2, \ldots, N_p$, defined in (6.3.12), satisfy the mapped physical jump conditions (2.2.9a) and (2.2.9b).*

Proof. The proof is similar to the proof of Lemma 6.3.1, and is omitted. □

Now, since the IFE shape functions $\hat{\varphi}_k,\ k = N_{p-1}+1, N_{p-1}+2, \ldots, N_p$, defined in (6.3.12) satisfy the jump conditions (2.2.9a) and (2.2.9b), we will select $c_{k,s},\ k = N_{p-1}+1, N_{p-1}+2, \ldots, N_p$,
$s = 2, \ldots, p$, such that

$$[\beta\ \frac{\partial^s \hat{\varphi}_k}{\partial \hat{\boldsymbol{n}}^s}(\hat{\xi}, 0)]_{\hat{\Gamma}} = 0, \tag{6.3.13}$$

which will lead to $\hat{\varphi}_k \in \mathcal{R}_2^p(T),\ k = N_{p-1}+1 \ldots N_p$.

We have the l-th normal derivative of $\hat{\varphi}_k,\ k = N_{p-1}+1, N_{p-1}+2, 3, \ldots, N_p$, where $2 \le l \le p$, is

$$\frac{\partial^l \hat{\varphi}_k}{\partial \hat{\boldsymbol{n}}^l}(\hat{\xi},\hat{\eta}) = \begin{cases} \sum_{v+w=l} \left(\frac{\partial^v \hat{\varphi}_i^1}{\partial \hat{\boldsymbol{n}}^v} \frac{\partial^w \hat{\varphi}_j^1}{\partial \hat{\boldsymbol{n}}^w} \right) + \sum_{s=l}^{p} \hat{c}_{k,s} \frac{s!}{(s-l)!} \hat{\eta}^{s-l}\ , & \text{on } \hat{T}^1, \\ \\ \sum_{v+w=l} \left(\frac{\partial^v \hat{\varphi}_i^2}{\partial \hat{\boldsymbol{n}}^v} \frac{\partial^w \hat{\varphi}_j^2}{\partial \hat{\boldsymbol{n}}^w} \right) & , \quad \text{on } \hat{T}^2. \end{cases} \tag{6.3.14}$$

Since $\hat{\varphi}_i$ and $\hat{\varphi}_j$ are, respectively, a linear and $(p-1)$-th degree IFE shape functions, then

$$\sum_{v+w=l} \left(\frac{\partial^v \hat{\varphi}_i}{\partial \hat{\boldsymbol{n}}^v} \frac{\partial^w \hat{\varphi}_j}{\partial \hat{\boldsymbol{n}}^w} \right) = \frac{\partial \hat{\varphi}_i}{\partial \hat{\boldsymbol{n}}} \frac{\partial^{l-1} \hat{\varphi}_j}{\partial \hat{\boldsymbol{n}}^{l-1}},$$

thus, the l-th normal derivative of $\hat{\varphi}_k,\ k = N_{p-1}+1, N_{p-1}+2, \ldots, N_p,\ 2 \le l \le p$, can be simplified as

$$\frac{\partial^l \hat{\varphi}_k}{\partial \hat{\boldsymbol{n}}^l}(\hat{\xi},\hat{\eta}) = \begin{cases} \frac{\partial \hat{\varphi}_i^1}{\partial \hat{\boldsymbol{n}}} \frac{\partial^{l-1} \hat{\varphi}_j^1}{\partial \hat{\boldsymbol{n}}^{l-1}} + \sum_{s=l}^{p} \frac{s!}{(s-l)!}\ \hat{c}_{k,s}\ \hat{\eta}^{s-l}\ , & \text{on } \hat{T}^1, \\ \frac{\partial \hat{\varphi}_i^2}{\partial \hat{\boldsymbol{n}}} \frac{\partial^{l-1} \hat{\varphi}_j^2}{\partial \hat{\boldsymbol{n}}^{l-1}} \qquad\qquad , & \text{on } \hat{T}^2. \end{cases} \tag{6.3.15}$$

On the interface, $\hat{\eta} = 0$, we have

$$\frac{\partial^l \hat{\varphi}_k}{\partial \hat{\boldsymbol{n}}^l}(\hat{\xi},0) = \begin{cases} \frac{\partial \hat{\varphi}_i^1}{\partial \hat{\boldsymbol{n}}}(\hat{\xi},0)\ \frac{\partial^{l-1} \hat{\varphi}_j^1}{\partial \hat{\boldsymbol{n}}^{l-1}}(\hat{\xi},0) + l!\ \hat{c}_{k,l}\ , & \text{on } \hat{T}^1, \\ \frac{\partial \hat{\varphi}_i^2}{\partial \hat{\boldsymbol{n}}}(\hat{\xi},0)\ \frac{\partial^{l-1} \hat{\varphi}_j^2}{\partial \hat{\boldsymbol{n}}^{l-1}}(\hat{\xi},0) \qquad , & \text{on } \hat{T}^2. \end{cases} \tag{6.3.16}$$

Enforcing (6.3.13) yields

$$\hat{\beta}^1\ \frac{\partial \hat{\varphi}_i^1}{\partial \hat{\boldsymbol{n}}}(\hat{\xi},0)\ \frac{\partial^{l-1} \hat{\varphi}_j^1}{\partial \hat{\boldsymbol{n}}^{l-1}}(\hat{\xi},0)\ +\ \hat{\beta}^1\ l!\ \hat{c}_{k,l}\ =\ \hat{\beta}^2\ \frac{\partial \hat{\varphi}_i^2}{\partial \hat{\boldsymbol{n}}}(\hat{\xi},0)\ \frac{\partial^{l-1} \hat{\varphi}_j^2}{\partial \hat{\boldsymbol{n}}^{l-1}}(\hat{\xi},0),$$

which leads to

$$\hat{c}_{k,l}\ = \frac{1}{l!\ \hat{\beta}^1}[\ \hat{\beta}\ \frac{\partial \hat{\varphi}_i}{\partial \hat{\boldsymbol{n}}}\ \frac{\partial^{l-1} \hat{\varphi}_j}{\partial \hat{\boldsymbol{n}}^{l-1}}]. \tag{6.3.17}$$

6.4 Approximation Capability of Cubic IFE Spaces

For all our numerical experiments, we consider the rectangular domain $\Omega = [0,1]^2$ subdivided into a uniform triangular mesh of size h denoted by $\mathscr{T}_h$. The set of interface elements that are cut by the interface is denoted by $\mathscr{T}_h^i$. The set of non-interface elements that are not cut by the interface is denoted by $\mathscr{T}_h^i$. Hence, $\mathscr{T}_h = \mathscr{T}_h^i \cup \mathscr{T}_h^c$.

The uniform triangular mesh $\mathscr{T}_h$ is formed by partitioning Ω into $(1/h)^2$ squares, with $h = 1/2^m,\ m = 2,3,4,5,6,7$, then forming the triangular elements by joining the lower right and upper left vertices of the squares. We define a piecewise cubic IFE interpolant $I_h u(x,y)$ of $u(x,y)$ such that $\forall\ T \in \mathscr{T}_h$

$$I_h u(x,y)|_T = \sum_{j=1}^{10} c_j \phi_j(x,y), \tag{6.4.1}$$

where $\phi_j(x,y),\ j = 1,\ldots,10$, are the ten cubic FE or IFE shape functions depending on whether T is a non-interface or an interface element, and $c_j,\ j = 1,\ldots,10$, are ten constants such that $I_h u(V_i) = u(V_i),\ i = 1,\ldots,10$, with $V_i,\ i = 1,\ldots,10$, being the nodes on T.

To measure the interpolation errors, we use the L^2-norm defined in (4.1.1a), and the broken H^1 norm defined in (4.1.3).

Example 6.4.1.

In this example we assume that the domain $\Omega = [0,1]^2$ is cut by the interface $y = x + \frac{1}{4}$ such that $\Omega^+ = \{y > x + \frac{1}{4}\}$ and $\Omega^- = \{y < x + \frac{1}{4}\}$. We test our spaces with the function u defined by

$$u(x,y) = \begin{cases} \frac{1}{\beta^+}\ (3y - x - \frac{3}{4})\ e^{y-x-\frac{1}{4}}, & \text{on } \Omega^+, \\ \left(\frac{1}{\beta^+} - \frac{1}{\beta^-}(1 - e^{y-x-\frac{1}{4}})\right)(x + y - \frac{1}{4}) - \frac{2}{\beta^-}(\frac{1}{4} + x - y)e^{y-x-\frac{1}{4}}, & \text{on } \Omega^-. \end{cases} \tag{6.4.2}$$

with $r = \frac{\beta^+}{\beta^-} = 5$ and $r = \frac{\beta^+}{\beta^-} = 10^3$ representing a moderate and a large jump in the coefficient β.

We present errors in $I_h u$ and their orders of convergence in Tables 6.1, 6.2, 6.3 and 6.4. We observe that the interpolant in $\mathcal{S}_h^{3,1}$ yields $\mathcal{O}(h^{3.5})$ sub-optimal convergence rates for u and about $\mathcal{O}(h^{2.5})$ sub-optimal rate for its derivatives. Similar results are obtained for the interpolation in the non-consistent IFE space $\mathcal{S}_h^{3,2}$.

These preliminary results for the cubic IFE spaces show an approximation capability higher than the capability of the quadratic IFE spaces, which shows the importance of cubic IFE spaces. However, the rate is still sub-optimal and lower than $p + 1 = 4$ in L^2 norm and lower than $p = 3$ in broken H^1 norm. These cubic IFE spaces are still the subject of further investigation in future works, in the goal of obtaining optimal convergence rates in both L^2 and broken H^1 norms.

h	$\|\|u - I_h u\|\|_0$	order	$\|\|u_x - (I_h u)_x\|\|_{\beta,h}$	order	$\|\|u_y - (I_h u)_y\|\|_{\beta,h}$	order
$\frac{1}{4}$	8.656226e-05	N/A	9.901610e-03	N/A	1.989246e-02	N/A
$\frac{1}{8}$	7.432903e-06	3.54174	1.553082e-03	2.67252	3.529185e-03	2.49481
$\frac{1}{16}$	6.481416e-07	3.51954	2.572915e-04	2.59365	6.680023e-04	2.40141
$\frac{1}{32}$	5.690995e-08	3.50955	4.396261e-05	2.54905	1.350986e-04	2.30584
$\frac{1}{64}$	5.013676e-09	3.50474	7.637296e-06	2.52514	2.916782e-05	2.21156
$\frac{1}{128}$	4.424254e-10	3.50236	1.338231e-06	2.5127	6.654561e-06	2.13196

Table 6.1: L^2 interpolation errors and orders for u, u_x and u_y for the function (6.4.2) with $r = 5$ using the IFE space $\mathcal{S}_h^{3,1}$.

h	$\|\|u - I_h u\|\|_0$	order	$\|\|u_x - (I_h u)_x\|\|_{\beta,h}$	order	$\|\|u_y - (I_h u)_y\|\|_{\beta,h}$	order
$\frac{1}{4}$	4.757337e-05	N/A	3.566275e+00	N/A	3.575101e+00	N/A
$\frac{1}{8}$	3.825033e-06	3.63661	5.878132e-01	2.60098	5.894140e-01	2.60063
$\frac{1}{16}$	3.180569e-07	3.58811	1.003102e-01	2.55088	1.005973e-01	2.55069
$\frac{1}{32}$	2.712293e-08	3.55170	1.742125e-02	2.52554	1.747246e-02	2.52543
$\frac{1}{64}$	2.350825e-09	3.52827	3.052465e-03	2.51280	3.061591e-03	2.51272
$\frac{1}{128}$	2.056610e-10	3.51482	5.372134e-04	2.50640	5.388447e-04	2.50634

Table 6.2: L^2 interpolation errors and orders for u, u_x and u_y for the function (6.4.2) with $r = 10^3$ using the IFE space $\mathcal{S}_h^{3,1}$.

h	$\|\|u - I_h u\|\|_0$	order	$\|\|u_x - (I_h u)_x\|\|_{\beta,h}$	order	$\|\|u_y - (I_h u)_y\|\|_{\beta,h}$	order
$\frac{1}{4}$	1.156719e-04	N/A	3.238563e-03	N/A	1.437396e-02	N/A
$\frac{1}{8}$	1.011418e-05	3.51558	5.265106e-04	2.62081	2.482972e-03	2.53331
$\frac{1}{16}$	8.910672e-07	3.50470	8.900746e-05	2.56446	4.957179e-04	2.32447
$\frac{1}{32}$	7.867069e-08	3.50163	1.537256e-05	2.53356	1.092707e-04	2.18161
$\frac{1}{64}$	6.950451e-09	3.50064	2.685359e-06	2.51717	2.555232e-05	2.09638
$\frac{1}{128}$	5.907281e-10	3.502750	1.888063e-07	2.50519	6.674447e-06	2.307792

Table 6.3: L^2 interpolation errors and orders for u, u_x and u_y for the function (6.4.2) with $r = 5$ using the IFE space $\mathcal{S}_h^{3,2}$.

h	$\|\|u - I_h u\|\|_0$	order	$\|\|u_x - (I_h u)_x\|\|_{\beta,h}$	order	$\|\|u_y - (I_h u)_y\|\|_{\beta,h}$	order
$\frac{1}{4}$	8.986771e-05	N/A	5.153758e+00	N/A	5.165334e+00	N/A
$\frac{1}{8}$	7.691480e-06	3.54647	8.618955e-01	2.58004	8.639681e-01	2.57981
$\frac{1}{16}$	6.681910e-07	3.52492	1.482111e-01	2.53986	1.485803e-01	2.53973
$\frac{1}{32}$	5.852642e-08	3.51310	2.584132e-02	2.51990	2.590691e-02	2.51983
$\frac{1}{64}$	5.148942e-09	3.50674	4.536760e-03	2.50994	4.548406e-03	2.50990
$\frac{1}{128}$	4.540284e-10	3.50342	7.992345e-04	2.50497	8.013055e-04	2.50493

Table 6.4: L^2 interpolation errors and orders for u, u_x and u_y for the function (6.4.2) with $r = 10^3$ using the IFE space $\mathcal{S}_h^{3,2}$

6.5 Conclusions

In this chapter, we have discussed how to construct p-th degree IFE spaces. A detailed description of cubic IFE spaces is given, hierarchical shape functions are constructed, and a general procedure for constructing general p-th degree IFE shape function is given. Numerical experiment show sub-optimal approximation capability of cubic IFE spaces. Hence, p-th degree IFE spaces proposed in this chapter are still the subject of further investigation; we will show that the dimension of each space is $\frac{(p+1)(p+2)}{2}$, we will show that the constructed p-th degree IFE shape functions form a basis of the corresponding p-th degree IFE space, and we will investigate numerical implementation or analytical correction in order to obtain optimal approximation capabilities and optimal convergence rates.

Chapter 7

Quadratic Immersed Finite Element Spaces for Arbitrary Interfaces

7.1 Introduction

In this chapter, we construct quadratic IFE spaces to be used with the interior penalty IFE method given in Chapter 5 to solve interface problems with an arbitrary smooth interface. In the first part of the chapter, we develop quadratic IFE spaces for quadratic interfaces, and will use them to handle interface problems with arbitrary smooth interfaces after interpolating the actual interface by a parabola. Quadratic IFE spaces for interface problems with quadratic interfaces are developed using two different approaches: (i) a piecewise isoparametric mapping which uses piecewise isoparametric mapping between the reference and the physical elements, and (ii) an affine mapping between the reference and the physical elements with weak flux jump conditions. We first discuss the jump conditions necessary to construct piecewise isoparametric IFE spaces. For each approach, we give procedure to construct IFE shape functions then present and discuss numerical results showing the approximation capability of IFE spaces. We present another quadratic IFE space constructed via an affine mapping, investigate its optimal approximation capability, and present numerical results showing optimal convergence. Finally, we present a procedure for approximating arbitrary smooth interfaces, investigate the approximation capability of the quadratic IFE space, and solve interface problems with arbitrary smooth interfaces using the interior penalty immersed finite element method (5.3.5). Again, numerical results show that the interior penalty method with the proposed quadratic IFE spaces exhibits optimal convergence rates.

We recall our model interface problem (1.1.1a), which is

$$\begin{cases} -\nabla(\beta\nabla u) &= f, \quad \text{on } \Omega, \\ u_{|\partial\Omega} &= g, \end{cases}$$

where $\Omega = \Omega^+ \cup \Omega^- \subset \mathbb{R}^2$ is a rectangular domain consisting of two sub-domains Ω^+ and

Ω^- separated by an interface Γ. The coefficient β is given by

$$\beta(x,y) = \begin{cases} \beta^+ > 0, & \text{on } \Omega^+, \\ \beta^- > 0, & \text{on } \Omega^-. \end{cases}$$

Following the notations of Chapter 2, we let $\mathcal{P}_k$ denote the two-dimensional polynomial space in $\mathbb{R}^2$ defined in (2.2.1). We also let $\mathscr{T}_h$ be a regular triangulation of the domain Ω, where h is the maximum diameter. The set of interface elements that are cut by the interface is denoted by $\mathscr{T}_h^i$, and we call the set of non-interface elements as $\mathscr{T}_h^c = \mathscr{T}_h \setminus \mathscr{T}_h^i$. Similarly, let $\mathscr{E}_h$, $\mathscr{E}_{h,0}$, $\mathscr{E}_h^i$, respectively, denote the set of all edges, interior edges and interface edges. As illustrated in Figure 7.1, every interface element $T = \triangle V_1V_2V_3$ can be split as

$$T = T^+ \cup T^-, \text{ where } T^\pm = T \cap \Omega^\pm.$$

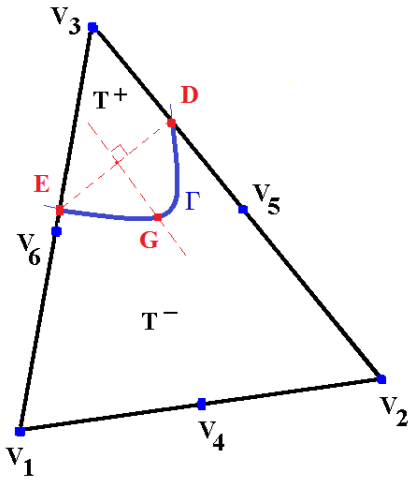

Figure 7.1: A physical interface element

In the discussion from now on, we will use V_4, V_5 and V_6 to denote the midpoints of the edges of a triangular element $T = \triangle V_1V_2V_3$ such that

$$V_4 = \frac{1}{2}(V_1 + V_2),\ V_5 = \frac{1}{2}(V_2 + V_3),\ V_6 = \frac{1}{2}(V_3 + V_1),$$

and we will use D and E to denote the intersection points of Γ with the edges of T. Guided by the standard isoparametric finite element ideas [10], we will denote by G the intersection point of Γ with the line orthogonal to the line segment DE and passing throw its midpoint, as shown in Figure 7.1.

Now, we start discussing the first approach to construct quadratic IFE spaces, using piecewise isoparametric mapping between the physical and the reference interface element. Our goal in this chapter is to propose IFE spaces for arbitrary interface, but we first start in sections 7.2 and 7.3 with discussing interface problems with a quadratic interface.

7.2 Piecewise Isoparametric IFE Spaces

In this section, we consider interface problems with a quadratic interface.

7.2.1 Jump Conditions and Piecewise Isoparametric IFE Spaces

Guided by our work for a linear interface in Chapter 2, we develop two IFE function spaces $\mathscr{R}_1(T)$ and $\mathscr{R}_2(T)$ on which an IFE solution U satisfies the physical jump conditions

$$[U]_{T\cap\Gamma} = 0, \tag{7.2.1a}$$

$$\int_{T\cap\Gamma} [\ \beta\ \frac{\partial U}{\partial \boldsymbol{n}}\ ]_\Gamma\ ds = 0, \tag{7.2.1b}$$

and the extended jump condition:

$$[\beta\Delta U]_{\Gamma\cap T} = 0, \qquad for\ U \in \mathscr{R}_1(T), \tag{7.2.2}$$

$$[\beta\frac{\partial^2 U}{\partial \boldsymbol{n}^2}]_{\Gamma\cap T} = 0, \qquad for\ U \in \mathscr{R}_2(T). \tag{7.2.3}$$

Hence, we define the following isoparametric IFE spaces on an arbitrary interface element T

$$\mathscr{R}_1(T) = \{U, |U|_{T^\pm} \in \mathcal{P}_2, [U]_{D,E,G} = [\ \beta\ \frac{\partial U}{\partial \boldsymbol{n}}\ ]_{Q_1,Q_2} = [\beta\Delta U]_G = 0\}, \tag{7.2.4}$$

$$\mathscr{R}_2(T) = \{U, |U|_{T^\pm} \in \mathcal{P}_2, [U]_{D,E,G} = [\ \beta\ \frac{\partial U}{\partial \boldsymbol{n}}\ ]_{Q1,Q2} = [\beta\frac{\partial^2 U}{\partial \boldsymbol{n}^2}]_G = 0\}, \tag{7.2.5}$$

with Q_1 and Q_2 being the nodes of the two points Gauss-Legendre quadrature, shifted to the curve $\Gamma \cap T$.

To define the global quadratic IFE spaces over the whole simulation domain Ω, we first recall the set of nodes $\mathcal{N}_h$ for the usual Lagrange quadratic finite element space defined on the mesh $\mathscr{T}_h$, and for each node $\mathbf{v}_i \in \mathcal{N}_h$, we define a piecewise quadratic IFE basis function ψ_i^k over Ω as follows

$$\psi_i^k|_T \in \begin{cases} \mathscr{R}_k(T)\ \forall\ T \in \mathscr{T}_h^i \\ \\ \mathcal{P}_2\ \forall\ T \in \mathscr{T}_h \setminus \mathscr{T}_h^i \end{cases}, \qquad \psi_i^k(\mathbf{v}_j) = \delta_{ij}\ \forall\ \mathbf{v}_j \in \mathcal{N}_h.$$

Without loss of generality, we assume that $\mathcal{N}_h$ contains N nodes among which the first N_I nodes are inside Ω while the rest of them are on the boundary of Ω. Finally, we define the global isoparametric IFE spaces over the domain Ω as

$$\mathcal{J}_h^k = span\{\psi_j^k,\ j = 1, \ldots, N\},\ k = 1, 2, \tag{7.2.6}$$

and we define the subsets of the spaces $\mathcal{J}_h^k,\ k = 1, 2$, consisting of functions interpolating the essential boundary condition g

$$\mathcal{J}_{h,E}^k = \left\{ U \in \mathcal{J}_h^k \,|\, U = \sum_{i=1}^{N_I} c_i \psi_i^k + \sum_{i=N_I+1}^{N} g(\mathbf{v}_i)\psi_i^k \right\}. \tag{7.2.7}$$

Next, we describe the main steps to construct the piecewise isoparametric IFE spaces $\mathscr{R}_k(T),\ k = 1, 2$. Thus, we map these piecewise isoparametric IFE spaces defined on an arbitrary element T to the reference interface triangle and derive new interface jump conditions.

7.2.2 Piecewise Isoparametric IFE Spaces on the Reference Element

In order to construct isoparametric IFE spaces on the reference element, we follow the steps:

1. *Step i.* We map each interface triangle T to the reference triangle $\hat{T}$ defined by the vertices $\hat{V}_1 = (0, 0)^t$, $\hat{V}_2 = (1, 0)^t$ and $\hat{V}_3 = (0, 1)^t$, using the standard affine mapping $F : T \to \hat{T}$ defined in (2.2.7), such that the vertex shared by the two interface edges is mapped to $\hat{V}_3$.
   Assuming that the interface Γ intersects two edges of T at two points E and D as illustrated in Figure 7.1, we approximate the interface on $\hat{T}$ given by $\hat{\Gamma} = F(\Gamma) \cap \hat{T}$ by the line segment $\tilde{\Gamma} = \hat{E}\hat{D}$ where $\hat{E} = F(E)$ and $\hat{D} = F(D)$ as illustrated in Figure 7.3, and let $\hat{G}$ denote the midpoint of $\hat{D}\hat{E}$.

   We assume that the interface intersects two edges of every interface triangle creating 12 possible cases similar to the cases with linear interface. Furthermore, interface elements can be grouped into three types, as illustrated in Figure 7.2. Each interface element of a given type is mapped to the corresponding reference interface triangle, as explained in Chapter 2.

   Thus, $\hat{T}$ is divided by $\hat{E}\hat{D}$ as $\hat{T} = \hat{T}^1 \cup \hat{T}^2$, while $\hat{T}^1 \cap \hat{T}^2 = \hat{E}\hat{D}$, where $\hat{T}^1$ is the sub-domain of $\hat{T}$ containing vertex $\hat{V}_3$; and $\hat{T}^2 = \hat{T} \setminus \hat{T}^1$.

2. *Step ii.* We construct a piecewise isoparametric mapping $\theta : T \to \hat{T}$, such that $\theta_1 = \theta|_{T^+}$ is obtained from a composition of an affine mapping and the inverse of a quadratic mapping, while $\theta_2 = \theta|_{T^-}$ is defined using a composition of a bilinear mapping and the inverse of a biquadratic mapping, as illustrated in Figures 7.3 and 7.4.

   Let $\hat{L}_i(\tilde{x}, \tilde{y}),\ i = 1, \ldots, 6$, be the standard Lagrange quadratic shape functions on the standard reference triangle Δ with vertices $(0, 0)$, $(1, 0)$, and $(0, 1)$. It is known that there exists an affine mapping ω_1 which maps that reference triangle Δ to the triangle $\hat{T}^1$, defined by

$$\omega_1(\tilde{x}, \tilde{y}) = \hat{E}\ (1 - \tilde{x} - \tilde{y}) + \hat{D}\ \tilde{x} + \hat{V}_3\ \tilde{y}.$$

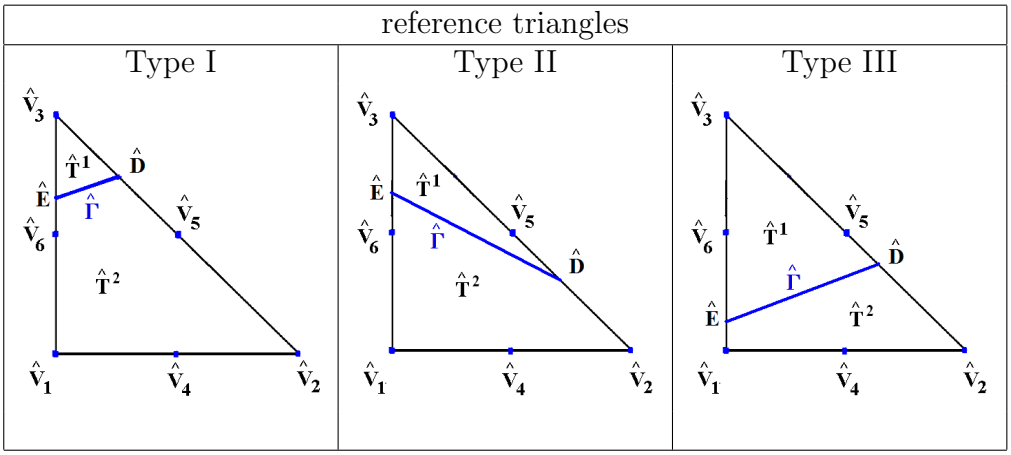

Figure 7.2: The three types of reference elements.

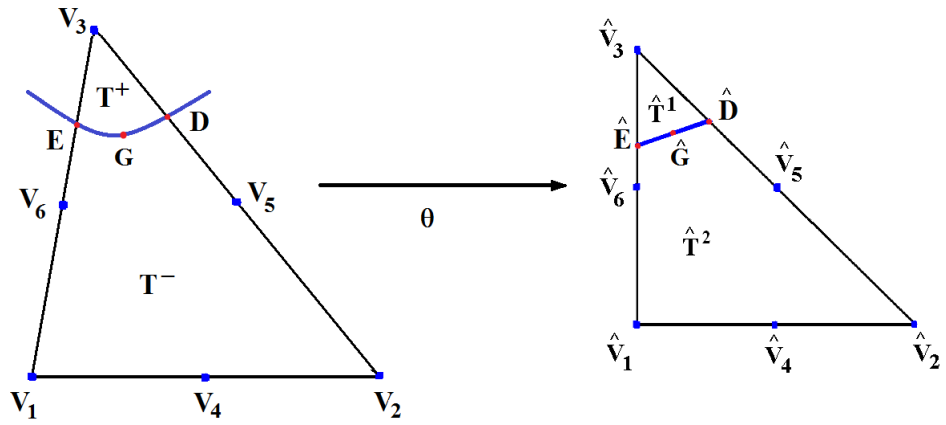

Figure 7.3: A physical interface element $T = T^+ \cup T^-$ and its mapping to a reference element $\hat{T} = \hat{T}^1 \cup \hat{T}^2$.

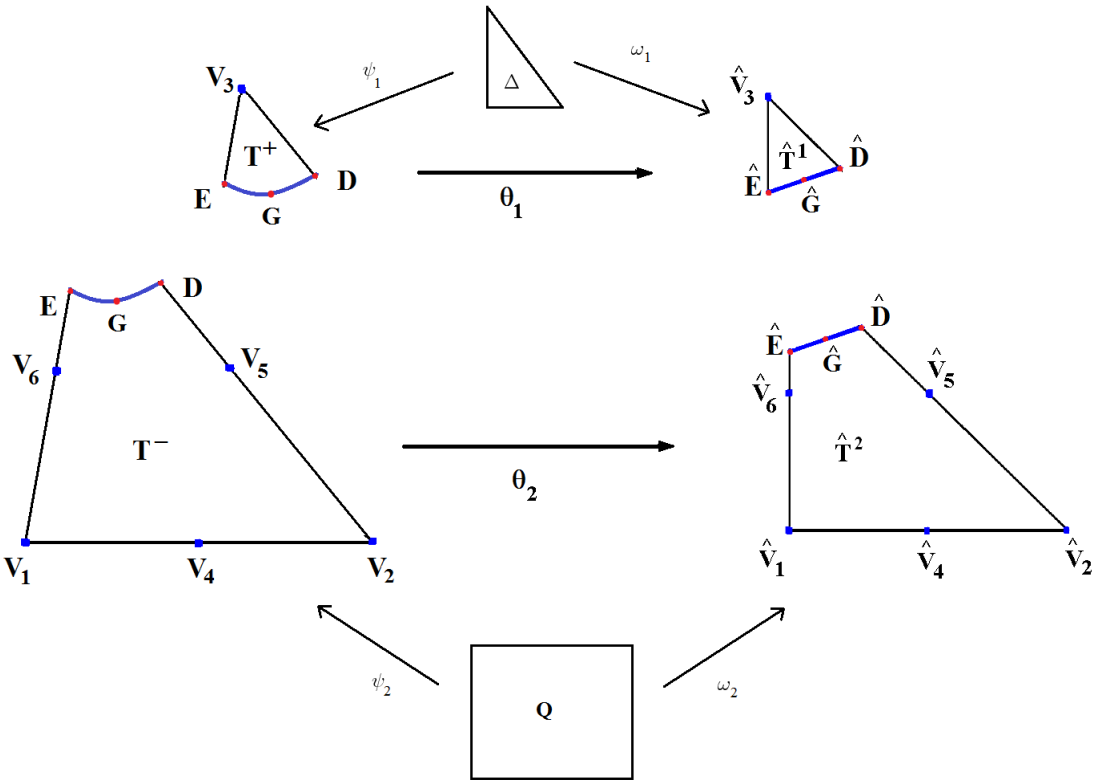

Figure 7.4: The mapping θ as a compositions of ω and ψ^{-1}.

We also define the quadratic mapping

$$\begin{aligned}\psi_1(\tilde{x},\tilde{y}) &= E\ \hat{L}_1(\tilde{x},\tilde{y}) + D\ \hat{L}_2(\tilde{x},\tilde{y}) + V_3\ \hat{L}_3(\tilde{x},\tilde{y}) + G\ \hat{L}_4(\tilde{x},\tilde{y}) \\ &\quad + \frac{D+V_3}{2}\ \hat{L}_5(\tilde{x},\tilde{y}) \ + \ \frac{E+V_3}{2}\ \hat{L}_6(\tilde{x},\tilde{y}).\end{aligned}$$

Thus, $\theta_1 = \omega_1 \circ \psi_1^{-1}$.

Similarly, let $\hat{N}_i(\tilde{x},\tilde{y}),\ i = 1,\ldots,9$, be the standard Lagrange biquadratic shape functions on the standard reference quadrilateral Q with vertices $(-1,-1)$, $(1,-1)$, $(1,1)$ and $(-1,1)$. It is known that there exists a bilinear mapping ω_2 which maps that reference quadrilateral Q to the quadrilateral $\hat{T}^2$, defined by

$$\begin{aligned}\omega_2(\tilde{x},\tilde{y}) &= \hat{V}_1\ \frac{(1-\tilde{x})(1-\tilde{y})}{4} + \hat{V}_2\ \frac{(1+\tilde{x})(1-\tilde{y})}{4} \\ &\quad + \hat{D}\ \frac{(1+\tilde{x})(1+\tilde{y})}{4} + \hat{E}\ \frac{(1-\tilde{x})(1+\tilde{y})}{4}.\end{aligned}$$

We also define the biquadratic mapping

$$\begin{aligned}\psi_2(\tilde{x},\tilde{y}) &= V_1\ \hat{N}_1(\tilde{x},\tilde{y}) + V_2\ \hat{N}_2(\tilde{x},\tilde{y}) + D\ \hat{N}_3(\tilde{x},\tilde{y}) + E\ \hat{N}_4(\tilde{x},\tilde{y}) \\ &\quad + \hat{V}_4\ \hat{N}_5(\tilde{x},\tilde{y}) \ + \ \frac{D+V_2}{2}\ \hat{N}_6(\tilde{x},\tilde{y}) \ + \ G\ \hat{N}_7(\tilde{x},\tilde{y}) \\ &\quad + \frac{E+V_1}{2}\ \hat{N}_8(\tilde{x},\tilde{y}) \ + \ \frac{G+V_4}{2}\ \hat{N}_9(\tilde{x},\tilde{y}).\end{aligned}$$

Thus, $\theta_2 = \omega_2 \circ \psi_2^{-1}$.

Hence, T is mapped to $\hat{T}$, through the mapping

$$\theta(x,y) = \begin{cases} \theta_1(x,y) = \omega_1 \circ \psi_1^{-1}(x,y)\ , & for\ (x,y) \in \hat{T}^1, \\ \theta_2(x,y) = \omega_2 \circ \psi_2^{-1}(x,y)\ , & for\ (x,y) \in \hat{T}^2, \end{cases} \tag{7.2.8}$$

and let us denote by $\mathbf{J}_\theta(x,y)$ the Jacobian matrix 2×2, of the mapping θ, defined by

$$\mathbf{J}_\theta(x,y) = \begin{pmatrix} \theta_x(x,y) & \theta_y(x,y) \end{pmatrix}. \tag{7.2.9}$$

The discontinuous material coefficient $\hat{\beta}$ on the reference interface triangle $\hat{T}$ is written as

$$\hat{\beta} = \begin{cases} \hat{\beta}^1, & \text{on } \hat{T}^1, \\ \hat{\beta}^2, & \text{on } \hat{T}^2, \end{cases} \tag{7.2.10}$$

where $\hat{\beta}^i = \beta^{\pm}$ if $\hat{T}^i = \theta(T^{\pm})$.

Remark 7.2.1. *Under the assumption that Γ is quadratic, the piecewise mapping θ, defined in (7.2.8), has the following properties:*

(a) θ is continuous across the interface $\Gamma \cap T$ and maps it into the linear segment $\hat{E}\hat{D}$, as illustrated in Figure 7.3.

(b) θ_1 satisfies

$$\begin{aligned}
&\theta_1(D) = \hat{D},\\
&\theta_1(E) = \hat{E},\\
&\theta_1(V_3) = \hat{V}_3,\\
&\theta_1(G) = \hat{G},\\
&\theta_1\left(\frac{1}{2}(D+V_3)\right) = \frac{\hat{D}+\hat{V}_3}{2},\\
&\theta_1\left(\frac{1}{2}(E+V_3)\right) = \frac{\hat{E}+\hat{V}_3}{2},
\end{aligned}$$

and we can also show that

$$\theta_1(T^1) = \hat{T}^1.$$

(c) θ_2 satisfies

$$\begin{aligned}
&\theta_2(V_1) = \hat{V}_1,\\
&\theta_2(V_2) = \hat{V}_2,\\
&\theta_2(D) = \hat{D},\\
&\theta_2(E) = \hat{E},\\
&\theta_2(G) = \hat{G},\\
&\theta_2(V_4) = \hat{V}_4,\\
&\theta_2\left(\frac{1}{2}(E+V_1)\right) = \frac{\hat{E}+\hat{V}_1}{2},\\
&\theta_2\left(\frac{1}{2}(D+V_2)\right) = \frac{\hat{D}+\hat{V}_2}{2},\\
&\theta_2\left(\frac{1}{2}(G+V_4)\right) = \frac{\hat{G}+\hat{V}_4}{2},
\end{aligned}$$

and we can also show that

$$\theta_2(T^2) = \hat{T}^2.$$

3. *Step iii.* We transform the interface jump conditions to the reference triangle $\hat{T}$ by θ and use them to construct piecewise quadratic IFE shape functions.

The mapping of the condition (7.2.1b) to the reference element yields

$$\int_{\hat{\Gamma}} [\ \hat{\beta}\ \hat{\boldsymbol{n}} \cdot \hat{\nabla}\hat{u}\ |\mathbf{J}_\theta^{-1}(\hat{x},\hat{y})|\ ]_{\tilde{\Gamma}}\ d\hat{s} = 0, \tag{7.2.11}$$

where $(\hat{x},\hat{y}) = \theta(x,y)$, $\hat{\Gamma} = \theta(T \cap \Gamma)$, $\hat{\nabla}\hat{u} = (\partial_{\hat{x}}\hat{u}, \partial_{\hat{y}}\hat{u})^t$, and if $\boldsymbol{n}(x,y)$ is the normal to Γ at (x,y), we let $\hat{\boldsymbol{n}} = \mathbf{J}_\theta(x,y)\ \boldsymbol{n}(x,y)$, where $\mathbf{J}_\theta$ is the Jacobian matrix of θ, and we also let $|\mathbf{J}_\theta^{-1}(\hat{x},\hat{y})|$ denote the determinant of the 2×2 matrix $\mathbf{J}_\theta^{-1}(\hat{x},\hat{y})$.

On the reference interface triangle $\hat{T}$, let $\hat{\varphi}(x,y)$ be a piecewise quadratic function written as

$$\hat{\varphi}(x,y) = \begin{cases} \hat{\varphi}^1(x,y)\ , & \text{on } \hat{T}^1, \\ \hat{\varphi}^2(x,y)\ , & \text{on } \hat{T}^2, \end{cases}$$

where $\hat{\varphi}^i(x,y) \in \mathcal{P}_2,\ i = 1,2.$

We let

$$\varphi(x,y) = \hat{\varphi}(\hat{x},\hat{y}) = \hat{\varphi}(\theta(x,y)).$$

with

$$\nabla\varphi = \mathbf{J}_\theta^t(x,y)\ \hat{\nabla}\hat{\varphi}$$

The interface jump conditions for the piecewise quadratic function $\hat{\varphi}$ on the interface $\tilde{\Gamma} = \theta(\Gamma \cap T)$, are as given below.

First, the jump condition (7.2.1a) becomes

$$[\hat{\varphi}]_{\tilde{\Gamma}} = 0, \tag{7.2.12}$$

which is enforced at $\hat{D}$, $\hat{E}$, and $\hat{G}$.

If $\boldsymbol{n}(x,y)$ is the normal to Γ at the point (x,y), the mapping of $\boldsymbol{n}(x,y)$ to $\hat{T}$ is

$$\hat{\boldsymbol{n}}(\hat{x},\hat{y}) = \mathbf{J}_\theta(x,y)\ \boldsymbol{n}(x,y), \qquad \text{where} \quad (\hat{x},\hat{y}) = \theta(x,y).$$

Guided by our work for the linear interface, described in Chapter 2, we enforce the condition (7.2.11) at two points $\hat{Q}_1$ and $\hat{Q}_2$ as

$$[\ \hat{\beta}\ \hat{\boldsymbol{n}} \cdot \hat{\nabla}\hat{\varphi}\ |\mathbf{J}_\theta^{-1}|\ ]_{\tilde{\Gamma}} = 0, \tag{7.2.13}$$

where $\hat{Q}_1 = \theta(Q_1)$ and $\hat{Q}_2 = \theta(Q_2)$ are the two nodes for Gauss-Legendre quadrature, shifted to the line segment $\tilde{\Gamma} = \hat{D}\hat{E}$.

Next, the conditions (7.2.2) and (7.2.3) are mapped to $\hat{T}$. By the chain rule $\nabla\varphi = \mathbf{J}_\theta^t(x,y)\hat{\nabla}\hat{\varphi}$, we write the Laplacian as

$$\Delta\varphi = \nabla \cdot \nabla\varphi = (\mathbf{J}_\theta^t\hat{\nabla}) \cdot (\mathbf{J}_\theta^t\hat{\nabla})\hat{\varphi}. \tag{7.2.14}$$

Thus, on $\hat{T}$, the extended jump condition (7.2.2) becomes

$$[\hat{\beta}(\mathbf{J}_\theta^t\hat{\nabla})\cdot(\mathbf{J}_\theta^t\hat{\nabla})\hat{\varphi}]|_{\hat{\Gamma}}=0. \tag{7.2.15}$$

Also, we note that the second normal derivative can be written as

$$\frac{\partial^2\varphi}{\partial\boldsymbol{n}^2}=(\boldsymbol{n}\cdot\nabla)\,(\boldsymbol{n}\cdot\nabla\varphi)\,. \tag{7.2.16}$$

Thus, (7.2.3) on $\hat{T}$ becomes

$$[\hat{\beta}(\hat{\boldsymbol{n}}\cdot\hat{\nabla})\left(\hat{\boldsymbol{n}}\cdot\hat{\nabla}\hat{\varphi}\right)\hat{\varphi}]|_{\hat{\Gamma}}=[\hat{\beta}\frac{\partial^2\hat{\varphi}}{\partial\hat{\boldsymbol{n}}^2}]_{\hat{\Gamma}}=0. \tag{7.2.17}$$

In summary, on a reference element $\hat{T}$, we define the following quadratic IFE spaces:

$$\hat{\mathscr{R}}_1(\hat{T})=\{\hat{U}\in\hat{\mathcal{P}}_2,|\,[\hat{U}]_{\hat{D},\hat{E},\hat{G}}=[\hat{\beta}\frac{\partial\hat{U}}{\partial\hat{\boldsymbol{n}}}\;|\mathbf{J}_\theta^{-1}(\hat{x},\hat{y})|\;]_{\hat{Q}_1,\hat{Q}_2}=[\hat{\beta}(\mathbf{J}_\theta^t\nabla).(\mathbf{J}_\theta^t\nabla)\hat{U}]_{\hat{G}}=0\}, \tag{7.2.18}$$

and

$$\hat{\mathscr{R}}_2(\hat{T})=\{\hat{U}\in\hat{\mathcal{P}}_2,|\,[\hat{U}]_{\hat{D},\hat{E},\hat{G}}=[\hat{\beta}\frac{\partial\hat{U}}{\partial\hat{\boldsymbol{n}}}\;|\mathbf{J}_\theta^{-1}(\hat{x},\hat{y})|\;]_{\hat{Q}_1,\hat{Q}_2}=[\hat{\beta}\frac{\partial^2\hat{U}}{\partial\hat{\boldsymbol{n}}^2}]_{\hat{G}}=0\}, \tag{7.2.19}$$

where $\hat{\mathcal{P}}_2$ is the polynomial space defined in (2.2.20).

7.2.3 Approximation Capability of Piecewise Isoparametric IFE Spaces

For all our numerical experiments, we consider the uniform triangular mesh $\mathscr{T}_h$ formed by partitioning $\Omega=[0,1]^2$ into $(1/h)^2$ squares, with $h=\frac{1}{2^m},\ m=2,3,4,5,6,7$, then forming the triangular elements by joining the lower right and upper left vertices of the squares.

We define a piecewise Lagrange type IFE interpolant $I_hu(x,y)$ of $u(x,y)$ such that $\forall\ T\in\mathscr{T}_h$

$$I_hu(x,y)|_T=\sum_{i=1}^{6}u(V_i)\phi_i(x,y), \tag{7.2.20}$$

where $V_i,\ i=1,\ldots,6$, are the nodes on T and $\phi_i(x,y),\ i=1,\ldots,6$, are the six Lagrange FE or IFE shape functions depending on whether T is a non-interface or an interface element.

To compute the interpolation errors, we use the L^2-norm defined in (4.1.1a). We also define, for a function w having partial derivatives in $L^2(T)$ for all T in $\mathscr{T}_h$, the following weighted

norm over $\mathscr{T}_h$:

$$||\nabla w||_{\beta,h} = \sum_{T\in\mathscr{T}_h^c} \beta \int_T \nabla w.\nabla w \; dxdy + \sum_{T\in\mathscr{T}_h^i} \left(\beta^+ \int_{T^+} \nabla w^+.\nabla w^+ \; dxdy + \beta^- \int_{T^-} \nabla w^-.\nabla w^- \; dxdy \right). \tag{7.2.21}$$

Example 7.2.1. *Circular interface and polynomial function*

Let us consider the interface $\Gamma : x^2 + (y-1)^2 = \left(\frac{5}{13}\right)^2$, which represents an arc of the circle centered at the point $(0,1)$ with radius equal to $\frac{5}{13}$, as illustrated in Figure 7.5. We denote $\Omega^+ = \{x^2 + (y-1)^2 < \left(\frac{5}{13}\right)^2\}$ and $\Omega^- = \{x^2 + (y-1)^2 > \left(\frac{5}{13}\right)^2\}$.

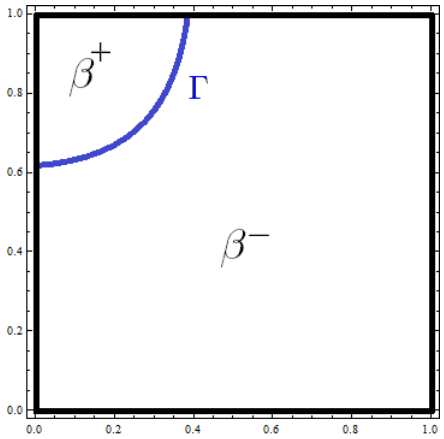

Figure 7.5: Geometry of Ω and the circular interface Γ in Example 7.2.1.

We test our space on the piecewise polynomial function

$$u(x,y) = \begin{cases} \frac{1}{\beta^+}\left((\frac{5}{13})^{10} - (x^2+(y-1)^2)^5\right) \; ; & \text{on } \Omega^+, \\ \\ \frac{1}{\beta^-}\left((\frac{5}{13})^{10} - (x^2+(y-1)^2)^5\right) \; ; & \text{on } \Omega^-, \end{cases} \tag{7.2.22}$$

with $r = \frac{\beta^+}{\beta^-} = 5$ and $r = \frac{\beta^+}{\beta^-} = 10^3$ representing a moderate and a large jump in the coefficient β.

We present interpolation errors in $I_h u$ in the L^2 norm $||u - I_h u||_0$ and the broken weighted H^1 norms $||u_x - (I_h u)_x||_{\beta,h}$ and $||u_y - (I_h u)_y||_{\beta,h}$, and compute their orders of convergence

in Tabes 7.1 and 7.2 for the isoparametric IFE space $\mathcal{J}_h^1$ defined in (7.2.6). The related numerical results show that the isoparametric IFE space $\mathcal{J}_h^1$ has optimal approximation capability for moderate and large jumps in β.

h	$\|\|u - I_h u\|\|_0$	order	$\|\|u_x - (I_h u)_x\|\|_{\beta,h}$	order	$\|\|u_y - (I_h u)_y\|\|_{\beta,h}$	order
$\frac{1}{4}$	1.413998e-01	N/A	6.519295e$_+$00	N/A	6.519295e$_+$00	N/A
$\frac{1}{8}$	1.903831e-02	2.892803	1.753818e$_+$00	1.894217	1.753818e$_+$00	1.894217
$\frac{1}{16}$	2.425719e-03	2.972421	4.467679e-01	1.972902	4.467679e-01	1.972902
$\frac{1}{32}$	3.046777e-04	2.993057	1.122208e-01	1.993185	1.122208e-01	1.993185
$\frac{1}{64}$	3.813064e-05	2.998261	2.808841e-02	1.998294	2.808841e-02	1.998294
$\frac{1}{128}$	4.767767e-06	2.999565	7.024180e-03	1.999573	7.024180e-03	1.999573

Table 7.1: L^2 interpolation errors and orders for u, u_x and u_y for the function (7.2.22) in Example 7.2.1 with $r = 5$ using the IFE space $\mathcal{J}_h^1$.

h	$\|\|u - I_h u\|\|_0$	order	$\|\|u_x - (I_h u)_x\|\|_{\beta,h}$	order	$\|\|u_y - (I_h u)_y\|\|_{\beta,h}$	order
$\frac{1}{4}$	1.414432e-01	N/A	9.219691e$_+$01	N/A	9.219691e$_+$01	N/A
$\frac{1}{8}$	1.903848e-02	2.893233	2.480273e$_+$01	1.894219	2.480273e$_+$01	1.894219
$\frac{1}{16}$	2.425764e-03	2.972407	6.318253e$_+$00	1.972901	6.318253e$_+$00	1.972901
$\frac{1}{32}$	3.046783e-04	2.993080	1.587042e$_+$00	1.993185	1.587042e$_+$00	1.993185
$\frac{1}{64}$	3.813320e-05	2.998167	3.972302e-01	1.998294	3.972302e-01	1.998294
$\frac{1}{128}$	4.768364e-06	2.999481	9.933694e-02	1.999573	9.933694e-02	1.999573

Table 7.2: L^2 interpolation errors and orders for u, u_x and u_y for the function (7.2.22) in Example 7.2.1 with $r = 1000$ using the IFE space $\mathcal{J}_h^1$.

Example 7.2.2. *Circular interface and non-polynomial function*

We consider the same geometry as in Example 7.2.1, with the following piecewise function

$$u(x,y) = \begin{cases} \frac{1}{\beta^+} \quad \sin\left(\frac{5^4}{13^4} - (x^2 + (y-1)^2)^2\right) \quad e^{x+y} \quad ; \qquad \text{on } \Omega^+, \\ \\ \frac{1}{\beta^-} \quad \sin\left(\frac{5^4}{13^4} - (x^2 + (y-1)^2)^2\right) \quad e^{x+y} \quad ; \qquad \text{on } \Omega^-, \end{cases} \tag{7.2.23}$$

and with $r = \frac{\beta^+}{\beta^-} = 5$ and $r = \frac{\beta^+}{\beta^-} = 1000$ representing a moderate and a large jump in the coefficient β.

We present interpolation errors in $I_h u$ in the L^2 norm $||u - I_h u||_0$ and the broken weighted H^1 norms $||u_x - (I_h u)_x||_{\beta,h}$ and $||u_y - (I_h u)_y||_{\beta,h}$, and their orders of convergence in Tabes 7.3 and 7.4 for the isoparametric IFE space $\mathcal{J}_h^1$. The related datum show that the isoparametric IFE space $\mathcal{J}_h^1$ has optimal approximation capability for moderate jumps in β, however its approximation capability is not optimal for large jumps in β. In the latter case, approximation error increases when the mesh is refined from $h = \frac{1}{16}$ to $h = \frac{1}{32}$.

h	$\|\|u - I_h u\|\|_0$	order	$\|\|u_x - (I_h u)_x\|\|_{\beta,h}$	order	$\|\|u_y - (I_h u)_y\|\|_{\beta,h}$	order
$\frac{1}{4}$	4.824161e-02	N/A	2.734412e$_+$00	N/A	1.009387e$_+$00	N/A
$\frac{1}{8}$	6.273018e-03	2.943046	7.106326e-01	1.944055	2.548546e-01	1.985733
$\frac{1}{16}$	7.920135e-04	2.985563	1.794048e-01	1.985885	6.384789e-02	1.996964
$\frac{1}{32}$	9.925303e-05	2.996342	4.496174e-02	1.996449	1.597071e-02	1.999210
$\frac{1}{64}$	1.241524e-05	2.998999	1.124759e-02	1.999082	3.993748e-03	1.999614
$\frac{1}{128}$	1.552248e-06	2.999681	2.812436e-03	1.999724	9.986877e-04	1.999638

Table 7.3: L^2 interpolation errors and orders for u, u_x and u_y for the function (7.2.23) in Example 7.2.2 with $r = 5$ using the IFE space $\mathcal{J}_h^1$.

h	$\|\|u - I_h u\|\|_0$	order	$\|\|u_x - (I_h u)_x\|\|_{\beta,h}$	order	$\|\|u_y - (I_h u)_y\|\|_{\beta,h}$	order
$\frac{1}{4}$	8.363956e-02	N/A	3.880933e$_+$01	N/A	1.500011e$_+$01	N/A
$\frac{1}{8}$	7.125662e-03	3.553089	1.005158e$_+$01	1.948981	3.607999e$_+$00	2.055703
$\frac{1}{16}$	1.119448e-03	2.670237	2.538815e$_+$00	1.985195	9.057510e-01	1.994012
$\frac{1}{32}$	1.070629e-04	3.386256	6.361169e-01	1.996792	2.268970e-01	1.997077
$\frac{1}{64}$	3.588604e-05	1.576964	1.597981e-01	1.993042	5.789657e-02	1.970488
$\frac{1}{128}$	6.029331e-06	2.573353	4.022456e-02	1.990101	1.548780e-02	1.902346

Table 7.4: L^2 interpolation errors and orders for u, u_x and u_y for the function (7.2.23) in Example 7.2.2 with $r = 1000$ using the IFE space $\mathcal{J}_h^1$.

Example 7.2.3. *Parabolic interface and non-polynomial function*

In this example, we consider the domain $\Omega = [0,1]^2$ cut by the parabolic interface $\Gamma : x^2 + \frac{5}{13} = y$, as illustrated in Figure 7.6. Let us denote $\Omega^+ = \{x^2 + \frac{5}{13} < y\}$ and $\Omega^- = \{x^2 + \frac{5}{13} > y\}$.

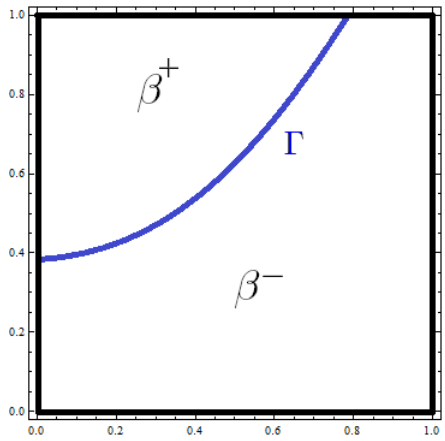

Figure 7.6: Geometry of Ω and the parabolic interface Γ in Example 7.2.3.

We consider the following piecewise polynomial function:

$$u(x,y) = \begin{cases} \frac{1}{\beta^+}\left(y^5 - \left(x^2 + \frac{5}{13}\right)^5\right) \; ; & \text{on } \Omega^+, \\ \\ \frac{1}{\beta^-}\left(y^5 - \left(x^2 + \frac{5}{13}\right)^5\right) \; ; & \text{on } \Omega^-, \end{cases} \tag{7.2.24}$$

with $r = \frac{\beta^+}{\beta^-} = 5$ and $r = \frac{\beta^+}{\beta^-} = 10^3$ representing a moderate and a large jump in the coefficient β.

We present interpolation errors in $I_h u$ in the L^2 norm $||u - I_h u||_0$ and the broken weighted H^1 norms $||u_x - (I_h u)_x||_{\beta,h}$ and $||u_y - (I_h u)_y||_{\beta,h}$, and their orders of convergence in Tabes 7.5 and 7.6 for the isoparametric IFE space $\mathcal{J}_h^1$. The related datum show that the isoparametric IFE space $\mathcal{J}_h^1$ has optimal approximation capability in L^2 and broken weighted H^1 norms for moderate jumps in β, however its approximation capability is not optimal for large jumps in β. In the latter case, approximation error presents oscillating behavior and sometimes increases when the mesh is refined. Hence, convergence is not guaranteed.

h	$\|\|u - I_h u\|\|_0$	order	$\|\|u_x - (I_h u)_x\|\|_{\beta,h}$	order	$\|\|u_y - (I_h u)_y\|\|_{\beta,h}$	order
$\frac{1}{4}$	3.459394e-02	N/A	9.094158e-01	N/A	7.924326e-02	N/A
$\frac{1}{8}$	4.854418e-03	2.833149	2.524779e-01	1.848783	1.979531e-02	2.001129
$\frac{1}{16}$	6.246270e-04	2.958232	6.486997e-02	1.960534	5.030076e-03	1.976507
$\frac{1}{32}$	7.869548e-05	2.988642	1.633445e-02	1.989633	1.174103e-03	2.099021
$\frac{1}{64}$	9.865019e-06	2.995887	4.096546e-03	1.995438	3.675446e-04	1.675567
$\frac{1}{128}$	1.236429e-06	2.996142	1.028685e-03	1.993607	1.202947e-04	1.611346

Table 7.5: L^2 interpolation errors and orders for u, u_x and u_y for the function (7.2.24) in Example 7.2.3 with $r = 5$ using the IFE space $\mathcal{J}_h^1$.

h	$\|\|u - I_h u\|\|_0$	order	$\|\|u_x - (I_h u)_x\|\|_{\beta,h}$	order	$\|\|u_y - (I_h u)_y\|\|_{\beta,h}$	order
$\frac{1}{4}$	3.444199e-02	N/A	1.486597e+00	N/A	1.297774e+00	N/A
$\frac{1}{8}$	7.860264e-03	2.131519	1.591171e+00	-0.098075	2.618612e+00	-1.012763
$\frac{1}{16}$	2.920444e-03	1.428390	4.476204e-01	1.829741	4.801507e-01	2.447243
$\frac{1}{32}$	2.078726e-04	3.812416	1.138936e-01	1.974589	2.593297e-01	0.888700
$\frac{1}{64}$	4.767483e-05	2.124400	2.497946e-02	2.188872	3.277577e-02	2.984086
$\frac{1}{128}$	1.112721e-05	2.099136	1.330385e-02	0.908898	1.973167e-02	0.732116

Table 7.6: L^2 interpolation errors and orders for u, u_x and u_y for the function (7.2.24) in Example 7.2.3 with $r = 1000$ using the IFE space $\mathcal{J}_h^1$.

Example 7.2.4. *Parabolic interface and non-polynomial function*

We consider the same geometry as in Example 7.2.3, with the following function now:

$$u(x,y) = \begin{cases} \frac{1}{\beta^+} \sin\left(y - \left(x^2 + \frac{5}{13}\right)\right) e^{x+y} \; ; & \text{on } \Omega^+ \\ \\ \frac{1}{\beta^-} \sin\left(y - \left(x^2 + \frac{5}{13}\right)\right) e^{x+y} \; ; & \text{on } \Omega^-, \end{cases} \tag{7.2.25}$$

with $r = \frac{\beta^+}{\beta^-} = 5$ and $r = \frac{\beta^+}{\beta^-} = 1000$ representing a moderate and a large jump in the coefficient β.

Similarly to the previous examples, we present interpolation errors in $I_h u$ in the L^2 norm $||u - I_h u||_0$ and the broken weighted H^1 norms $||u_x - (I_h u)_x||_{\beta,h}$ and $||u_y - (I_h u)_y||_{\beta,h}$, and their orders of convergence in Tabes 7.7 and 7.8 for the isoparametric IFE space $\mathcal{J}_h^1$. The related numerical results show that the isoparametric IFE space $\mathcal{J}_h^1$ has sub-optimal approximation capability in L^2 and broken H^1 norms for moderate jumps in β, however for large jumps in β, no convergence is observed.

h	$\|\|u - I_h u\|\|_0$	order	$\|\|u_x - (I_h u)_x\|\|_{\beta,h}$	order	$\|\|u_y - (I_h u)_y\|\|_{\beta,h}$	order
$\frac{1}{4}$	2.967310e-02	N/A	8.279107e-01	N/A	3.498072e-01	N/A
$\frac{1}{8}$	4.069140e-03	2.866360	2.231471e-01	1.891480	9.729916e-02	1.846061
$\frac{1}{16}$	5.246915e-04	2.955183	5.739643e-02	1.958962	2.526647e-02	1.945203
$\frac{1}{32}$	6.617925e-05	2.987018	1.444219e-02	1.990671	5.998010e-03	2.074668
$\frac{1}{64}$	8.444594e-06	2.970279	3.712273e-03	1.959915	1.724310e-03	1.798465
$\frac{1}{128}$	1.103960e-06	2.935340	9.975386e-04	1.895858	5.370624e-04	1.682858

Table 7.7: L^2 interpolation errors and orders for u, u_x and u_y for the function (7.2.25) in Example 7.2.4 with $r = 5$ using the IFE space $\mathcal{J}_h^1$.

h	$\|\|u - I_h u\|\|_0$	order	$\|\|u_x - (I_h u)_x\|\|_{\beta,h}$	order	$\|\|u_y - (I_h u)_y\|\|_{\beta,h}$	order
$\frac{1}{4}$	3.012856e-02	N/A	3.146196e+00	N/A	4.405796e+00	N/A
$\frac{1}{8}$	2.660075e-02	0.179665	5.696345e+00	-0.856428	9.426773e+00	-1.097361
$\frac{1}{16}$	1.043958e-02	1.349404	1.654902e+00	1.783291	1.784794e+00	2.401006
$\frac{1}{32}$	8.624706e-04	3.597444	4.831597e-01	1.776174	9.591359e-01	0.895951
$\frac{1}{64}$	1.852222e-04	2.219218	9.349951e-02	2.369469	1.269951e-01	2.916963
$\frac{1}{128}$	4.224783e-05	2.132308	5.583083e-02	0.743897	7.710323e-02	0.719909

Table 7.8: L^2 interpolation errors and orders for u, u_x and u_y for the function (7.2.25) in Example 7.2.4 with $r = 1000$ using the IFE space $\mathcal{J}_h^1$.

In summary, we see from Examples 7.2.1, 7.2.2, 7.2.3, and 7.2.4, that for low or moderate ratios $\frac{\beta^+}{\beta^-}$, isoparametric IFE space $\mathcal{J}_h^1$ exhibits optimal or nearly optimal approximation capability in some cases and sub-optimal approximation capability in other cases. However, when the ratio $\frac{\beta^+}{\beta^-}$ is large, the space fails to have the optimal approximation capability or fails to provide any convergence. One possible reason causing the suboptimal approximation capability or the non-convergence in the space $\mathcal{J}_h^1$ with high ratios is the ill-conditioned matrices obtained when constructing the isoparametric IFE shape functions.

Next, we propose and discuss another approach of constructing the IFE spaces when the interface Γ is quadratic.

7.3 Piecewise Quadratic IFE Space by Affine Mapping and Weak Flux Jump Conditions

In this section also, we consider interface problems with a quadratic interface.

7.3.1 Weak Formulation of the Problem and Jump Conditions

We multiply the first equation of the model interface problem (1.1.1a) by a test function v, then we integrate over the domain Ω to obtain

$$\int_\Omega -\nabla(\beta\nabla u)\ v\ dxdy = \int_\Omega f\ v\ dxdy,$$

which can be written as

$$\sum_{T\in\mathscr{T}_h}\int_T -\nabla(\beta\nabla u)\ v\ dxdy = \int_\Omega f\ v\ dxdy.$$

We recall that a regular triangular mesh of size h is denoted by $\mathscr{T}_h = \mathscr{T}_h^c \cup \mathscr{T}_h^i$, $\mathscr{T}_h^i$ is the set of interface elements that are cut by the interface, and $\mathscr{T}_h^c$ is the set of non-interface elements that are not cut by the interface. Hence, we can write the previous equation as

$$\sum_{T\in\mathscr{T}_h^c}\int_T -\nabla(\beta\nabla u)\ v\ dxdy + \sum_{T\in\mathscr{T}_h^i}\int_T -\nabla(\beta\nabla u)\ v\ dxdy = \int_\Omega f\ v\ dxdy.$$

Integrating by parts the left-hand side yields

$$\sum_{T\in\mathscr{T}_h^c}\int_T \beta\nabla u\cdot\nabla v\ dxdy+\sum_{T\in\mathscr{T}_h^i}\int_{T\cap\Omega^+}\beta\nabla u\cdot\nabla v\ dxdy+\sum_{T\in\mathscr{T}_h^i}\int_{T\cap\Omega^-}\beta\nabla u\cdot\nabla v\ dxdy$$
$$-\sum_{T\in\mathscr{T}_h^c}\int_{\partial T}\beta\ \frac{\partial u}{\partial \boldsymbol{n}}\ v\ ds-\sum_{T\in\mathscr{T}_h^i}\int_{\partial(T\cap\Omega^+)}\beta\ \frac{\partial u}{\partial \boldsymbol{n}}\ v\ ds-\sum_{T\in\mathscr{T}_h^i}\int_{\partial(T\cap\Omega^-)}\beta\ \frac{\partial u}{\partial \boldsymbol{n}}\ v\ ds$$
$$=\int_\Omega f\ v\ dxdy. \tag{7.3.1}$$

The first three terms in (7.3.1) can be combined as

$$\sum_{T\in\mathscr{T}_h}\int_T \beta\nabla u\cdot\nabla v\ dxdy$$

The last two terms on the left-hand side of (7.3.1) can be written as

$$\sum_{T\in\mathscr{T}_h^i}\int_{\partial(T\cap\Omega^+)}\beta\ \frac{\partial u}{\partial \boldsymbol{n}}\ v\ ds+\sum_{T\in\mathscr{T}_h^i}\int_{\partial(T\cap\Omega^-)}\beta\ \frac{\partial u}{\partial \boldsymbol{n}}\ v\ ds=\sum_{T\in\mathscr{T}_h^i}\int_{\partial T}\beta\ \frac{\partial u}{\partial \boldsymbol{n}}\ v\ ds+\int_\Gamma[\beta\ \frac{\partial u}{\partial \boldsymbol{n}}]_\Gamma\ v\ ds$$

Thus, equation (7.3.1) becomes

$$\sum_{T\in\mathscr{T}_h}\int_T \beta\nabla u\cdot\nabla v\ dxdy-\sum_{T\in\mathscr{T}_h^c}\int_{\partial T}\beta\ \frac{\partial u}{\partial \boldsymbol{n}}\ v\ ds-\sum_{T\in\mathscr{T}_h^i}\int_{\partial T}\beta\ \frac{\partial u}{\partial \boldsymbol{n}}\ v\ ds-\int_\Gamma[\beta\ \frac{\partial u}{\partial \boldsymbol{n}}]_\Gamma\ v\ ds$$
$$=\int_\Omega f\ v\ dxdy,$$

which is equivalent to

$$\sum_{T\in\mathscr{T}_h}\int_T \beta\nabla u\cdot\nabla v\ dxdy-\sum_{T\in\mathscr{T}_h}\int_{\partial T}\beta\ \frac{\partial u}{\partial \boldsymbol{n}}\ v\ ds-\int_\Gamma[\beta\ \frac{\partial u}{\partial \boldsymbol{n}}]_\Gamma\ v\ ds=\int_\Omega f\ v\ dxdy. \tag{7.3.2}$$

Thus, we will impose

$$\int_\Gamma[\ \beta\ \frac{\partial u}{\partial \boldsymbol{n}}\ ]_\Gamma\ v\ ds=0, \tag{7.3.3}$$

which can be written also as

$$\sum_{T\in\mathscr{T}_h^i}\int_{T\cap\Gamma}[\ \beta\ \frac{\partial u}{\partial \boldsymbol{n}}\ ]_{T\cap\Gamma}\ v\ ds=0. \tag{7.3.4}$$

Hence, a sufficient condition is

$$\forall\ T\in\mathscr{T}_h^i,\quad \int_{T\cap\Gamma}[\ \beta\ \frac{\partial u}{\partial \boldsymbol{n}}\ ]_{T\cap\Gamma}\ v\ ds=0. \tag{7.3.5}$$

Hence, we introduce the following piecewise quadratic IFE space locally on an arbitrary interface element T:

$$\mathcal{R}(T) = \{U,\ |\ U|_{T^{\pm}} \in \mathcal{P}_2,\ [U]_{D,E,G} = 0,\ \int_{T\cap\Gamma} [\ \beta\ \boldsymbol{n}\cdot\nabla U\ ]_{T\cap\Gamma}\ v_i\ ds = 0,\ i = 1,2,3\ \},\ (7.3.6)$$

with $v_i,\ i = 1,2,3$, being 3 linearly independent polynomials in $\mathcal{P}_1$, determined by the mappings from the reference interface element to the physical element T of the three polynomials $\hat{v}_i,\ i = 1,2,3$, defined on the reference interface element and given later in (7.3.11).

Again, to define the global quadratic IFE space over the whole simulation domain Ω, we recall the set of nodes $\mathcal{N}_h$ for the usual Lagrange quadratic finite element space defined on the mesh $\mathscr{T}_h$, and for each node $\mathbf{v}_i \in \mathcal{N}_h$, we define a piecewise quadratic IFE basis function ψ_i^k over Ω as follows

$$\psi_i|_T \in \begin{cases} \mathscr{R}(T)\ \forall\ T \in \mathscr{T}_h^i \\ \\ \mathcal{P}_2\ \forall\ T \in \mathscr{T}_h \setminus \mathscr{T}_h^i \end{cases}, \qquad \psi_i(\mathbf{v}_j) = \delta_{ij}\ \forall\ \mathbf{v}_j \in \mathcal{N}_h.$$

We also recall that $\mathcal{N}_h$ contains N nodes among which the first N_I nodes are inside Ω while the rest of them are on the boundary of Ω, and we define the global quadratic IFE space over the domain Ω as

$$\mathcal{J}_h = span\{\psi_j,\ j = 1,\ldots,N\}, \tag{7.3.7}$$

and the subsets of the space $\mathcal{J}_h$, consisting of functions interpolating the essential boundary condition g

$$\mathcal{J}_{h,E} = \left\{ U \in \mathcal{J}_h \,|\, U = \sum_{i=1}^{N_I} c_i\psi_i^k + \sum_{i=N_I+1}^{N} g(\mathbf{v}_i)\psi_i^k \right\}. \tag{7.3.8}$$

Next, we map the piecewise quadratic IFE space on an arbitrary element $\mathcal{R}(T)$ into the reference interface triangle and discuss the new interface jump conditions on the reference element.

7.3.2 Piecewise Quadratic IFE Space on the Reference Interface Element

Here, we describe the construction of piecewise quadratic functions on the reference interface triangle $\hat{T}$ with vertices $\hat{V}_1 = (0,0)^t$, $\hat{V}_2 = (1,0)^t$ and $\hat{V}_3 = (0,1)^t$, for quadratic interface Γ. The method consists of the following two steps:

1. *Step i:* We map an interface element $T = T^+ \cup T^-$ to a reference triangle $\hat{T}$ using the standard affine mapping F, defined in (2.2.7), as illustrated in Figure 7.7. We note

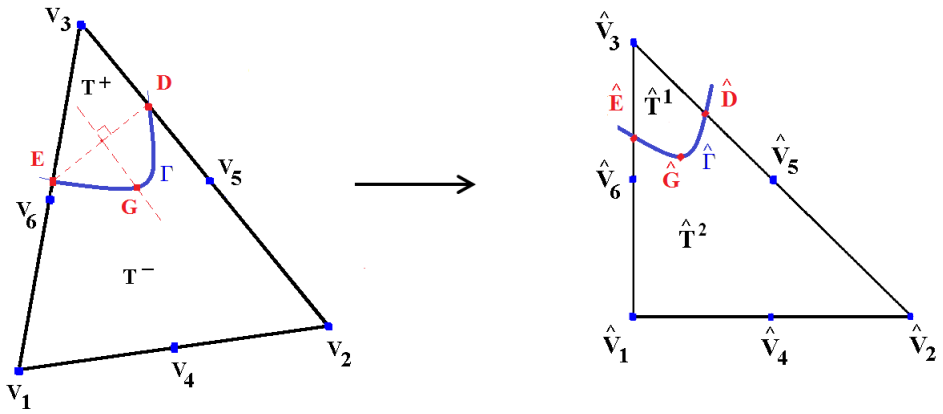

Figure 7.7: A physical interface element and its mapping to a reference element.

that $\hat{\Gamma} = F(\Gamma \cap T)$ is still quadratic, and let $\hat{D} = F(D)$ and $\hat{E} = F(E)$, $\hat{G} = F(G)$. As explained in section 7.2.2, the interface intersects two edges of every interface triangle creating 12 possible cases, furthermore, interface elements can be grouped into three types, as previously illustrated in Figure 7.2. The discontinuous material coefficient $\hat{\beta}$ on the reference interface triangle $\hat{T}$ is written as

$$\hat{\beta} = \begin{cases} \hat{\beta}^1, & \text{on } \hat{T}^1, \\ \hat{\beta}^2, & \text{on } \hat{T}^2, \end{cases} \tag{7.3.9}$$

where $\hat{\beta}^i = \beta^{\pm}$ if $\hat{T}^i = F(T^{\pm})$.

2. *Step ii.* We map the interface jump conditions across $\Gamma \cap T$ by the affine mapping to new jump conditions across $\hat{\Gamma}$ which are used to construct piecewise quadratic interface shape functions. These conditions lead to a unique set of Lagrange piecewise quadratic IFE shape functions.

   Next, we map the jump condition (7.3.5) to the reference element using the mapping F, which yields

$$\int_{\hat{\Gamma}} [\ \hat{\beta}\ \hat{\boldsymbol{n}} \cdot \hat{\nabla} \hat{u}\ ]_{\hat{\Gamma}}\ \hat{v}_i\ d\hat{s} = 0, \quad i = 1, 2, 3, \tag{7.3.10}$$

   where $(\hat{x}, \hat{y}) = F(x, y)$, $\hat{\Gamma} = F(T \cap \Gamma)$, $\hat{\nabla} \hat{u} = (\partial_{\hat{x}} \hat{u}, \partial_{\hat{y}} \hat{u})^t$, and if $\boldsymbol{n}(x, y)$ is the normal to Γ, we let $\hat{\boldsymbol{n}} = \mathbf{J}\ \boldsymbol{n}(x, y)$, where $\mathbf{J}$ is the Jacobian of F at (x, y).

In our computations, we use in (7.3.10):

$$\hat{v}_1(\hat{x}, \hat{y}) = 1,\ \hat{v}_2(\hat{x}, \hat{y}) = \hat{x},\ \hat{v}_3(\hat{x}, \hat{y}) = \hat{y}, \tag{7.3.11}$$

to define the following quadratic IFE space:

$$\hat{\mathcal{R}}(\hat{T}) = \{\hat{U} \in \hat{\mathcal{P}}_2(\hat{T}), |\ [\hat{U}]_{\hat{D},\hat{E},\hat{G}} = 0, \int_{\hat{\Gamma}} [\ \hat{\beta}\ \hat{\boldsymbol{n}} \cdot \hat{\nabla} \hat{U}\ ]_{\hat{\Gamma}}\ \hat{v}_i\ d\hat{s} = 0, i = 1, 2, 3\}, \tag{7.3.12}$$

where $\hat{\mathcal{P}}_2(\hat{T})$ is the polynomial space defined in (2.2.20).

7.3.3 Approximation Capability

In this section, we use the norms defined in (4.1.1a) and (7.2.21) to compute the interpolation errors using Lagrange piecewise quadratic immersed finite element shape functions constructed in this section and discuss the approximation capability of the piecewise quadratic IFE space $\mathcal{J}_h$.

For all our numerical experiments, we consider the rectangular domain $\Omega = [0,1]^2$ and the uniform triangular mesh $\mathscr{T}_h = \mathscr{T}_h^i \cup \mathscr{T}_h^c$ of size h defined in Section 7.2.3. Again, $\mathscr{T}_h$ is formed by partitioning Ω into $(1/h)^2$ squares, with $h = \frac{1}{2^m},\ m = 2, \ldots, 7$, then forming the triangular elements by joining the lower right and upper left vertices of the squares. Using the same definition in Section 7.2.3, a piecewise Lagrange type IFE interpolant $I_h u(x,y)$ of $u(x,y)$ is defined by (7.2.20).

Example 7.3.1. *Circular interface and polynomial function*

We consider the same domain $\Omega = [0,1]^2$ of Example 7.2.1, cut by the same circular interface $\Gamma : x^2 + (y-1)^2 = \left(\frac{5}{13}\right)^2$, illustrated in Figure 7.5.

We also test our IFE space on the same piecewise polynomial function:

$$u(x,y) = \begin{cases} \frac{1}{\beta^+}\left((\frac{5}{13})^{10} - (x^2 + (y-1)^2)^5 \right) \ ; & \text{on } \Omega^+, \\ \\ \frac{1}{\beta^-}\left((\frac{5}{13})^{10} - (x^2 + (y-1)^2)^5 \right) \ ; & \text{on } \Omega^-, \end{cases}$$

with $r = \frac{\beta^+}{\beta^-} = 5$ and $r = \frac{\beta^+}{\beta^-} = 10^3$ representing a moderate and a large jump in the coefficient β.

We present interpolation errors in $I_h u$ in the L^2 norm $||u - I_h u||_0$ and the broken weighted H^1 norms $||u_x - (I_h u)_x||_{\beta,h}$ and $||u_y - (I_h u)_y||_{\beta,h}$, and compute their orders of convergence in Tabes 7.9 and 7.10 for the quadratic IFE space $\mathcal{J}_h$. The related numerical results show that the quadratic IFE space $\mathcal{J}_h$ has optimal approximation capability for moderate and large jumps in β in both L^2 and broken H^1 norms.

h	$\|\|u - I_h u\|\|_0$	order	$\|\|u_x - (I_h u)_x\|\|_{\beta,h}$	order	$\|\|u_y - (I_h u)_y\|\|_{\beta,h}$	order
$\frac{1}{4}$	1.413998e-01	N/A	2.915527e$_+$00	N/A	2.915527e$_+$00	N/A
$\frac{1}{8}$	1.903831e-02	2.892803	7.843313e-01	1.894222	7.843313e-01	1.894222
$\frac{1}{16}$	2.425719e-03	2.972421	1.998007e-01	1.972902	1.998007e-01	1.972902
$\frac{1}{32}$	3.046777e-04	2.993057	5.018669e-02	1.993185	5.018669e-02	1.993185
$\frac{1}{64}$	3.813064e-05	2.998261	1.256152e-02	1.998294	1.256152e-02	1.998294
$\frac{1}{128}$	4.767767e-06	2.999565	3.141309e-03	1.999573	3.141309e-03	1.999573

Table 7.9: Interpolation errors and orders for u, u_x and u_y for the function (7.2.22) in Example 7.3.1 with $r = 5$.

h	$\|\|u - I_h u\|\|_0$	order	$\|\|u_x - (I_h u)_x\|\|_{\beta,h}$	order	$\|\|u_y - (I_h u)_y\|\|_{\beta,h}$	order
$\frac{1}{4}$	1.413998e-01	N/A	2.915678e$_+$00	N/A	2.915678e$_+$00	N/A
$\frac{1}{8}$	1.903831e-02	2.892804	7.843328e-01	1.894294	7.843328e-01	1.894294
$\frac{1}{16}$	2.425719e-03	2.972421	1.998008e-01	1.972903	1.998008e-01	1.972903
$\frac{1}{32}$	3.046777e-04	2.993057	5.018669e-02	1.993186	5.018669e-02	1.993186
$\frac{1}{64}$	3.813064e-05	2.998261	1.256152e-02	1.998294	1.256152e-02	1.998294
$\frac{1}{128}$	4.767767e-06	2.999565	3.141309e-03	1.999573	3.141309e-03	1.999573

Table 7.10: Interpolation errors and orders for u, u_x and u_y for the function (7.2.22) in Example 7.3.1 with $r = 1000$.

Example 7.3.2. *Circular interface and non-polynomial function*

We consider the same domain, same interface, and we test our IFE space with the same function of Example 7.2.2:

$$u(x,y) = \begin{cases} \frac{1}{\beta^+}\left((\frac{5}{13})^6 - (x^2+(y-1)^2)^3\right)\ e^{x+y} \ ; & \text{on } \Omega^+, \\ \\ \frac{1}{\beta^-}\left((\frac{5}{13})^6 - (x^2+(y-1)^2)^3\right)\ e^{x+y} \ ; & \text{on } \Omega^-, \end{cases}$$

with $r = \frac{\beta^+}{\beta^-} = 5$ and $r = \frac{\beta^+}{\beta^-} = 1000$ representing a moderate and a large jump in the coefficient β.

We present interpolation errors in $I_h u$ in the L^2 norm $||u - I_h u||_0$ and the broken weighted H^1 norms $||u_x - (I_h u)_x||_{\beta,h}$ and $||u_y - (I_h u)_y||_{\beta,h}$, and compute their orders of convergence in Tabes 7.11 and 7.12 for the quadratic IFE space $\mathcal{J}_h$. Again, the related numerical results show that the quadratic IFE space $\mathcal{J}_h$ has optimal approximation capability for moderate and large jumps in β in both L^2 and broken H^1 norms.

h	$\|\|u - I_h u\|\|_0$	order	$\|\|u_x - (I_h u)_x\|\|_{\beta,h}$	order	$\|\|u_y - (I_h u)_y\|\|_{\beta,h}$	order
$\frac{1}{4}$	4.825487e-02	N/A	1.224001e$_+$00	N/A	4.527345e-01	N/A
$\frac{1}{8}$	6.273074e-03	2.943430	3.178465e-01	1.945202	1.140196e-01	1.989383
$\frac{1}{16}$	7.920179e-04	2.985568	8.023689e-02	1.985993	2.855912e-02	1.997258
$\frac{1}{32}$	9.925107e-05	2.996379	2.010815e-02	1.996485	7.142981e-03	1.999353
$\frac{1}{64}$	1.241420e-05	2.999092	5.030122e-03	1.999115	1.785962e-03	1.999825
$\frac{1}{128}$	1.552015e-06	2.999776	1.257722e-03	1.999781	4.465018e-04	1.999964

Table 7.11: Interpolation errors and orders for u, u_x and u_y for the function (7.2.23) in Example 7.3.2 with $r = 5$.

h	$\|\|u - I_h u\|\|_0$	order	$\|\|u_x - (I_h u)_x\|\|_{\beta,h}$	order	$\|\|u_y - (I_h u)_y\|\|_{\beta,h}$	order
$\frac{1}{4}$	4.828089e-02	N/A	1.237437e$_+$00	N/A	4.885675e-01	N/A
$\frac{1}{8}$	6.273523e-03	2.944105	3.185202e-01	1.957899	1.152139e-01	2.084243
$\frac{1}{16}$	7.920937e-04	2.985533	8.036762e-02	1.986698	2.881601e-02	1.999373
$\frac{1}{32}$	9.925487e-05	2.996461	2.012172e-02	1.997861	7.176632e-03	2.005492
$\frac{1}{64}$	1.241940e-05	2.998542	5.034252e-03	1.998904	1.795437e-03	1.998972
$\frac{1}{128}$	1.552357e-06	3.000063	1.258256e-03	2.000352	4.476989e-04	2.003734

Table 7.12: Interpolation errors and orders for u, u_x and u_y for the function (7.2.23) in Example 7.3.2 with $r = 1000$.

Example 7.3.3. *Parabolic interface and polynomial function*

In this example, we consider the same domain $\Omega = [0,1]^2$ of Example 7.2.3, cut by the same parabolic interface $\Gamma : x^2 + \frac{5}{13} = y$, illustrated in Figure 7.6.

We also test our IFE space on the same piecewise polynomial function:

$$u(x,y) = \begin{cases} \frac{1}{\beta^+}\left(y^5 - \left(x^2 + \frac{5}{13}\right)^5\right) \ ; & \text{on } \Omega^+, \\ \\ \frac{1}{\beta^-}\left(y^5 - \left(x^2 + \frac{5}{13}\right)^5\right) \ ; & \text{on } \Omega^-, \end{cases}$$

with $r = \frac{\beta^+}{\beta^-} = 5$ and $r = \frac{\beta^+}{\beta^-} = 10^3$ representing a moderate and a large jump in the coefficient β.

We present interpolation errors in $I_h u$ in the L^2 norm $||u - I_h u||_0$ and the broken weighted H^1 norms $||u_x - (I_h u)_x||_{\beta,h}$ and $||u_y - (I_h u)_y||_{\beta,h}$, and compute their orders of convergence in Tabes 7.13 and 7.14 for the quadratic IFE space $\mathcal{J}_h$. Moreover, least square fits showing the global rate of convergence for u, u_x and u_y are illustrated, respectively, in Figures 7.8, 7.9, and 7.10. From the data tables, as well as the figures, we conclude that $\mathcal{J}_h$ has optimal approximation capability in L^2 norm, and overall optimal approximation capability in broken weighted H^1 norms, for both moderate and large jumps in β. The global convergence rate for the interpolation errors is:

$$\begin{aligned} ||u - I_h u||_0 &\approx Ch^{2.929}, \\ ||ux - (I_h u)_x||_{\beta,h} &\approx Ch^{2.051}, \\ ||uy - (I_h u)_y||_{\beta,h} &\approx Ch^{2.259}. \end{aligned}$$

h	$\|\|u - I_h u\|\|_0$	order	$\|\|u_x - (I_h u)_x\|\|_{\beta,h}$	order	$\|\|u_y - (I_h u)_y\|\|_{\beta,h}$	order
$\frac{1}{4}$	3.474993e-02	N/A	9.183850e-01	N/A	7.966278e-02	N/A
$\frac{1}{8}$	4.875259e-03	2.833460	2.538371e-01	1.855196	1.957757e-02	2.024704
$\frac{1}{16}$	6.256799e-04	2.961982	6.502423e-02	1.964854	4.577233e-03	2.096654
$\frac{1}{32}$	7.870814e-05	2.990840	1.635672e-02	1.991094	1.040536e-03	2.137149
$\frac{1}{64}$	9.855414e-06	2.997524	4.096404e-03	1.997454	2.522337e-04	2.044493
$\frac{1}{128}$	1.232477e-06	2.999356	1.024724e-03	1.999123	6.213368e-05	2.021314

Table 7.13: Interpolation errors and orders for u, u_x and u_y for the function (7.2.24) in Example 7.3.3 with $r = 5$.

h	$\|\|u - I_h u\|\|_0$	order	$\|\|u_x - (I_h u)_x\|\|_{\beta,h}$	order	$\|\|u_y - (I_h u)_y\|\|_{\beta,h}$	order
$\frac{1}{4}$	3.497570e-02	N/A	1.525384e+00	N/A	7.955109e-01	N/A
$\frac{1}{8}$	4.888972e-03	2.838750	3.463162e-01	2.139011	1.951546e-01	2.027264
$\frac{1}{16}$	7.691961e-04	2.668108	8.858531e-02	1.966951	4.488528e-02	2.120303
$\frac{1}{32}$	8.160749e-05	3.236578	1.781173e-02	2.314240	6.127606e-03	2.872847
$\frac{1}{64}$	1.153552e-05	2.822619	5.643782e-03	1.658093	2.003142e-03	1.613059
$\frac{1}{128}$	1.392790e-06	3.050033	1.182215e-03	2.255170	3.211796e-04	2.640812

Table 7.14: Interpolation errors and orders for u, u_x and u_y for the function (7.2.24) in Example 7.3.3 with $r = 1000$.

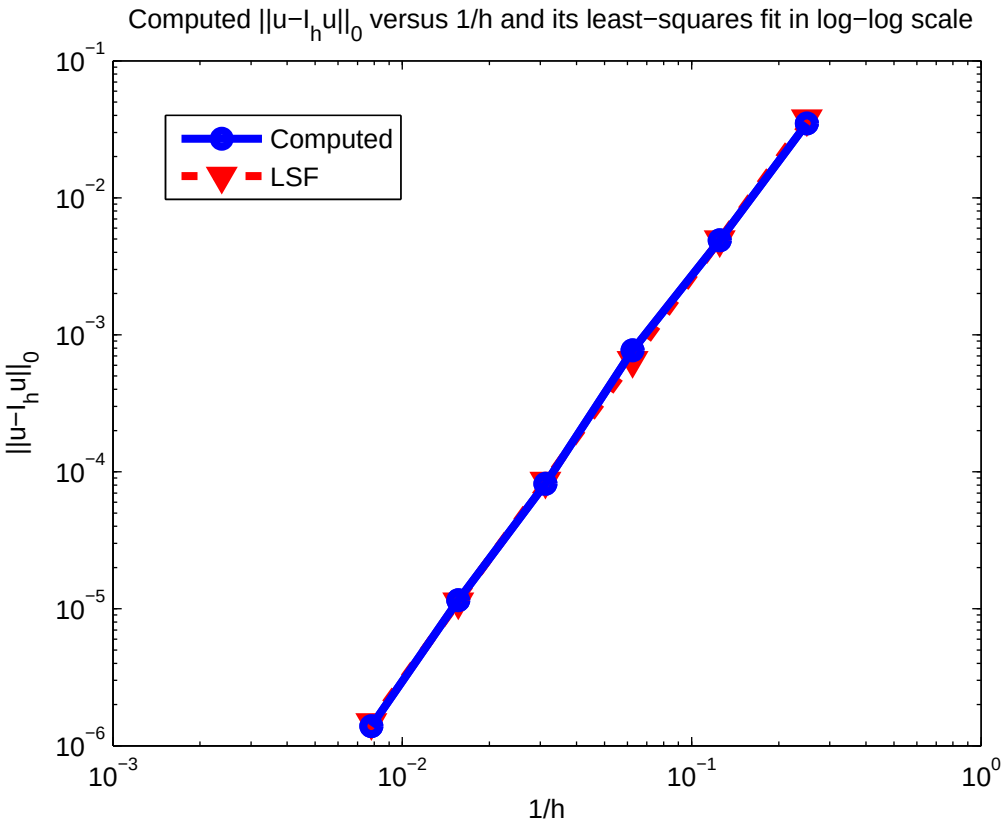

Figure 7.8: Least-squares fit in log-log scale of $||u - I_h u||_0$ versus $\frac{1}{h}$, for Example 7.3.3. Global order of convergence = 2.929

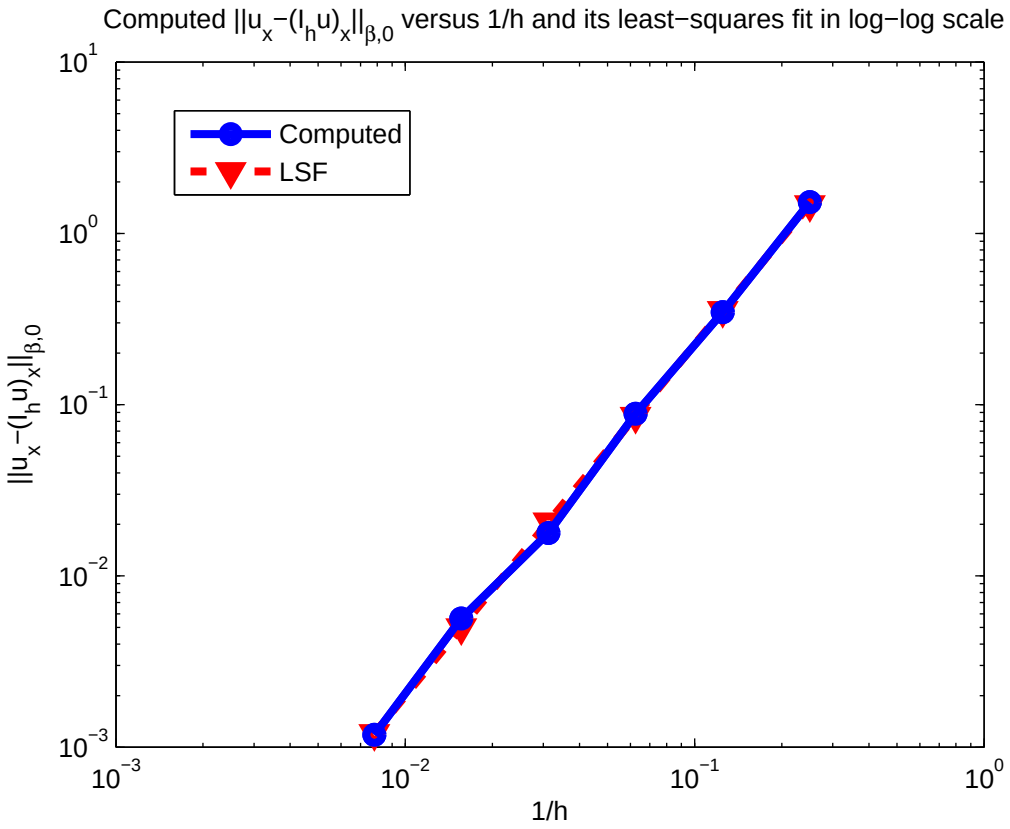

Figure 7.9: Least-squares fit in log-log scale of $||u_x - (I_h u)_x||_{\beta,h}$ versus $\frac{1}{h}$, for Example 7.3.3. Global order of convergence = 2.051

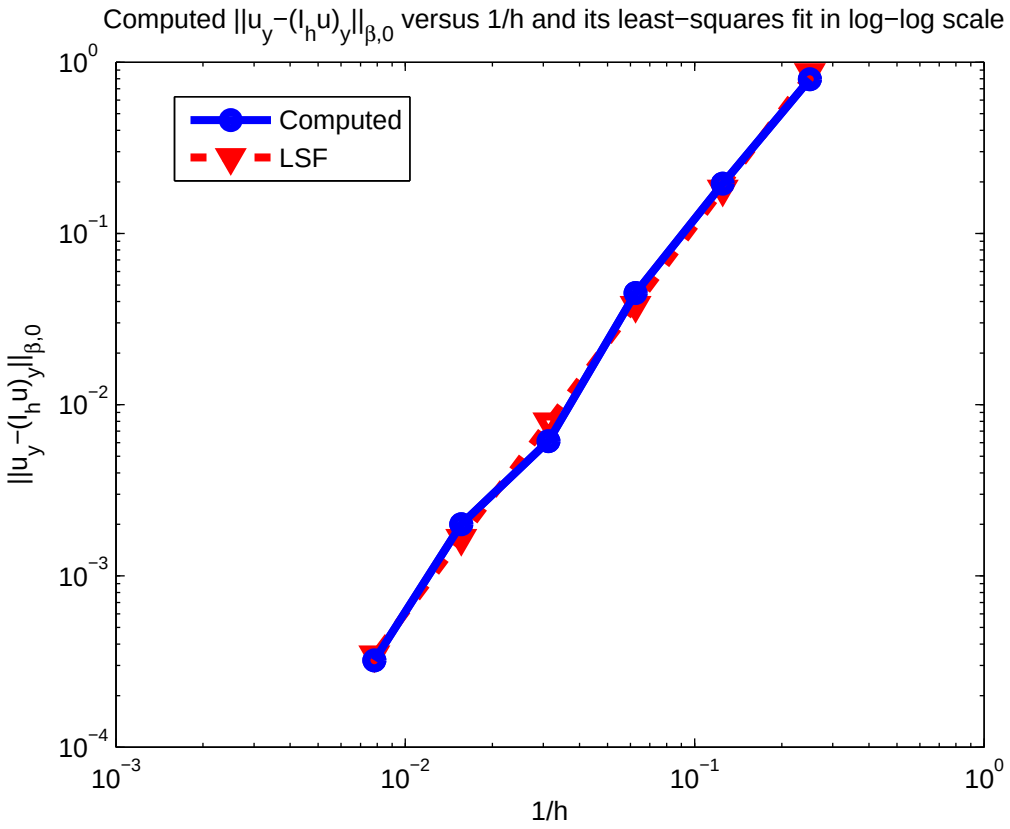

Figure 7.10: Least-squares fit in log-log scale of $||u_y - (I_h u)_y||_{\beta,h}$ versus $\frac{1}{h}$, for Example 7.3.3. Global order of convergence = 2.259

Example 7.3.4. *Parabolic interface and non-polynomial function*

We consider the same domain, the same interface, and the same true solution of Example 7.2.4:

$$u(x,y) = \begin{cases} \frac{1}{\beta^+}\left(y^3 - \left(x^2 + \frac{5}{13}\right)^3\right)\ e^{x+y} \ ; & \text{on } \Omega^+ \\ \\ \frac{1}{\beta^-}\left(y^3 - \left(x^2 + \frac{5}{13}\right)^3\right)\ e^{x+y} \ ; & \text{on } \Omega^-, \end{cases}$$

We present interpolation errors in $I_h u$ in the L^2 norm $||u - I_h u||_0$ and the broken weighted H^1 norms $||u_x - (I_h u)_x||_{\beta,h}$ and $||u_y - (I_h u)_y||_{\beta,h}$, and compute their orders of convergence in Tabes 7.15 and 7.16 for the quadratic IFE space $\mathcal{J}_h$. Least-squares fits showing the global rate of convergence for u, u_x and u_y are also illustrated, respectively, in Figures 7.11, 7.12, and 7.13, which show again the overall optimal approximation capability of the IFE space $\mathcal{J}_h$ in both L^2 and broken weighted H^1 norms. The global convergence rate for the interpolation errors is:

$$\begin{aligned} ||u - I_h u||_0 &\approx Ch^{2.782}, \\ ||ux - (I_h u)_x||_{\beta,h} &\approx Ch^{2.104}, \\ ||uy - (I_h u)_y||_{\beta,h} &\approx Ch^{2.253}. \end{aligned}$$

h	$\|\|u - I_h u\|\|_0$	order	$\|\|u_x - (I_h u)_x\|\|_{\beta,h}$	order	$\|\|u_y - (I_h u)_y\|\|_{\beta,h}$	order
$\frac{1}{4}$	3.115047e-02	N/A	8.686810e-01	N/A	3.181307e-01	N/A
$\frac{1}{8}$	4.172492e-03	2.900273	2.259787e-01	1.942640	7.583309e-02	2.068720
$\frac{1}{16}$	5.227874e-04	2.996613	5.655063e-02	1.998572	1.846379e-02	2.038128
$\frac{1}{32}$	6.519298e-05	3.003436	1.412117e-02	2.001684	4.486127e-03	2.041157
$\frac{1}{64}$	8.146633e-06	3.000441	3.531473e-03	1.999517	1.110646e-03	2.014072
$\frac{1}{128}$	1.018208e-06	3.000172	8.836072e-04	1.998793	2.764321e-04	2.006402

Table 7.15: Interpolation errors and orders for u, u_x and u_y for the function (7.2.25) in Example 7.3.4 with $r = 5$.

h	$\|\|u - I_h u\|\|_0$	order	$\|\|u_x - (I_h u)_x\|\|_{\beta,h}$	order	$\|\|u_y - (I_h u)_y\|\|_{\beta,h}$	order
$\frac{1}{4}$	3.635535e-02	N/A	3.139787e+00	N/A	2.351817e+00	N/A
$\frac{1}{8}$	4.315064e-03	3.074714	6.182118e-01	2.344493	5.552316e-01	2.082614
$\frac{1}{16}$	1.510766e-03	1.514102	1.887628e-01	1.711527	1.410038e-01	1.977356
$\frac{1}{32}$	9.234845e-05	4.032049	2.399016e-02	2.976060	1.873054e-02	2.912270
$\frac{1}{64}$	1.851802e-05	2.318158	1.023904e-02	1.228362	5.291982e-03	1.823512
$\frac{1}{128}$	2.303581e-06	3.006979	2.047640e-03	2.322047	1.024755e-03	2.368529

Table 7.16: Interpolation errors and orders for u, u_x and u_y for the function (7.2.25) in Example 7.3.4 with $r = 1000$.

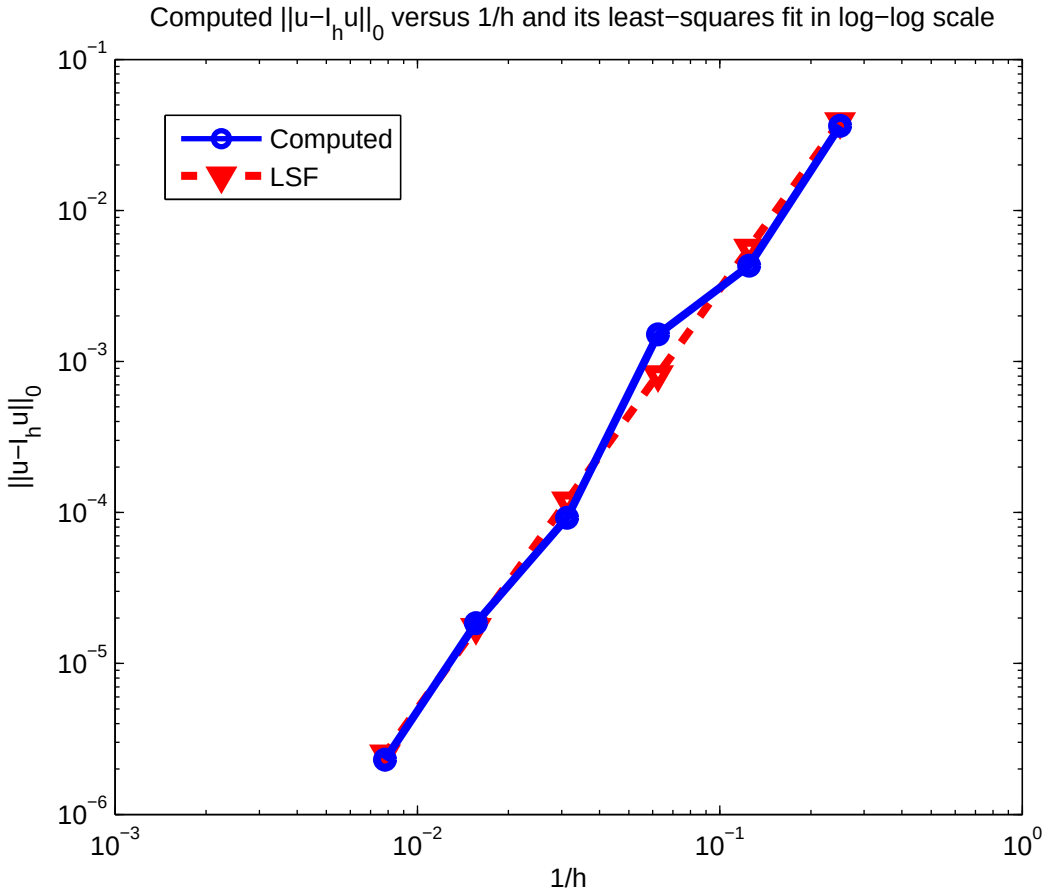

Figure 7.11: Least-squares fit in log-log scale of $||u - I_h u||_0$ versus $\frac{1}{h}$, for Example 7.3.4. Global order of convergence = 2.782

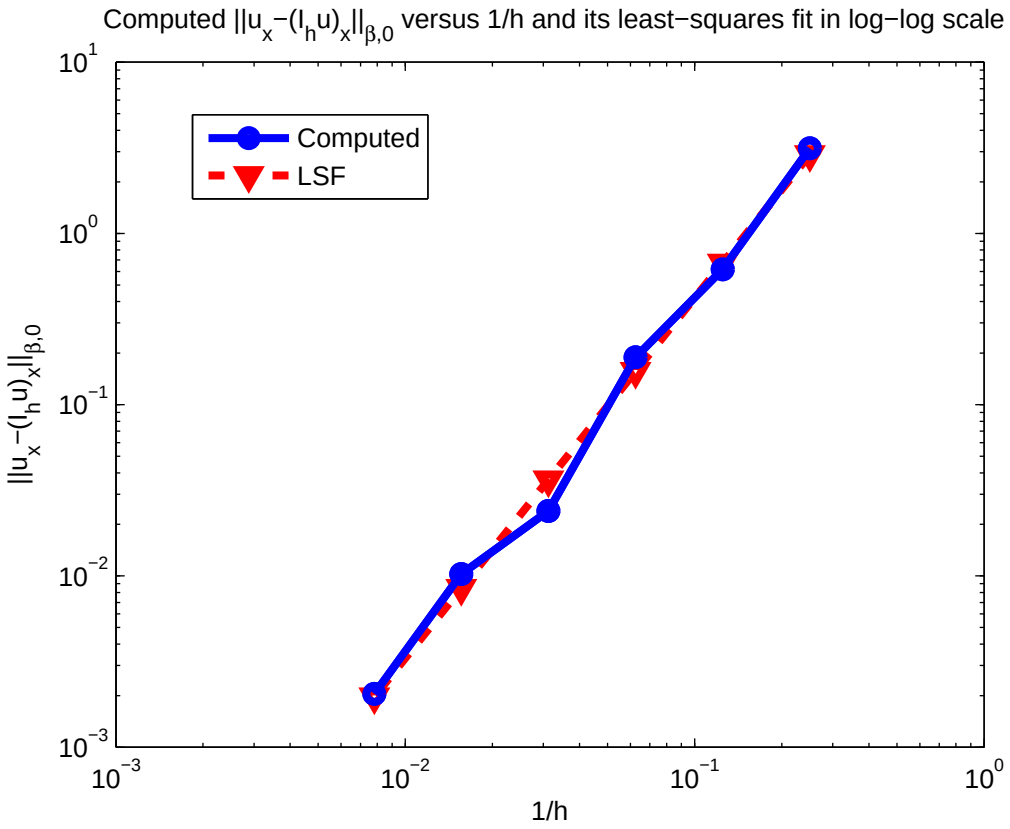

Figure 7.12: Least-squares fit in log-log scale of $||u_x - (I_h u)_x||_{\beta,h}$ versus $\frac{1}{h}$, for Example 7.3.4. Global order of convergence = 2.104

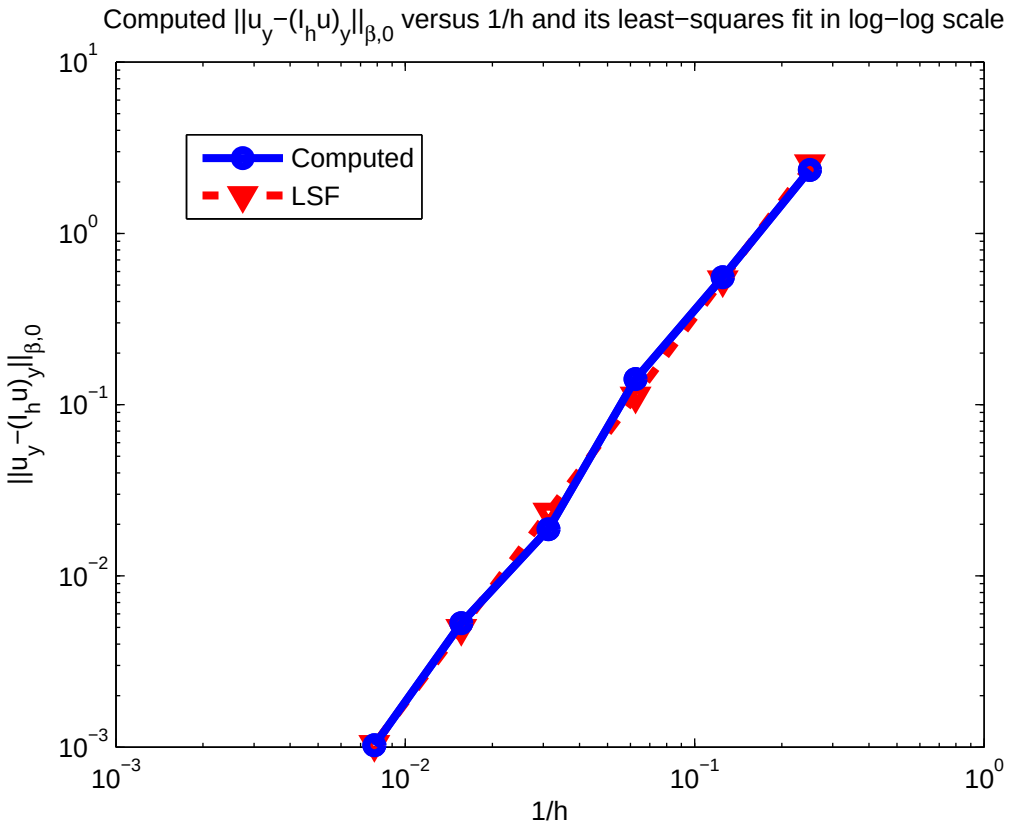

Figure 7.13: Least-squares fit in log-log scale of $||u_y - (I_h u)_y||_{\beta,h}$ versus $\frac{1}{h}$, for Example 7.3.4. Global order of convergence = 2.253

7.3.4 Application to Interface Problems

In this section, we present numerical results for the interior penalty IFE method (5.3.5) with the quadratic IFE space $\mathcal{J}_h$, considering several interface problems. We will use the norms (4.1.1a) and (7.2.21) to measure the finite element errors.

For all our numerical experiments, we consider the rectangular domain $\Omega = [0,1]^2$ and the uniform triangular mesh $\mathscr{T}_h = \mathscr{T}_h^i \cup \mathscr{T}_h^c$ of size h defined in Section 7.2.3. Here, $\mathscr{T}_h$ is formed by partitioning Ω into $(1/h)^2$ squares, with $h = \frac{1}{5m},\ m = 2, \ldots, 20$, then forming the triangular elements by joining the lower right and upper left vertices of the squares.

Example 7.3.5. *Circular interface and polynomial solution*

We consider the circular interface $\Gamma : x^2 + (y-1)^2 = \left(\frac{5}{13}\right)^2$ defined in Example 7.2.1. We solve the interface problem (1.1.1a), where the true solution is (7.2.22) from Example 7.3.1, with $r = \frac{\beta^+}{\beta^-} = 5$, then with $r = \frac{\beta^+}{\beta^-} = 10^3$. The L^2 error $||u - U^h||_0$, the weighted errors $||u_x - U_x^h||_{\beta,h}$ and $||u_y - U_y^h||_{\beta,h}$, and their orders of convergence are presented in Tables 7.17 and 7.18. Moreover, global rates of convergence are computed using least-squares fit. A computation of the global convergence rates for $r = 5$ reveals the following:

$$||u - U^h||_0 \approx C\ h^{2.9975}, \tag{7.3.13a}$$
$$||u_x - U_x^h||_{\beta,h} \approx C\ h^{1.9938}, \tag{7.3.13b}$$
$$||u_y - U_y^h||_{\beta,h} \approx C\ h^{1.9938}, \tag{7.3.13c}$$

and a computation of the global convergence rates for $r = 1000$ yields:

$$||u - U^h||_0 \approx C\ h^{2.9975}, \tag{7.3.14a}$$
$$||u_x - U_x^h||_{\beta,h} \approx C\ h^{1.9937}, \tag{7.3.14b}$$
$$||u_y - U_y^h||_{\beta,h} \approx C\ h^{1.9937}. \tag{7.3.14c}$$

From these results, we can easily observe that the interior penalty IFE method with the IFE space $\mathcal{J}_h$ performs optimally for interface problems with circular interfaces.

h	$\|\|u-U^h\|\|_0$	order	$\|\|u_x-U_x^h\|\|_{\beta,h}$	order	$\|\|u_y-U_y^h\|\|_{\beta,h}$	order
$\frac{1}{10}$	9.920905e-03	N/A	5.043181e-01	N/A	5.043181e-01	N/A
$\frac{1}{15}$	2.951582e-03	2.989907	2.266310e-01	1.972757	2.266310e-01	1.972757
$\frac{1}{20}$	1.247098e-03	2.994701	1.279919e-01	1.986068	1.279919e-01	1.986068
$\frac{1}{25}$	6.389956e-04	2.996623	8.207010e-02	1.991512	8.207010e-02	1.991512
$\frac{1}{30}$	3.699488e-04	2.997633	5.705259e-02	1.994280	5.705259e-02	1.994280
$\frac{1}{35}$	2.330340e-04	2.998237	4.194281e-02	1.995882	4.194281e-02	1.995882
$\frac{1}{40}$	1.561430e-04	2.998633	3.212579e-02	1.996892	3.212579e-02	1.996892
$\frac{1}{45}$	1.096784e-04	2.998907	2.539061e-02	1.997571	2.539061e-02	1.997571
$\frac{1}{50}$	7.996305e-05	2.999107	2.057062e-02	1.998049	2.057062e-02	1.998049
$\frac{1}{55}$	6.008170e-05	2.999254	1.700311e-02	1.998399	1.700311e-02	1.998399
$\frac{1}{60}$	4.628075e-05	2.999368	1.428900e-02	1.998662	1.428900e-02	1.998662
$\frac{1}{65}$	3.640264e-05	2.999459	1.217635e-02	1.998865	1.217635e-02	1.998865
$\frac{1}{70}$	2.914701e-05	2.999530	1.049975e-02	1.999025	1.049975e-02	1.999025
$\frac{1}{75}$	2.369827e-05	2.999588	9.146984e-03	1.999154	9.146984e-03	1.999154
$\frac{1}{80}$	1.952723e-05	2.999636	8.039726e-03	1.999258	8.039726e-03	1.999258
$\frac{1}{85}$	1.628030e-05	2.999677	7.121978e-03	1.999345	7.121978e-03	1.999345
$\frac{1}{90}$	1.371509e-05	2.999710	6.352840e-03	1.999417	6.352840e-03	1.999417
$\frac{1}{95}$	1.166169e-05	2.999739	5.701879e-03	1.999478	5.701879e-03	1.999478
$\frac{1}{100}$	9.998566e-06	2.999764	5.146070e-03	1.999529	5.146070e-03	1.999529

Table 7.17: L^2 errors and orders for u, u_x and $u_y$in Example 7.3.5 with $r = 5$, using the interior penalty IFE method with the IFE space $\mathcal{J}_h$.

h	$\|\|u-U^h\|\|_0$	order	$\|\|u_x-U_x^h\|\|_{\beta,h}$	order	$\|\|u_y-U_y^h\|\|_{\beta,h}$	order
$\frac{1}{10}$	9.920794e-03	N/A	5.043182e-01	N/A	5.043182e-01	N/A
$\frac{1}{15}$	2.951572e-03	2.989887	2.266310e-01	1.972757	2.266310e-01	1.972757
$\frac{1}{20}$	1.247096e-03	2.994696	1.279919e-01	1.986068	1.279919e-01	1.986068
$\frac{1}{25}$	6.389948e-04	2.996621	8.207010e-02	1.991512	8.207010e-02	1.991512
$\frac{1}{30}$	3.699485e-04	2.997630	5.705259e-02	1.994280	5.705259e-02	1.994280
$\frac{1}{35}$	2.330338e-04	2.998236	4.194281e-02	1.995882	4.194281e-02	1.995882
$\frac{1}{40}$	1.561430e-04	2.998632	3.212579e-02	1.996892	3.212579e-02	1.996892
$\frac{1}{45}$	1.096783e-04	2.998907	2.539061e-02	1.997571	2.539061e-02	1.997571
$\frac{1}{50}$	7.996303e-05	2.999105	2.057062e-02	1.998049	2.057062e-02	1.998049
$\frac{1}{55}$	6.008168e-05	2.999254	1.700311e-02	1.998399	1.700311e-02	1.998399
$\frac{1}{60}$	4.628074e-05	2.999368	1.428900e-02	1.998662	1.428900e-02	1.998662
$\frac{1}{65}$	3.640263e-05	2.999458	1.217870e-02	1.996447	1.217801e-02	1.997162
$\frac{1}{70}$	2.914700e-05	2.999530	1.049975e-02	2.001637	1.049975e-02	2.000864
$\frac{1}{75}$	2.369827e-05	2.999588	9.146984e-03	1.999154	9.146984e-03	1.999154
$\frac{1}{80}$	1.952723e-05	2.999636	8.039726e-03	1.999258	8.039726e-03	1.999258
$\frac{1}{85}$	1.628030e-05	2.999676	7.121978e-03	1.999345	7.121978e-03	1.999345
$\frac{1}{90}$	1.371509e-05	2.999710	6.352840e-03	1.999417	6.352840e-03	1.999417
$\frac{1}{95}$	1.166169e-05	2.999739	5.701879e-03	1.999478	5.701879e-03	1.999478
$\frac{1}{100}$	9.998565e-06	2.999764	5.146070e-03	1.999529	5.146070e-03	1.999529

Table 7.18: L^2 errors and orders for u, u_x and $u_y$in Example 7.3.5 with $r = 1000$, using the interior penalty IFE method with the IFE space $\mathcal{J}_h$.

Example 7.3.6. *Circular interface and non-polynomial solution*

We consider the circular interface $\Gamma : x^2 + (y-1)^2 = \left(\frac{5}{13}\right)^2$ defined in Example 7.2.1. We solve the interface problem (1.1.1a), where the true solution now is (7.2.23) from Example 7.3.2, with $r = \frac{\beta^+}{\beta^-} = 5$, then $r = \frac{\beta^+}{\beta^-} = 10^3$. The L^2 error $||u - U^h||_0$, the weighted errors $||u_x - U_x^h||_{\beta,h}$ and $||u_y - U_y^h||_{\beta,h}$, and their orders of convergence are presented in Tables 7.19 and 7.20. Moreover, global rates of convergence are computed using least-squares fit. A computation of the global convergence rates for $r = 5$ reveals the following:

$$||u - U^h||_0 \approx C\ h^{2.9976}, \tag{7.3.15a}$$
$$||u_x - U_x^h||_{\beta,h} \approx C\ h^{1.9971}, \tag{7.3.15b}$$
$$||u_y - U_y^h||_{\beta,h} \approx C\ h^{1.9997}, \tag{7.3.15c}$$

and a computation of the global convergence rates for $r = 1000$ yields:

$$||u - U^h||_0 \approx C\ h^{2.99767}, \tag{7.3.16a}$$
$$||u_x - U_x^h||_{\beta,h} \approx C\ h^{1.97901}, \tag{7.3.16b}$$
$$||u_y - U_y^h||_{\beta,h} \approx C\ h^{1.96896}, \tag{7.3.16c}$$

which show, again, that the interior penalty IFE method with the IFE space $\mathcal{J}_h$ performs optimally for interface problems with circular interfaces and non-polynomial solutions.

h	$\|\|u-U^h\|\|_0$	order	$\|\|u_x-U_x^h\|\|_{\beta,h}$	order	$\|\|u_y-U_y^h\|\|_{\beta,h}$	order
$\frac{1}{10}$	3.229994e-03	N/A	2.041102e-01	N/A	7.308307e-02	N/A
$\frac{1}{15}$	9.610371e-04	2.989709	9.119304e-02	1.987055	3.250186e-02	1.998444
$\frac{1}{20}$	4.060531e-04	2.994726	5.139232e-02	1.993485	1.828574e-02	1.999346
$\frac{1}{25}$	2.080509e-04	2.996731	3.291990e-02	1.996076	1.170370e-02	1.999681
$\frac{1}{30}$	1.204460e-04	2.997895	2.287196e-02	1.997380	8.127812e-03	1.999839
$\frac{1}{35}$	7.586684e-05	2.998509	1.680878e-02	1.998113	5.971575e-03	1.999868
$\frac{1}{40}$	5.083280e-05	2.998830	1.287166e-02	1.998582	4.572027e-03	1.999935
$\frac{1}{45}$	3.570546e-05	2.999057	1.017152e-02	1.998897	3.612485e-03	1.999955
$\frac{1}{50}$	2.603114e-05	2.999322	8.239691e-03	1.999125	2.926119e-03	1.999978
$\frac{1}{55}$	1.955875e-05	2.999374	6.810136e-03	1.999269	2.418292e-03	1.999948
$\frac{1}{60}$	1.506592e-05	2.999460	5.722709e-03	1.999393	2.032046e-03	1.999949
$\frac{1}{70}$	9.488126e-06	2.999681	4.204748e-03	1.999775	1.492939e-03	2.000618
$\frac{1}{75}$	7.714381e-06	2.999656	3.662902e-03	1.999608	1.300521e-03	1.999942
$\frac{1}{80}$	6.356575e-06	2.999704	3.219417e-03	1.999666	1.143038e-03	1.999979
$\frac{1}{85}$	5.299579e-06	2.999811	2.851853e-03	1.999703	1.012519e-03	1.999974
$\frac{1}{90}$	4.464538e-06	2.999763	2.543821e-03	1.999733	9.031432e-04	1.999980
$\frac{1}{95}$	3.796103e-06	2.999796	2.283127e-03	1.999758	8.105789e-04	1.999964
$\frac{1}{100}$	3.254710e-06	2.999841	2.060544e-03	1.999791	7.315474e-04	2.000000

Table 7.19: L^2 errors and orders for u, u_x and u_y in Example 7.3.6, with $r = 5$, using the interior penalty IFE method with the IFE space $\mathcal{J}_h$.

h	$\|\|u-U^h\|\|_0$	order	$\|\|u_x-U_x^h\|\|_{\beta,h}$	order	$\|\|u_y-U_y^h\|\|_{\beta,h}$	order
$\frac{1}{10}$	3.229947e-03	N/A	2.041205e-01	N/A	7.310329e-02	N/A
$\frac{1}{15}$	9.610814e-04	2.989559	9.119421e-02	1.987148	3.250514e-02	1.998877
$\frac{1}{20}$	4.060663e-04	2.994773	5.139263e-02	1.993508	1.828708e-02	1.999442
$\frac{1}{25}$	2.080578e-04	2.996729	3.292034e-02	1.996043	1.170491e-02	1.999550
$\frac{1}{30}$	1.204491e-04	2.997935	2.287224e-02	1.997387	8.128520e-03	1.999924
$\frac{1}{35}$	7.586832e-05	2.998548	1.680880e-02	1.998182	5.971847e-03	2.000137
$\frac{1}{40}$	5.083382e-05	2.998825	1.287173e-02	1.998550	4.572258e-03	1.999898
$\frac{1}{45}$	3.570583e-05	2.999141	1.017155e-02	1.998920	3.612615e-03	2.000078
$\frac{1}{50}$	2.603144e-05	2.999311	8.239703e-03	1.999140	2.926194e-03	2.000078
$\frac{1}{55}$	1.955890e-05	2.999411	6.810154e-03	1.999256	2.418355e-03	1.999946
$\frac{1}{60}$	1.506601e-05	2.999485	5.722711e-03	1.999419	2.032066e-03	2.000132
$\frac{1}{70}$	9.488159e-06	2.999669	4.204746e-03	1.999529	1.492948e-03	1.999993
$\frac{1}{75}$	7.714410e-06	2.999651	3.662902e-03	1.999599	1.300530e-03	1.999925
$\frac{1}{80}$	6.356590e-06	2.999728	3.219419e-03	1.999656	1.143050e-03	1.999920
$\frac{1}{85}$	5.299601e-06	2.999779	2.851855e-03	1.999702	1.012531e-03	1.999960
$\frac{1}{90}$	4.464552e-06	2.999781	2.543824e-03	1.999726	9.031563e-04	1.999937
$\frac{1}{95}$	3.796118e-06	2.999784	2.283130e-03	1.999760	8.105896e-04	1.999986
$\frac{1}{100}$	3.254718e-06	2.999867	2.060545e-03	1.999805	7.315551e-04	2.000053

Table 7.20: L^2 errors and orders for u, u_x and u_y in Example 7.3.6, with $r = 1000$, using the interior penalty IFE method with the IFE space $\mathcal{J}_h$.

Example 7.3.7. *Parabolic interface and polynomial solution*

We consider the parabolic interface $\Gamma : x^2 + \frac{5}{13} = y$ defined in Example 7.2.3. We solve the interface problem (1.1.1a), where the true solution is (7.2.24) from Example 7.3.3, with $r = \frac{\beta^+}{\beta^-} = 5$, then with $r = \frac{\beta^+}{\beta^-} = 10^3$. The L^2 error $||u - U^h||_0$, the weighted errors $||u_x - U_x^h||_{\beta,h}$ and $||u_y - U_y^h||_{\beta,h}$, and their orders of convergence are presented in Tables 7.21 and 7.22. Moreover, global rates of convergence are estimated using least-squares fit. A computation of the global convergence rates for $r = 5$ reveals the following:

$$||u - U^h||_0 \approx C\ h^{2.9929}, \tag{7.3.17a}$$
$$||u_x - U_x^h||_{\beta,h} \approx C\ h^{1.9924}, \tag{7.3.17b}$$
$$||u_y - U_y^h||_{\beta,h} \approx C\ h^{2.0772}, \tag{7.3.17c}$$

and a computation of the global convergence rates for $r = 1000$ yields:

$$||u - U^h||_0 \approx C\ h^{2.9956}, \tag{7.3.18a}$$
$$||u_x - U_x^h||_{\beta,h} \approx C\ h^{1.9951}, \tag{7.3.18b}$$
$$||u_y - U_y^h||_{\beta,h} \approx C\ h^{2.1942}, \tag{7.3.18c}$$

From these datum, we can easily observe that the interior penalty IFE method with the IFE space $\mathcal{J}_h$ performs optimally for interface problems with a parabolic interface as well.

h	$\|\|u-U^h\|\|_0$	order	$\|\|u_x-U_x^h\|\|_{\beta,h}$	order	$\|\|u_y-U_y^h\|\|_{\beta,h}$	order
$\frac{1}{10}$	2.525076e-03	N/A	1.638644e-01	N/A	1.243936e-02	N/A
$\frac{1}{15}$	7.579464e-04	2.967984	7.376399e-02	1.968526	5.189900e-03	2.155921
$\frac{1}{20}$	3.212902e-04	2.983390	4.168838e-02	1.983608	2.809850e-03	2.132852
$\frac{1}{25}$	1.648662e-04	2.990051	2.673622e-02	1.990661	1.756249e-03	2.106048
$\frac{1}{30}$	9.551739e-05	2.993754	1.859234e-02	1.992468	1.200794e-03	2.085309
$\frac{1}{35}$	6.019374e-05	2.995381	1.367139e-02	1.994440	8.701925e-04	2.089022
$\frac{1}{40}$	4.033938e-05	2.997348	1.047311e-02	1.995737	6.591854e-04	2.079733
$\frac{1}{45}$	2.833958e-05	2.997619	8.277809e-03	1.997174	5.148535e-04	2.098115
$\frac{1}{50}$	2.066508e-05	2.997461	6.706355e-03	1.998117	4.145262e-04	2.057188
$\frac{1}{55}$	1.552752e-05	2.998964	5.543901e-03	1.997238	3.422886e-04	2.009038
$\frac{1}{60}$	1.196112e-05	2.999062	4.659276e-03	1.997881	2.863186e-04	2.052019
$\frac{1}{70}$	7.533877e-06	2.998867	3.423875e-03	1.999071	2.090348e-04	2.028754
$\frac{1}{75}$	6.125551e-06	2.999456	2.982921e-03	1.998321	1.820412e-04	2.004084
$\frac{1}{80}$	5.047563e-06	2.999187	2.621957e-03	1.998529	1.598343e-04	2.015784
$\frac{1}{85}$	4.208302e-06	2.999548	2.322736e-03	1.998777	1.414404e-04	2.016650
$\frac{1}{90}$	3.546245e-06	2.994658	2.072317e-03	1.995834	1.278549e-04	1.766717
$\frac{1}{95}$	3.014609e-06	3.004025	1.859572e-03	2.003444	1.128617e-04	2.306992
$\frac{1}{100}$	2.584696e-06	2.999653	1.678383e-03	1.998620	1.018723e-04	1.997210

Table 7.21: L^2 errors and orders for u, u_x and u_y in Example 7.3.7, with $r = 5$, using the interior penalty IFE method with the IFE space $\mathcal{J}_h$.

h	$\|\|u - U^h\|\|_0$	order	$\|\|u_x - U_x^h\|\|_{\beta,h}$	order	$\|\|u_y - U_y^h\|\|_{\beta,h}$	order
$\frac{1}{10}$	2.551402e-03	N/A	1.654924e-01	N/A	2.194710e-02	N/A
$\frac{1}{15}$	7.602739e-04	2.986001	7.410100e-02	1.981665	7.614243e-03	2.610864
$\frac{1}{20}$	3.217974e-04	2.988565	4.174217e-02	1.994970	3.343147e-03	2.861172
$\frac{1}{25}$	1.651798e-04	2.988605	2.677903e-02	1.989270	2.192454e-03	1.890672
$\frac{1}{30}$	9.568744e-05	2.994420	1.862140e-02	1.992675	1.466491e-03	2.205715
$\frac{1}{35}$	6.028625e-05	2.996958	1.369206e-02	1.994772	1.066627e-03	2.065325
$\frac{1}{40}$	4.038199e-05	3.000944	1.048364e-02	1.999533	7.582384e-04	2.555641
$\frac{1}{45}$	2.837200e-05	2.996876	8.287931e-03	1.995325	6.295192e-04	1.579527
$\frac{1}{50}$	2.069309e-05	2.995457	6.714537e-03	1.998143	4.920329e-04	2.338740
$\frac{1}{55}$	1.554739e-05	2.999752	5.550803e-03	1.996978	4.020716e-04	2.118508
$\frac{1}{60}$	1.196849e-05	3.006683	4.663336e-03	2.002169	3.186921e-04	2.670971
$\frac{1}{70}$	7.538037e-06	2.997339	3.426542e-03	1.997143	2.336102e-04	2.014726
$\frac{1}{75}$	6.129100e-06	2.999063	2.985319e-03	1.997960	2.031375e-04	2.025874
$\frac{1}{80}$	5.049692e-06	3.001630	2.623982e-03	1.999016	1.762868e-04	2.196682
$\frac{1}{85}$	4.209215e-06	3.002921	2.323780e-03	2.004099	1.501000e-04	2.652569
$\frac{1}{90}$	3.546278e-06	2.998293	2.072888e-03	1.998876	1.357462e-04	1.758530
$\frac{1}{95}$	3.015784e-06	2.996983	1.860605e-03	1.998268	1.225038e-04	1.898470
$\frac{1}{100}$	2.585757e-06	2.999256	1.679389e-03	1.997766	1.110096e-04	1.920819

Table 7.22: L^2 errors and orders for u, u_x and u_y in Example 7.3.7, with $r = 1000$, using the interior penalty IFE method with the IFE space $\mathcal{J}_h$.

Example 7.3.8. *Parabolic interface and non-polynomial solution*

We consider the parabolic interface $\Gamma : x^2 + \frac{5}{13} = y$ and we solve the interface problem (1.1.1a), where the true solution now is (7.2.25) from Example 7.3.4, with $r = \frac{\beta^+}{\beta^-} = 5$, then $r = \frac{\beta^+}{\beta^-} = 10^3$. The L^2 error $||u - U^h||_0$, the weighted errors $||u_x - U^h_x||_{\beta,h}$ and $||u_y - U^h_y||_{\beta,h}$, and their orders of convergence are presented in ables 7.23 and 7.24. Moreover, global rates of convergence are estimated using least-squares fit. A computation of the global convergence rates for $r = 5$ reveals the following:

$$||u - U^h||_0 \approx C\ h^{2.9987}, \tag{7.3.19a}$$
$$||u_x - U^h_x||_{\beta,h} \approx C\ h^{1.9952}, \tag{7.3.19b}$$
$$||u_y - U^h_y||_{\beta,h} \approx C\ h^{2.0091}, \tag{7.3.19c}$$

and for $r = 1000$ we have:

$$||u - U^h||_0 \approx C\ h^{3.0161}, \tag{7.3.20a}$$
$$||u_x - U^h_x||_{\beta,h} \approx C\ h^{2.0118}, \tag{7.3.20b}$$
$$||u_y - U^h_y||_{\beta,h} \approx C\ h^{2.0837}, \tag{7.3.20c}$$

which show, again, that the interior penalty IFE method with the IFE space $\mathcal{J}_h$ performs optimally for interface problems with parabolic interface and non-polynomial solutions.

h	$\|\|u-U^h\|\|_0$	order	$\|\|u_x-U_x^h\|\|_{\beta,h}$	order	$\|\|u_y-U_y^h\|\|_{\beta,h}$	order
$\frac{1}{10}$	2.125261e-03	N/A	1.427377e-01	N/A	4.625662e-02	N/A
$\frac{1}{15}$	6.320709e-04	2.990759	6.380530e-02	1.985800	2.045580e-02	2.012351
$\frac{1}{20}$	2.672648e-04	2.992059	3.599501e-02	1.989891	1.146448e-02	2.012682
$\frac{1}{25}$	1.370015e-04	2.994699	2.304987e-02	1.997461	7.325164e-03	2.007399
$\frac{1}{30}$	7.928318e-05	3.000008	1.602543e-02	1.993638	5.074330e-03	2.013591
$\frac{1}{35}$	4.991351e-05	3.001831	1.178381e-02	1.994477	3.719078e-03	2.015682
$\frac{1}{40}$	3.340636e-05	3.007123	9.027088e-03	1.995762	2.842370e-03	2.013291
$\frac{1}{45}$	2.344816e-05	3.005138	7.132285e-03	2.000273	2.240621e-03	2.019688
$\frac{1}{50}$	1.709740e-05	2.997948	5.775917e-03	2.002026	1.813249e-03	2.008656
$\frac{1}{55}$	1.284315e-05	3.001944	4.775571e-03	1.995417	1.499094e-03	1.996214
$\frac{1}{60}$	9.888557e-06	3.004580	4.013516e-03	1.997967	1.258273e-03	2.012617
$\frac{1}{70}$	6.227418e-06	2.999099	2.949095e-03	2.000630	9.234705e-04	2.002585
$\frac{1}{75}$	5.062902e-06	3.000631	2.569454e-03	1.997384	8.044457e-04	1.999994
$\frac{1}{80}$	4.171588e-06	3.000424	2.258735e-03	1.997079	7.069451e-04	2.001912
$\frac{1}{85}$	3.477592e-06	3.001368	2.001133e-03	1.997390	6.262011e-04	2.000532
$\frac{1}{90}$	2.950525e-06	2.875465	1.792670e-03	1.924607	5.644307e-04	1.816949
$\frac{1}{95}$	2.491233e-06	3.129537	1.601821e-03	2.081942	5.010097e-04	2.204518
$\frac{1}{100}$	2.135870e-06	3.000461	1.445933e-03	1.996103	4.522272e-04	1.997158

Table 7.23: L^2 errors and orders for u, u_x and u_y in Example 7.3.8, with $r = 5$, using the interior penalty IFE method with the IFE space $\mathcal{J}_h$.

h	$\|\|u-U^h\|\|_0$	order	$\|\|u_x-U_x^h\|\|_{\beta,h}$	order	$\|\|u_y-U_y^h\|\|_{\beta,h}$	order
$\frac{1}{10}$	2.256364e-03	N/A	1.513580e-01	N/A	6.355162e-02	N/A
$\frac{1}{15}$	6.462930e-04	3.083514	6.598873e-02	2.047437	2.470430e-02	2.330349
$\frac{1}{20}$	2.718617e-04	3.010127	3.648725e-02	2.059639	1.252624e-02	2.360771
$\frac{1}{25}$	1.392322e-04	2.998742	2.335671e-02	1.999065	7.977940e-03	2.021773
$\frac{1}{30}$	8.045833e-05	3.007894	1.622591e-02	1.997982	5.471738e-03	2.068236
$\frac{1}{35}$	5.053732e-05	3.016706	1.195077e-02	1.983861	4.137388e-03	1.813367
$\frac{1}{40}$	3.372831e-05	3.028311	9.114979e-03	2.028559	3.032793e-03	2.325899
$\frac{1}{45}$	2.369025e-05	2.999363	7.205945e-03	1.995303	2.407545e-03	1.960183
$\frac{1}{50}$	1.729647e-05	2.985567	5.836048e-03	2.001247	1.934437e-03	2.076598
$\frac{1}{55}$	1.297266e-05	3.018130	4.826299e-03	1.993217	1.591429e-03	2.047879
$\frac{1}{60}$	9.942338e-06	3.057553	4.044378e-03	2.031370	1.315736e-03	2.186339
$\frac{1}{70}$	6.257379e-06	2.992100	2.966947e-03	2.156679	9.571431e-04	2.064204
$\frac{1}{75}$	5.087214e-06	3.000760	2.585443e-03	1.994938	8.339202e-04	1.997528
$\frac{1}{80}$	4.187838e-06	3.014415	2.273210e-03	1.994218	7.345698e-04	1.965535
$\frac{1}{85}$	3.487463e-06	3.018741	2.009258e-03	2.035928	6.410587e-04	2.246017
$\frac{1}{90}$	2.938364e-06	2.997310	1.791958e-03	2.002453	5.733330e-04	1.953420
$\frac{1}{95}$	2.500780e-06	2.982404	1.609012e-03	1.991751	5.141116e-04	2.016497
$\frac{1}{100}$	2.143854e-06	3.002296	1.453480e-03	1.981923	4.676192e-04	1.847923

Table 7.24: L^2 errors and orders for u, u_x and u_y in Example 7.3.8, with $r = 1000$, using the interior penalty IFE method with the IFE space $\mathcal{J}_h$.

In summary, we developed a quadratic IFE space that has an optimal approximation capability of $p+1=3$ in L^2 norm, and $p=2$ in the weighted H^1 norms. The quadratic IFE space performs optimally in producing solutions to interface problems with quadratic interfaces via the interior penalty immersed finite element method (5.3.5). In the following section, we discuss the approximation capability and the convergence rates of solutions produced by the interior penalty IFE method for interface problems with arbitrary smooth interface.

7.4 Piecewise Quadratic IFE Spaces for Arbitrary Interfaces

In many practical problems, the interface is usually not a quadratic polynomial, hence an extension of the method presented in the previous section is necessary to handle higher-order polynomial interfaces and arbitrary smooth interfaces. In this sections, we consider interface problems (1.1.1a) with an arbitrary smooth interface Γ defined as:

$$y = \gamma(x), \tag{7.4.1a}$$

or

$$\begin{cases} x = \gamma_1(t), \\ \\ y = \gamma_2(t), \end{cases} \qquad t \in I \subset \mathbb{R}. \tag{7.4.1b}$$

7.4.1 Quadratic IFE Spaces for Arbitrary Smooth Interfaces

We extend the quadratic IFE space $\mathcal{J}_h$ proposed in Section 7.3 for arbitrary smooth interfaces.

First, we interpolate Γ by a quadratic interface Π, as shown in Figure 7.14, using the three points $P_1 = E$, $P_2 = D$, and $P_3 = G$, as:

$$\Pi = \left\{ (x,y) \in \mathbb{R}^2 \mid (x,y)^t = P_1\, l_1(t) + P_2\, l_2(t) + P_3\, l_3(t),\ t \in [-1,1] \right\}, \tag{7.4.2}$$

where $l_i(t)$ are one-dimensional Lagrange quadratic polynomials:

$$l_1(t) = \frac{1}{2}\, t\, (t-1), \quad l_2(t) = \frac{1}{2}\, t\, (t+1), \quad l_3(t) = (1-t)\, (1+t), \quad t \in [-1,1].$$

Then, we use the quadratic IFE space defined in (7.3.6), for the quadratic approximation Π of Γ:

$$\mathcal{R}(T) = \{ U,\ \mid U|_{T^{\pm}} \in \mathcal{P}_2,\ [U]_{D,E,G} = 0,\ \int_{T \cap \Pi} [\ \beta\ \boldsymbol{n} \cdot \nabla U\ ]_{T \cap \Pi}\ v_i\ ds = 0,\ i = 1,2,3\ \},$$

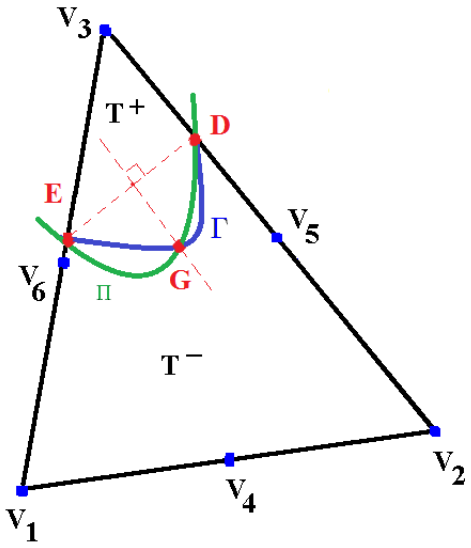

Figure 7.14: Approximation of the general interface Γ by a quadratic curve Π on a physical interface element T.

with $v_i,\ i = 1, 2, 3$, being the three quadratic polynomials given in Section 7.3.

Finally, using the standard affine mapping F defined in (2.2.7), we map the interface element $T = T^+ \cup T^-$ to $\hat{T} = \hat{T}^1 \cup \hat{T}^2$ and we let $\hat{\Gamma} = F(\Gamma \cap T)$, the quadratic curve $\hat{\Pi} = F(\Pi \cap T)$, $\hat{D} = F(D)$, $\hat{E} = F(E)$, and $\hat{G} = F(G)$. Thus, on $\hat{T}$, we use the quadratic IFE space defined in (7.3.12):

$$\hat{\mathcal{R}}(\hat{T}) = \{\hat{U} \in \hat{\mathcal{P}}_2(\hat{T}), \mid [\hat{U}]_{\hat{D},\hat{E},\hat{G}} = 0, \int_{\hat{\Pi}} [\ \hat{\beta}\ \hat{\boldsymbol{n}} \cdot \hat{\nabla}\hat{U}\ ]_{\hat{\Pi}}\ \hat{v}_i\ d\hat{s} = 0, i = 1, 2, 3\},$$

where $\hat{\mathcal{P}}_2(\hat{T})$ is the polynomial space defined in (2.2.20), and $\hat{v}_i,\ i = 1, 2, 3$, are given in (7.3.11).

7.4.2 Approximation Capability

In this section, we use the norms defined in (4.1.1a) and (7.2.21) to compute the interpolation errors using Lagrange piecewise quadratic immersed finite element shape functions constructed in this section and discuss the approximation capability of the piecewise quadratic IFE space $\mathcal{J}_h$.

For all our numerical experiments, we consider the rectangular domain $\Omega = [0, 1]^2$ and the uniform triangular mesh $\mathcal{T}_h = \mathcal{T}_h^i \cup \mathcal{T}_h^c$ of size h defined in Section 7.2.3. Here, $\mathcal{T}_h$ is formed by partitioning Ω into $(1/h)^2$ squares, with $h = \frac{1}{5m},\ m = 2, \ldots, 20$, then forming the triangular elements by joining the lower right and upper left vertices of the squares. Using

the same definition in Section 7.2.3, a piecewise Lagrange type IFE interpolant $I_h u(x, y)$ of $u(x, y)$ is defined by (7.2.20).

Example 7.4.1. *Polynomial interface*

In this example, we consider the cubic interface

$$y = (x+1)^3 - \frac{13}{27}, \tag{7.4.3}$$

such that $\Omega^+ = \{y > (x+1)^3 - \frac{13}{27}\}$ and $\Omega^- = \{y < (x+1)^3 - \frac{13}{27}\}$, as illustrated in Figure 7.15.

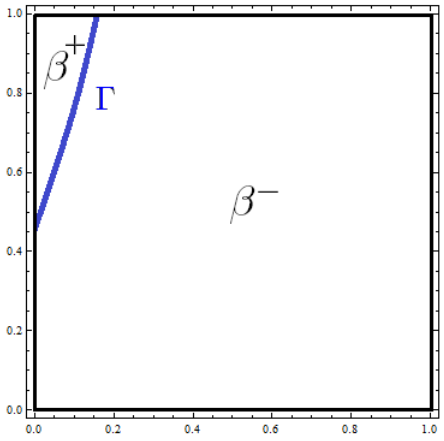

Figure 7.15: Geometry of Ω and the circular interface Γ in Example 7.4.1.

We test our space on the function defined by

$$u(x,y) = \begin{cases} \frac{1}{\beta^+}\ \left(y^2 - (x+1)^6 + \frac{26}{27}(x+1)^3 - \frac{169}{729}\right); & \text{on } \Omega^+, \\ \\ \frac{1}{\beta^-}\ \left(y^2 - (x+1)^6 + \frac{26}{27}(x+1)^3 - \frac{169}{729}\right); & \text{on } \Omega^-, \end{cases} \tag{7.4.4}$$

with $r = \frac{\beta^+}{\beta^-} = 5$ and $r = \frac{\beta^+}{\beta^-} = 10^3$ representing a moderate and a large jump in the coefficient β.

We present interpolation errors in $I_h u$ in the L^2 norm $||u - I_h u||_0$ and the broken weighted H^1 norms $||u_x - (I_h u)_x||_{\beta,h}$ and $||u_y - (I_h u)_y||_{\beta,h}$, and compute their orders of convergence in Tabes 7.25 and 7.26. Moreover, global rates of convergence are estimated using least-squares fit, thus computation for $r = 5$ reveals the following:

$$||u - U^h||_0 \approx C\ h^{3.0037}, \tag{7.4.5a}$$

$$||u_x - (I_h u)_x||_{\beta,h} \approx C\ h^{2.0029}, \tag{7.4.5b}$$

$$||u_y - (I_h u)_y||_{\beta,h} \approx C\ h^{1.9901}, \tag{7.4.5c}$$

and for $r = 1000$:

$$||u - U^h||_0 \approx C\ h^{3.0058}, \tag{7.4.6a}$$
$$||u_x - (I_h u)_x||_{\beta,h} \approx C\ h^{2.0090}, \tag{7.4.6b}$$
$$||u_y - (I_h u)_y||_{\beta,h} \approx C\ h^{2.3182}, \tag{7.4.6c}$$

We observe that, the interpolant in $\mathcal{J}_h$ yields $\mathcal{O}(h^3)$ optimal convergence rates for u and $\mathcal{O}(h^2)$ for its derivatives.

h	$\|\|u - I_h u\|\|_0$	order	$\|\|u_x - (I_h u)_x\|\|_{\beta,h}$	order	$\|\|u_y - (I_h u)_y\|\|_{\beta,h}$	order
$\frac{1}{10}$	2.551402e-03	N/A	1.654924e-01	N/A	2.194710e-02	N/A
$\frac{1}{15}$	7.602739e-04	2.986001	7.410100e-02	1.981665	7.614243e-03	2.610864
$\frac{1}{20}$	3.217974e-04	2.988565	4.174217e-02	1.994970	3.343147e-03	2.861172
$\frac{1}{25}$	1.651798e-04	2.988605	2.677903e-02	1.989270	2.192454e-03	1.890672
$\frac{1}{30}$	9.568744e-05	2.994420	1.862140e-02	1.992675	1.466491e-03	2.205715
$\frac{1}{35}$	6.028625e-05	2.996958	1.369206e-02	1.994772	1.066627e-03	2.065325
$\frac{1}{40}$	4.038199e-05	3.000944	1.048364e-02	1.999533	7.582384e-04	2.555641
$\frac{1}{45}$	2.837200e-05	2.996876	8.287931e-03	1.995325	6.295192e-04	1.579527
$\frac{1}{50}$	2.069309e-05	2.995457	6.714537e-03	1.998143	4.920329e-04	2.338740
$\frac{1}{55}$	1.554739e-05	2.999752	5.550803e-03	1.996978	4.020716e-04	2.118508
$\frac{1}{60}$	1.196849e-05	3.006683	4.663336e-03	2.002169	3.186921e-04	2.670971
$\frac{1}{70}$	7.538037e-06	2.997339	3.426542e-03	1.997143	2.336102e-04	2.219487
$\frac{1}{75}$	6.129100e-06	2.999063	2.985319e-03	1.997960	2.031375e-04	2.025874
$\frac{1}{80}$	5.049692e-06	3.001630	2.623982e-03	1.999016	1.762868e-04	2.196682
$\frac{1}{85}$	4.209215e-06	3.002921	2.323780e-03	2.004099	1.501000e-04	2.652569
$\frac{1}{90}$	3.546278e-06	2.998293	2.072888e-03	1.998876	1.357462e-04	1.758530
$\frac{1}{95}$	3.015784e-06	2.996983	1.860605e-03	1.998268	1.225038e-04	1.898470
$\frac{1}{100}$	2.585757e-06	2.999256	1.679389e-03	1.997766	1.110096e-04	1.920819

Table 7.25: L^2 interpolation errors and orders for u, u_x and u_y for the function (7.4.4) in Example 7.4.1 with $r = 5$ using the IFE space $\mathcal{J}_h$.

h	$\|\|u - I_h u\|\|_0$	order	$\|\|u_x - (I_h u)_x\|\|_{\beta,h}$	order	$\|\|u_y - (I_h u)_y\|\|_{\beta,h}$	order
$\frac{1}{10}$	2.902580e-03	N/A	1.889123e-01	N/A	1.724591e-02	N/A
$\frac{1}{15}$	8.664496e-04	2.981641	8.467745e-02	1.979045	5.877450e-03	2.654858
$\frac{1}{20}$	3.656831e-04	2.998577	4.771452e-02	1.993915	3.421939e-03	1.880255
$\frac{1}{25}$	1.879772e-04	2.982144	3.059199e-02	1.991979	1.963108e-03	2.490228
$\frac{1}{30}$	1.087109e-04	3.003641	2.125966e-02	1.996073	1.234201e-03	2.545533
$\frac{1}{35}$	6.844872e-05	3.001009	1.560643e-02	2.005366	8.831184e-04	2.171379
$\frac{1}{40}$	4.577955e-05	3.012380	1.193365e-02	2.009422	6.617328e-04	2.161271
$\frac{1}{45}$	3.209026e-05	3.016435	9.408357e-03	2.018656	4.850404e-04	2.637303
$\frac{1}{50}$	2.344631e-05	2.978722	7.635093e-03	1.982177	3.799262e-04	2.318281
$\frac{1}{55}$	1.765097e-05	2.978931	6.337409e-03	1.954514	3.483634e-04	0.909985
$\frac{1}{60}$	1.350404e-05	3.077778	5.272476e-03	2.114321	2.308328e-04	4.729870
$\frac{1}{65}$	1.066547e-05	2.948145	4.516585e-03	1.933267	2.177341e-04	0.729850
$\frac{1}{70}$	8.522844e-06	3.026140	3.885557e-03	2.030683	1.783014e-04	2.696054
$\frac{1}{75}$	6.944937e-06	2.967511	3.390017e-03	1.977468	1.541468e-04	2.109923
$\frac{1}{80}$	5.724670e-06	2.993994	2.981470e-03	1.989798	1.339706e-04	2.173671
$\frac{1}{85}$	4.758380e-06	3.049549	2.635209e-03	2.036367	1.186658e-04	2.000992
$\frac{1}{90}$	4.007628e-06	3.004066	2.347704e-03	2.021128	9.801092e-05	3.345646
$\frac{1}{95}$	3.407662e-06	2.999474	2.106766e-03	2.002761	8.514347e-05	2.603077
$\frac{1}{100}$	2.925962e-06	2.971208	1.903870e-03	1.974242	7.714460e-05	1.923372

Table 7.26: L^2 interpolation errors and orders for u, u_x and u_y for the function (7.4.4) in Example 7.4.1 with $r = 10^3$ using the IFE space $\mathcal{J}_h$.

Example 7.4.2. *Non-polynomial interface*

In this example, we consider the smooth interface

$$y = \frac{9}{23}\, e^{\frac{23}{9}x}, \tag{7.4.7}$$

such that $\Omega^+ = \{y > \frac{9}{23}\, e^{\frac{23}{9}x}\}$ and $\Omega^- = \{y < \frac{9}{23}\, e^{\frac{23}{9}x}\}$, as illustrated in Figure 7.16.

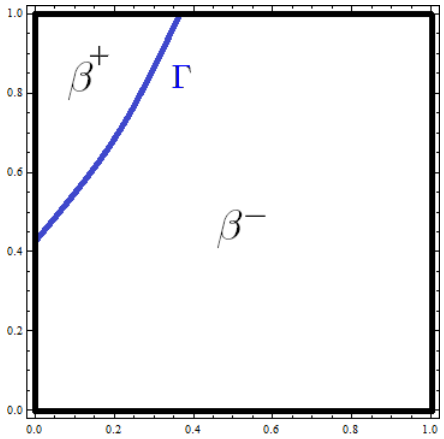

Figure 7.16: Geometry of Ω and the circular interface Γ in Example 7.4.2.

We test our space on the function defined by

$$u(x,y) = \begin{cases} \frac{1}{\beta^+}\, \left(y^2 - \frac{9}{49}\, e^{\frac{14}{3}x}\right)(x^4 + y^4 - 1); & \text{on } \Omega^+, \\ \\ \frac{1}{\beta^-}\, \left(y^2 - \frac{9}{49}\, e^{\frac{14}{3}x}\right)(x^4 + y^4 - 1); & \text{on } \Omega^-. \end{cases} \tag{7.4.8}$$

with $r = \frac{\beta^+}{\beta^-} = 5$ and $r = \frac{\beta^+}{\beta^-} = 10^3$ representing a moderate and a large jump in the coefficient β.

We present interpolation errors in $I_h u$ in the L^2 norm $||u - I_h u||_0$ and the broken weighted H^1 norms $||u_x - (I_h u)_x||_{\beta,h}$ and $||u_y - (I_h u)_y||_{\beta,h}$, and compute their orders of convergence in Tabes 7.27 and 7.28. Moreover, global rates of convergence are estimated using least-squares fit, thus computation for $r = 5$ reveals the following:

$$||u - U^h||_0 \approx C\, h^{3.0139}, \tag{7.4.9a}$$
$$||u_x - (I_h u)_x||_{\beta,h} \approx C\, h^{2.0130}, \tag{7.4.9b}$$
$$||u_y - (I_h u)_y||_{\beta,h} \approx C\, h^{1.9990}, \tag{7.4.9c}$$

and for $r = 1000$:

$$||u - U^h||_0 \approx C\ h^{3.0359}, \tag{7.4.10a}$$
$$||u_x - (I_h u)_x||_{\beta,h} \approx C\ h^{2.0370}, \tag{7.4.10b}$$
$$||u_y - (I_h u)_y||_{\beta,h} \approx C\ h^{2.0789}, \tag{7.4.10c}$$

We observe that, the interpolant in $\mathcal{J}_h$ yields $\mathcal{O}(h^3)$ optimal convergence rates for u and $\mathcal{O}(h^2)$ for its derivatives, for problems with arbitrary smooth interface.

h	$\|\|u - I_h u\|\|_0$	order	$\|\|u_x - (I_h u)_x\|\|_{\beta,h}$	order	$\|\|u_y - (I_h u)_y\|\|_{\beta,h}$	order
$\frac{1}{10}$	1.699731e-02	N/A	1.104897e$_+$00	N/A	1.116721e-01	N/A
$\frac{1}{15}$	5.177615e-03	2.931721	5.039784e-01	1.935983	4.956516e-02	2.003325
$\frac{1}{20}$	2.205908e-03	2.965792	2.861189e-01	1.967887	2.780693e-02	2.009173
$\frac{1}{25}$	1.134620e-03	2.979433	1.839079e-01	1.980664	1.778061e-02	2.003986
$\frac{1}{30}$	6.582537e-04	2.986278	1.280147e-01	1.987094	1.234638e-02	2.000561
$\frac{1}{35}$	4.151538e-04	2.990200	9.418530e-02	1.990785	9.071267e-03	1.999675
$\frac{1}{40}$	2.783939e-04	2.992645	7.217724e-02	1.993085	6.944009e-03	2.001272
$\frac{1}{45}$	1.956562e-04	2.994302	5.706490e-02	1.994647	5.486736e-03	1.999827
$\frac{1}{50}$	1.427018e-04	2.995448	4.624337e-02	1.995730	4.442792e-03	2.003128
$\frac{1}{55}$	1.072522e-04	2.996264	3.823048e-02	1.996482	3.671316e-03	2.001178
$\frac{1}{60}$	8.263390e-05	2.996881	3.213242e-02	1.997066	3.084912e-03	2.000049
$\frac{1}{65}$	6.500750e-05	2.997367	2.738453e-02	1.997523	2.628723e-03	1.999244
$\frac{1}{70}$	5.205740e-05	2.997730	2.361591e-02	1.997865	2.266498e-03	2.000627
$\frac{1}{75}$	4.233029e-05	2.998051	2.057468e-02	1.998170	1.974306e-03	2.000479
$\frac{1}{80}$	3.488292e-05	2.998296	1.808508e-02	1.998401	1.735079e-03	2.001350
$\frac{1}{85}$	2.908477e-05	2.998492	1.602138e-02	1.998580	1.536920e-03	2.000384
$\frac{1}{90}$	2.450351e-05	2.998657	1.429171e-02	1.998736	1.370904e-03	1.999885
$\frac{1}{95}$	2.083595e-05	2.998796	1.282769e-02	1.998868	1.230419e-03	1.999651
$\frac{1}{100}$	1.786522e-05	2.998911	1.157760e-02	1.998976	1.110398e-03	2.000967

Table 7.27: L^2 interpolation errors and orders for u, u_x and u_y for the function (7.4.8) with $r = 5$ using the IFE space $\mathcal{J}_h$.

h	$\|\|u - I_h u\|\|_0$	order	$\|\|u_x - (I_h u)_x\|\|_{\beta,h}$	order	$\|\|u_y - (I_h u)_y\|\|_{\beta,h}$	order
$\frac{1}{10}$	1.714986e-02	N/A	1.119257e+00	N/A	3.012172e-01	N/A
$\frac{1}{15}$	5.179029e-03	2.953084	5.048667e-01	1.963489	1.260394e-01	2.148736
$\frac{1}{20}$	2.213310e-03	2.955097	2.888171e-01	1.941382	4.747032e-02	3.394337
$\frac{1}{25}$	1.165268e-03	2.875000	1.910798e-01	1.851285	2.809431e-02	2.350674
$\frac{1}{30}$	6.693974e-04	3.040390	1.310251e-01	2.069433	2.016063e-02	1.820056
$\frac{1}{35}$	4.271893e-04	2.913712	9.816282e-02	1.873241	1.557361e-02	1.674686
$\frac{1}{40}$	2.803987e-04	3.152925	7.311965e-02	2.205701	1.078490e-02	2.751640
$\frac{1}{45}$	2.018427e-04	2.790928	5.928024e-02	1.781421	9.274539e-03	1.280951
$\frac{1}{50}$	1.460310e-04	3.072025	4.766894e-02	2.069049	6.839196e-03	2.891052
$\frac{1}{55}$	1.096380e-04	3.007385	3.949958e-02	1.972400	5.678366e-03	1.951593
$\frac{1}{60}$	8.404491e-05	3.055150	3.289203e-02	2.103860	4.576480e-03	2.479370
$\frac{1}{65}$	6.577258e-05	3.062720	2.797231e-02	2.024112	3.828347e-03	2.230021
$\frac{1}{70}$	5.423521e-05	2.602591	2.482379e-02	1.611332	3.657976e-03	0.614282
$\frac{1}{75}$	4.342667e-05	3.221440	2.129136e-02	2.224885	3.040456e-03	2.680026
$\frac{1}{80}$	3.564611e-05	3.059164	1.862702e-02	2.071442	2.552502e-03	2.710529
$\frac{1}{85}$	2.981036e-05	2.949033	1.659959e-02	1.900803	2.326269e-03	1.530863
$\frac{1}{90}$	2.479243e-05	3.224677	1.454810e-02	2.307929	1.865568e-03	3.861207
$\frac{1}{95}$	2.112974e-05	2.956632	1.311400e-02	1.919465	1.718203e-03	1.521928

Table 7.28: L^2 interpolation errors and orders for u, u_x and u_y for the function (7.4.8) with $r = 10^3$ using the IFE space $\mathcal{J}_h$.

7.4.3 Application to Interface Problems

In this section, we will show that the interior penalty IFE methods can produce solutions to the interface problems with optimal convergence rates, when the arbitrary interface is approximated by a parabola. Again, we consider the rectangular domain $\Omega = [0,1]^2$ and the uniform triangular mesh $\mathscr{T}_h = \mathscr{T}_h^i \cup \mathscr{T}_h^c$ of size h and formed by partitioning Ω into $(1/h)^2$ squares, with $h = \frac{1}{5m},\ m = 2, \ldots, 20$, then forming the triangular elements by joining the lower right and upper left vertices of the squares.

We solve the interface problem by the interior penalty IFE method (5.3.5) using the quadratic IFE space $\mathscr{J}_h$ after approximating the smooth interface by a parabola. Again, we use the norms defined in (4.1.1a) and (7.2.21) to compute the finite element errors.

Example 7.4.3. *Polynomial interface*

In this example we consider the interface problem (1.1.1) with the same cubic interface Γ as in Example 7.4.1, and the same true solution (7.4.4), where $\frac{\beta^+}{\beta^-} = 5$ and $r = \frac{\beta^+}{\beta^-} = 10^3$ representing a moderate and a large jump in the coefficient β.

The L^2 error $||u - U^h||_0$, the weighted errors $||u_x - U_x^h||_{\beta,h}$ and $||u_y - U_y^h||_{\beta,h}$, and their orders of convergence are presented in Tables 7.29 and 7.30. Moreover, global rates of convergence are computed using least-squares fit. A computation of the global convergence rates for $r = 5$ reveals the following:

$$||u - U^h||_0 \approx C\ h^{2.9993}, \tag{7.4.11a}$$
$$||u_x - U_x^h||_{\beta,h} \approx C\ h^{1.9990}, \tag{7.4.11b}$$
$$||u_y - U_y^h||_{\beta,h} \approx C\ h^{2.4788}, \tag{7.4.11c}$$

and a computation of the global convergence rates for $r = 1000$ yields:

$$||u - U^h||_0 \approx C\ h^{2.9995}, \tag{7.4.12a}$$
$$||u_x - U_x^h||_{\beta,h} \approx C\ h^{1.9993}, \tag{7.4.12b}$$
$$||u_y - U_y^h||_{\beta,h} \approx C\ h^{2.6027}. \tag{7.4.12c}$$

From these results, we can easily observe that the quadratic IFE solutions produced by the interior penalty IFE method converge, optimally, to the true solution under mesh refinement.

h	$\|\|u-U^h\|\|_0$	order	$\|\|u_x-U_x^h\|\|_{\beta,h}$	order	$\|\|u_y-U_y^h\|\|_{\beta,h}$	order
$\frac{1}{10}$	2.899860e-03	N/A	1.880082e-01	N/A	3.483171e-03	N/A
$\frac{1}{15}$	8.603341e-04	2.996798	8.367956e-02	1.996450	1.203510e-03	2.620943
$\frac{1}{20}$	3.630880e-04	2.998711	4.709601e-02	1.998061	6.130976e-04	2.344509
$\frac{1}{25}$	1.859435e-04	2.998977	3.014791e-02	1.999039	3.477050e-04	2.541726
$\frac{1}{30}$	1.076189e-04	2.999353	2.094071e-02	1.998778	2.088457e-04	2.795932
$\frac{1}{35}$	6.777613e-05	2.999573	1.538693e-02	1.999191	1.455473e-04	2.342478
$\frac{1}{40}$	4.540754e-05	2.999532	1.178173e-02	1.999297	1.054068e-04	2.416464
$\frac{1}{45}$	3.189438e-05	2.999145	9.309876e-03	1.999217	8.020644e-05	2.319719
$\frac{1}{50}$	2.325005e-05	3.000391	7.541025e-03	1.999968	5.903307e-05	2.909116
$\frac{1}{55}$	1.746825e-05	2.999914	6.232484e-03	1.999610	4.703199e-05	2.384529
$\frac{1}{60}$	1.345512e-05	2.999892	5.237230e-03	1.999535	3.724430e-05	2.681593
$\frac{1}{65}$	1.058308e-05	2.999688	4.462642e-03	1.999579	3.312126e-05	1.465760
$\frac{1}{70}$	8.473537e-06	2.999797	3.847941e-03	1.999821	2.544384e-05	3.558343
$\frac{1}{75}$	6.889329e-06	2.999937	3.352065e-03	1.999653	2.360024e-05	1.090213
$\frac{1}{80}$	5.676736e-06	2.999717	2.946223e-03	1.999617	1.913173e-05	3.252459
$\frac{1}{85}$	4.732668e-06	3.000221	2.609785e-03	2.000117	1.558269e-05	3.384552
$\frac{1}{95}$	3.390021e-06	3.001063	2.089365e-03	2.000469	1.282193e-05	2.555210
$\frac{1}{100}$	2.906747e-06	2.998475	1.885675e-03	1.999760	1.107957e-05	2.847424

Table 7.29: L^2 errors and orders for u and its derivatives for Example 7.4.3 with $r = 5$ using the interior penalty IFE method with $\mathcal{J}_h$.

h	$\|\|u - U^h\|\|_0$	order	$\|\|u_x - U_x^h\|\|_{\beta,h}$	order	$\|\|u_y - U_y^h\|\|_{\beta,h}$	order
$\frac{1}{10}$	2.901402e-03	N/A	1.880265e-01	N/A	7.374314e-03	N/A
$\frac{1}{15}$	8.606145e-04	2.997305	8.381076e-02	1.992826	4.547137e-03	1.192470
$\frac{1}{20}$	3.631552e-04	2.999201	4.710949e-02	2.002512	1.126703e-03	4.849806
$\frac{1}{25}$	1.859255e-04	3.000240	3.014439e-02	2.000845	5.343896e-04	3.342806
$\frac{1}{30}$	1.076227e-04	2.998628	2.094128e-02	1.997988	4.198616e-04	1.322938
$\frac{1}{35}$	6.777466e-05	2.999941	1.538827e-02	1.998804	2.865423e-04	2.478347
$\frac{1}{40}$	4.540548e-05	2.999711	1.178177e-02	1.999918	1.982708e-04	2.757795
$\frac{1}{45}$	3.189182e-05	2.999442	9.309575e-03	1.999526	1.381337e-04	3.068452
$\frac{1}{50}$	2.324839e-05	3.000304	7.540672e-03	2.000105	1.065611e-04	2.463009
$\frac{1}{55}$	1.746809e-05	2.999261	6.232846e-03	1.998509	9.092746e-05	1.664632
$\frac{1}{60}$	1.345460e-05	3.000235	5.237341e-03	1.999957	7.248108e-05	2.605826
$\frac{1}{70}$	8.473160e-06	2.999734	3.847871e-03	2.003552	4.571573e-05	2.646847
$\frac{1}{75}$	6.888963e-06	3.000063	3.352112e-03	1.999186	4.079426e-05	1.650910
$\frac{1}{80}$	5.676519e-06	2.999485	2.946217e-03	1.999866	3.514241e-05	2.310754
$\frac{1}{85}$	4.732434e-06	3.000408	2.609839e-03	1.999744	2.905503e-05	3.137623
$\frac{1}{90}$	3.986739e-06	2.999837	2.327922e-03	1.999918	2.513948e-05	2.532472
$\frac{1}{95}$	3.389855e-06	2.999719	2.089393e-03	1.999407	2.242515e-05	2.113230
$\frac{1}{100}$	2.906357e-06	3.000137	1.885632e-03	2.000474	1.920455e-05	3.022536

Table 7.30: L^2 errors and orders for u and its derivatives for Example 7.4.3 with $r = 10^3$ using the interior penalty IFE method with $\mathcal{J}_h$.

Example 7.4.4. *Non-polynomial interface*

In this example we consider the interface problem (1.1.1) with the same interface Γ as in Example 7.4.2, and the same true solution (7.4.8), where $\frac{\beta^+}{\beta^-} = 5$ and $r = \frac{\beta^+}{\beta^-} = 10^3$ representing a moderate and a large jump in the coefficient β.

We solve the interface problem by the interior penalty IFE method (5.3.5) using quadratic IFE space $\mathcal{J}_h$ after approximating the smooth interface by a parabola. Numerical results are presented in Tables 7.31 and 7.32, and global rates of convergence are computed using least-squares fit. The computation of the global convergence rates for $r = 5$ reveals the following:

$$||u - U^h||_0 \approx C\ h^{2.9848}, \tag{7.4.13a}$$
$$||u_x - U^h_x||_{\beta,h} \approx C\ h^{1.9849}, \tag{7.4.13b}$$
$$||u_y - U^h_y||_{\beta,h} \approx C\ h^{2.0295}, \tag{7.4.13c}$$

and a computation of the global convergence rates for $r = 1000$ yields:

$$||u - U^h||_0 \approx C\ h^{2.9848}, \tag{7.4.14a}$$
$$||u_x - U^h_x||_{\beta,h} \approx C\ h^{1.9849}, \tag{7.4.14b}$$
$$||u_y - U^h_y||_{\beta,h} \approx C\ h^{2.0333}. \tag{7.4.14c}$$

These results show that the quadratic IFE solutions produced by the interior penalty IFE method converge, optimally, to the true solution under mesh refinement for problems with arbitrary smooth interfaces.

h	$\|\|u-U^h\|\|_0$	order	$\|\|u_x-U_x^h\|\|_{\beta,h}$	order	$\|\|u_y-U_y^h\|\|_{\beta,h}$	order
$\frac{1}{10}$	1.699713e-02	N/A	1.101882e+00	N/A	1.207078e-01	N/A
$\frac{1}{15}$	5.176745e-03	2.932109	5.032243e-01	1.932939	5.204139e-02	2.074983
$\frac{1}{20}$	2.205532e-03	2.965801	2.858501e-01	1.965949	2.875123e-02	2.062551
$\frac{1}{25}$	1.134463e-03	2.979291	1.837880e-01	1.979376	1.820885e-02	2.046989
$\frac{1}{30}$	6.581809e-04	2.986124	1.279533e-01	1.986149	1.256710e-02	2.033909
$\frac{1}{35}$	4.151138e-04	2.990108	9.415069e-02	1.990056	9.195197e-03	2.026596
$\frac{1}{40}$	2.783712e-04	2.992532	7.215618e-02	1.992517	7.019079e-03	2.022366
$\frac{1}{45}$	1.956432e-04	2.994176	5.705151e-02	1.994162	5.534215e-03	2.017966
$\frac{1}{50}$	1.426938e-04	2.995351	4.623447e-02	1.995329	4.475063e-03	2.016215
$\frac{1}{55}$	1.072469e-04	2.996190	3.822427e-02	1.996166	3.693743e-03	2.013218
$\frac{1}{60}$	8.263029e-05	2.996816	3.212796e-02	1.996798	3.100961e-03	2.010404
$\frac{1}{65}$	6.500497e-05	2.997307	2.738126e-02	1.997283	2.640366e-03	2.008862
$\frac{1}{70}$	5.205562e-05	2.997666	2.361342e-02	1.997670	2.275227e-03	2.008392
$\frac{1}{75}$	4.232905e-05	2.997980	2.057278e-02	1.997981	1.980951e-03	2.007492
$\frac{1}{80}$	3.488202e-05	2.998242	1.808361e-02	1.998232	1.740314e-03	2.006732
$\frac{1}{85}$	2.908406e-05	2.998470	1.602022e-02	1.998438	1.541046e-03	2.005850
$\frac{1}{90}$	2.450296e-05	2.998618	1.429077e-02	1.998609	1.374185e-03	2.004964
$\frac{1}{95}$	2.083553e-05	2.998753	1.282693e-02	1.998754	1.233045e-03	2.004430
$\frac{1}{100}$	1.786489e-05	2.998876	1.157697e-02	1.998882	1.112559e-03	2.004630

Table 7.31: L^2 errors and orders for u and its derivatives for Example 7.4.4 with $r = 5$ using the interior penalty IFE method with $\mathcal{J}_h$.

h	$\|\|u-U^h\|\|_0$	order	$\|\|u_x-U_x^h\|\|_{\beta,h}$	order	$\|\|u_y-U_y^h\|\|_{\beta,h}$	order
$\frac{1}{10}$	1.699693e-02	N/A	1.101920e+00	N/A	1.219824e-01	N/A
$\frac{1}{15}$	5.177086e-03	2.931918	5.032453e-01	1.932920	5.248303e-02	2.080047
$\frac{1}{20}$	2.205725e-03	2.965725	2.858584e-01	1.965994	2.892295e-02	2.071226
$\frac{1}{25}$	1.134543e-03	2.979367	1.837936e-01	1.979369	1.832758e-02	2.044550
$\frac{1}{30}$	6.581905e-04	2.986430	1.279549e-01	1.986246	1.262462e-02	2.044512
$\frac{1}{35}$	4.151203e-04	2.990100	9.415161e-02	1.990075	9.228481e-03	2.032778
$\frac{1}{40}$	2.783759e-04	2.992526	7.215674e-02	1.992533	7.039568e-03	2.027595
$\frac{1}{45}$	1.956458e-04	2.994202	5.705207e-02	1.994144	5.551056e-03	2.016917
$\frac{1}{50}$	1.426961e-04	2.995324	4.623493e-02	1.995327	4.487497e-03	2.018717
$\frac{1}{55}$	1.072489e-04	2.996161	3.822468e-02	1.996159	3.704651e-03	2.011391
$\frac{1}{60}$	8.263096e-05	2.996944	3.212818e-02	1.996840	3.108308e-03	2.017098
$\frac{1}{65}$	6.500547e-05	2.997312	2.738140e-02	1.997303	2.645234e-03	2.015414
$\frac{1}{70}$	5.205592e-05	2.997693	2.361354e-02	1.997676	2.279190e-03	2.009763
$\frac{1}{75}$	4.232929e-05	2.997979	2.057291e-02	1.997964	1.984712e-03	2.005221
$\frac{1}{80}$	3.488228e-05	2.998216	1.808370e-02	1.998249	1.743317e-03	2.009415
$\frac{1}{85}$	2.908435e-05	2.998430	1.602030e-02	1.998431	1.543845e-03	2.004351
$\frac{1}{90}$	2.450308e-05	2.998710	1.429083e-02	1.998642	1.376133e-03	2.011938
$\frac{1}{95}$	2.083559e-05	2.998786	1.282697e-02	1.998761	1.234578e-03	2.007642
$\frac{1}{100}$	1.786494e-05	2.998879	1.157702e-02	1.998864	1.114081e-03	2.002203

Table 7.32: L^2 errors and orders for u and its derivatives for Example 7.4.4 with $r = 10^3$ using the interior penalty IFE method with $\mathcal{J}_h$.

7.5 Conclusions

In this chapter, we first presented two different approaches to construct quadratic IFE spaces to be used with a penalized finite element formulation or a with a discontinuous finite element formulation to solve elliptic interface problems with quadratic interfaces. Then, a procedure of handling arbitrary interfaces through the interpolation of the actual interface by a quadratic interface was presented and discussed. Numerical results have shown that IFE spaces constructed using the isoparametric approach have the optimal approximation capability for moderate jumps in the coefficient β, however they fail to have the optimal approximation capability with high jumps. Unlike the isoparametric approach, the second approach, which can be considered more straight-forward, generated a quadratic IFE space that was able to provide optimal solutions for the interface problems with both moderate and high jumps. Numerical results obtained with this latter quadratic IFE space using the interior penalty formulation developed in Chapter 5, showed that the method exhibits optimal convergence rates when the actual interface is quadratic (parabola or circle) as well as when the interface is arbitrary and smooth.

Chapter 8

Conclusions and Future Work

8.1 Contributions

Many interesting applications and real life problems in sciences and engineering involve interface problems, such as problems in elasticity, electromagnetism, fluid-dynamics, and material sciences. There exist several numerical methods for solving interface problems with discontinuous coefficients. The main topic of this thesis is the immersed finite element method which is one of the most efficient methods to solve interface problems. One of the main advantages of the IFE method for interface problems is that it does not require the mesh to be aligned with interfaces. Many applications can take advantage of this feature of the IFE method. For instance, this method is more efficient than the standard finite element method for solving problems involving thin layers and/or moving interfaces.

Our work mainly consisted of developing IFE spaces with optimal approximation capability to produce accurate numerical solutions to second-order elliptic interface problems. Then, we presented an interior penalty immersed finite element method that relies on the developed IFE spaces. Numerical results for several interface problems with different interface geometries have shown the optimality of the method.

We started with interface problems having linear interfaces. Based on two different sets of jump conditions on the interface, we presented two IFE spaces $\mathcal{S}_{h,E}^k,\ k = 1, 2$, where we justified the use of each set of jump conditions, and constructed local IFE spaces on arbitrary interface elements. The dimension of a local quadratic IFE space was proven to be equal to 6. We constructed Lagrange and hierarchical shape functions on interface elements. We presented general formulas to construct functions belonging to both spaces $\mathcal{S}_h^k,\ k = 1, 2$, and proved the existence of Lagrange shape functions which form a basis for the space $\mathcal{S}_h^2$, and a partition of unity. Similar reasoning can be applied to the space $\mathcal{S}_h^1$, and to other IFE spaces. We have numerically shown that our IFE spaces have optimal approximation capability where the interpolation error is $\mathcal{O}(h^3)$ in the L^2-norm and $\mathcal{O}(h^2)$ in broken H^1-

norm, under mesh refinement.

We presented an interior penalty IFE method which relies on the proposed quadratic IFE spaces $\mathcal{S}_h^k,\ k = 1, 2$, and based on the NIPG method developed by Wheeler *et al.* [57]. We presented several numerical results and computational examples which showed that this method leads to $\mathcal{O}(h^3)$ and $\mathcal{O}(h^2)$ optimal convergence rates, respectively, in the L^2 and broken H^1 norms. Moreover, we showed via a numerical example involving a thing layer, the efficiency of this method compared to the standard finite element method especially in applications involving thin layers. Such advantage can be seen in applications involving moving interfaces as well.

An extension of hierarchical shape functions to a general p-th degree is presented and a procedure to construct higher-degree IFE shape functions of degree p was given for problems with linear interfaces. Few properties of p-th degree IFE spaces were proved. Hence, p-th degree IFE spaces can be the subject of further investigation and numerical results can be presented in forthcoming work.

We further constructed quadratic IFE spaces that can be used to compute numerical solutions for interface problem with quadratic interfaces. Two different approaches were used to construct such quadratic IFE spaces. Finally, a procedure for solving problems with arbitrary interfaces was presented and discussed. An arbitrary smooth interface was interpolated by a parabola, then the procedure for quadratic IFE space can be used in solving such interface problem. Numerical results have shown that IFE spaces constructed using the isoparametric approach have optimal approximation capability only for moderate jumps in the coefficient β, however IFE space constructed using the second approach has optimal approximation capability for moderate and high jumps. This latter IFE space was also able to provide optimal solutions for interface problems using the interior penalty formulation developed in Chapter 5 for polynomial and general smooth interfaces.

8.2 Future Work

There are several long term goals and future work that can follow this dissertation. Here, we present some possible extensions to our work and give ideas and perspectives on how these problems may be treated.

8.2.1 Discontinuous Galerkin Methods for Interface Problems

Numerical results presented in Chapter 5 for the convergence of the immersed finite element solution are computed with Lagrange basis of the IFE spaces. Computation of IFE solutions using hierarchical basis of the spaces and a penalized formulation does not show optimal rates of convergence. Hence, a discontinuous Galerkin (DG) formulation is neces-

sary to obtain optimal convergence rates in L^2 and H^1 norms. In fact, the main feature of DG methods is their flexibility and ability to exhibit optimal convergence rates for problems having non-smooth solutions, although the cost of computation for these methods is higher. A future work will consist of testing a discontinuous Galerkin (DG) formulation with the quadratic IFE spaces developed in this thesis and compare obtained numerical results with results obtained by the Galerkin IFE method and the interior penalty IFE method discussed in this work. Moreover, guided by the work performed by X. He, T. Lin, and Y.Lin [32], a selective discontinuous Galerkin method (SDG) can be discussed and implemented as well. The main feature of the SDG method is its computational cost which is much lower than the known DG methods.

8.2.2 p-th degree IFE Spaces and Order of Approximation of the Interface

We have numerically shown in Chapter 7 that quadratic IFE spaces exhibit optimal convergence rates when an arbitrary interface is interpolated by a quadratic curve. We have also investigated p-th degree IFE spaces for interface problems with linear interface, in Chapter 6. Future work will include extending the proposed method to p-th degree polynomial approximations yielding exponential convergence rates for problems with arbitrary interfaces. Extended jump conditions will be investigated and applied to construct generalized higher-order IFE. The optimality of the interior penalty IFE methods and/or discontinuous Galerkin methods with higher-order IFE spaces and arbitrary smooth interfaces will be discussed. A very interesting research direction in this context would be to investigate the optimal order of approximation for a general interface that leads to optimal convergence rates, when polynomials of degree p are used. Our expectations are the following: when p-th degree IFE are used and the arbitrary interface is interpolated by a polynomial curve of the same degree p, optimal convergence rates will be obtained in L^2 and H^1 norms. Such result is not guaranteed in H^1 norm with the use of standard finite element method, since it was shown in [40] that optimal convergence rates are obtained in H^1 norm, only when the interface is interpolated by polynomials of degree $2p$ or higher. Furthermore, elements cut by multiple interfaces can be considered and an extension of this work to multi-material domains can be performed as well.

8.2.3 *A priori* Error Analysis

We have shown, numerically, that the interpolation error in the quadratic IFE spaces for problems with arbitrary smooth interfaces satisfy the inequalities (4.1.5). A future work consists of developing rigorous mathematical proofs for these inequalities. First, we can

show that for an element T_i of type $i,\ i = \text{I, II, III}$, the interpolation errors satisfy:

$$||u - I_h u||_{0,T_i} \ \leq \ C_{0,i} h^3, \tag{8.2.1a}$$

$$||ux - (I_h u)_x||_{0,T_i} \ \leq \ C_{1,i} h^2, \tag{8.2.1b}$$

$$||uy - (I_h u)_y||_{0,T_i} \ \leq \ C_{2,i} h^2, \tag{8.2.1c}$$

where $I_h u$ is the interpolant of the function u on the element T_i of size h, and $C_{k,i},\ k = 0, 1, 2$, are three positive constants.

We can then conclude that, if the interface element T of size h preserves the same type under h refinement, then we have:

$$||u - I_h u||_{0,T} \ \leq \ C_{0,T} h^3, \tag{8.2.2a}$$

$$||ux - (I_h u)_x||_{0,T} \ \leq \ C_{1,T} h^2, \tag{8.2.2b}$$

$$||uy - (I_h u)_y||_{0,T} \ \leq \ C_{2,T} h^2, \tag{8.2.2c}$$

where $I_h u$ is the interpolant of the function u on the element T of size h.

Finally, we can prove that the global interpolation errors on a mesh of size h satisfy:

$$||u - I_h u||_0 \ \leq \ C_0 h^3, \tag{8.2.3a}$$

$$||ux - (I_h u)_x||_{0,h} \ \leq \ C_1 h^2, \tag{8.2.3b}$$

$$||uy - (I_h u)_y||_{0,h} \ \leq \ C_2 h^2. \tag{8.2.3c}$$

For simplicity, we can first perform the above analysis for interface problems with linear interfaces then generalize the theory to quadratic and arbitrary smooth interfaces.

Following the same reasoning as for the interpolation error, we can prove that the immersed finite element errors satisfy the inequalities (5.1.3) which were shown numerically in this thesis.

8.2.4 Mathematical Proof of the Existence of Quadratic IFE Shape Functions for Problems with Arbitrary Interface

We proved the existence of Lagrange shape functions forming a partition of unity and a basis for the space $\mathcal{S}_h^2$ defined in Chapter 2. An immediate future work will consist of following the same reasoning to prove the existence of a Lagrange basis for the space $\mathcal{S}_h^1$. Moreover, other future work will consist of proving the existence of piecewise quadratic IFE shape functions forming a basis of the isoparametric IFE spaces $\mathcal{J}_h^k,\ k = 1, 2$, and the existence of piecewise quadratic IFE shape functions forming a basis of the piecewise quadratic IFE space $\mathcal{J}_h$, for problems with quadratic interfaces and problems with arbitrary smooth interface approximated by a parabola.

An interesting idea, to prove the existence of a basis of the piecewise quadratic IFE spaces for problems with parabolic interfaces and arbitrary interfaces approximated by parabolas, is to perform a coordinates change from the Cartesian coordinates (x, y) to an interface coordinates system based on parabolic coordinates (σ, τ), defined by

$$\begin{cases} x = \sigma\tau, \\ y = \frac{1}{2}\left(\tau^2 - \sigma^2\right), \end{cases} \tag{8.2.4}$$

where the physical interface Γ is given by $\tau = 0$.

For instance, in the parabolic coordinates system (σ, τ), we can write a function φ in the piecewise quadratic IFE space $\mathcal{J}_h$ as:

$$\varphi(\sigma, \tau) = \begin{cases} \varphi^+(\sigma, \tau), & \text{on } T^+, \\ \varphi^-(\sigma, \tau), & \text{on } T^-. \end{cases} \tag{8.2.5}$$

Given $\varphi^+(\sigma, \tau)$, we can write $\varphi^-(\sigma, \tau)$ as:

$$\varphi^-(\sigma, \tau) = \frac{\beta^+}{\beta^-}\ \left(\varphi^+(\sigma, \tau) - \varphi^+(\sigma, 0)\right) + \sum_{i=1}^{3} \varphi^+(P_i)\ l_i(\sigma)\ , \tag{8.2.6}$$

where $P_i,\ i = 1, 2, 3$, are respectively, the points D, E, and G defined in Chapter 7, and l_i are Lagrange one-dimensional quadratic polynomials shifted to the curve $\Gamma : \tau = 0$.

The formula (8.2.6) will be a starting point for the proof of the existence of a basis for the piecewise quadratic IFE space $\mathcal{J}_h$.

8.2.5 Time Dependent Interface Problems

Many practical applications include time dependent problems, such as interface problems with moving interface. In [34], He, Lin, and Zhang, investigated moving interface applications for parabolic equations using bilinear immersed finite element developed by X. He *et al.* [30]. Similar work can be performed using quadratic immersed finite elements developed in this thesis. Applications with moving interfaces show the high efficiency of the immersed finite element method, since the mesh will not be regenerated at every iteration; instead, the solution space will be regenerated. In many applications, regenerating the solution space is less expensive than regenerating the mesh. Hence, a future work will consist of using our quadratic IFE to treat and compute numerical solutions for model problems with moving interfaces.

8.2.6 Three-Dimensional Interface Problems

Three-dimensional interface problems were treated by Kafafy, Lin, Lin, and Wang who presented two IFE methods for solving the elliptic interface problem arising from electric field

simulation in composite materials [37]. A future work related to this thesis will consist of developing three-dimensional quadratic IFE spaces that are able to handle arbitrary three-dimensional interfaces and yield optimal convergence rates in L^2 and broken H^1 norms.

Bibliography

[1] S. Adjerid, M. Aiffa, and J.E. Flaherty. Hierarchical finite element bases for triangular and tetrahedral elements. *Computer Methods in Applied Mechanics and Engineering*, 190:2925–2941, 1999.

[2] S. Adjerid and T. Lin. Higher-order immersed discontinuous Galerkin methods. *International journal of information and systems sciences*, 3:558–565, 2007.

[3] S. Adjerid and T. Lin. A p^{th}-degree immersed finite element method for boundary value problems with discontinuous coefficients. *Applied Numerical Mathematics*, 59:1303–1321, 2009.

[4] D.N. Arnold, F. Brezzi, B. Cockburn, and D. Marini. Discontinuous Galerkin methods for elliptic problems. In B. Cockburn, G. Karniadakis, and C.-W. Shu, editors, *Discontinuous Galerkin Methods: Theory, Computation and Applications*, volume 11 of *Lecture Notes in Computational Science and Engineering*, pages 89–102, Berlin, 2000. Springer.

[5] I. Babuska. The finite element method for elliptic equations with discontinuous coefficients. *Computing*, 5:207–213, 1970.

[6] I. Babuska. The finite element method with penalty. *Math. Comp.*, 27:221–228, 1973.

[7] I. Babuska and J. E. Osborn. Generalized finite element methods: their performance and relation to mixed methods. *SIAM J. Numer. Anal.*, 20(3):510–536, 1983.

[8] I. Babuska and J. E. Osborn. Finite element methods for the solution of problems with rough input data. In P. Grisvard, W. Wendland, and J.R. Whiteman, editors, *Singular and Constructive Methods for their Treatment, Lecture Notes in Mathematics, #1121*, pages 1–18, New York, 1985. Springer-Verlag.

[9] I. Babuska and J. E. Osborn. Can a finite element method perform arbitrarily badly? *Math. Comp.*, 69(230):443–462, 2000.

[10] John W. Barrett and Charles M. Elliott. Fitted and unfitted finite-element methods for elliptic equations with smooth interfaces. *IMA J. Numer. Anal.*, 7:283–300, 1987.

[11] R. Becker and P. Hansbo. A finite element method for domain decomposition with non-matching grids. *Tech. Report 3613, INRIA*, 1999.

[12] G. Birkhoff and R.E. Lynch. *Numerical Solution of Elliptic Problems*. SIAM Studies in Applied Mathematics, SIAM, Philadelphia, 1984.

[13] J. H. Bramble and J. T. King. A finite element method for interface problems in domains with smooth boundary and interfaces. *Adv. Comput. Math.*, 6:109–138, 1996.

[14] S.C. Brenner and L.R. Scott. *The Mathematical Theory of Finite Element Methods*. Texts in Applied Mathematics, Springer, 1994.

[15] F. Brezzi, B. Cockburn, L.D. Marini, and E. Suli. Stabilization mechanisms in discontinuous Galerkin finite element methods. *Comput. methods in Appl. Mech. Engrg.*, 2005.

[16] F. Brezzi, M. Manzini, D. Marini, P. Pietra, and A. Russo. Discontinuous finite elements for diffusion problems. Atti Convegno in onore Di F. Brioschi (Milano 1997), Instituto Lombardo, Accademia di Scienze e Lettere, 1999.

[17] B. Camp, T. Lin, Y. Lin, and W.-W. Sun. Quadratic immersed finite element spaces and their approximation capabilities. *Advances in Computational Mathematics*, 24:81–112, 2006.

[18] Z. Chen and J. Zou. Finite element methods and their convergence for elliptic and parabolic interface problems. *Numer. Math.*, 79:175–202, 1998.

[19] A. J. Chorin. A numerical method for solving incompressible viscous flow problems. *J. Comput. Phys*, 2:12, 1967.

[20] A. J. Chorin. Numerical solution of the navier-stokes equations. *Math. Comp.*, 22:745762, 1968.

[21] R.W. Clough and J.L. Tocher. Finite element stiffness matrices for analysis of plates in bending. In *Matrix Methods in Structual Mechanics, The Proceedings of the Conference held at Wright-Parrterson Air Force Base, Ohio, 26-28, October, 1965, edited by J.R. Prezemieniecki et al*, pages 515–545. National Technical Information Service, U.S. Department of Commerce, Virginia, 1966.

[22] M. Delves and C.A. Hall. An implicit matching principle for global element calculations. *J. Inst. Math. Appl*, 23:223–234, 1979.

[23] LD. Marini D.N. Arnold F. Brezzi, B. Cockburn. Unified analysis of discontinuous galerkin methods for elliptic problems. *SIAM J. Numer. Anal.*, 39:1749–1779, 2000.

[24] John Dolbow and Isaac Harari. An efficient finite element method for embedded interface problems. *Int. J. Numer. Meth. Engng*, 78:229252, 2009.

[25] James R. Gaier. The effects of lunar dust on eva systems during the apollo missions. *Glenn Research Center, Cleveland, Ohio*, NASA/TM2005-213610.

[26] A. Gersborg-Hansen, M. P. Bendsoe, and O. Sigmund. Topology optimization of heat conduction problems using the finite volume method. *Struct. Multidisc. Optim.*, 31:251–259, 2006.

[27] Y. Gong, B. Li, and Z. Li. Immersed-interface finite-element methods for elliptic interface problems with non-homogeneous jump conditions. *SIAM J. Numer. Anal.*, 46:472–495, 2008.

[28] H. Han. The numerical solutions of the interface problems by finite element methods. *Numer. Math.*, 39:39–50, 1982.

[29] X. He. *Bilinear Immersed Finite Elements For Interface Problems*. PhD thesis, Virginia Polytechnic Institute and State University, 2009.

[30] X. He, T. Lin, and Y. Lin. Approximation capability of a bilinear immersed finite element space. *Numerical Methods for Partial Differential Equations*, 24:1265–1300, 2008.

[31] X. He, T. Lin, and Y. Lin. A bilinear immersed finite volume element method for the diffusion equation with discontinuous coefficient. *Communications in Computational Physics*, 6(1):185–202, 2009.

[32] X. He, T. Lin, and Y. Lin. Interior penalty bilinear IFE discontinuous Galerkin methods for elliptic equations with discontinuous coefficient. *J Syst Sci Complex*, 23:467483, 2010.

[33] X. He, T. Lin, and Y. Lin. Immersed finite element methods for elliptic interface problems with non-homogeneous jump conditions. *International Journal of Numerical Analysis & Modeling*, (submitted) 2009.

[34] X. He, T. Lin, and X. Zhang. Immersed finite element methods for parabolic equations with moving interface. submitted, 2010.

[35] S.-M. Hou and X.-D. Liu. A numerical method for solving variable coefficient elliptic equation with interfaces. *J. Comput. Phys.*, 202:411–445, 2005.

[36] J. Douglas Jr. and T. Dupont. Interior penalty procedures for elliptic and parabolic Galerkin methods. *Lecture Notes in Physics*, 58:207–216, 1976.

[37] R. Kafafy, T. Lin, Y. Lin, and J. Wang. 3-D immersed finite element methods for electric field simulation in composite materials. *International Journal for Numerical Methods in Engineering*, 64:904–972, 2005.

[38] R. J. LeVeque and Z. Li. The immersed interface method for elliptic equations with discontinuous coefficients and singular sources. *SIAM Journal of Numerical Analysis*, 34:1019–1044, 1994.

[39] R. J. LeVeque and Z. Li. Immersed interface methods for stokes flow with elastic boundaries or surface tension. *SIAM Journal on Scientific Computing*, 18(3):709–735, 1997.

[40] Jingzhi Li, Jens Markus Melenk, Barbara Wohlmuth, and Jun Zou. Optimal a priori estimates for higher order finite elements for elliptic interface problems. *Applied Numerical Mathematics*, 60:1937, 2010.

[41] Z. Li. The immersed interface method using a finite element formulation. *Applied Numer. Math.*, 27:253–267, 1998.

[42] Z. Li, T. Lin, Y. Lin, and R. Rogers. An immersed finite element space and its approximation capability. *Numerical Methods for Partial Differential Equations*, 20(3):338–367, 2004.

[43] Z. Li, T. Lin, and X. Wu. New Cartesian grid methods for interface problems using finite element formulation. *Numerische Mathematik*, 96(1):61–98, 2003.

[44] T. Lin, Y. Lin, R. C. Rogers, and L. M. Ryan. A rectangular immersed finite element method for interface problems. In P. Minev and Y. Lin, editors, *Advances in Computation: Theory and Practice, Vol. 7*, pages 107–114. Nova Science Publishers, Inc., 2001.

[45] Tao Lin, Yanping Lin, Robert Rogers, and Lynne Ryan. A rectangular immersed finite element space for interface problems. *Advances in Computation: Theory and Practice*, 7:107–114, 2001.

[46] Wing Kam Liu, Yaling Liu, David Farrell, Lucy Zhang, X. Sheldon Wang, Yoshio Fukui, Neelesh Patankar, Yongjie Zhang, Chandrajit Bajaj, Junghoon Lee, Juhee Hong, Xinyu Chen, and Huayi Hsu. Immersed finite element method and its applications to biological systems. *Comput. Methods Appl. Mech. Engrg.*, 195:17221749, 2006.

[47] Rajat Mittal and Gianluca Iaccarino. Immersed boundary methods. *Annu. Rev. Fluid Mech.*, 37:239–261, 2005.

[48] J.A. Nitsche. Uber ein variationsprinzip zur losung dirichlet-problemen bei verwendung von teilraumen, die keinen randbedingungen unteworfen sind. *Abh. Math. Sem. Univ. Hamburg*, 36:9–15, 1971.

[49] J.T. Oden, Ivo Babuska, and C.E. Baumann. A discontinuous hp finite element method for diffusion problems. *J. Comput. Phys.*, 146:491–519, 1998.

[50] C. S. Peskin. Flow patterns around heart valves. *J. Comput. Phys.*, 10:252–271, 1972.

[51] C. S. Peskin. Numerical analysis of blood flow in the heart. *J. Comput. Phys.*, 25:220–252, 1977.

[52] C. S. Peskin. Lectures on mathematical aspects of physiology. *Lectures in Appl. Math.*, 19:69–107, 1981.

[53] A. G. Piano. *Hierarchies of Conforming Finite Elements*. PhD thesis, Sever Institute of Technology, Washington University, St.Louis, 1975.

[54] A. G. Piano. Hierarchies of conforming finite elements for plane elasticity and plate bending. *Comp. & Meths. with Appls.*, 2:211–224, 1976.

[55] A. G. Piano. Conforming approximation for kirchhoff plates and shells. *Int. J. Num. Meth. Engng.*, 14:1273–1291, 1979.

[56] B. Riviere, M. Wheeler, and V. Girault. Improved energy estimates for interior penalty, constrained and discontinuous Galerkin methods for elliptic problems. part i. *Comp. Geosci.*, 3:337–360, 1999.

[57] B. Riviere, M.F. Wheeler, and V. Giraut. Improved energy estimates for finite elements methods based on discontinuous approximations spaces for elliptic problems. *SIAM Journal on Numerical Analysis*, 39:902–931, 2001.

[58] T. Rusten, P.S. Vassilevski, and R. Winther. Interior penalty preconditioners for mixed finite element approximations of elliptic problems. *Math. Comp.*, 65:447–466, 1996.

[59] Shephard, Dey, and Flaherty. A straightforward structure to construct shape functions for variable p-order meshes. *Computer Methods in Applied Mechanics and Engineering*, 147:209–233, 1997.

[60] E. Süli, C. Schwab, and P. Houston. hp-dgfem for partial differential equations with non-negative characteristic form. In B. Cockburn, G. Karniadakis, and C.-W. Shu, editors, *Discontinuous Galerkin Methods: Theory, Computation and Application*, volume 11 of *Lecture Notes in Computational Science and Engineering*, pages 221–230, Berlin, 2000. Springer.

[61] B. Szabo and I. Babuska. *Finite Element Analysis*. John Wiley, New York, 1991.

[62] Joseph Wang, Xiaoming He, and Yong Cao. Modeling electrostatic levitation of dust particles on lunar surface. *IEEE Transactions On Plasma Science*, 36:2459–2466, October 2008.

[63] M.F. Wheeler. An elliptic collocation-finite element method with interior penalties. *SIAM Journal on Numerical Analysis*, 15:152–161, 1978.

[64] J. Xu. Error estimates of the finite element method for the 2nd order elliptic equations with discontinuous coecients. *J. Xiangtan University*, 1:1–5, 1982.